CHEMICAL GENETICS OF NEW NITRO-CONTAINING COMPOUNDS THAT INHIBIT THE
GROWTH OF *MYCOBACTERIUM TUBERCULOSIS* AND *M. ABSCESSUS*

By

Ifeanyichukwu Emmanuel Eke

A DISSERTATION

Submitted to
Michigan State University
in partial fulfillment of the requirements
for the degree of

Microbiology and Molecular Genetics – Doctor of Philosophy

2024

ABSTRACT

Tuberculosis (**TB**), caused by *Mycobacterium tuberculosis* (**Mtb**), is a respiratory infection with a global distribution. TB chemotherapy is faced with many challenges, including the continual evolution of drug-resistant Mtb and the treatment failures resulting from the inactivity of many drugs against latent TB. These challenges highlight the need to develop more effective TB drugs. With the approval of pretomanid and delamanid for TB treatment, nitro-containing compounds have remerged as promising antimycobacterial compounds that can be developed into TB drugs.

In this dissertation, I describe the mechanisms-of-action of 10 new nitro-containing compounds that have potent antitubercular activities. These compounds were discovered from our previous high throughput screen of the Molecular Libraries Small Molecule Repository (**MLSMR**). Using a forward genetic selection approach, I showed that three of these compounds, the nitrofuranyl piperazines (HC2209, HC2210, HC2211), depend on the cofactor F_{420} (deazaflavin) activation machinery for their antimycobacterial activity. This is a well-characterized activation system that is used by pretomanid and delamanid for their reductive activation into toxic metabolites. Unlike pretomanid that completely loses its activity against Mtb in the absence of the deazaflavin-dependent nitroreductase (**Ddn**), I showed that these three compounds partially depend on Ddn and possibly, a secondary unknown F_{420}-dependent nitroreductase. Therefore, these nitrofurans have the possibility of being used in the treatment of pretomanid-resistant TB cases that are caused by *ddn* mutations. Additionally, these three nitrofurans differ from pretomanid in their activity against *M. abscessus* (**Mab**), a mycobacterial species with high intrinsic drug resistance. While pretomanid is inactive against Mab, the nitrofurans maintain their inhibitory activities against the pathogen. Additionally, I used a transcriptional profiling approach to demonstrate that HC2210 has differing effects on both Mab and Mtb. While HC2210 is bactericidal in Mtb and impacts different genes, including those involved in respiration; in Mab, HC2210 is bacteriostatic and does not affect the expression of respiratory genes. Interestingly,

the genetic selection of HC2210-resistant mutants in Mab identified glycerol kinase (**GlpK**) as a resistance factor in Mab. Much is known about the role of this gene in driving antibiotic resistance in Mtb, but little is known about it in Mab. The works presented in this dissertation remains one of the few reports of these protein as a resistance driver in Mab.

In addition to the nitrofuranyl piperazines, I genetically characterized the mechanism-of-action of four dinitrobenzamides (HC2217, HC2226, HC2238, and HC2239) and showed that they lose their activity against *dprE1* mutants in both Mtb and *M. smegmatis*. This is predictable since many dinitrobenzamide-based compounds have been biochemically characterized as DprE1 inhibitors. Interestingly, HC2250, a nitrofuranyl hydrazide, also loses its activity against the mutant, suggesting a DprE1-dependent mechanism. Transcriptional profiling of HC2250-treated and HC2238-treated cultures supports the possibility that HC2250 is a DprE1 inhibitor. This is the first report of a nitrofuran scaffold as a putative DprE1 inhibitor. However, HC2250 differs from the dinitrobenzamides in its bactericidal activity against dormant Mtb under hypoxic conditions, with this activity occurring in a DprE1-independent manner. I have also demonstrated that HC2250 and HC2210 have *in vivo* efficacy in a murine model of TB, indicating their promising potential for development as TB drugs.

Lastly, a targeted mutant screening approach and cheminformatics was used to provide an early assessment of the mechanisms-of-action of some growth inhibitors from the MLSMR screen. Surprisingly, this approach identified isoniazid analogs that partially retain their antimycobacterial activity against a *Tn:katG* mutant. Additionally, I identified many nitro-containing clusters in the MLSMR dataset, including the nitrofuranyl benzothiazoles that show enhanced activity against a *mmpL3* mutant pool and a *Tn:katG* mutant. This is a classic example of collateral sensitivity. Overall, this dissertation used chemical-genetic approaches to characterize the mechanisms-of-action of new nitro-containing compounds and provides proof-of-concept for their potential development as TB drugs.

I dedicate this dissertation to my wonderful parents,
Mr. and Mrs. Eke Kalu,
and to my younger siblings – Chidi, Nelson, Eke, and Stephen.
Your prayers and encouragements mean a lot to me!

ACKNOWLEDGEMENTS

TABLE OF CONTENTS

LIST OF ABBREVIATIONS

Mtb — *Mycobacterium tuberculosis*

Mab — *Mycobacterium abscessus*

Ddn — Deazaflavin-dependent nitroreductase

Fgd — F_{420}-dependent glucose-6-phosphate dehydrogenase

GlpK — Glycerol kinase

NRP — Non-replicating persistent

DprE1 — Decaprenylphosphoryl-β-D-ribose oxidase

DprE2 — Decaprenylphosphoryl-D-2-keto-ribose reductase

DPA — Decaprenylphosphoryl-D-arabinose

DPR — Decaprenylphosphoryl-β-D-ribose

DPX — Decaprenylphosphoryl-D-2-keto-ribose

PPP — Pentose phosphate pathway

MLSMR — Molecular Libraries Small Molecule Repository

WT — Wild type

CFU — Colony forming units

CHAPTER ONE: Functions of Nitroreductases in Mycobacterial Physiology and Drug Susceptibility

Abstract:

Tuberculosis is a respiratory infection that is caused by members of the *Mycobacterium tuberculosis* complex, with *M. tuberculosis* (**Mtb**) being the predominant cause of the disease in humans. The approval of pretomanid and delamanid, two nitroimidazole-based compounds, for the treatment of tuberculosis encourages the development of more nitro-containing drugs that target Mtb. Similar to the nitroimidazoles, many antimycobacterial nitro-containing scaffolds are prodrugs that require reductive activation into metabolites that inhibit the growth of the pathogen. This reductive activation is mediated by mycobacterial nitroreductases, highlighting the specificity of the nitro prodrugs for mycobacteria. In addition to their prodrug-activating activities, these nitroreductases have different native activities that support the growth of the bacteria. This chapter summarizes the activities of different mycobacterial nitroreductases with respect to their activation of different nitro prodrugs and highlights their physiological functions in the bacteria.

Introduction:

Tuberculosis (**TB**) is a respiratory infection that is caused by a phylogenetically related group of species known as the *Mycobacterium tuberculosis* complex (**MBTC**). Members of this complex include *Mycobacterium tuberculosis* (**Mtb**), *Mycobacterium africanum*, *Mycobacterium bovis*, *Mycobacterium orygis*, and *Mycobacterium canettii* amongst others, with Mtb being the predominant cause of TB in humans. With the introduction of antimycobacterial drugs such as streptomycin, isoniazid, rifampicin, pyrazinamide, and ethambutol, the 20th century gave birth to modern TB chemotherapy. While the latter four drugs remain the standards for TB treatment, their effectiveness is hampered by the evolution and spread of drug resistant strains. Additionally, TB treatment with these drugs is limited by the long courses of treatment needed to effectively sterilize the body of the pathogen[1-12]. These challenges require the discovery and development of new drugs to treat TB.

Nitric oxide is part of the body's innate immune system against mycobacterial infections[1, 13, 14]. Not surprisingly, nitro-containing compounds have emerged as important additions to the TB drug repository[1, 3, 8, 15]. Many nitro-containing compounds are prodrugs, requiring the reductive activation of their pharmacophoric nitro groups in order to exert their antimycobacterial activities[6, 16]. The reduction of the nitro prodrugs is usually mediated by cofactor-dependent mycobacterial nitroreductases, making these compounds to be specific for mycobacteria.

One of these mycobacterial nitroreductases is the deazaflavin-dependent nitroreductase (**Ddn**). Much is known about Ddn because of its role as the sole nitroreductase involved in the activation of pretomanid and delamanid, two nitro-containing drugs that have been approved for TB treatment[1, 3, 6-9, 17]. There are also other mycobacterial nitroreductases such as NfnB, Acg, DsbA, DprE1, Rv3368c, and Rv3131 (**Figure 1.1**), and they activate different nitro-containing scaffolds (**Figure A.1.1**). In this chapter, emphasis is placed on discussing the mechanistic basis for the prodrug-activating activities of the nitroreductases. Where it is known, the native activity of

the nitroreductases is also discussed and gaps in our understanding of the systems are highlighted. Current challenges with the use of nitro-containing compounds for TB chemotherapy, and possible solutions and therapeutic opportunities are also discussed.
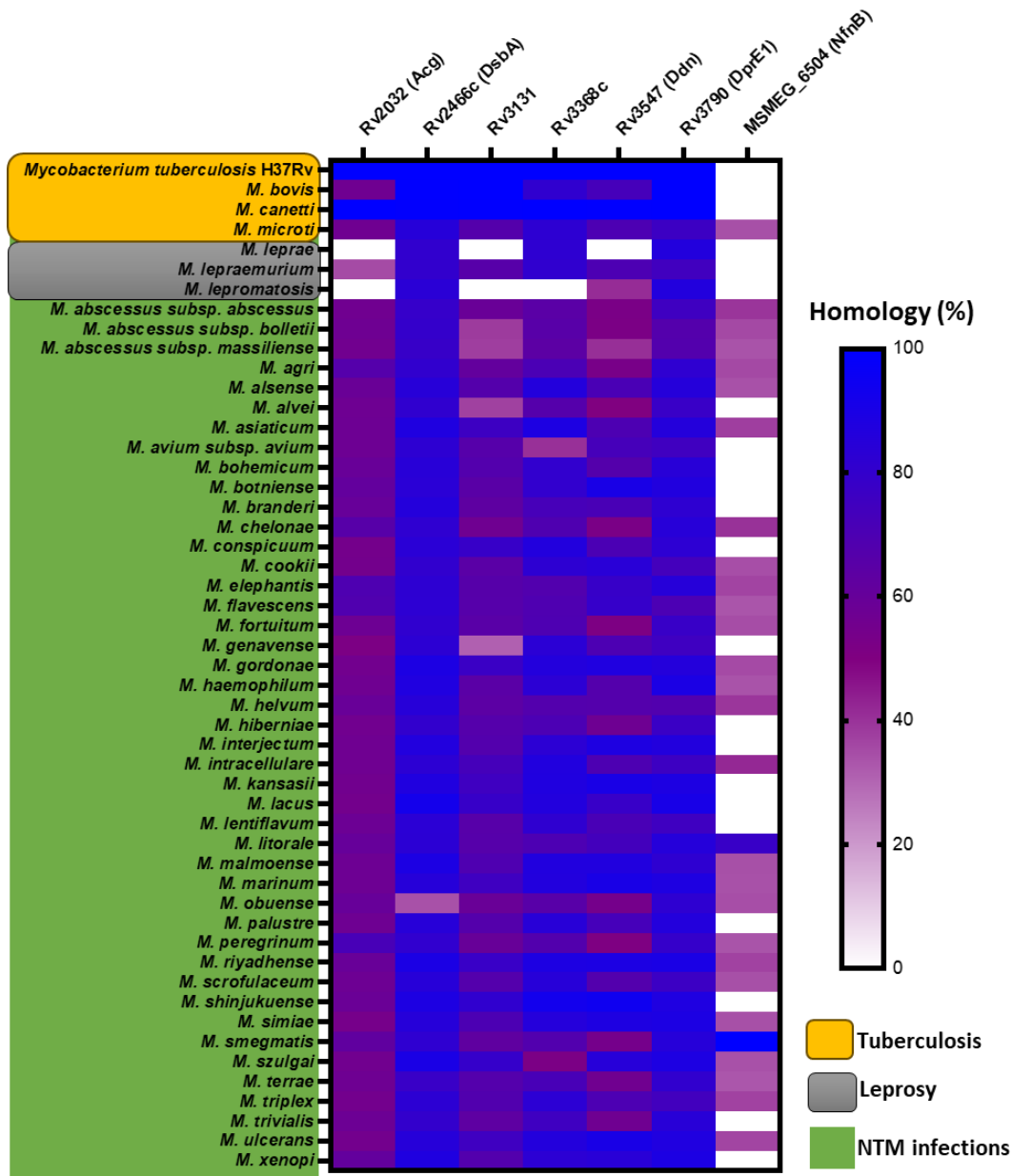
Figure 1.1. The conservation of mycobacterial nitroreductases across different species. The color gradient is the percentage homology of the amino acid sequences of the enzymes with respect to the *M. tuberculosis* H37Rv homolog (for Rv2032, Rv2466c, Rv3131, Rv3368c, Rv3547, and Rv3790) or *M. smegmatis* MC^2-155 homolog (for MSMEG_6504). Homologs were determined using a threshold e-value of 1×10^{-14}.

Deazaflavin-dependent nitroreductase (Ddn/Rv3547):

Native function of Ddn

Ddn (**Rv3547**) and its homologs (**Rv1558, Rv1261c, and Rv3178**) are classified as $F_{420}H_2$-dependent quinone reductases because of their obligatory use of cofactor F_{420} to reduce different quinone-based substrates such as menaquinone, menadione, plumbagin amongst others[18]. However, it is the reduction of menaquinone that is physiologically most relevant[17, 18] and accordingly, Ddn is functionally annotated as an $F_{420}H_2$-dependent menaquinone reductase[17]. In the mycobacterial electron transport system, menaquinone serves as an essential intermediate that shuttles electrons from the membrane-bound NADH dehydrogenases and succinate dehydrogenases to the cytochrome complexes (cyt-*bc₁-aa₃* or cyt-*bd*). The shuttled electrons can then be used to reduce oxygen or other terminal electron acceptors, producing a proton motive force that is used to power ATP generation[19]. Interestingly, the menaquinone reductase activity of Ddn has been associated with energy generation[17] (**Figure 1.2**). Here, Ddn is proposed to use $F_{420}H_2$ as a respiratory electron source to reduce menaquinone into its reduced form, menaquinol. The reduced menaquinone donates its electrons to cytochrome *bd* oxidase, with the subsequent activity of the oxidase leading to oxygen reduction and ATP production. As a word of caution, this model was built from data generated from purified membrane fractions[17] and needs to be verified using orthogonal approaches in an intact cell. Regardless, it is interesting to think of $F_{420}H_2$ as part of the mycobacterial pool of respiratory electron donors. This might also provide metabolic flexibility since cytochrome *bd* oxidase is an energetically inefficient complex that serves as the major cytochrome in hypoxic and stressful conditions[19, 20]. This oxidase has a high affinity for oxygen and a limited ability to generate a proton gradient that powers ATP generation[19, 20]. Therefore, the menaquinone-reductase activity of Ddn coupled with the activity of cytochrome *bd* oxidase may help in maintaining the proton motive force in non-replicating persistent Mtb, a hypothesis that still needs to be tested.
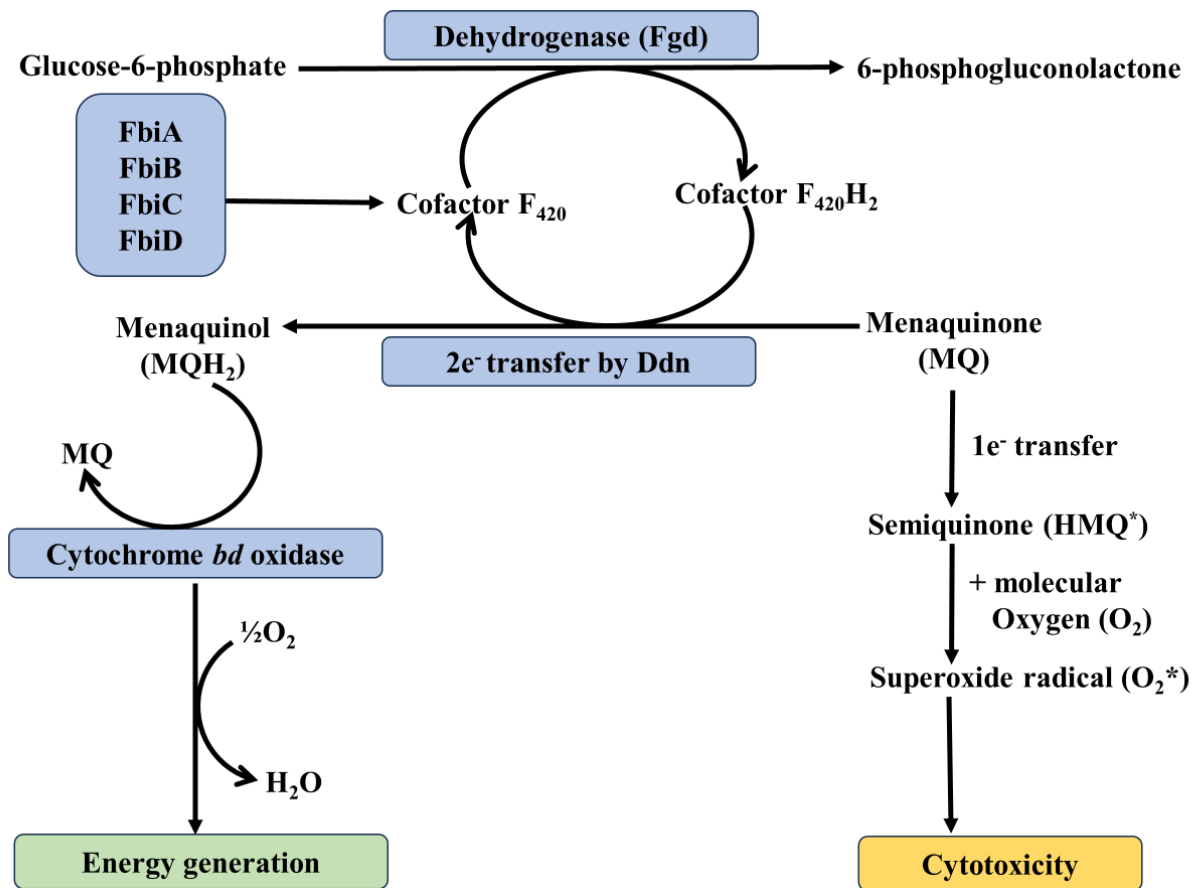
Figure 1.2. Schematic on the native activity of Ddn. First, FbiA, FbiB, FbiC, FbiD work together in the biosynthesis of cofactor F_{420}. This oxidized cofactor can be converted into the reduced form through the activity of Fgd in the pentose phosphate pathway. The reduced cofactor can be used by Ddn to reduce menaquinone into the menaquinol form in a 2-electron transfer. Menaquinol can subsequently transfer electrons to the terminal cytochrome bd oxidase, leading to the reduction of oxygen and energy production. Alternatively, in the absence of the menaquinone-reductase activity of Ddn, menaquinone is reduced in a 1-electron transfer to unstable semiquinone that can react with molecular oxygen to form superoxide radicals, leading to the death of the cells.

In addition to respiration, the quinone reductase activity of Ddn has been linked to resistance against oxidative stress in mycobacteria[17, 18, 21, 22]. Guerra-Lopez *et al*. reported that *M. smegmatis* mutants deficient in cofactor F_{420} biosynthesis are more sensitive to quinone-based oxidative stress agents[21]. This report was also replicated in F_{420}-deficient Mtb strains[18] and was

closely followed by the works of Hasan and colleagues who observed a reduction in the intracellular levels of glucose-6-phosphate in mycobacterial cells that were challenged with quinone-based oxidative stress agents, and the disruption of the F_{420}-dependent glucose-6-phosphate dehydrogenase (**fgd**) making the cells more sensitive to these agents[22]. This led them to hypothesize glucose-6-phosphate and $F_{420}H_2$ as electron storage molecules that maintain the redox balance of the cell during oxidative stress. However, when they introduced oxidative stress agents into a cell lysate containing $F_{420}H_2$, there was no observable reduction of these agents. Considering this, they speculated that the protective effects conferred by the reducing power of $F_{420}H_2$ might be occurring through an enzyme intermediate that was not in sufficient amount in the cell lysate. Indeed, this was later found to be true when Gurumurthy and colleagues conclusively showed that Ddn uses $F_{420}H_2$ to reduce different quinone substrates[18]. Interestingly, reducing cofactors such as NADH or NADPH are not used by the enzyme, nor does it depend on metal ions for its activity[2, 18]. Taking this further, Gurumurthy and colleagues proposed a Ddn-dependent oxidative stress resistance where Ddn, in a two-electron transfer, uses $F_{420}H_2$ to reduce quinones such as menaquinone into the quinol form[18] (**Figure 1.2**). This two-electron transfer by Ddn competes with the toxic one-electron reduction of quinones that normally leads to the generation of the unstable semiquinone molecule. While quinols can easily be detoxified, the semiquinones reacts with molecular oxygen to form superoxide radicals that kill the cells. Therefore, in mediating the conversion of menaquinone into the quinols instead of the semiquinones, the menaquinone-reductase activity of Ddn is protecting against oxidative stress. Despite the biochemical plausibility of this model, it needs to be tested since quinols can also be oxidized to cytotoxic semiquinones[18].

Lastly, the $F_{420}H_2$-dependent quinone reductase activity of Ddn and its homologs can be considered as an important recycling system to regenerate the oxidized cofactor. As alluded previously, the oxidized cofactor is used by Fgd in the pentose phosphate pathway (**PPP**) to oxidize glucose-6-phosphate into phosphogluconoate, generating $F_{420}H_2$. Of note, the oxidized cofactor can also be used by a structural homolog of Fgd – Rv0132c – initially annotated as

Fgd2[23, 24]. Rv0132c is not a glucose-6-phosphate dehydrogenase since it cannot oxidize glucose-6-phosphate[23, 24]. However, it is involved in the biosynthesis of mycolic acids where it uses cofactor F_{420} in the oxidation of hydroxy-mycolic acid into keto-mycolic acid[23]. Therefore, Rv0132c has been re-annotated as F_{420}-dependent Hydroxy Mycolic Acid Dehydrogenase (**FHMAD**)[23, 25]. Additionally, Fgd was previously annotated as Fgd1, but we now know that there is no other F_{420}-dependent homolog that carries out the oxidation of glucose-6-phosphate in the PPP[23, 24]. Both Fgd and FHMAD utilizes cofactor F_{420} to catalyze different reactions, producing $F_{420}H_2$; however, Fgd is the primary source of $F_{420}H_2$ since many $F_{420}H_2$-dependent reactions cannot occur when Fgd is genetically ablated[25]. A possible explanation for this is that the Fgd-linked PPP is a pathway that occurs multiple times throughout the lifecycle of the bacteria, serving as a rich source of ribose sugars and reducing equivalents such as $F_{420}H_2$. This contrasts with the Rv0132c-linked generation of $F_{420}H_2$ that occurs only during mycolic acid synthesis in preparation for cellular division. In any case, the $F_{420}H_2$ produced by either enzyme needs to be recycled into an oxidized form that can be reused. This is where Ddn comes into play to regenerate the oxidized cofactor. In addition to Ddn, it is important to note that Rv2951c, a phthiodiolone ketoreductase, can also recycle $F_{420}H_2$ into an oxidized form through its participation in the biosynthesis of phthiocerol dimycocerosates[25]. The same is applicable to Rv2074, an $F_{420}H_2$-dependent biliverdin reductase, that uses $F_{420}H_2$ to reduce heme-derived biliverdin into bilirubin[26]. Therefore, Ddn, Rv2951c, and Rv2074 are some of the few reductases that recycle F_{420} into an oxidized form. It can be argued that without the reductase activity of these enzymes, the cell would always turn to the metabolically burdensome *de novo* biosynthesis of cofactor F_{420} to satisfy its need for the oxidized form that is needed by Fgd and FHMAD. Taken together, Ddn is proposed to be part of the energy-generating machinery and oxidative stress defense system of mycobacteria.

Cellular Localization of Ddn

The cellular localization of Ddn is still an unsettled question, although evidence points to its possible localization to the bacterial membrane. The strongest empirical evidence on the membrane localization of Ddn is the identification of the protein during proteomic profiling of mycobacterial membrane extracts[27, 28]. These proteomic profiling studies coupled with *in silico* predictions pointed to the possibility that Ddn might be peripherally linked to the outer membrane of Mtb, but this opens up the question of the extra-cytoplasmic presence of cofactor F_{420}. A study by Bashiri and group showed the cytosolic binding of cofactor F_{420} to FHMAD prior to Tat-dependent export to the mycobacterial cell envelope[24]. While there are yet no reports of a translocation system that possibly exports Ddn to the cell envelope, it is reasonable to speculate that if such is found, Ddn will be bound to its cofactor prior to being exported to the mycobacterial cell envelope.

Additional evidence supporting the possible membrane localization of Ddn is that the enzymatic activity of the protein is significantly improved by the addition of Triton X-100, a detergent, into the buffer composition[2]. This enhanced activity might be due to the ability of the detergent to prevent the aggregation of the protein while simultaneously simulating the potential membrane-like environment of the protein. In fact, Triton X-100 has been successfully used with phosphatidylcholines to generate stable planar bilayers for solid-state NMR spectroscopy of membrane proteins[29]. The detergent has also been used to induce the *in vitro* assembly and insertion of proteins into purified outer membrane fractions of gram-negative bacteria[30]. Finally, the detergent is typically recommended for maximal yield of most membrane proteins during cellular extraction since it binds efficiently to membrane proteins and has very low affinity for hydrophilic proteins[31, 32]. Taken together, the enhanced enzymatic activity of Ddn in the presence of Triton X-100 might be an indication that it is a membrane protein.

Lastly, Ddn has stretches of hydrophobic amino acids that can enable it to associate with the amphipathic phospholipid bilayer of the membrane or the mycolic acid-rich cell envelope. This can be visualized with a Kyte-Doolittle hydropathy plot of Ddn that shows uninterrupted regions of hydrophobic amino acids in the amino acid sequence of Ddn (**Figure A.1.2A**), a typical property of membrane proteins[33]. However, unexposed interior regions of globular cytosolic proteins can also have these hydrophobic patches[33]; hence, the hydropathy plot does not conclusively prove Ddn as a membrane protein. Additionally, the Grand Average of Hydropathy (**GRAVY**) score of Ddn indicates that it might not be a membrane protein. The GRAVY score is a value that is generated by dividing the sum of the hydropathy values of all the amino acids that make up a protein by the total number of the amino acids[27, 33]. The GRAVY score of Ddn is -0.544. As a benchmark for comparison, the probability of a protein being a membrane protein is higher when its GRAVY score is higher than -0.4 [27, 33, 34]. Going further, DeepTMHMM, an *in-silico* prediction platform for transmembrane proteins, predicts no transmembrane domain in Ddn (**Figure A.1.2B**). Moreover, SignalP-5.0, another *in-silico* tool, predicts the absence of different translocation signals such as the Tat signal peptide, general Secretion signal, or lipoprotein peptide in the amino acid sequence of Ddn, indicating that Ddn is neither secreted nor translocated to the membrane. Nevertheless, these *in-silico* predictions do not rule out the possibility that Ddn might be directly bound to the membrane or is indirectly linked to the membrane through its possible interaction with membrane-bound proteins. As shown in **Figure A.1.2C**, the interaction network of Ddn in the STRING database include Rv0132 (**FHMAD**), a protein that is responsive to the Tat transport system and is anchored to the cell envelope[24]. Moreover, the native substrate of Ddn is menaquinone, a membrane-bound lipid-soluble molecule[17, 18]. Therefore, it is reasonable to speculate that Ddn will also be co-localized to the membrane with its substrate.

Prodrug activating activity of Ddn

Ddn is commonly known for its role as the sole nitroreductase in the reductive bioactivation of the nitroimidazole-based TB drugs, pretomanid and delamanid[1, 3, 6-8, 16, 17]. However, two other categories of cofactor F_{420}-dependent nitro compounds have been reported in literature (**Figure 1.3**). First, there are those that require Ddn and possibly another F_{420}-dependent nitroreductase for their activity. These include the nitrofuranyl piperazines (HC2209, HC2210, and HC2211) that we discovered in our lab[15], with the elucidation of their mechanisms-of-action forming the major chapters of this dissertation, and the nitrofuranyl triazines[9].
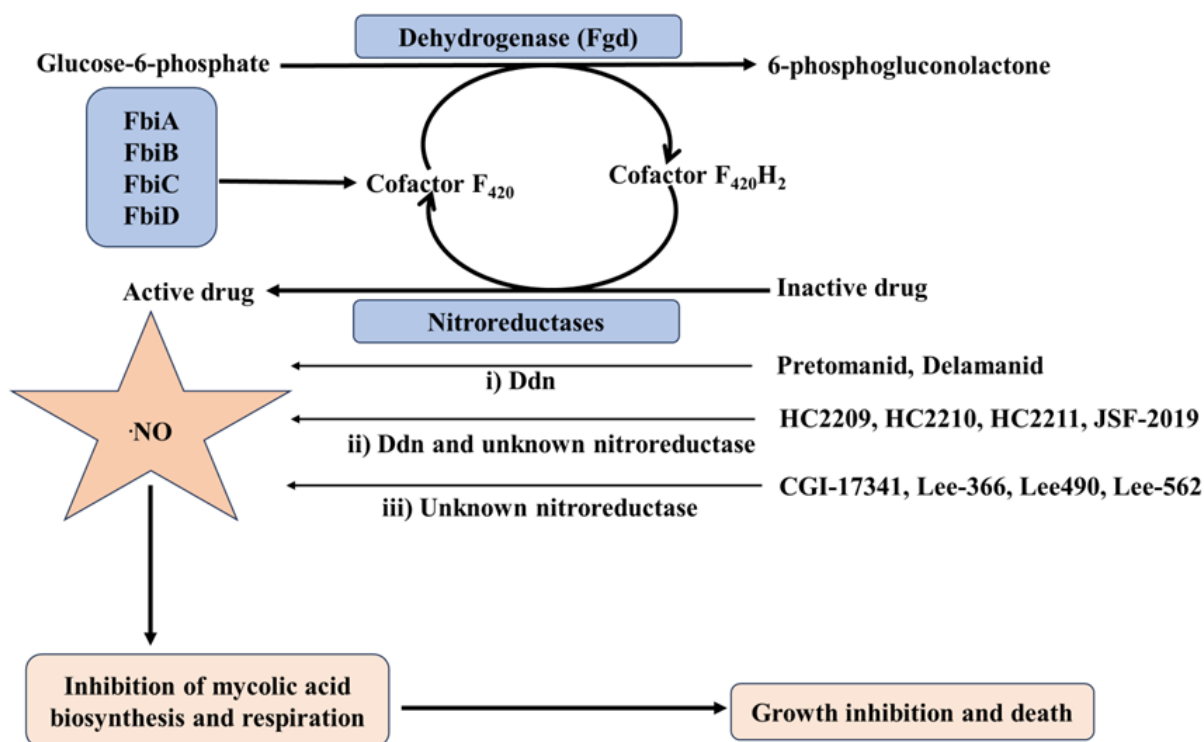
Figure 1.3. Schematic on the activation of different F_{420}-dependent compounds. The reduced cofactor F_{420} that is produced by Fgd is used by nitroreductases to reductively activate different nitro-containing compounds. Ddn is the exclusive nitroreductase for pretomanid and delamanid. HC2209, HC2210, HC2211, and JSF-2019 depend on Ddn and another F_{420}-dependent nitroreductase that is unknown. CGI-17341, Lee-366, Lee-490, Lee-562 need the reduced cofactor F_{420} for their activation, although the utilizing nitroreductase is yet to be discovered. Upon reductive activation, nitric oxide species are proposed to be produced and these inhibit the biosynthesis of mycolic acid and poison the electron transport chain, leading to growth inhibition and death.

Then, there are those that depend on cofactor F_{420} but not Ddn for their activation. For such compounds, the activating nitroreductase is yet to be identified, but it is predicted that the enzyme must depend on cofactor F_{420} for its activity. A good example is CGI-17341, the parent analog for pretomanid and delamanid, that retains its activity against *ddn* mutants[6]. Intriguingly, while CGI-17341 is able to inhibit the growth of *ddn* mutants[2, 6], *in vitro* biochemical characterization shows that Ddn can reduce the compound albeit at a lower rate compared to pretomanid[2]. This suggests that redundant Ddn homologs might be playing a role in its activation inside the cell. Another example is the nitrofuranylamides that retain their antimycobacterial activity in the absence of Ddn, but lose it in the absence of cofactor F_{420} or *fgd*[16].

Inasmuch as Ddn can reductively activate a variety of nitro prodrugs, a detailed biochemical and structural basis for this reductive activation is only available for pretomanid, and this will only be discussed here. The crystal structure of Ddn was solved by Cellitti and group[1], but generating the cocrystal structure of Ddn and pretomanid has proven to be a daunting task[1, 17]. Considering this, different molecular docking tools have been used to model the interactions of pretomanid with the protein[1, 2, 35]. In this section, I first provide a summary of the crystal structure of the Ddn holoenzyme before moving on to discuss the interactions of pretomanid with the Ddn:F_{420} complex.

The Ddn structure has a split barrel-like topology and a positively charged groove that interacts with the complementary negatively charged oligoglutamyl tail of cofactor F_{420}[1]. These interactions occur through a network of salt bridges and hydrogen bonding. In addition to the oligoglutamyl tail, different components of the cofactor such as the phosphate group, the ribityl moiety, and the deazaflavin ring interact with the enzyme to stabilize the binding of the cofactor. On the side of the enzyme, residues such as R54, K55, T56, R60, N62, P63, Y65, A76, S78, K79, M87, W88, N91, and Y133 amongst others participate in these interactions. Additionally, water molecules can mediate some interactions between the enzyme and the cofactor. Cellitti *et al.*

proposed that a combination of all these interactions leads to the orientation of the *Re* face of cofactor F_{420} towards pretomanid[1]. Predictably, resistance to pretomanid and other Ddn-dependent compounds have been linked to mutations in these residues[1, 6, 15, 17, 35]. The *Re* orientation of F_{420} for pretomanid activation in Ddn contrasts with Fgd and many other F_{420}-dependent enzymes that catalyzes reactions at the *Si* face of the cofactor[1].

In the molecular docking of pretomanid to Ddn, the drug is first placed in the protein such that its nitroimidazole group is close to the carbon-5 of the deazaflavin ring of cofactor F_{420}[1]. Upon docking to Ddn, the nitroimidazole group of pretomanid is positioned near the *Re* face of cofactor F_{420} and the hydrophobic tail of the drug is oriented towards the N-terminus of the protein[1, 2]. Additionally, the nitro group of pretomanid interacts with S78, Y130, and Y136 through hydrogen bonding[1, 17]. While it is tempting to suggest that Ddn directly participates in the transfer of the hydride electrons from the cofactor to the drug, the absence of classic catalytic residues at the active site of Ddn argues against this possibility[1]. In this case, Ddn functions primarily by precisely positioning the nitroimidazole head group of pretomanid near the *Re* face of F_{420} for an efficient hydride transfer from F_{420} and possibly aiding in the stabilization of the transition state of the drug-F_{420} complex[1]. Subsequently, the electron-deficient imidazole group of pretomanid is subject to a hydride attack from the deazaflavin ring of cofactor F_{420}[2, 7]. This attack occurs at the carbon-3 position of the imidazole ring, leading to the reduction of the ring and a concomitant formation of three intermediates of the drug. One of these intermediates further decomposes to release a mycobactericidal burst of nitric oxide[2, 7, 36].

Conservation of Ddn

Ddn is highly conserved across many mycobacterial species but is lacking in *M. leprae* (**Figure 1.1**). Mutants deficient in F_{420} biosynthesis and *ddn* mutants do not show any growth defect under normal laboratory conditions[18, 35, 37], supporting it is not essential for growth. There are varying numbers of Ddn homologs in different mycobacterial species[1, 6, 17, 18, 35], with three in

Mtb and as many as 11 in *M. abscessus*. Remarkably, none of the three homologs in Mtb has been shown to be involved in the activation of any prodrug nor can they serve as a replacement for Ddn in the activation of pretomanid and delamanid. Nonetheless, these homologs have quinone reductase activity like Ddn and are part of the defense system against oxidative stress[18].

Some mycobacterial species that have a Ddn ortholog are unable to activate pretomanid and delamanid, possibly due to differences in the key residues that interact with the drug or cofactor[1, 17]. For example, the Ddn ortholog of Mtb and *M. marinum* share a high similarity of essential residues necessary for prodrug activation, making both species to be susceptible to pretomanid and delamanid treatment[17, 38, 39]. *M. kansasii* and *M. xenopi* are also susceptible to pretomanid[38, 39]. However, *M. smegmatis*, *M. ulcerans*, *M. avium, M. intracellulare*, *M. gordonae*, *M. chelonae*, *M. fortuitum*, *M. scrofulaceum*, *M. gilvum*, and *M. abscessus* are resistant to pretomanid[6, 17, 38-40]. In my recently published work[15] that forms chapter two of this dissertation, I showed that both pretomanid and the nitrofuranyl piperazines (HC2209, HC2210, and HC2211) are active against Mtb, but only the latter three retain their activity against *M. abscessus*. Pretomanid depends exclusively on Ddn for activation, while the nitrofurans depend on Ddn and possibly another F_{420}-dependent nitroreductase for their activation. In chapter three of this dissertation, I used forward genetic selection to show that, similar to what is obtainable in Mtb, the nitrofurans depend on the cofactor F_{420} machinery of *M. abscessus* for activation. However, I could not recover any *ddn* mutant in *M. abscessus,* suggesting the possibility of multiple Ddn homologs mediating the activity of the nitrofurans in Mab, or another F_{420}-dependent, nitroreductase-independent mechanism.

Cofactor F_{420} and its biosynthesis

Cofactor F_{420} is so named because of the characteristic peak absorbance of its oxidized state at 420 nm[8, 37, 41]. It is a deazaflavin-based molecule that is conjugated to an oligoglutamyl tail of varying lengths. Structurally, cofactor F_{420} is similar to riboflavin cofactors such as FAD and

FMN, but biochemically, it functions more like the nicotinamides such as NAD and NADP[36, 37, 41, 42]. It is an obligatory redox carrier of two electrons and participates in hydride transfer. It has a low standard redox potential range of -340 mV to -360mV, compared to -205 mV to -220 mV for the flavins and -320 mV for nicotinamides[23, 37, 41]. The lower redox potential of cofactor F_{420} translates to a stronger reducing power and enables it to reduce a variety of substrates[1, 2, 18, 37]. This property has been proposed to allow the cofactor to serve as an electron carrier in low-oxygen or highly anaerobic environments[6, 23, 37]. This biochemical property can also explain the taxonomical restriction of the cofactor to few groups such as archaea and actinobacteria where they participate in metabolically challenging transformations such as methanogenesis and sulfate reduction[37]. However, evidence has recently arisen on the possible widespread distribution of the cofactor in non-actinobacterial phyla, although the physiological role of the molecule in these bacteria is still unclear[41].

The biosynthesis of cofactor F_{420} is a multi-enzymatic process that involves precursor molecules such as phosphoenolpyruvate, GTP, deazaflavin (F_0), lactate, tyrosine, and glutamate amongst others[8, 35, 37, 42]. A detailed review of the biosynthesis of cofactor F_{420} was provided by Greening and collaborators[37]. First, F_0, a biosynthetic intermediate of cofactor F_{420}, is produced through the condensation activity of F_0 synthase using precursors such as tyrosine and the pyrimidine, ribityldiaminouracil. In Mtb, this synthase is a single protein (FbiC), but in archaea, it is composed of two proteins (CofG and CofH). Next, enzymes such as CofA, CofB, and CofC (FbiD) work together to produce a lactate-derived intermediate that condenses with F_0 to form F_{420}-0. Recently, Bashiri *et al.* proposed a revision to this condensation reaction in prokaryotes where a phosphoenolpyruvate intermediate instead of a lactate-derived intermediate is involved[42]. Either way, the condensation reaction is catalyzed by FbiA or CofD, and the final product, F_{420}-0, is highly similar to cofactor F_{420} except that it lacks an oligoglutamyl tail. Lastly, cofactor F_{420} is generated through the sequential addition of glutamate residues to F_{420}-0. This reaction occurs in a GTP-dependent manner and is catalyzed by an F_{420}:γ-L-glutamyl ligase, CofE or FbiB. The

number of glutamate residues in the cofactor is also highly dependent on the species, with some having as many as seven residues[37]. The physiological importance of this variation is not yet clear, but it is known that the length of the oligoglutamyl tail does not affect the reductase activity of Ddn[1, 2]. Cofactor F_{420} of varying glutamate residues can bind with similar affinity to the protein. Furthermore, it should be noted that the genes involved in F_{420} biosynthesis seems to be functionally non-redundant in Mtb since the disruption of any of these genes leads to a halt in the biosynthesis of the cofactor and a concomitant resistance to different F_{420}-dependent drugs[8, 35].

Other Mycobacterial Nitroreductases:

NfnB (MSMEG_6505)

NfnB is an FMN-dependent nitroreductase that uses NADPH or NADH in a double-displacement reaction to reduce nitro-containing substrates into different derivatives[43, 44]. NfnB first reduces its prosthetic FMN group using NADPH or NADH as the electron source. Subsequently, it uses the reduced FMN to reduce the nitro groups of different nitro-aromatics, generating amino or hydroxylamino derivatives[43]. As shown in **Figure 1.1,** NfnB is lacking in many mycobacterial species including the MTBC. However, it is present in some fast-growing species such as *M. smegmatis*, and much of what is currently known for mycobacterial NfnB came from the homolog, *MSMEG_6505*.

The expression of *MSMEG_6505* is controlled by the neighboring transcriptional repressor, MSMEG_6503, that binds to conserved operator sites in *MSMEG_6505* and represses the expression of the enzyme[44]. Genetic ablation of *MSMEG_6503* leads to the overexpression of MSMEG_6505[44-46]. Many of the studies identifying MSMEG_6505 as a nitroreductase for different prodrugs resulted from forward genetic selections where the expression of *MSMEG_6503* is disrupted[15, 44-46]. None of the campaigns have ever reported spontaneous mutations in *MSMEG_6505*, bringing up the question of why the regulator is easily disrupted in different genetic selection studies while the nitroreductase stays intact. A possible answer to this

question might be that *MSMEG_6505* has a low tolerance for replication errors because of its physiological essentiality. However, we know this to be untrue since *MSMEG_6505* can be knocked out in *M. smegmatis*[44]. An alternative hypothesis is that the nucleotide sequence of *MSMEG_6503* might have regions that are more prone to replication errors. For instance, homopolymeric tracts or short sequence repeats in a gene can make it susceptible to strand mispairing and errors during replication[47, 48]. Another possibility is that MSMEG_6503 might be regulating some genes that might promote its selection over the nitroreductase in forward genetic selections. These hypotheses need to be subjected to rigorous scientific inquiry using a combination of computational, structural, and biochemical tools.

The native physiological activity of MSMEG_6505 remains enigmatic; hence, the protein has primarily been studied in the context of the modification of exogenous nitro-containing substrates. Unlike most mycobacterial nitroreductases that only have a prodrug-activating activity, MSMEG_6505 can activate or inactivate a nitro prodrug, and this seems to be dependent on the type of scaffold that is possessed by the nitro substrate[15, 44-46]. For instance, benzothiazinones, nitroimidazoles, and dinitrobenzamides are modified by MSMEG_6505 into inactive amino or hydroxylamine derivatives[44, 45, 49, 50]. I have also shown in chapter two of this dissertation that the dintrobenzamides in our collection lose their activity against *MSMEG_6503* mutants, presumably due to the increased expression of MSMEG_6505[15]. Contrastingly, the nitazoxanides are reductively activated by the enzyme into toxic hydroxylamine intermediates that kill the bacteria[46]. Additionally, overexpression of the enzyme in *M. smegmatis* increases the susceptibility of the bacteria to thienopyrimidines[51].

While MSMEG_6505 is not found in Mtb, the insights provided by the study of MSMEG_6505 activity in *M. smegmatis* raises the possibility of mammalian nitroreductases using the same mechanism to inactivate nitro-based TB drugs in the body[44, 45, 50]. However, it remains to be studied whether nitroreductases from the intestinal microbiota or mammalian systems affect

17

the *in vivo* pharmacodynamics of known TB nitro compounds. In any case, studies can be prioritized towards designing new nitro analogs that uses MSMEG_6505 to their advantage or are resistant to the enzyme[44, 49]. For instance, PBTZ169 is an analog of BTZ043 and is less susceptible to MSMEG_6505-mediated reduction than its parent compound[49]. This may translate to the protection of PBTZ169 from the potential reductive activity of mammalian nitroreductases or intestinal flora.

DprE1 (Rv3790)

DprE1, decaprenylphosphoryl-β-D-ribose oxidase/Rv3790, is a highly conserved protein that is well known for its role in the biosynthesis of the mycobacterial cell envelope (**Figure 1.1; Figure 1.4**). DprE1 forms a heteromeric membrane-bound epimerase complex with DprE2 (decaprenylphosphoryl-D-2-keto-ribose reductase/Rv3791). Together, they catalyze an essential two-step epimerization reaction that leads to the formation of decaprenylphosphoryl-D-arabinose (**DPA**), the only known source of arabinofuranosyl residues that are used by the mycobacterial arabinosyltransferases in the biosynthesis of important cell wall components such as arabinogalactan and lipoarabinomannan[10, 11, 44, 45, 49, 50, 52-59].

The epimerization reaction catalyzed by the DprE1/E2 complex starts with decaprenylphosphoryl-β-D-ribose (**DPR**) as the initial substrate and proceeds through a decaprenylphosphoryl-D-2-keto-ribose (**DPX**) intermediate to give rise to DPA, and this is a two-step oxidation-reduction reaction[10, 11, 49, 52-59] (**Figure 1.4**). First, DprE1 uses FAD as a cofactor to oxidize the 2'-hydroxyl group of DPR, generating a reduced flavin cofactor and DPX[10, 11, 49, 53, 55-58]. The reduced FAD can be recycled to an oxidized form through the action of electron acceptors such as molecular oxygen or menaquinone[11, 53]. Subsequently, DprE2 uses NADH (or NADPH) as a cofactor to reduce DPX to the final product, DPA[53-59]. This two-step epimerization reaction is proposed to occur at the periplasmic space of the mycomembrane[55], highlighting DprE1/DprE2 as vulnerable therapeutic targets.

Indeed, owing to the essential nature of the reactions catalyzed by DprE1/DprE2, many compounds have been developed to target either protein, although efforts have largely been focused on DprE1. The nitrobenzothiazinones (**BTZs**) were one of the first compounds reported to target DprE1[10, 11, 45, 52, 55, 57]. The BTZs work as mechanism-based inhibitors of DprE1, where
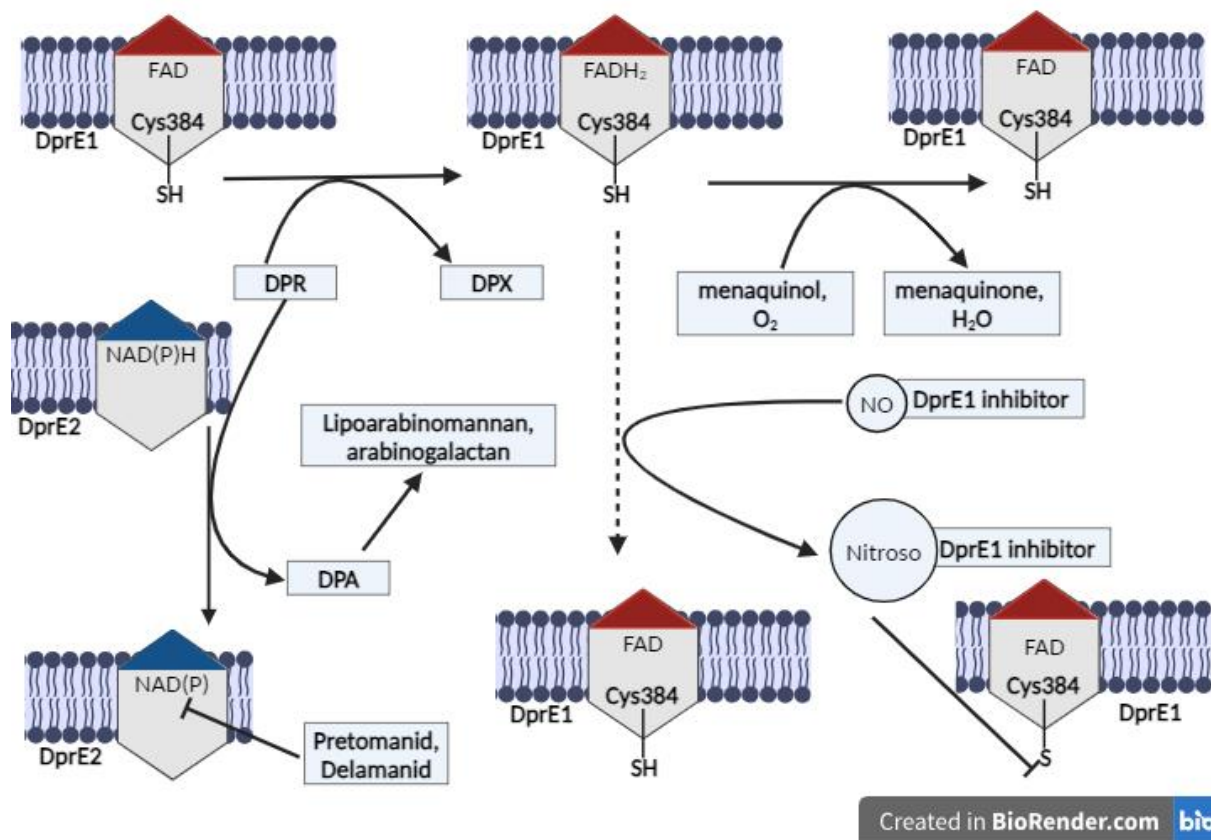
Figure 1.4. Activity of DprE1 mechanism-based inhibitors and DprE2 inhibitors. DPR (Decaprenylphosphoryl-β-D-ribose) is converted to DPX (Decaprenylphosphoryl-D-2-keto-ribose) through the catalytic activity of DprE1. This reaction produces the reduced form of the bound coenzyme, $FADH_2$. Under normal condition, the oxidized coenzyme is regenerated through the oxidizing activities of menaquinol or molecular oxygen. However, nitro-containing DprE1 inhibitors can regenerate the bound oxidized coenzyme through a DprE1-mediated activity, forming a nitroso intermediate of the inhibitors. Subsequently, the nitroso intermediates form a covalent bound with the thiol group of Cys387 at the active site of DprE1. This covalent modification inhibits the activity of DprE1. The DPX that is produced by DprE1 is converted to DPA through the activity of DrpE2. DPA is the sole source of arabinosyl groups that are used in the biosynthesis of the lipoarabinomannan and arabinogalactan components of the mycobacterial cell envelope. Pretomanid and delamanid inhibit the activity of DprE2 by forming an adduct with the protein.

the protein is both the activator of the prodrug and the target of the activated compound (**Figure 1.4**). Here, DprE1 serves as a nitroreductase that uses its FADH$_2$ prosthetic group to reductively activate the nitro group of the BTZs into a nitroso intermediate. The activated intermediate is an electrophile and is predicted to be susceptible to a nucleophilic attack by the thiol group of Cys387, an essential residue at the active site of DprE1. The electrophilic nitroso intermediate forms a covalent adduct with Cys387, irreversibly inhibiting the activity of the protein[10, 11, 45, 49, 52, 53, 57]. Covalent inhibitors of DprE1 share the same mechanism of action as BTZs and are generally characterized by three properties: the presence of a nitro group; their dependence on the reductase activity of DprE1 for their activation into active intermediates; and lastly, their loss of inhibitory activity against Mtb mutants that have mutations in *dprE1* Cys387. There are several distinct covalent DprE1 inhibitors including dinitrobenzamides, trinitroxanthones, nitrobenzoquinoxalines, nitrotriazoles, nitrobenzothiazoles, and the more recently described, nitrofuranyl hydrazides[11, 12, 15, 45, 50, 52, 55, 60, 61]. The latter scaffold (HC2250) was first reported as a putative DprE1 inhibitor in my recently published work[15] that I discussed in chapter two of this dissertation. In chapter four, I followed up and showed that HC2250 has a DprE1-independent activity against dormant Mtb and exhibits *in vivo* efficacy in an acute murine model of TB.

Noncovalent DprE1 inhibitors lack a nitro group and do not require the reductase activity of DprE1. Therefore, DprE1 is not a nitroreductase for these compounds. Instead, these compounds inhibit DprE1 by forming noncovalent interactions with different residues of the protein[55]. Some of these noncovalent DprE1 inhibitors include chemical classes such as azaindoles, thiadiazoles, benzothiazoles, carboxyquinoxalines, and dihydroquinolones[55, 61].

Inhibitors of DprE2 have only recently been reported [58, 59], and this began with the work of Batt *et al*. who observed that the overexpression of DprE2 and not DprE1 in a whole-cell target-based screening reduced the potency of two nitrofuran-based compounds[59]. They speculated that the compounds might be DprE2 inhibitors. However, when they followed up their observation with

an *in vitro* biochemical assay for DprE2, they did not observe any inhibitory effect of the compounds on the enzymatic activity of DprE2. This was suggested to be due to the possibility that the compounds are prodrugs that need to be activated into a form that can interact with DprE2. Indeed, subsequent forward genetic selection proved this correct, with the implication of the cofactor F_{420} system as the activation machinery. However, the activating nitroreductase was never reported. In a latter report by the same group, they showed that DprE2 is also a molecular target for the Ddn-activated pretomanid and delamanid[58]. The activated nitroimidazole drugs were showed to form NAD adducts that inhibit the activity of DprE2 (**Figure 1.4**). While the two studies from Batt *et al.* and Abrahams *et al.* are currently the only reports on DprE2 inhibitors[58, 59], it is intriguing that neither of them implicated the enzyme as a nitroreductase. As discussed previously, DprE2 works as a reductase to convert DPX to DPA using NADH or NADPH as a cofactor[54-59]. Therefore, it is reasonable to argue that DprE2 might be able to reduce nitro-containing substrates. It is likely that as more DprE2 inhibitors are discovered, we will see nitro-containing compounds that require the reductase activity of the protein for their activation. Conversely, there is also the possibility that the thermodynamic property of the bound NADH, especially in terms of the high redox potential, makes the protein unable to serve as a nitroreductase.

Mrx2 (Rv2466c)

Rv2466c (DsbA/Mrx2) is a mycothiol-dependent cytosolic thioredoxin-like oxidoreductase that is directly induced by SigH as part of the bacterial response against oxidative stress[14, 51, 62-64]. SigH also induces the expression of thioredoxin reductase/thioredoxin genes (*trxB2*/*trxC*)[62]. During oxidative stress, the bacteria use these SigH-induced proteins to reduce unneeded disulfide bonds of different proteins, maintaining the cellular redox balance and protein conformations [51, 62-64]. Notably, the mycothiol-dependence of Rv2466c is critical to the protective activity of the protein against oxidative insults[14, 63, 64]. Mycothiol is a low-molecular weight pseudodisaccharide that is composed of a 1-D-*myo*-inosityl 2-amino-2-deoxy-α-D-

21

glucopyranoside conjugated with *N*-acetylcysteine. The molecule is not found in eukaryotes, and its distribution seems to be limited to actinomycetes such as mycobacteria[65, 66]. It is present in high levels in these actinomycetes, where it serves as the major low-molecular weight thiol. This contrasts with most bacteria and eukaryotes that predominantly use glutathione, a tripeptide thiol, to maintain redox homeostasis inside the cells[64, 65, 67]. Mycothiol is considered a functional analogue of glutathione since it can mediate the same activities of the tripeptide molecule[67]. The disruption of the multi-step biosynthetic machinery for mycothiol leads to enhanced susceptibility of the mycobacteria to oxidative stress[65-67]. As part of the cellular defense system against oxidative stress, mycothiol forms a chemical linkage with cysteine residues in different proteins, a phenomenon known as protein S-mycothiolation[64]. This protects the residues from excessive oxidation, maintaining the structural integrity of the proteins. Unsurprisingly, Mtb strains that are deficient in the biosynthesis of mycothiol also have an increased sensitivity to hydroxyl radical-producing antibiotics such as rifampin[65, 66]. The same can be said for *sigH* or *rv2466c* mutants under oxidative stress conditions[14, 64].

The limited species distribution of mycothiol makes it an attractive target for mycobacteria-specific drugs[66], and this might be where Rv2466c comes into play. Rv2466c is a mycothiol-dependent nitroreductase that was first shown to reductively activate thienopyrimidine derivatives, with the mechanistic basis being worked out to be a series of dithiol-disulfide formations[51, 63, 64]. Albesa-Jove *et al*. provided a structural model that suggests that the conformation of Rv2466c is strongly controlled by its redox state, and this in turn, controls the catalytic activity of the protein[63]. In the oxidized state, Cys19 and Cys22 at the active site of the protein form a disulfide bond with each other and trigger an inactive open conformation of the protein. Upon reduction, the protein switches to an active closed conformation that can catalytically activate thienopyrimidines. Upon reductive activation of thienopyrimidines, the Cys19-Cys22 disulfide bond at the active site of the enzyme is formed again. This leads to a local conformational change that opens the protein to release the activated prodrug. Taking this further, Rosado and group worked out a biochemical

model where Cys19 and Cys22 are in direct competition with each other[64]. Cys22 promotes the formation of intramolecular disulfide bond with Cys19, making the protein unable to activate the prodrug. This is akin to the oxidized inactive state that was proposed in the structural model of Albesa and colleagues[63]. Cys19 reacts with two mycothiol molecules, giving rise to a reduced protein and an outgoing mycothione molecule (**Figure 1.5**). It is this reduced Rv2466c, through an initial nucleophilic attack by Cys19, that activates thienopyrimidines into active metabolites including nitric oxide species that kill Mtb[51, 63, 64, 68].
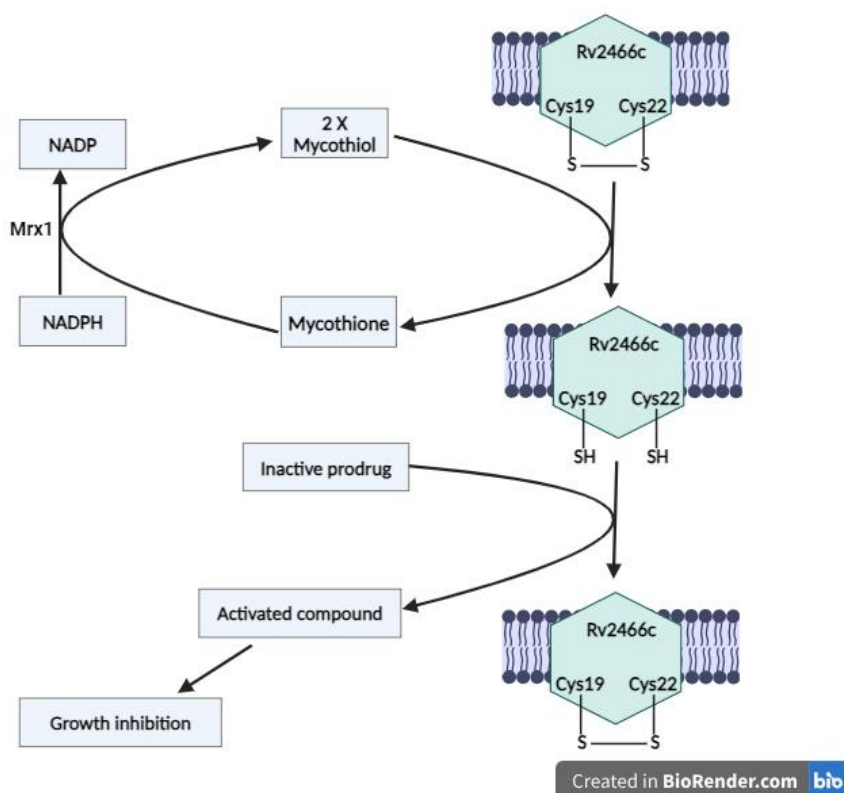
Figure 1.5. Activation mechanism of Rv2466c-dependent compounds. Two cysteine residues at the active site of Rv2466c form a disulfide bond that is broken down in a mycothiol-dependent manner. This generates a mycothione molecule that is recycled back to two mycothiol molecules through the catalytic activity of Mrx1, an enzyme that utilizes the reducing power of NADPH. The reduced Rv2466c enzyme can then activate nitro prodrugs into active metabolites that kill the bacteria. This also regenerates the oxidized form of the enzyme that can participate in multiple cycles of the reaction.

Mycothione, a molecule formed from the intramolecular disulfide linkage of two oxidized mycothiol molecules, can be recycled back to the reduced form through the action of mycothione reductase (**Mrx1**), with NADPH as an electron donor[64]. Since Rv2466c is a mycothiol-dependent nitroreductase, it has been renamed as **Mrx2**[64, 68, 69]. While Rv2466c is considered a nonessential gene under normal laboratory conditions, it might play critical roles during the pathogenesis of the bacteria. This idea is driven by the conservation of a homologous gene in *M. leprae* (**Figure 1.1**), a species that has undergone extensive genomic reduction and is presumed to only retain genes that are essential to its physiology and pathogenesis.

Besides thienopyrimidines, Rv2466c reductively activates nitrofuranylcalanolides (**NFCs**) into a fluorescent amine-based product, ANI[14]. While NFCs have a high mycobactericidal activity, treatment of Mtb with a synthetic ANI shows a very weak cidal effect. This discrepancy in the mycobactericidal activity of the two compounds was proposed to be due to the poor cellular entry of ANI, although this remains to be tested. Alternatively, it is possible that ANI is not the bactericidal product of NFC and like most activated nitro compounds, the activated intermediates are too unstable to be reliably detected by existing tools. In such cases, carefully designed and well-timed experiments coupled with advanced molecular technologies need to be used to identify the active intermediates. Nevertheless, the intrinsic fluorescence property of the activated NFC has been successfully applied towards the development of diagnostic assays for Mtb[14, 70, 71]. There are three intertwined reasons for the use of NFCs in Mtb diagnosis. First, NFCs have a narrow spectrum of activity[70, 72], with the conjugation of a trehalose moiety further increasing their specificity for mycobacteria[71, 73]. Second, NFCs need to be activated by Rv2466c, an enzyme that depends on the mycobacterial-restricted thiol cofactor, mycothiol, further highlighting the specificity of NFCs for mycobacteria[14, 70]. Lastly, NFC has a coumarin core whose intrinsic fluorescence is quenched by the inclusion of an electron-withdrawing nitro group on the heteroatom at the 7-position of the core[70, 74]. Therefore, the reduction of the nitro group to an amine derivative by the mycobacterial Rv2466c unmasks the intrinsic fluorescence of coumarin,

serving as a rapid high throughput readout for Mtb in different clinical samples[70]. In line with this, works from Liu's group have demonstrated the diagnostic utility of the NFC reduction, where the fluorescence readout from NFCs reduction in TB-positive sputum samples and clinical isolates was used to rapidly confirm TB diagnosis in a low-cost, high-throughput fashion[70, 71, 73].

Rv3368c

Rv3368c is an oxidoreductase that is conserved in different mycobacterial species (**Figure 1.1**). It is upregulated in oxygen-starved non-replicating mycobacteria, pointing to a possible role in protection against oxidative stress[75]. While Rv3368c is annotated as a nitroreductase, biochemical evidence to this effect is limited. Recently, Hong *et al*. showed that Rv3368c is possibly a nitroreductase that activates a cyanine-based nitro-containing probe for TB diagnosis[76]. Here, the intrinsic fluorescence of cyanine is blocked by conjugating with a nitrobenzyl ring. The reductive activity of Rv3368c is suggested to generate an amine derivative that allows the fluorescence of the cyanine probe to be detected. When the cyanine-nitrobenzyl probe was further conjugated with trehalose, it allows for the specific labeling of live mycobacteria in clinical samples. Specifically, the trehalose in the cyanine-nitrobenzyl probe is incorporated into the mycobacterial cell wall by actively replicating bacteria, allowing the probe to serve as a viability marker. Notably, this differs from standard diagnostic sputum smear reagents such as the fluorescent dye, Auramine O, and the Ziehl-Neelsen staining that cannot differentiate between live and dead mycobacteria. Further biochemical analysis is needed to confirm the nitroreductase status of Rv3368c and to define the cofactor(s) needed for its activity. This will allow the development of Rv3368c-dependent diagnostic kits, and possibly drugs for TB chemotherapy.

Rv3131

Rv3131 is a *dosR*-regulated putative nitroreductase that is proposed to be part of the bacterial response to host-generated nitrosative stress during latent infection[77-79]. It is immunogenic, stimulating the expression of proinflammatory cytokines[80]. Due to its

immunostimulatory property, Rv3131 has been considered as a potential vaccine candidate to protect against the hypervirulent Beijing Mtb strain[78, 81].

Rv3131 is an FMN-bound protein that depends on NADPH for its oxidoreductase activity[82, 83], although its nitroreductase status is disputed[83]. Recently, Dong and group provided preliminary biochemical evidence on the nitroreductase function of Rv3131[82]. They showed that the protein uses NADPH to reductively activate metronidazole, with two cysteine residues – Cys75 and Cys279 – playing a role in this process. Further genetic studies could be used to decipher if Rv3131 is indeed the nitroreductase that activates metronidazole in Mtb. Metronidazole is a nitroimidazole-based drug that has been used in the treatment of different anaerobic infections[84-86]. The low reduction potential of metronidazole ensures that it can only be reduced inside anaerobic organisms. In such organisms, different systems such as the malate/pyruvate:ferrodoxin oxidoreductases and hydrogenases reductively activate the drug[6, 84, 86, 87].

Metronidazole is not currently used for TB treatment, probably because of its inactivity in aerobic conditions. Inasmuch as it cannot be used for active TB cases, it has been proposed for the treatment of latent TB[82]. This is understandable since latent TB is characterized by hypoxic granuloma, a condition that favors the activation of the drug. In fact, metronidazole is active against non-replicating persistent Mtb in anaerobic conditions[88] and has been shown to prevent the reactivation of latent TB in non-human primates[89]. It is also effective against intracellular Mtb in macrophages[82]. Since Rv3131 is part of the 48-member DosRST regulon that is strongly upregulated in hypoxia-driven latent TB, it is possible it might indeed be the nitroreductase that allows metronidazole to exert its antimycobacterial activity only in low-oxygen environment[82]. Bioinformatic analyses suggest some similarity between Rv3131 and RdxA, a nitroreductase in *Helicobacter pylori* that is involved in the activation of metronidazole in the bacteria, reinforcing the possibility that Rv3131 is a metronidazole-activating nitroreductase in Mtb[82, 86]. However, it

cannot be ruled out the possibility that Acg, another DosR-regulated gene, might be the nitroreductase for metronidazole in Mtb.

Acg (Rv2032)

Rv2032 (Acg) is a monomeric FMN-bound protein that is induced by DosR[90, 91]. Therefore, the gene is strongly upregulated during hypoxic conditions or during the infection of macrophages[79, 90, 91]. Acg is generally classified as a nitroreductase[79, 90], although the evidence for this classification is contested. The strongest support on the nitroreductase nature of Acg came from the work of Chauviac and group who provided the first crystal structure of the protein[90]. They showed that Acg has a structural fold that is reminiscent of classical nitroreductases. The protein can structurally superimpose with NfnB, a mycobacterial nitroreductase that is not found in Mtb, although this is not a perfect superimposition. Going further, they showed that, like NfnB and many other nitroreductases, Acg uses FMN as a prosthetic group to accept or donate electrons. The FMN group can be reduced by dithionite in anaerobic conditions. Interestingly, Acg diverges from other FMN-bound nitroreductases in its inability to use NADH or NADPH as an electron source. Additionally, the Acg protein has a lid that may restrict the access of different substrates to the bound FMN pocket. This restrictive lid raises the question of which type of molecules can gain access to the binding pocket and if the protein even has any native nitroreductase activity. Evidence against the nitroreductase nature of Acg can be seen by the increased sensitivity of an *acg* knockout mutant to nitrofuran-based prodrugs[91]. These drugs need to be reductively activated, and the fact that the mutant shows collateral susceptibility to the drugs suggests at least that the protein is not an activating enzyme for this nitro chemotype. However, it might also be that other nitro chemotypes can be reduced by Acg, and these were not tested in the study. In any case, Chauviac and group proposed a model to explain the increased susceptibility of the *acg* mutant to the nitrofurans[90]. They suggested that Acg might be sequestering the FMN cofactor needed by other nitroreductases, serving as a storage site for the cofactor. The inactivation of

Acg will increase the cellular availability of the FMN cofactor and this can be used by other nitroreductases to reductively activate the nitrofuran prodrugs. Alternatively, it can be speculated that Acg might be functioning as an NfnB-like nitroreductase that inactivates the nitrofurans, hence the increased susceptibility of the mutants to the compounds. These are all plausible scenarios that need to be worked out in the lab.

Another piece of evidence against the nitroreductase function of Acg is that it differs from other mycobacterial nitroreductases in its inability to protect against oxidative and nitrosative stresses[91]. Interestingly, the protein has been shown to be a virulence factor that is required during infection, with a knockout strain suffering a remarkable defect in its ability to grow and survive in mice and macrophages[91]. However, the molecular mechanisms for this virulence activity remain to be fully defined.

Molecular targets of nitro-containing compounds:

With the exception of the DprE1 mechanism-based inhibitors, where DprE1 is both the activator and target, the molecular targets of most nitro-containing compounds are poorly defined. The reductive activation of the aromatic nitro groups of these compounds is proposed to release radical nitrogen species that rarely have only a single cellular target[5, 6]. These species damage different cellular components including DNA, RNA, and proteins, explaining for their high potency[87].

Most nitro-containing compounds are effective against both active and non-replicating persistent Mtb. This contrasts with many TB drugs that are only active against actively replicating Mtb. The potency of nitro prodrugs against active and dormant Mtb may be attributed to the ability of the compounds to target mycolic acid biosynthesis and respiration under different physiological conditions. This is a hypothesis that was primarily built from the transcriptional profiling of pretomanid[5, 40] but can be generalized to other nitro-containing compounds[9, 92]. Part of the activities that occurs in an actively replicating Mtb is the biosynthesis of mycolic acids[5]. In such

organisms, nitro compounds exert their antitubercular activity by inhibiting different enzymes involved in the biosynthesis of mycolic acids, and some of these effects have been biochemically validated. For instance, JSF-2019, a nitrofuranyl triazine, has been shown to be a direct inhibitor of InhA, an enzyme involved in the FAS-II pathway of mycolic acid biosynthesis[9]. Pretomanid reduces the levels of ketomycolates and allows the accumulation of the precursor, hydroxy-mycolates, possibly by its direct inhibition of FHMAD, an enzyme that converts hydroxy-mycolic acids into ketomycolic acids[23, 37, 40]. As mentioned previously, pretomanid and delamanid have recently been shown to be inhibitors of DprE2, another protein involved in the biosynthesis of the mycobacterial cell envelope[58]. Despite the subtle differences in the ability of nitro compounds to inhibit different genes involved in mycolic acid biosynthesis, a uniting feature seen in the transcriptional profiling of most nitro compounds is the upregulation of the *iniBAC* operon[5, 9, 92]. This operon is typically upregulated by inhibitors of mycobacterial cell wall biosynthesis[5].

On the other hand, cell envelope biosynthesis is limited in non-replicating Mtb, making drugs such as isoniazid, ethambutol, DprE1 inhibitors, and other drugs that target mycolic acid biosynthesis ineffective against dormant Mtb[5, 10, 15, 40]. The minimal basal transcriptional state of dormant cells also makes it unreasonable to conduct transcriptional studies in such cells[5]. However, transcriptional profiling in aerobically growing cells coupled with biochemical studies in dormant cells have led to a model where the nitro compounds primarily inhibit respiratory activities in dormant Mtb[5, 7, 9, 92]. In aerobic conditions, the released nitric oxide can be easily detoxified by molecular oxygen; but in anaerobic conditions, the free nitric oxide species are sufficient to drive the antimycobacterial activities of the compounds[68, 92]. Dormant mycobacterial cells show some levels of respiration that is needed to maintain critical cellular processes such as membrane potential, and the bactericidal activity of the nitro compounds can be explained by the ability of the released nitric oxide to serve as an electron sink[5, 7, 35, 69, 87, 92]. Like the respiratory inhibitor, potassium cyanide, the released toxic nitric oxide is proposed to interact with cytochromes or cytochrome oxidases in the electron transport chain, although this interaction have never been

elucidated for any of the nitro compounds[5, 7]. This hypothesis is inferred from the differential expression of sentinel respiratory genes such as the *cydABDC* operon that encodes cytochrome *bd* oxidase, the nitrate reductase *narGHIJ*, the type 1 NADH dehydrogenase *rv1854c*, and cytochrome genes such as *rv0327c* and *rv0136* amongst others[5, 68, 92]. Biochemically, this respiratory poisoning normally manifests as a rapid decrease in the intracellular concentrations of ATP and a change in the redox status of the dormant Mtb[5].

Nitro compounds can also target genes that are clearly far from pathways related to respiration or mycolic acid biosynthesis. For example, Mori and coworkers used a combination of genetics and click chemistry to demonstrate that TP053, a DsbA-activated thienopyrimidine, directly interacts with Rv0579, a non-essential mycobacterial protein that is proposed to have RNase activity[69]. The physiological activities of Rv0579 are still unclear, although it is suggested to be involved in RNA metabolism. Thus, in addition to other mechanisms, TP053 may be interrupting the metabolism or turnover rate of the mycobacterial RNA pool by targeting Rv0579. Nitro compounds can also modulate genes that are part of the defense system of the bacteria against oxidative stress, an observation I made from the transcriptional profiling of HC2250-treated cells as discussed in chapter four of this dissertation.

Issues and prospects:

Nitro prodrugs and mutagenicity

Generally, nitro-containing compounds are considered as therapeutic liabilities and tend to be avoided by most researchers. This is due to the laboratory association of such compounds with increased mutagenicity and genotoxicity, and their overall cytotoxicity[4, 15, 40, 68, 93]. However, the significance of such laboratory studies in human medicine has been hotly contested in some quarters due to a variety of reasons[87, 94, 95].

First, *ex in vivo* studies on the mutagenicity of nitro prodrugs mostly employ microsomal liver extracts to reduce the compounds, followed by the classical Ames test to check for the

mutagenic properties of the reduced metabolites[4, 16, 87, 93]. Microsomal liver extracts are highly concentrated in oxygen-consuming proteins that rapidly create an anaerobic environment. This environment has a very low redox potential that cannot be reached inside human cells. Since low redox potential favors the reduction of nitro compounds into different metabolites, it follows that the generation of mutagenic metabolites from nitro compounds in liver microsomes is physiologically questionable in humans[87, 93].

Second, most nitro prodrugs need a nitroreductase, especially of microbial origin, for activation. Through passive diffusion, nitro compounds are proposed to enter the microbial cytosol or periplasm, where they are subsequently reduced to active forms by appropriate enzymes. Microbial nitroreductases have little sequence conservation and substrate specificity with the mammalian counterparts, making it harder for the antimicrobial nitro prodrugs to be reductively activated by the mammalian enzymes. Thus, the cytotoxic activities of the nitro prodrugs tend to be restricted to microbes that express the activating nitroreductase[8, 93]. This also ensures that these prodrugs have little or no inhibitory impact on the composition of the normal flora, a beneficial property that most antibiotics lack.

Lastly, there are conflicting reports on the risk of tumor formation by nitro prodrugs in different models. For instance, metronidazole has been reported to increase the incidence of different types of cancer in animals[87, 96, 97], while other reports dispute the carcinogenicity of the drug[87]. Indeed, the routine use of metronidazole in different clinical settings has greatly increased, and this is probably because of different epidemiological studies that show no association between the drug usage and cancer incidence in humans[94, 95]. Another example is pretomanid that was recently shown to have no carcinogenic potential in a transgenic rasH2 mice[93]. This mice model expresses the human proto-oncogene, *c-Ha-ras*, that increases the sensitivity of the mice to carcinogens and is associated with a high frequency of spontaneous tumors. Interestingly, the

rasH2 mice did not develop tumors even when treated with very high doses of pretomanid that exceeds normal therapeutic exposure for humans.

While the mutagenic potential of nitro prodrugs cannot be quickly dismissed, more thorough epidemiological studies should be done to assess their carcinogenic potential in humans. Additionally, cellular biology approaches should be used to elucidate the mechanisms of the antimicrobial activity and genotoxicities of nitro prodrugs. This will aid medicinal chemistry efforts that will develop potent antitubercular nitro molecules that have little to no mutagenic activity. To see the possible fruit of this approach, it is important to discuss the historical evolution of CGI-17341 from a mutagenic pariah to the only two nitro-containing drugs that are currently used for TB treatment – pretomanid and delamanid.

CGI-17341 is arguably the most consequential nitroimidazole molecule discovered at the early stages of modern TB drug research[98]. This compound was found to be active against multi-drug resistant Mtb strains and had an *in vitro* potency comparable to those of isoniazid and rifampicin. *In vivo* studies showed the compound to increase the survival rate of Mtb-infected mice[98]. Unfortunately, drug discovery efforts towards CGI-17341 and indeed for most nitro compounds were rightly approached with skepticism early on due to the potential mutagenicity of the compounds. A significant breakthrough in the potential use of nitroimidazoles in TB therapy came from the report of Stover *et al.* who profiled more than 300 CGI-17341 analogs for their antitubercular activity and mutagenic properties[40]. These analogs have substantial modifications at the carbon-3 position of the parent structure. More than 100 compounds from this series exhibited significant antitubercular activity while showing no detectable mutagenic effect in the test system. A structure-activity relationship analysis showed that the stereochemistry at the carbon-3 position played essential roles in the antitubercular activity of the molecules, with the R enantiomers generally showing reduced activity compared to the S enantiomers. Among the numerous substitutions made at the carbon-3 position, the lipophilic modifications showed higher

potencies, probably because of increased permeability and diffusion across the lipid-rich envelope of mycobacteria. The lead compound from this series was PA-824 and is generically known as pretomanid. Pretomanid has undergone clinical trials and further pharmacological characterizations and is currently approved as part of a TB drug regimen in different countries. Another compound that has some structural similarity to CGI-17341 but lacks mutagenetic effect and has made it to the clinic is OPC-67683[4, 9]. It is marketed in different parts of the world as delamanid.

Nitro prodrugs and mycobacterial resistance

Unlike most pathogens, mycobacterial drug resistance is driven primarily by chromosomal mutations instead of the acquisition of extra-chromosomal entities such as plasmids and transposons. These chromosomal mutations can have a multiplicative effect especially when they occur early during infection or treatment, producing many drug-resistant clones[99]. Drug resistance remains a huge problem in the TB drug discovery field, and nitro-containing compounds are not spared from the menace.

As emphasized throughout this chapter, most nitro-containing antimycobacterial compounds are prodrugs that require a nitroreductase in order to be activated into a form that inhibits the growth of the bacteria. These nitroreductases depend on a reduced cofactor to exert their reductive activation on the compound. Therefore, the pathogen can easily acquire resistance to the antimycobacterial nitro prodrug from mutations of either the nitroreductase, the biosynthetic machinery of the cofactor, or the dehydrogenase that produces the reduced form of the cofactor. For instance, mycobacterial resistance to pretomanid and delamanid is driven by mutations in any of the genes involved in cofactor F_{420} synthesis, or *fgd*, or *ddn*[1, 3, 4, 6, 8, 15, 17, 35, 40]. Not surprisingly, the *in vitro* frequency of resistance for either of the two compounds is relatively high to moderate (10^{-5} to 10^{-7}) [6, 8, 35, 40]. This is similar to what is obtainable for isoniazid (10^5 to 10^{-6}) [8, 40], a first-line TB prodrug that requires the activating activity of a catalase-peroxidase, KatG. Predictably, a

slightly lower frequency of resistance (10^{-6} to 10^{-8}) is reported for nitro-containing compounds that have more than one activating nitroreductase[9, 15]. Add to this, most of the genes involved in the activation of the nitro prodrugs are classically considered to be non-essential under normal laboratory conditions. That is, the bacteria can lose these genes and acquire resistance to the nitro compounds without suffering from fitness defect in standard growth conditions.   An exception to this rule is DprE1, a nitroreductase that is also an essential protein involved in mycobacterial cell wall biosynthesis. Most resistance to nitro-containing DprE1 inhibitors is driven by point mutations in C387. Therefore, these DprE1 mechanism-based inhibitors have a frequency of resistance that goes as low as 10^{-9}, although it must be pointed out that some of this resistance may also be driven by drug efflux pumps. Remarkably, the frequency of resistance to DprE1 inhibitors is generally lower than what has been reported for rifampicin (10^{-6} to 10^{-7})[8, 16], a first-line TB drug whose resistance is primarily driven by mutations in its target, the β-subunit of bacterial RNA polymerase[100]. These resistance mutations can occur in different parts of the polymerase[100], while resistance to the covalent DprE1 inhibitors occurs mostly in one residue – C387. This raises the question of what drives the mutation-proneness of an essential gene and if those genetic changes have an associated pleiotropic effect on the bacteria in terms of long-term fitness and transmissibility.

One of the ways to tackle the issue of resistance to nitro-containing compounds is to use a structure-guided approach to design analogs that either use an alternative activation system or compounds that do not require any activation. Little is known about this approach for nitro prodrugs; however, serendipity has led to the discovery of non-nitro InhA inhibitors that acts in a KatG-independent manner[101]. In chapter five of this dissertation, I also report our fortuitous discovery of some isoniazid analogs that retain some of their activity against a *Tn:katG*. Taken together, this highlights the possibility of discovering nitro compounds that do not require any bacterial enzyme-dependent activation. Also, nitroreductases normally interact with their nitro

prodrug substrates, and mutations in the interacting residues can guide the synthesis of analogs that are less susceptible to these mutations.

In terms of combination regimens, a bedrock of TB chemotherapy, there is a silver lining with mutations that drive resistance to nitro-containing compounds. As highlighted throughout this chapter, the native activity of most nitroreductases enables the pathogen to survive harsh conditions such as oxidative stress. Therefore, it stands to reason that the genetic disruptions of these nitroreductases or the biosynthesis machinery for the cofactors will make the pathogen to be more susceptible to the stress agent. For instance, F_{420}-deficient or *fgd* mutants are known to be hypersusceptible to oxidative stress[18, 21]. Of note is that F_{420}-deficient mutants are also hypersensitive to oxidative stress-elevating drugs such as isoniazid, moxifloxacin, and clofazimine[18], highlighting the concept of collateral sensitivity. Hence, these drugs can be used in combination with F_{420}-dependent compounds for TB treatment. This will ensure that resistance to these F_{420}-dependent compounds that are conferred by the disruptions in the biosynthesis of F_{420}, reduction, or recycling will come with a collateral cost in terms of increased susceptibility to these drugs. A model can be proposed for the increased susceptibility of F_{420}-deficient mutants to isoniazid. Mtb uses NADH and $F_{420}H_2$ to reduce oxidizing agents, producing NAD and F_{420}. When $F_{420}H_2$ is no longer there to partake in the reduction, NADH is overburdened with this reaction, perturbing the cellular NADH/NAD ratio[18]. This high concentration of NAD is conducive for the formation of the isoniazid-NAD adduct, a complex that is required for the mycobactericidal activity of the drug. While this model was proposed for isoniazid and F_{420}-deficient mutants, it may also be applicable to drugs such as ethionamide that forms an NAD adduct. It may also be applicable to nitroreductases that require different cofactors such as mycothiol, NADPH, or $FADH_2$ since these cofactors are part of the machinery that the pathogen uses against oxidative stress.

Also, the hypersusceptibility of the nitroreductase mutants to oxidative stress provides a therapeutic opening to design drugs that may prevent the reactivation of latent TB[37]. Latent TB is

characterized by hypoxic granuloma, a protective lesion of immune cells, that prevents the growth and extra-pulmonary dissemination of Mtb in an infected host. When Mtb is emerging from hypoxia-induced dormancy, the sudden introduction of oxygen potentially leads to the formation of toxic oxygen radicals[18]. These radicals need to be curtailed by the oxidative stress defense system of the bacteria, and that includes most nitroreductases. In fact, F_{420}-deficient Mtb and *ddn* mutants are known to be growth-defective when emerging from hypoxia-induced dormancy[17, 18]. One of the genes involved in F_{420} biosynthesis, *fbiC*, and *ddn* were found to be upregulated during hypoxia and re-aeration, respectively, speaking to the possible function of the system in either anaerobic energy generation or oxidative stress response[18]. Therefore, mechanism-based inhibitors that have nitroreductases as both their activating enzymes and targets can be designed to target the reemergence of the pathogen from dormancy.

Drug delivery of nitro prodrugs

Like most drugs, nitro-containing compounds are subject to hepatic first-pass metabolism where the pharmacophoric nitro group can be modified into inactive amines or other metabolites that are excreted. This leads to sub-optimal concentrations of the drugs in different tissues of the body. Hence, a big challenge for TB chemotherapy is the specific delivery of the drugs to the region of the body where they are mostly needed – the lungs. Apart from reducing the side-effects associated with the parenteral or oral administration of the drugs, this approach should potentially increase the therapeutic efficacy of the drugs[102]. Indeed, pulmonary delivery approaches have shown promising results for some TB drugs including nitro-containing compounds such as pretomanid, delamanid, and BTZ043[102-107]. However, this technology is still in its infancy especially for TB chemotherapy, and questions remain about its commercial scalability and deployment to different parts of the world. Since oral drug delivery remains the preferred administration route, more efforts can be made towards improving the pharmaceutics of TB drugs. This may be in terms of formulating them with exotic excipients that increase their oral

bioavailability and volume of distribution, necessitating their penetration into the lungs, granuloma and other tissues where they kill the pathogen.

Concluding Remarks:

In this chapter, I have provided an overview of different nitroreductases involved in the activation of nitro prodrugs and have placed emphasis on the mechanistic basis of these activities. Additionally, I have also highlighted the physiological activities of these nitroreductases in mycobacteria and have shown that most of them are part of the defense system of the bacteria against stressful environments. These include nitroreductases such as Ddn, Rv2466c, Rv3368c, and Rv3131, and most of these enzymes are non-essential under normal laboratory conditions. DprE1 is the only essential nitroreductase that has been reported so far in literature and it is involved in the biosynthesis of the mycobacterial cell envelope. Nitro-containing inhibitors against DprE1 work through a mechanism-based system, where DprE1 serves as both the activator and the target. In the latter parts of this dissertation, I will discuss new compounds that target DprE1 as well as compounds that depend on the mycobacterial cofactor F_{420} activation machinery.

In chapter two, I first describe the discovery and initial characterization of novel nitro-containing compounds and provide findings underlying their mechanisms-of-action in Mtb. In chapter three, I followed up with some of the compounds that had activity against *M. abscessus* and defined the basis for their activity against the pathogen. In chapter four, I present findings on a novel scaffold that targets DprE1 and showed that it has *in vivo* efficacy in a murine model of TB. In chapter five, I used a targeted mutant study and cheminformatics to explore the activity of some hits, including nitro-containing compounds, that we got from our initial high throughput screen. Together, this dissertation defines new chemical matter that can be developed into new anti-*M. abscessus* or TB therapeutics and has uncovered new insights into the biology of these mycobacterial species in response to these novel chemotypes.

CHAPTER TWO: Discovery and characterization of antimycobacterial nitro-containing compounds with distinct mechanisms of action and *in vivo* efficacy

Works presented in this chapter have been previously published as:

Author contributions for the study:

I.E.E., J.T.W., and R.B.A. conceived and designed the studies. J.T.W. conducted prioritization studies of MLSMR primary hits (including EC_{50}, cytotoxicity studies, and activity against Mtb in macrophages). **I.E.E.** conducted the remaining *in vitro* and genetic characterization studies. **I.E.E.,** E.R.H., V.J.A., and H.M.M. conducted the *in vivo* efficacy study. B.J.A. generated the Msm-resistant mutants. **I.E.E.** and R.B.A. wrote the manuscript. All authors reviewed the manuscript.

Abstract:

Nitro-containing compounds have emerged as important agents in the control of tuberculosis (**TB**). From a whole cell high-throughput screen for *Mycobacterium tuberculosis* (**Mtb**) growth inhibitors, ten nitro-containing compounds were prioritized for characterization and mechanism of action studies. HC2209, HC2210, and HC2211 are nitrofuran-based prodrugs that need the cofactor F_{420} machinery for activation. Unlike pretomanid which depends only on deazaflavin-dependent nitroreductase (**Ddn**), these nitrofurans depend on Ddn and possibly another F_{420}-dependent reductase for activation. These nitrofurans also differ from pretomanid in their potent activity against *Mycobacterium abscessus*. Four dinitrobenzamides (HC2217, HC2226, HC2238, and HC2239) and a nitrofuran (HC2250) are proposed to be inhibitors of decaprenyl-phosphoryl-ribose 2'-epimerase 1 (**DprE1**), based on isolation of resistant mutations in *dprE1*. Unlike other DprE1 inhibitors, HC2250 was found to be potent against non-replicating persistent bacteria, suggesting additional targets. Two of the compounds, HC2233 and HC2234, were found to have potent, sterilizing activity against replicating and non-replicating Mtb *in vitro*, but a proposed mechanism of action could not be defined. In a pilot *in vivo* efficacy study, HC2210 was orally bioavailable and efficacious in reducing bacterial load by ~1 log in a chronic murine TB infection model.

Introduction:

The high prevalence of tuberculosis (**TB**), coupled with growing antibiotic resistance, highlights the need to develop new TB drugs [108]. With the recent approval of pretomanid and delamanid for TB treatment [9, 109], nitro-containing compounds have emerged as important agents to control TB. Pretomanid and delamanid are classified as nitroimidazoles. Other antitubercular nitro-containing chemical scaffolds include benzothiazinones, dinitrobenzamides, nitrobenzamides, and nitrofurans, among others [9, 50, 110]. Some compounds from these series such as PBTZ-169 and BTZ-043 have been shown to be efficacious in clinical trials for TB treatment [109].

Pretomanid and delamanid kill *Mycobacterium tuberculosis* (**Mtb**) by targeting essential cellular processes such as respiration or cell wall biogenesis and are effective against nonreplicating Mtb [1, 5, 7, 40, 92, 111]. They are prodrugs and require reductive activation by the mycobacterial-specific deazaflavin-dependent nitroreductase (**Ddn**) [1, 6, 8]. Their prodrug status enables them to specifically inhibit the growth of the infecting Mtb while limiting dysbiotic effect on the host microbiome. Despite their promising use for TB treatment, pretomanid and delamanid have some limitations. There are reports of Mtb isolates that are naturally resistant to either drug due to genetic polymorphism in Ddn or other genes in the F_{420} biosynthesis pathway, and the F_{420}-dependent glucose-6-phosphate dehydrogenase-1 (***fgd***). [3, 17]. Fgd mediates one of the earliest steps in the pentose phosphate pathway of mycobacteria. It uses F_{420}, instead of the canonical NAD(P), in catalyzing its reaction. In this process, F_{420} is reduced and can be used by Ddn in the activation of pretomanid or delamanid [1, 2, 6-8, 35]. Clinical strains that have developed resistance to either pretomanid or delamanid have been isolated in different parts of the world [17, 111]. The pharmacokinetic profile and side effects of the compounds can make them less ideal for certain patients. Delamanid has a relatively poor oral bioavailability and can have a modest effect on QT

prolongation [9, 111, 112]. Due to these challenges, there are ongoing efforts to develop new antitubercular nitro-containing compounds with improved properties.

Our lab previously conducted a whole cell high-throughput screen of the ~340,000 compound Molecular Libraries Small Molecular Repository (**MLSMR**) for inhibitors of the DosRST two-component regulatory system[113]. From this primary HTS, we identified compounds that inhibited Mtb growth independent of the targeted pathway. We noted many of these growth inhibiting compounds contained a nitro group as a presumptive pharmacophore. The goal of this study is to decipher the possible mechanisms of action of 10 nitro-containing compounds that inhibit mycobacterial growth and prioritize analogs for continued development. Here, we provide a genetic basis for the antimycobacterial activities of the compounds. We show that, like pretomanid and delamanid, several of the nitrofurans depend on cofactor F_{420}-dependent enzymes for activation. Unlike the nitroimidazoles that depend only on Ddn, these nitrofurans partially depend on Ddn and possibly a second, unknown F_{420}-dependent enzyme for activation. Additionally, we show that the nitrofurans are active against *Mycobacterium abscessus* (**Mab**), whereas pretomanid had limited inhibition of Mab growth. Other nitro-containing compounds, including dinitrobenzamides and a nitrofuran in this study, are proposed to target decaprenyl-phosphoryl-ribose 2'-epimerase 1 (**DprE1**), an essential protein involved in cell wall biogenesis. These putative DprE1 inhibitors were active against both Mtb and *Mycobacterium smegmatis* (**Msm**). Lastly, we demonstrate that a novel nitrofuran-piperazine-nitrophenol compound, HC2210, is effective, when delivered orally, in a chronic murine Mtb infection model.

Results:

New nitro-containing compounds have potent antitubercular activities

As part of our efforts towards developing a mechanistic understanding for the antimycobacterial activity of the small molecules discovered from the previous high-throughput screen of the MLSMR, we selected 10 nitro-containing compounds (**Figure 2.1**) and characterized their mechanisms of action. Six of these compounds are nitrofurans and they include **HC2209** (1-(4-fluorophenyl)-4-[(5-nitro-2-furyl)methyl]piperazine), **HC2210** (1-[(5-nitro-2-furyl)methyl]-4-(4-nitrophenyl)piperazine oxalate), **HC2211** (1-[(5-nitro-2-furyl)methyl]-4-phenylpiperazine), **HC2233** (N-{4-[4-(2-methylpropanoyl)piperazin-1-yl]phenyl}-5-nitrofuran-2-carboxamide), **HC2234** (N-{4-[4-(2,2-dimethylpropanoyl)piperazin-1-yl]phenyl}-5-nitrofuran-2-carboxamide), and **HC2250** (N'-[(E)-(5-nitrofuran-2-yl)methylidene]-2-phenoxyacetohydrazide). Previously, nitrofuran piperazine and nitrofuran triazine compounds have been reported as Mtb growth inhibitors [9, 114]. The other four compounds, with their nitro groups attached to a parent benzene ring, are dinitrobenzamides and they include **HC2217** (N-(2-morpholin-4-yl-2-thiophen-2-ylethyl)-3,5-dinitrobenzamide), **HC2226** (N-(cyclopropylmethyl)-3,5-dinitrobenzamide), **HC2238** (N-[(4-fluorophenyl)methyl]-4-methyl-3,5-dinitrobenzamide), and **HC2239** (N-[2-(3-methoxyphenoxy)ethyl]-3,5-dinitrobenzamide). Notably, related dinitrobenzamide compounds have previously been described as DprE inhibitors [45, 50, 109].
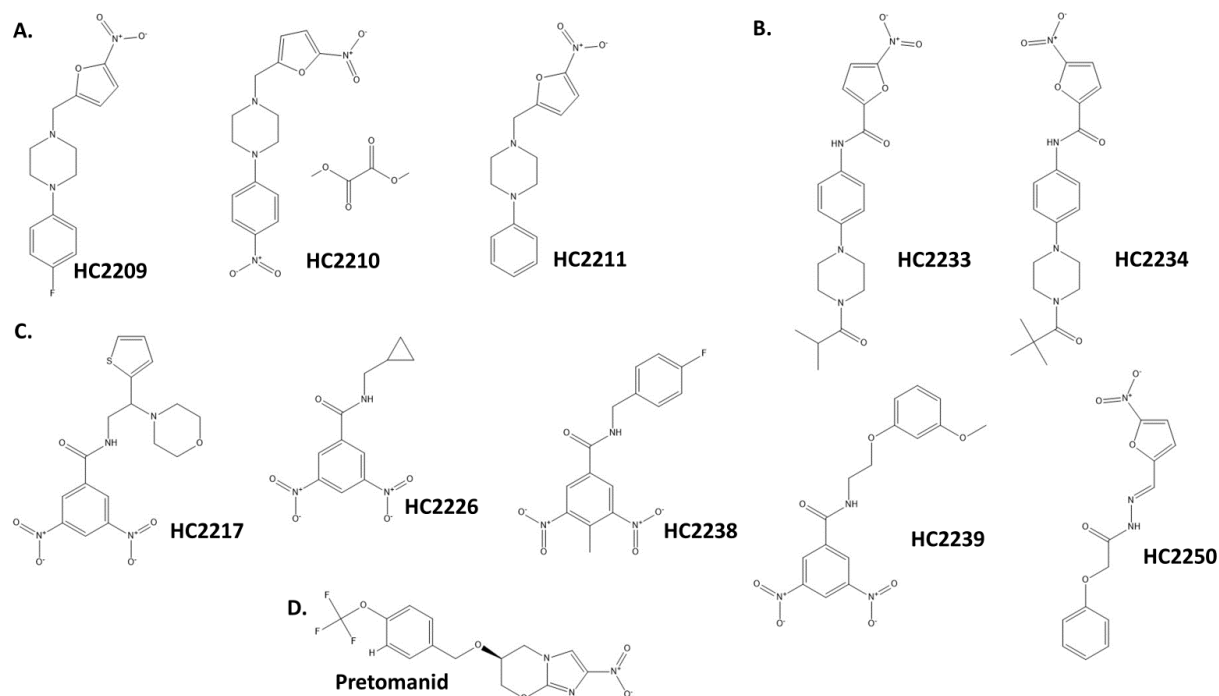
Figure 2.1. Nitro-containing compounds that inhibit Mtb growth. A. Fgd-dependent nitrofurans. **B.** Fgd-independent nitrofurans. **C.** Dinitrobenzamides that are putative DrpE inhibitors. **D.** Pretomanid, a nitro-containing FDA approved TB drug.

An *in vitro* dose-response study against Mtb show all the compounds are relatively potent with half-maximal effective concentrations (EC_{50}) ranging from 0.05 µM to 6.86 µM (**Figure 2.2, Table 2.1**). Of particular interest is HC2210, a nitrofuran-piperazine-nitrophenol compound that has an EC_{50} of 50 nM. By comparison, in this assay, HC2210 is >2X more potent than isoniazid (EC_{50} = 140 nM), and 12X more potent than pretomanid (EC_{50} = 620 nM). During infection, Mtb can replicate inside macrophages, therefore we tested compound activity against intracellular Mtb and for cytotoxicity against murine bone marrow-derived macrophages. In a dose-response study, all the nitro-containing compounds exhibited high potency against intracellular Mtb and had limited eukaryotic cytotoxicity (**Table 2.1**). These data demonstrate that the compounds can selectively inhibit intracellular Mtb with no or limited cytotoxicity on macrophages.
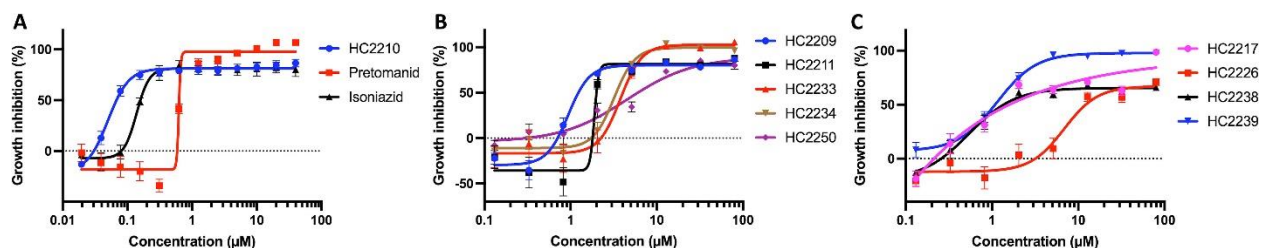
Figure 2.2. **Nitro-containing compounds inhibit Mtb growth in a dose-dependent manner.**
A. Dose response curves for HC2210 inhibition of Mtb growth relative to pretomanid and isoniazid.
B. Dose response curves for other nitrofurans. **C.** Dose response curves for the dinitrobenzamides. The dotted line represents the growth inhibition of the negative control (DMSO). The error bars represent the standard deviations of two to three biological replicates. All experiments were independently conducted at least twice with similar results.

Table 2.1. Potency of nitro-containing compounds against Mycobacterial and non-mycobacterial species

Compds	In vitro EC$_{50}$ (µM) of compounds								Ex vivo EC$_{50}$ (µM)	CC$_{50}$ (µM)
	Mtb	**Msm**	**Mab**	**Eco**	**Pae**	**Staph**	**Efae**	**Pvul**		
HC2209	0.94	>200	<5.12	>200	>200	>200	>200	>200	<0.13	>80
HC2210	0.05	>200	<0.82	56.83	>200	>200	>200	>200	<0.13	>32
HC2211	1.89	>200	2.81	>200	>200	>200	>200	>200	<0.33	>80
HC2217	<2.05	<2.05	>200	>200	>200	>200	>200	>200	<0.13	>80
HC2226	6.86	<32	>80	>200	>200	>200	>200	>200	<0.83	>80
HC2233	3.78	>200	<80	>200	>200	>200	>200	>200	<0.33	>80
HC2234	3.20	>200	<32	>200	>200	>200	>200	>200	<32	>80
HC2238	0.54	1.25	>80	>200	>200	>200	>200	>200	<0.13	>80
HC2239	1.15	0.63	>80	>200	>200	>200	>200	>200	<0.13	>80
HC2250	4.52	<5.12	>80	>200	>200	>200	>200	25.48	<0.33	>80
PA824	0.62	>80	<80	>200	>200	>200	>200	>200	ND	ND
Isoniazid	0.14	39.88	ND	ND	ND	ND	ND	ND	ND	ND
ETH	10.41	<0.82	ND	ND	ND	ND	ND	ND	ND	ND

ND = not determined; Mtb = *Mycobacterium tuberculosis*; Msm = *Mycobacterium smegmatis*; Mab = *Mycobacterium abscessus*; Eco = *Escherichia coli*; Pae = *Pseudomonas aeruginosa*; Staph = *Staphylococcus aureus*; Efae = *Enterobacter faecalis*; Pvul = *Proteus vulgaris*; *Ex vivo* EC$_{50}$ (µM) = EC$_{50}$ of compounds against intracellular Mtb in bone marrow-derived macrophages; and CC$_{50}$ (µM) = macrophage cytotoxicity. Compds = compounds; PA824 = pretomanid; ETH = ethambutol.

Next, we sought to determine whether the compounds were bactericidal or bacteriostatic against Mtb. For most antibiotics, it is important to note that this classification system depends on the dose and time allowed for treatment [115, 116]. Treatment of Mtb with HC2210, pretomanid and isoniazid showed the compounds are bactericidal at the tested concentrations (**Figure 2.3A**). Three other nitrofurans in this study (HC2233, HC2234, and HC2250) were also bactericidal at the tested concentrations and time points, with 50 µM of HC2233 or HC2234 completely sterilizing the culture after 4 or 10 days of treatment, respectively **(Figure 2.3B)**. For the dinitrobenzamides, we tested HC2217, HC2226, and HC2238. At 4 days of incubation, all the compounds exhibited bactericidal activity even at the lowest test concentrations (**Figure 2.3C**). We noticed interesting differences at 10 days of incubation. While HC2238 continued to kill the pathogen at 10 days of incubation, HC2217 and HC2226 start to lose their bactericidal activity at this time point. In fact, the two test concentrations of HC2217 completely lose their bactericidal profile at this time point. While we do not know the exact cause of this lost activity, we presume that it may be due to instability of the compounds.
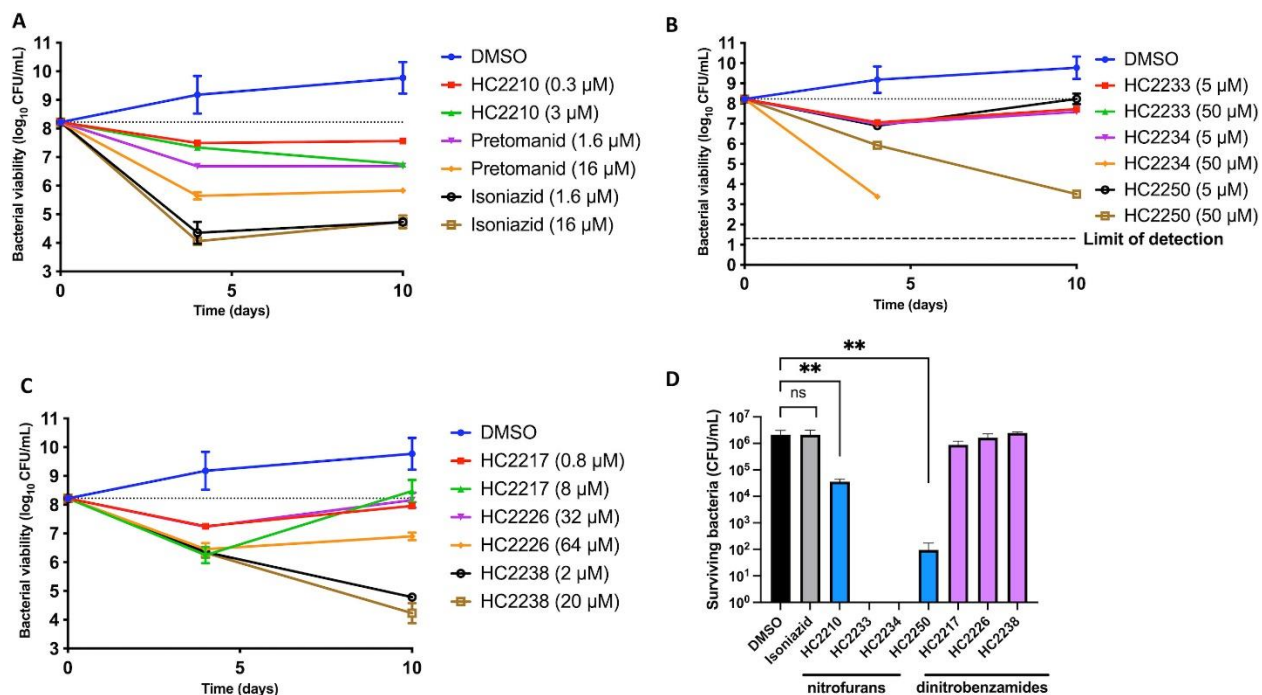
Figure 2.3. *In vitro* time and concentration dependent killing of Mtb. A. Comparing the bactericidal activity of HC2210 with those of pretomanid and isoniazid shows that it is weakly bactericidal. **B.** The other tested nitrofurans killed Mtb in a dose- and time-dependent manner. For both time points, HC2233 completely sterilized the culture at 50 μM. Hence, the line is not shown in the graph. After 10 days of treatment, 50 μM of HC2234 completely sterilized the culture below the limit of detection. Hence, the graph line ended at 4 days. **C.** The time- and dose-dependent killing of Mtb by the tested dinitrobenzamides. **D.** The bactericidal activity of the compounds against non-replicating Mtb in a hypoxic shift-down assay. The upper black dotted lines in **A**, **B**, and **C** represent the starting cell concentration of 1.7×10^8 CFU/mL. The limit of detection in this assay is ~20 CFU. The errors bars represent the standard deviations of two technical replicates for **A-C** or two biological replicates for **D**. Asterisks denote statistically significant differences between the compared groups in an unpaired Student's t-test (**p value $\leq$ 0.01). ns = statistically nonsignificant with p value > 0.05.

HC2210, HC2233, HC2234, and HC2250 are active against non-replicating Mtb

In response to different environmental signals such as hypoxia during infection, Mtb can transition into a non-replicating persistent (NRP) state that is non-responsive to many antibiotics [117, 118]. One of the goals of modern TB chemotherapy is to develop drugs that can kill Mtb in this dormant state [113, 119]. Using a hypoxic shiftdown assay [120], we investigated the effect of the nitro-containing compounds on the survival of NRP Mtb. All the tested dinitrobenzamides (HC2217,

HC2226, HC2238) had no impact on viability of the pathogen relative to the DMSO-vehicle control (**Figure 2.3D**). Isoniazid, a cell wall inhibitor, was used as a control in this assay and was inactive against NRP bacteria. In contrast, all the tested nitrofuran compounds (HC2210, HC2233, HC2234, HC2250) significantly reduced the viability of the NRP bacteria relative to the control, with HC2233 and HC2234 again showing sterilizing activity, suggesting that these compounds may be inhibiting essential cellular activities during Mtb dormancy.

HC2209, HC2210, and HC2211 are cofactor F$_{420}$-dependent nitrofurans

Due to the presence of one or more nitro groups in these compounds, we reasoned that, like other nitro containing compounds, they might be prodrugs that need mycobacterial proteins for activation. Isolation of resistant mutants has previously been used to identify activating enzymes [6, 9, 45, 51]. Spontaneous mutants resistant to HC2210 were isolated on media supplemented with either 0.1 µM or 0.3 µM HC2210 with a frequency of 1.6×10^{-6}, similar to what we observed for pretomanid (1.8×10^{-6}).

Ten resistant colonies from each plate were isolated and confirmed for resistance against HC2210 (**Figure A.2.1; Figure 2.4**). Notably, two resistance patterns were observed from the dose-response curves, 1) partial resistance with an EC$_{50}$ of 5 µM, and 2) total resistance at all concentrations tested. The partially resistant mutants were isolated from both the 0.1 µM and 0.3 µM HC2210 selection plates, while the fully resistant clones were only observed in the 0.3 µM selection plate. The absence of fully resistant clones from the 0.1 µM HC2210 plate may be due to a lower selective pressure to evolve full resistance to the compound.
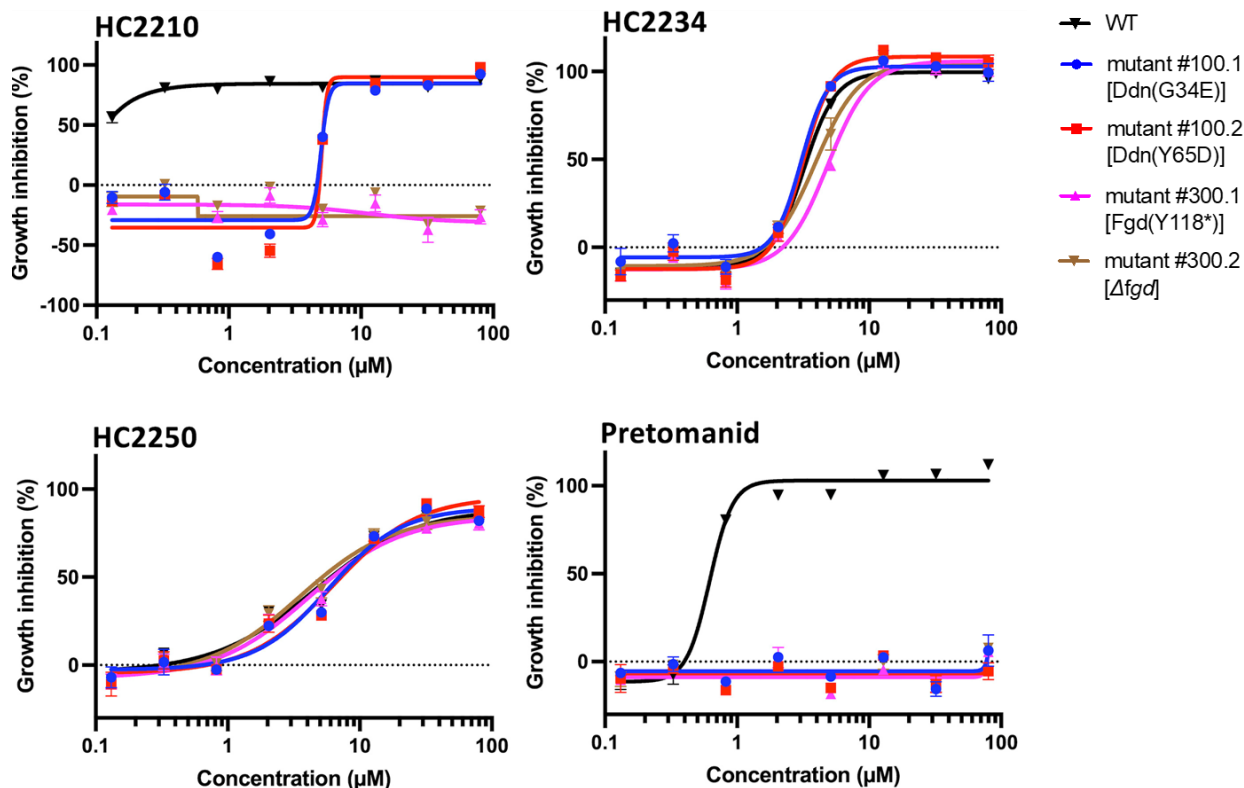
Figure 2.4. Resistance of the *ddn* and *fgd* spontaneous mutants against the tested nitrofurans and pretomanid. *fgd* mutants provide full resistance and *ddn* mutants provide partial resistance against HC2210. Pretomanid entirely loses its activity in the tested *fgd* and *ddn* mutants. *fgd* and *ddn* mutants did not provide resistance to HC2234 or HC2250. The dotted lines represent the growth inhibition of the negative control (DMSO). The error bars represent the standard deviations of three biological replicates. All experiments were independently repeated three times with similar results.

To ascertain mutations that cause these resistance patterns, we sequenced the genomes of the isolated resistant mutants. For the fully resistant clones, we identified nonsense, insertion, and deletion mutations of *fgd*, while the partially resistant clones harbored missense mutations or deletion in *ddn* (**Table 2.2**). Since we selected mutants in these genes, we hypothesized that HC2210 shares a related activation mechanism with pretomanid and delamanid. Notably, partial resistance of the *ddn* mutants for HC2210 suggests that a second nitroreductase may be required for its activation, as was previously observed for nitro-containing triazines [9]. As expected, cross-

resistance screening of two *fgd* spontaneous mutants against pretomanid showed a full loss of activity of the drug (**Figure 2.4**). The *ddn* spontaneous mutants also showed full resistance to high concentrations of pretomanid, further highlighting the role of the nitroreductase in the activation of the compound. Cross-resistance profiling of the spontaneous mutants also showed HC2209 and HC2211 to be dependent on Fgd and Ddn for activation (**Figure A.2.2**), with *fgd* mutants providing full resistance and the *ddn* mutants providing partial resistance.

Table 2.2. Mutations of *ddn* and *fgd* in resistant clones

Resistance	Mutant strain #	SNP location (nt)	Gene	Nucleotide Change	Amino acid substitution
Partial	100.1	3,967,990	*ddn*	GGG→GAG	G34E
	100.2	3,968,082	*ddn*	TAC→GAC	Y65D
	100.3	3,966,767	*[fadA5], ddn [ERDMAN_3893]*	Δ2,315 bp	
	100.4	3,967,990	*ddn*	GGG→GAG	G34E
Full	300.1	492,852	*fgd*	TAC→TAA	Y118*
	300.2	490,918	*[pks6], fgd, [pta]*	Δ2,760 bp	
	300.3	492,727	*fgd*	$(C)_{5\rightarrow6}$	coding (231/1011 nt)
	300.5	493,331	*fgd*	CAG→TAG	Q279*

The three other nitrofurans in this study (HC2233, HC2234, and HC2250) retained their full potency against the *fgd* and *ddn* spontaneous mutants (**Figure 2.4; Figure A.2.2**). This suggests that they do not depend on the F_{420} machinery for their activity. The same can be said for all the dinitrobenzamides since they did not show any change in their potency against the spontaneous mutants (**Figure A.2.3**), consistent with their presumed target of DprE. Overall, HC2209, HC2210, and HC2211 are the only compounds in this study that depended on the F_{420} bioreductive activation system.

Mutations in *dprE* confer resistance to the nitrofuran HC2250 and dinitrobenzamides

Dinitrobenzamides are known DprE1 inhibitors [45, 50, 109, 121]. To determine if the compounds are potential DprE1 inhibitors, we isolated resistant mutants to HC2238 and confirmed their resistance in a dose-response study (**Figure A.2.4**; **Figure 2.5**). Whole genome sequencing identified the mutants harbored single nucleotide variants leading to a C384S substitution in DprE1. DprE1 is a conserved protein that catalyzes an essential epimerization step during the synthesis of mycobacterial arabinogalactan [45, 122-124]. Cross-resistance profiling of the mutants against other dinitrobenzamides in this study further confirmed that they share the same likely target (**Figure 2.5; Figure A.2.4**). As expected, the mutants did not show any cross-resistance against a common cell wall inhibitor such as ethambutol (**Figure A.2.4**), indicating that they target different proteins in the cell wall biogenesis pathway.
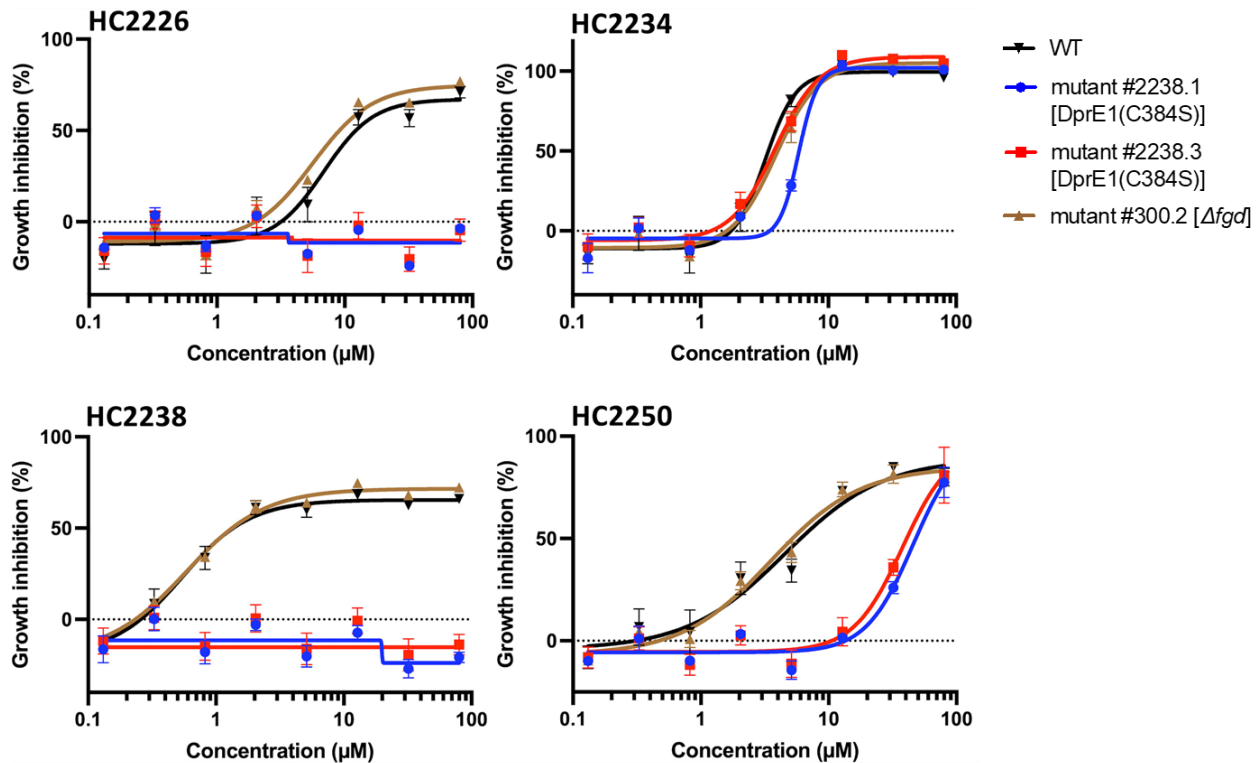
Figure 2.5. Resistance to dinitrobenzamides and HC2250 in *dprE1* mutants. HC2238 and HC2226 lose activity against the spontaneous *dprE1* mutants, while partial resistance is observed towards HC2250. HC2234 is active against the tested *dprE* mutant. The dotted lines represent the growth inhibition of the negative control (DMSO). The *fgd* mutant is included as a control showing the compounds are independent of the F_{420}-dependent activation. The error bars represent the standard deviations of three biological replicates. All experiments were independently conducted two times with similar results.

Since HC2233, HC2234, and HC2250 remained the only compounds in this study whose mechanism of action remained unknown, we attempted to select resistant mutants on agar plates amended with the respective compounds at various concentrations. However, these efforts were unsuccessful. We also examined their inhibitory activity against the *dprE1* mutants. HC2233 and HC2234 retained their full potency against the mutants, indicating that they likely do not target DprE1 or that other mutations are required for resistance (**Figure 2.5**; **Figure A.2.4**). HC2250 had reduced potency in these mutants, indicating that it might be a DprE1 inhibitor (**Figure 2.5**).

Recently, Batt *et al*. showed that nitrofurans can also target DprE [59]. Together, these findings support the potential for developing nitrofuran scaffolds as DprE1 inhibitors.

All the nitro-containing compounds have a narrow spectrum of activity

Several of the nitro compounds need a mycobacterial-specific target or system for activation, therefore, we hypothesized they would have a narrow spectrum of activity. To test this hypothesis, we carried out a dose-response study of the compounds against *Escherichia coli*, *Pseudomonas aeruginosa*, *Proteus vulgaris*, *Enterobacter faecalis*, and *Staphylococcus aureus*. We also used pretomanid as a control. As expected, pretomanid did not affect any of the test organisms, indicating a narrow spectrum of activity (**Table 2.1**). Similarly, the nitro-containing compounds had a narrow spectrum of activity displaying little or no effect on the tested pathogens not belonging to the genus *Mycobacterium* (**Table 2.1**).

HC2209, HC2210, and HC2211 are active against *M. abscessus*

The inhibitory activity of the prioritized compounds was next tested against the mycobacterial species*, M. smegmatis* (Msm) and *M. abscessus* (Mab). These organisms retain some degree of genome homology with Mtb, suggesting that the compounds may also inhibit these mycobacterial species. Interestingly, we observed different inhibitory profiles for the nitro-containing scaffolds with respect to the test species.

Pretomanid and the F_{420}-dependent nitrofurans had no inhibitory effects on Msm (**Table 2.1**). This agrees with previous reports on the loss of activity of pretomanid against Msm [17, 39, 125]. However, when tested against Mab, the F_{420}-dependent nitrofurans diverged from pretomanid (**Table 2.1, Figure A.2.5**). While pretomanid did not inhibit the pathogen even at high concentrations, the F_{420}-dependent nitrofurans showed potency against the pathogen (EC_{50} = 0.81 – 5 µM) that is better or comparable to amikacin (EC_{50} = 5.4 µM). Studies are currently underway to decipher the mechanisms of action of these nitrofurans against Mab.

While the putative DprE1 inhibitors (HC2217, HC2226, HC2238, HC2239, and HC2250) retain their activity against Msm, they lose their activity against Mab (**Table 2.1**). Indeed, the isolation and whole-genome sequencing of Msm-resistant mutants further confirmed the compounds are likely DprE1 inhibitors in Msm (**Figures A.2.6 and A.2.7, Supplemental Data 2.1**). From the genome sequence analysis, we also observed that mutations in the regulator, MSMEG_6503, caused resistance against the tested putative DprE inhibitors. This corroborates previous studies that show mutations in *MSMEG_6503* lead to the overexpression of a nearby nitroreductase, NfnB, in Msm [44, 45]. NfnB can subsequently inactivate the exposed nitro groups of the compounds, reducing their potency. The Msm-resistant mutants retained their susceptibility to other cell wall inhibitors such as isoniazid and ethambutol (**Figure A.2.7**), further confirming the different cellular targets of the compounds.

HC2210 is orally bioavailable and efficacious in a chronic murine Mtb infection model

Based on the promising drug-like potency of HC2210, we examined its efficacy in a murine model of chronic tuberculosis. C57Bl/6 mice were aerosol infected with Mtb Erdman and the infection was allowed to progress for 39 days before initiating treatment. For treatment, one group was treated by oral gavage with HC2210 at 75mg/kg, dosed once daily, five days a week. The other groups were either treated twice daily with rifampicin (10mg/kg) as a positive control or sham control (corn oil/DMSO). After 4 weeks of treatment, compared to the vehicle control group, HC2210 reduced the bacterial burden by 1.1-log and 1.2-log CFU in the lungs and spleens of infected mice, respectively (**Figure 2.6**). Overall, these data show HC2210 is orally bioavailable and efficacious in a mouse model of Mtb infection and support its further development.
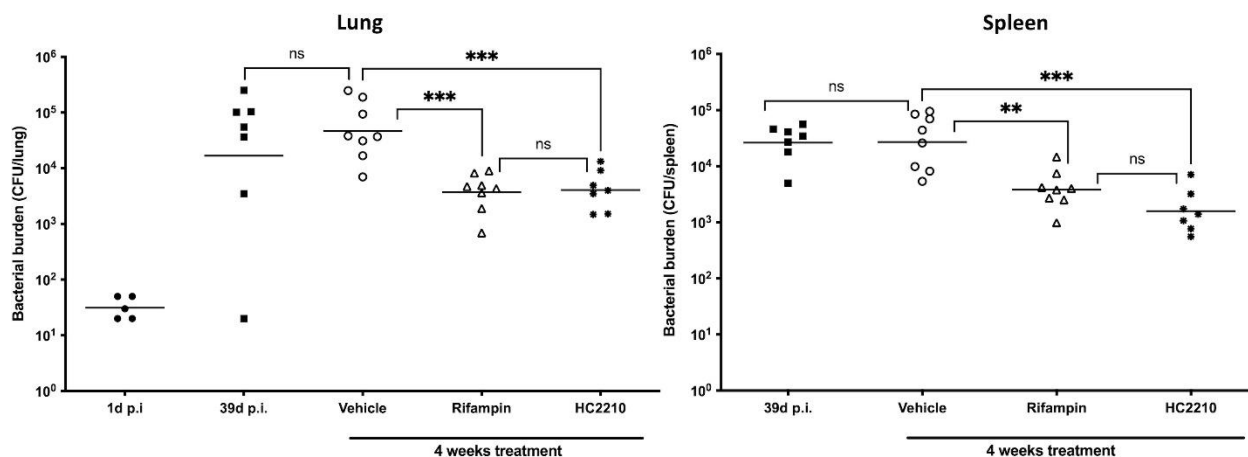
Figure 2.6. HC2210 delivered orally reduces Mtb survival in a chronic model of Mtb infection. Mycobacterial burden is reduced in the lung and spleen of infected C57Bl/6 mice following four weeks of treatment with HC2210. HC2210 treatment was performed by oral gavage once daily, 5 days a week at 75 mg/kg. Rifampin treatment was twice daily, 5 days a week at 10 mg/kg. p.i is acronym for post-infection. 1d p.i is the mycobacterial burden of the mice a day after infection. 39d p.i is the mycobacterial burden of the untreated mice 39 days post-infection, prior to treatment. The vehicle control is 95% corn oil/5% DMSO. Asterisks denote statistically significant differences between the compared groups in an unpaired Student's t-test (**p value $\leq$ 0.01; ***p value $\leq$ 0.001). ns = statistically nonsignificant with p value > 0.05.

Discussion:

The nitro-containing compounds in this study have potent antimycobacterial activities against both Mtb and Mab. Other nitrofurans or dinitrobenzamides have been previously described [9, 45, 50, 110], however, several of the tested compounds are chemically distinct, and based on their potency warranted further characterization. Using a genetic selection method, we found that nitrofurans such as HC2209, HC2210, and HC2211 depend on the *fgd* activation system for their antimicrobial activities. This system of activation is also used by pretomanid and delamanid, two clinically approved TB drugs. Fgd provides the reduced form of cofactor F_{420} that Ddn uses to activate the nitro-containing compounds into active metabolites. To date, Ddn is the only nitroreductase that has been described in the activation of pretomanid and delamanid [1, 2, 6-8, 17, 35, 40, 111]. We further confirmed this with the full loss of activity of pretomanid when tested against the *ddn* mutants in this study. Interestingly, the Fgd-dependent nitrofurans did not fully lose their

potency against the *ddn* mutants. They retained some levels of antimycobacterial activities at high concentrations (**Figure 2.4; Figure A.2.2**). This suggests the presence of other Fgd-dependent reductases (**FDORs**) that may be playing a role in the activation of the compounds. A similar observation was made by Wang *et al.* [9] for JSF-2019, another nitrofuran. Deletion of *fgd* led to a large loss in the activity of JSF-2019, while perturbation of *ddn* only led to a slight potency loss. This led the authors to suggest that Ddn is not the primary reductase for JSF-2019. In this case, we observed a large potency loss when we tested the *ddn* spontaneous mutants against the nitrofurans. We propose Ddn as the primary nitroreductase for these Fgd-dependent nitrofurans and suggest a possible role for other secondary FDORs in the activation of the compounds. Many computationally and functionally annotated FDORs exist in the literature [37, 125, 126], but only Ddn is involved in the activation of different antimycobacterial nitro compounds. Interestingly, CGI-17341, a parent nitroimidazole molecule for pretomanid and delamanid [4, 40, 98], depends on Fgd but not Ddn for activation [2, 6]. This same conclusion was made in another study that associated a full loss of antitubercular activity of some nitrofurans with spontaneous mutations in *fgd* or the F_{420} biosynthesis pathway [16]. These compounds, however, retained their efficacy against a *ddn* mutant. Taken together, these studies suggest the possibility of uncovering other clinically relevant FDORs.

The Fgd-dependent nitrofurans were also different from pretomanid in their activity against growth of Mab. While pretomanid did not have any inhibitory effect on Mab, HC2209, HC2210, and HC2211 retained their activity against the pathogen. Mab is a challenging to treat pathogen that is non-responsive to many antibiotics. The intrinsic resistance of Mab limits the chemotherapeutic strategies for treating the infection [127]. Among other factors, the intrinsic resistance of Mab may be attributed to its highly efficient efflux system. Genetic polymorphic differences may also explain the lack of activity of pretomanid against the pathogen. Indeed, phylogenetic analysis and multiple sequence alignment showed a low homology or relatedness between the Ddn in Mtb and Mab [39]. However, these reasons do not fully explain why we see

differences in the susceptibility of Mab to pretomanid and the Fgd-dependent nitrofurans described here. We suggest two hypotheses to further explain the susceptibility of Mab to these nitrofurans. Ddn of Mtb and its Mab homolog may share residues that interact with these nitrofurans but not pretomanid. This can be tested through detailed biochemical studies and co-crystallization of the compounds with the Ddn of both species. Unfortunately, researchers have been unable to isolate co-crystals of pretomanid with Ddn [1]. Only the crystal structure of Mtb Ddn has been solved, and molecular docking has been used to identify residues that interact with pretomanid [1, 2, 17, 125]. Our second hypothesis, reinforced by the partial resistance of the Mtb *ddn* mutants to the tested nitrofurans, is that Mab may be using an unknown FDOR to activate these compounds. This FDOR may be found in both species but can only activate the nitrofurans described in this study. This hypothesis can be tested by the selection of spontaneous mutants or targeted disruption of candidate FDORs in Mab and testing for resistance. This study also identified two nitrofurans – HC2233 and HC2234 – which did not depend on either Fgd or Ddn for activation and do not elicit resistance in DprE1 mutants. It is possible that these compounds may not be prodrugs and do not require a nitroreductase for activation or they are prodrugs that require unknown activation systems.

The other five nitro-containing compounds in this study (HC2217, HC2226, HC2238, HC2239, and HC2250) are proposed to be DprE1 inhibitors. These inhibitors were potent against Mtb and Msm, probably owing to the high homology of DprE1 between both species [11, 128]. Generally, DprE1 inhibitors can be classified as covalent or noncovalent inhibitors [11, 123]. Resistance to covalent DprE1 inhibitors is usually characterized by the substitution of C387/384 to different residues [11, 122, 123]. Due to the generation of C384S spontaneous mutants resistant to these compounds, we can speculate that they may be covalent DprE1 inhibitors. However, this can only be conclusively determined with detailed biochemical and structural analyses. Additionally, HC2250 seems to be different from other DprE1 inhibitors in terms of its bactericidal activity against NRP bacilli. During dormancy, cell wall biosynthesis, replication, or

translation are minimized. Hence, drugs that target these physiologic activities in actively replicating cells are less effective against Mtb in the NRP state. As expected, NRP Mtb tolerated all the tested dinitrobenzamides (HC2217, HC2226, and HC2238) since these compounds likely target DprE1, an enzyme in the cell wall biosynthesis pathway. However, HC2250, a putative DprE1 inhibitor, continued to kill the bacilli even in the NRP phase. This suggests that HC2250 may also be targeting a cellular process that is needed by Mtb during dormancy. In the isolated *dprE1* Msm mutants (**Supplementary Dataset 2.1**), we observed partial resistance of F346C spontaneous mutants against the tested DprE1 inhibitors. The putative DprE1 inhibitors did not have any inhibitory activity against Mab, agreeing with a study done with PBTZ169, a covalent DprE1 inhibitor that have undergone clinical trials for TB treatment [124].

Apart from identifying potential chemical probes that can be used to further understand Mtb physiology, a critical end goal of most drug discovery efforts is to move potent compounds from the lab into the clinic. The *in vitro* inhibitory activities of most antitubercular compounds can be difficult to translate into *in vivo* potency due to the complex nature of Mtb infection and the pharmacokinetic considerations [9, 129]. These factors lead to a high attrition rate for most antitubercular agents. In this pilot study, without optimizations, HC2210 significantly reduced the burden of Mtb in both the lung and spleen of the infected mice when delivered orally. This finding shows the promise of HC2210 as a potential TB drug. HC2210 is a nitrofuran with a piperazine backbone. HC2210 has two nitro groups, and an important question is whether one or both nitro groups are necessary for the full antimycobacterial activity of the compound. Secondly, are there functional groups in the compound that might pose a significant metabolic liability in a human host? These questions seem to have been partly answered in an earlier structure-activity relationship (**SAR**) study of antimycobacterial nitrofuranyl methyl piperazine series [114]. The furan ring was preferred to other heterocycles in order to maintain the antitubercular activities of the compounds, while the piperazine ring was preferred to substituents such as morpholine or piperidine. These nitrofuranyl series only had one nitro group, and as will be expected, removal

of the nitro group abolished the antitubercular activities of the compounds. This SAR study established the nitro group as the pharmacophore, but it does not show if the presence of two nitro groups may contribute to the overall potency of the compounds. Review of the related HC2209, HC2210, HC2211 structures showed that the three compounds are similar except that HC2210 has two nitro groups. The potency of HC2210 is in the nanomolar range, while those of HC2209 and HC2211 is in the low micromolar range, indicating that the additional nitro group of HC2210 may play a role in its high potency. Structure activity relationship studies involving the synthesis of new analogs will be needed to address this question.

Overall, this report characterizes 10 antitubercular nitro-containing compounds from the MLSMR collection and showed their potential development as TB drugs. Genetic analyses provided evidence supporting distinct mechanisms of action. Some compounds are putative DprE1 inhibitors, while others depend on Fgd for activation and likely inhibit Mtb following mechanisms similar to pretomanid. We also highlighted the possibility of unknown FDORs involved in further activating HC2209, HC2210, and HC2211. Notably, for HC2233 and HC2234 we could only rule out resistance in mutants we have isolated in *fgd, ddn,* and *dprE*. A drawback of this chemical genetics approach is the need for more biochemical experiments to define the specific mechanisms of action. However, this problem is remedied by the established body of biochemical and structural knowledge already available on the subject. Additionally, the resistance of the *ddn* and *fgd* spontaneous mutants to pretomanid serves as a probe-based confirmation that these genes are driving the resistance of some of the compounds reported in this study. A significant takeaway from this study is the possibility of developing HC2210 as an orally bioavailable TB drug. The compound is also active against Mab, a pathogen that is recalcitrant to most drugs, highlighting the possible use of this compound to treat the infection.

Acknowledgments:

Materials and Methods:

Culture conditions, strains, and compounds

Unless otherwise specified, streptomycin-resistant or wild type Erdman and CDC1551 Mtb strains were used. The strains were maintained in 7H9 Middlebrook medium supplemented with 10% oleic acid-albumin-dextrose-catalase (**OADC**), 0.05% Tween 80, and with or without 0.2% cycloheximide and were incubated at 37°C and 5% CO_2 in standing vented flasks. *M. smegmatis* mc^{2}155 and *M. abscessus* ATCC 19977 were grown shaking in 7H9/OADC media at 37°C. Other cultures used in this study include *Staphylococcus aureus* Wichita (29213) or Seattle (25923), *Escherichia coli* (Migula), *Pseudomonas aeruginosa* (Schroeter), *Proteus vulgaris* (Hauser emend. Judicial Commission), and *Enterococcus faecalis* (Andrewes and Horder). Except for *E. faecalis* which was grown in either brain heart infusion medium or Luria-Bertani (**LB**), all the non-mycobacterial cultures were grown exclusively in LB broth at 37°C.

Antimycobacterial compounds were purchased from commercial vendors that supply compounds with >90% purity. HC2209, HC2210, and HC2211 were supplied by Chembridge; HC2217 by Enamine; HC2226 from Chemdiv; HC2233 and HC2234 from Specs; and, HC2238, HC2239 and HC2250 from Vitas-M. To authenticate the supplied compounds, the mass of the compounds was examined by electrospray ionization (ESI) mass spectrometry in the positive

mode. All of the tested compounds had observed masses matching the predicted masses (**Table A.1.1**). For HC2210 the oxalic acid cannot be detected using the ESI method.

***In vitro* dose response study in *M. tuberculosis* and spectrum of activity in other mycobacteria and non-mycobacterial species**

Mtb cultures were aliquoted (0.2 mL) into 96-well assay plates to an initial optical density (**OD**) of 0.1. Starting at 80 µM, the cultures were treated with an 8-point (2.5-fold) dilution series of the test compounds (HC2209, HC2210, HC2211, HC2217, HC2226, HC2233, HC2234, HC2238, HC2239, HC2250, pretomanid, isoniazid, and ethambutol). For comparative study of the most potent compounds (HC2210, pretomanid, and isoniazid), a 12-point (2-fold) dilution series starting from 40 µM were used. The treated cultures were incubated for 6 days at 37°C and in 5% CO_2. After incubation, the OD of the cultures was measured in a plate reader (PerkinElmer Enspire) at 595nm, and the growth of the cultures was normalized based on the OD relative to a rifampicin-positive control (100% growth inhibition) and a DMSO-negative control (0% growth inhibition). The half-maximal effective concentrations (EC_{50s}) of each compound were determined by fitting the normalized data to a four-parameter logistic equation using GraphPad Prism software package.

For Msm and Mab, the cultures were diluted to an initial OD of 0.1 and aliquoted into 96-well plates (0.2 mL) or 384-well plates (0.05 mL). This is followed by the treatment of the cultures with 2.5-fold serial dilutions of the compounds starting from either 200 µM or 80 µM. The cultures were incubated for 3 days before measuring the OD. Growth was normalized based on a positive control (kanamycin for Msm or amikacin for Mab) and a DMSO negative control. The EC_{50s} of the compounds were determined by fitting the normalized data to a four-parameter logistic equation using GraphPad Prism software package.

For the non-mycobacterial cultures, an initial OD of 0.05 was prepared and aliquoted into 96-well plates (0.2 mL) or 384-well plates (0.05 mL). The cultures were treated with 2.5-fold serial

dilutions of the compounds starting from either 200 µM or 80 µM and were incubated for 5 – 8 hours before measuring the OD. Except for *P. aeruginosa* which was normalized with tobramycin-positive control (100% inhibition), other cultures were normalized with kanamycin (100% inhibition). DMSO was used as the negative control (0% inhibition). The normalized data was fitted to a four-parameter logistic equation to calculate the EC_{50s} of the compounds using GraphPad Prism software package.

Kinetic killing assays

For Mtb, an initial OD of 0.1 OD was prepared and dispensed in 0.2 mL aliquots into 96-well assay plates. The cultures were treated with two different doses of the compounds, with an equivalent volume of DMSO used as a negative control. After 4- and 10-days incubation at 37°C and in 5% CO_2, the cultures were diluted serially in phosphate-buffered saline-Tween-80 solution and plated for colony forming units (CFU) in 7H10/OADC agar quadrant plates. The bactericidal activity was determined by comparing the CFU of the initial inoculum to the bacterial CFU after treatment.

Hypoxic shift-down assay to test activity against NRP Mtb

The hypoxic shift-down assay [120] was used to generate NRP bacilli and was performed as previously described with slight modifications [113]. Briefly, 0.2 mL aliquots of CDC1551 (*hspX'::*GFP) culture in 7H9/OADC medium was dispensed into 96-well assay plates to an initial OD of 0.25. The cultures were incubated at 37°C in an anaerobic chamber (BD GasPak). At 4 days of incubation, cultures have become completely anaerobic as indicated by the methylene blue indicator turning to colorless. This was considered to be the first day of anaerobiosis. Aliquots of cultures from day 1 were collected and plated onto 7H10/OADC to quantify the initial CFU. Subsequently, 20 µM of the test compounds were added to the cultures and incubated for 10 days in the anaerobic chamber. DMSO was used as the negative control. The surviving bacterial CFU at different treatments was enumerated at day 10 by plating onto 7H10/OADC agar.

Isolation of resistant mutants

The isolation and confirmation of resistant mutants were done as previously described [130]. Briefly, 1×10^9 CFU streptomycin-resistant Erdman culture was plated onto 7H10/OADC agar plates containing 0.3 µM or 0.1 µM HC2210. The plates were incubated at 37°C until colonies appeared. Colonies were randomly picked from each plate and grown in 7H9/OADC broths. The broth cultures were subjected to a dose-response study using HC2210 as previously described above. Resistance was confirmed by an increase in the EC_{50s} of the mutants when compared to that of the Erdman streptomycin-resistant culture.

To generate mutants resistant to HC2238, mutant #300.1 (*Δfgd*) from the above setup was used. Briefly, 1×10^9 of mutant #300.1 was plated onto 7H10/OADC agar plates supplemented with 5 µM or 20 µM of HC2238 and incubated at 37°C until colonies appeared. Colonies were grown in broth cultures and subjected to a dose-response study with HC2238 as the test compound. Resistance was confirmed by an increase in the EC_{50} values of the spontaneous mutants with respect to that of mutant #300.2. The same protocol was used in generating HC2238- and HC2217-resistant mutants in *M. smegmatis* background except that the agar plates were amended with 10 µM or 20 µM of the compounds.

Whole-genome sequencing and analysis

The genomic DNAs of the confirmed resistant mutants and an Erdman streptomycin-resistant control (or Msm wild-type control) were extracted and submitted for Illumina-based whole-genome sequencing. The breseq computational pipeline was used to analyze the sequence reads and identify single-nucleotide variations [131, 132]. Erdman reference genome (for Mtb) or mc^{2}155 (for Msm) was used in the analysis. After subtracting the mutations shared by the resistant mutants with the Erdman streptomycin-resistant control (for HC2210-resistant mutants), mutant #300.2 control (for HC2238-resistant mutants), or mc^{2}155 WT (for Msm), all the unique

mutations in the resistant mutant strains are presented in **Supplemental Dataset 2.1** (for Msm) or **Supplemental Dataset 2.2** (for Mtb).

Inhibitory activity against intracellular *M. tuberculosis*

A previously described protocol was adapted in testing the efficacy of the compounds against intracellular M. tuberculosis [130]. Briefly, primary bone marrow-derived macrophages were harvested from C57BL/6 mice and distributed into 96-well assay plates in preparation for mycobacterial infection. The macrophages were infected for 1 h with CDC1551 luciferase reporter strain, followed by treatment with different concentrations of the nitro-containing compounds (80 μM to 0.136 μM). Rifampicin and DMSO were used as negative and positive controls, respectively. After incubating the samples for 6 days at 37°C and 5% CO_2, bacterial survival was measured in a luciferase readout assay. The EC_{50s} of the compounds against intracellular *M. tuberculosis* were determined by fitting the normalized data to a four-parameter logistic equation using GraphPad Prism software package.

Eukaryotic cytotoxicity assay

Murine primary bone marrow-derived macrophages were distributed into 96-well assay plates as described above. Different concentrations of the indicated inhibitors, ranging from 80 μM to 0.136 μM, were used in treating the macrophages. Cells were treated with DMSO as a positive control, while 4% Triton X-100 served as the negative control. Following a 3-day incubation of the macrophages at 37°C and in 5% CO_2, the viability of the cells was assessed with the CellTiter-Glo (Promega) luciferase assay kit. The half-maximal cell cytotoxicity concentration (CC_{50}) values were calculated by fitting the normalized data into a non-linear four-parameter least squares regression model in the GraphPad prism package.

Evaluation of the efficacy of HC2210 is a chronic murine TB infection model

All animal studies were approved by the Michigan State University Institutional Animal Care and Use Committee. Female, ~8-week-old C57BL/6 mice purchased from Jackson Laboratories were

used in this study. Low dose infection was initiated by aerosol exposure to 100 CFU of *M. tuberculosis* Erdman strain using a Glas-Col aerosol inhalation exposure device. One day after infection, 5 mice were euthanized, and the lungs were aseptically collected to assess the initial infection dose. The remaining mice were randomly distributed into three groups of eight mice and allowed for 38 days to develop a chronic infection. Treatment was then initiated by administering the mice with oral doses of the vehicle (corn oil/5% DMSO), 75mg/kg of HC2210, or 10mg/kg rifampicin through oral gavage. HC2210 was administered once daily, while rifampicin and vehicle doses were given twice daily. The mice were treated five days a week, with a two-day resting period. The treatment lasted four weeks after which the mice were euthanized. The lungs and spleens were aseptically removed and homogenized, and the mycobacterial burdens were assessed by enumerating CFUs. For statistical analysis, one-way ANOVA was used to determine the effects of the treatments on the mycobacterial load of the tissues. The mean differences between the groups were compared in an unpaired Student's t-test and were considered statistically significant at a 95% confidence interval.

CHAPTER THREE: Defining the mechanisms-of-action of nitrofuranyl piperazines against

Mycobacterium abscessus

This work is in preparation for journal submission. The authors and their affiliations are listed below:

Ifeanyichukwu E. Eke[1], Maria S. Escobar[1], Andrew Olive[1], Allison Carey[2], and Robert B. Abramovitch[1]*

[1]Department of Microbiology, Genetics, and Immunology, Michigan State University, East Lansing, Michigan, 48824, United States, and [2]Department of Pathology, University of Utah, Salt Lake City, Utah, 84112, United States

Contributions:

I.E.E. and R.B.A. conceived and designed the studies. M.S.E., A.O., and A.C. provided the clinical isolates of Mab and conducted the initial drug susceptibility testing. **I.E.E.** conducted all the experiments including the *in vitro* and genetic characterization studies. **I.E.E.** and R.B.A. wrote the manuscript.

Abstract:

Mycobacterium abscessus (**Mab**) is well-known for its intrinsic resistance to diverse classes of antibiotics, making many non-tuberculous mycobacterial (**NTM**) infections challenging to treat. Our lab previously reported three nitrofuranyl piperazines – HC2209, HC2210, HC2211 – that are active against *M. tuberculosis* (**Mtb**). In this current report, we show these agents are also active against Mab and define their mechanisms-of-action in Mab. HC2210 is about 5X more potent than amikacin, a standard-of-care drug for Mab infections and retains its antimycobacterial activities against multidrug-resistant clinical isolates of Mab. Isolation of resistant mutants suggests that the compounds require the cofactor F_{420} activation machinery, although an activating nitroreductase could not be identified. Additionally, resistance mutations in glycerol kinase (**GlpK**) were selected against HC2210. The potencies of the nitro-containing inhibitors significantly improved in a glycerol-containing medium, suggesting a possible potentiating activity of glycerol. Transcriptional profiling shows that HC2210 primarily exerts its inhibitory effects against Mab through oxidative stress and the modulation of lipid metabolism. Our findings demonstrate the potential of developing these nitro-containing compounds as drugs to treat Mab infections.

Introduction:

Nontuberculous mycobacterial infections (**NTMI**) are caused by mycobacterial species other than *Mycobacterium tuberculosis* (**Mtb**) or *M. leprae*[133]. These infections are major causes of pulmonary comorbidities in people with preexisting lung conditions such as cystic fibrosis and can also manifest as skin and soft tissue infections[127, 133]. They are mostly caused by fast-growing species such as the *M. abscessus* (**Mab**) complex, and slower-growing species such as the *M. avium* complex, *M. kansasii*, and *M. ulcerans*[133]. Mab is well-known for its high intrinsic antibiotic resistance system that includes but are not limited to the highly impermeable cell envelope, enzyme modification pathways, efflux proteins, polymorphism of target or prodrug-activating genes, and a high-functioning *whiB7* regulon, making many antimycobacterial drugs to be ineffective against the pathogen[127, 133]. Currently, macrolides such as erythromycin, azithromycin, and clarithromycin, and aminoglycosides such as amikacin are the mainstay of chemotherapeutic interventions for Mab infections[133, 134]. However, these drugs have limited efficacy against Mab infections, with the treatment success ranging from 30 to 50%[133, 134]. Additionally, a combination-based therapy involving multiple drugs is normally used to treat Mab infections and this treatment can extend to several years[134]. Overall, these challenges call for more effective drugs to treat Mab infections.

Recently, our group discovered new nitro-containing compounds that are active against Mtb[15]. In that study, we characterized the mechanisms-of-action of the compounds against Mtb and their spectrum of activity against other pathogens including Mab. We showed that the nitrofuranyl piperazines (**HC2209, HC2210, and HC2211**) are prodrugs that require the deazaflavin-dependent nitroreductase (**Ddn**) and possibly another cofactor F_{420}-dependent nitroreductase for their inhibitory activity in Mtb. They differ from pretomanid, an FDA-approved nitroimidazole-based tuberculosis drug, that depends solely on Ddn for its activation. Interestingly,

the nitrofuranyl piperazines inhibited the growth of Mab, while pretomanid was inactive against the pathogen.

In this current study, we examined the mechanisms-of-action of these nitrofuranyl piperazines against Mab. We showed that HC2210 is a potent bacteriostatic inhibitor of Mab growth that is also active against clinical strains of Mab. Forward genetic selection implicated the cofactor F_{420} activation machinery in the possible reductive activation of the nitrofuranyl piperazines in Mab. Interestingly, the genetic disruption of glycerol kinase (**glpK**), an enzyme involved in glycerol utilization, led to reduced potency of the compounds against Mab. While much is known about GlpK and its role in antitubercular drug resistance, this represents one of the few reports of this protein as a resistance factor in Mab[135]. We also showed that the growth-inhibiting activity of the compound against Mab is glycerol-dependent. Lastly, transcriptional profiling showed that HC2210 possibly inhibits the growth of the bacteria by modulating the metabolism of lipids and causing oxidative stress.

Results:

HC2210 is potent against *M. abscessus* ATCC 19977

In our previous characterization of antitubercular nitro-containing compounds, we showed three nitrofuranyl piperazines (**Figure 3.1A**) – **HC2209** (1-(4-fluorophenyl)-4-[(5-nitro-2-furyl)methyl]piperazine), **HC2210** (1-[(5-nitro-2-furyl)methyl]-4-(4-nitrophenyl)piperazine oxalate, and **HC2211** (1-[(5-nitro-2-furyl)methyl]-4-phenylpiperazine) – to also inhibit the growth of Mab[15]. HC2210 was the most potent compound among the three nitrofuranyl piperazines and is the major focus of the present study.

To benchmark HC2210 against other antimicrobial drugs, we examined the half-maximal effective concentrations (EC_{50}) of HC2210 and several known Mab inhibitors against a reference strain of Mab (***M. abscessus* subspecies *abscessus* ATCC 19977**). HC2210 had a potent EC_{50} of 0.720 μM against Mab (**Figure 3.1B, Table 3.1**), recapitulating our initial report[15]. When

compared with other drugs, the efficacy of HC2210 against Mab was similar to moxifloxacin (0.699 μM) and rifabutin (0.920 μM). Rifampin, the parent analog of rifabutin and a first-line antitubercular drug, had a poor activity against Mab (EC$_{50}$ = 21.050 μM), agreeing with previous reports[136, 137]. We also observed a general trend where common antimycobacterial drugs such as clofazimine (EC$_{50}$ = 2.397 μM) and bedaquiline (EC$_{50}$ = 0.159 μM) that target energy production were relatively potent against Mab, while those that target cell wall biosynthesis such as ethambutol (EC$_{50}$ = 31.570 μM), isoniazid (33.250 μM), and meropenem (30.970 μM) had poor activity against the pathogen. We did not include pretomanid in the study since we[15] and others[39] have previously reported the drug to be inactive against Mab. Interestingly, HC2210 was about 5X more potent than amikacin (EC$_{50}$ = 3.800 μM), an aminoglycoside that is generally used for the treatment of Mab infections. Together, these data show HC2210 is a potent compound against Mab.
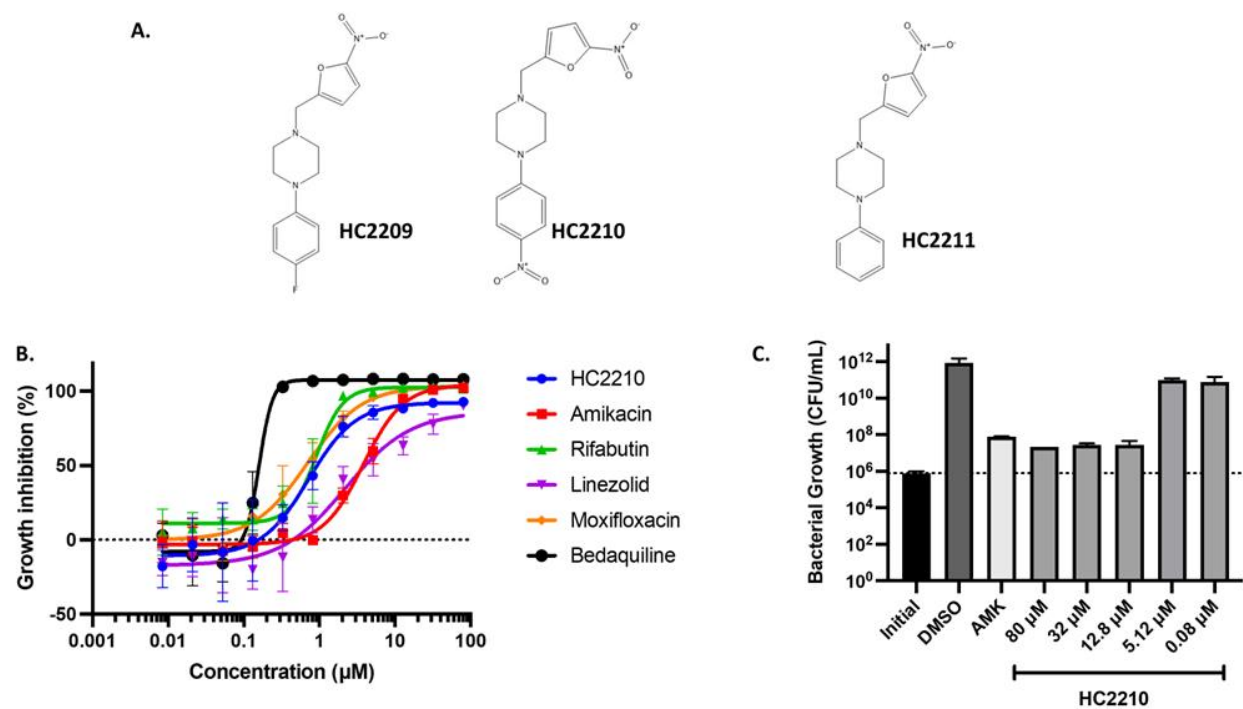
Figure 3.1. HC2210 is a potent nitrofuranyl piperazine that inhibits the growth of Mab. A. Structures of the nitrofuranyl piperazines included in the study. **B.** Dose response curves of HC2210 and common drugs used in the treatment of *M. abscessus* infections **C.** HC2210 is bacteriostatic against Mab. The dotted line in **B** represents the growth inhibition of the negative control (DMSO), while the dotted line in **C** is a trace of the starting concentration (7.933×10^5 CFU/mL). The error bars represent the standard deviation of at least two biological replicates.

Table 3.1. *In vitro* potency of HC2210 and other antimicrobial compounds against *M. abscessus*

Targeted Cellular Pathway	Antibiotic	EC$_{50}$ (μM)
Multiple targets	HC2210	0.72
Cell wall biosynthesis	Ethambutol	31.57
	Isoniazid	33.25
	Meropenem	30.97
Respiration	Bedaquiline	0.16
	Clofazamine	2.40
Translation	Amikacin	3.80
	Doxycycline	34.90
	Kanamycin	16.78
	Linezolid	2.19
Transcription	Rifabutin	0.92
	Rifampicin	21.05
DNA topology	Ciprofloxacin	6.75
	Moxifloxacin	0.70

EC$_{50}$ is the half-maximal effective concentration of the compound.

HC2210 is bacteriostatic against *M. abscessus*

Next, we sought to determine if the inhibitory activity of HC2210 is bactericidal or bacteriostatic. To do this, we treated a culture of Mab for four days with different concentrations of HC2210 (80 μM – 0.08 μM) and used DMSO and a single concentration of amikacin (20 μM) as vehicle and positive controls, respectively. Bacterial viability was determined by enumerating CFUs. As shown in **Figure 3.1C**, HC2210 is not bactericidal against Mab as the burden of the treated cells does not fall below the initial inoculum even at high concentrations. However, a strong bacteriostatic effect was observed for the compound, suppressing the growth of the treated cells relative to the DMSO control by as much as 10,000-fold. In contrast, HC2210 and other *ddn*-dependent nitro-containing compounds are bactericidal in Mtb[15], revealing a difference in

compound activities between the species. Amikacin was also bacteriostatic against Mab at the tested concentration. These findings are consistent with other reports of the bacteriostatic activity of Mab antibiotics[138-140], although there are promising exceptions such as rifabutin, moxifloxacin, clarithromycin, and EC/11716 that have been reported to be bactericidal against Mab[136, 138].

HC2210 has varying efficacy against antibiotic-resistant clinical isolates of Mab

Having established the efficacy of HC2210 against a laboratory-adapted reference strain of Mab, we examined its potency against a clinical collection of 28 Mab strains that were isolated from different sources such as the sputum, wound, and skin of infections in humans. Using the CLSI guideline, most of these clinical isolates were clinically classified to be resistant to common antibiotics used for Mab treatment and these include but are not limited to macrolides (clarithromycin), aminoglycosides (amikacin, tobramycin), and fluoroquinolones (ciprofloxacin, moxifloxacin). Therefore, this collection of multidrug resistant Mab isolates represents a rich resource to test the potential clinical utility of HC2210.

HC2210 had varying levels of antimycobacterial activity against all the tested drug-resistant clinical isolates (**Table 3.2**). About half of the tested isolates were resistant to low concentrations of HC2210 but were susceptible when treated at higher concentrations (32 μM or 80 μM). The other half of the tested isolates were susceptible even to lower concentrations of HC2210, giving rise to EC_{50} values that ranged from 0.539 μM to 4.713 μM. Notably, the efficacy of HC2210 was not dependent on the smooth or rough morphotype of the strains. Taken together, HC2210 shows promise for possible development as a drug for the treatment of multidrug-resistant Mab infections, however, it would be limited to specific susceptible clinical strains.

Table 3.2. Inhibitory activity of HC2210 against drug-resistant clinical isolates of *M. abscessus*

Isolate code	Morphology	Isolation site	HC2210 EC$_{50}$ (µM)
MAB002	Smooth	Arm	> 32
MAB006	Smooth	Sputum	> 32
MAB007	Smooth	Spine	4.71
MAB010	Smooth	Lung	> 0.33
MAB011	Smooth	Sputum	0.58
MAB014	Rough	Sputum	0.71
MAB015	Rough	Sputum	> 0.33
MAB016	Smooth	Breast	1.17
MAB018	Smooth	Sputum	> 32
MAB019	Rough	Bronchial Wash	0.846
MAB022	Smooth	Sputum	> 12.5
MAB023	Smooth	Sputum	> 32
MAB025	Rough	Sputum	> 12.5
MAB026	Smooth	Abscess	0.840
MAB028	Rough	BAL	> 12.5
MAB029	Smooth	Sputum	> 12.5
MAB035	Smooth	Bronchial Wash	> 32
MAB041	Rough	Sputum	> 32
MAB048	Smooth	Not indicated	> 32
MAB051	Smooth	Bronchial Wash	0.884
MAB052	Smooth	Bronchial Wash	0.943
MAB053	Rough	Sputum	> 32
MAB056	Smooth	Skin	> 32
MAB057	Smooth	Not indicated	1.066
MAB058	Smooth	Sputum	0.908
MAB086	Smooth	Sputum	1.696
MAB088	Rough	Ear	0.539
MAB089	Smooth	Arm	> 32

HC2210 activity depends on the cofactor F$_{420}$ activation machinery in Mab

In Mtb, HC2210 and other nitrofuranyl piperazines depend on the cofactor F$_{420}$ machinery and *ddn* for presumed activation into antimycobacterial metabolites[15]. To determine if the mechanism is shared in Mab, we conducted a forward genetic selection for HC2210-resistant mutants. Mab was inoculated onto 7H10 agar plates amended with high concentrations of

HC2210 (200 μM and 80 μM) and incubated for 14 days to allow for resistant colonies to emerge. Resistance to HC2210 was confirmed (**Figure A.3.1**), followed by whole-genome sequencing of selected mutants. Most of the sequenced resistant mutants had mutations in genes involved in the biosynthesis of cofactor F_{420} (*MAB_3289*, *MAB_1319*, *MAB_3607*) or in the dehydrogenase that generates the reduced form of the cofactor (*MAB_4230c* or *fgd*) (**Table 3.3; Figure 3.2A, 3.2B**), implicating the cofactor F_{420} activation machinery of the pathogen. In Mtb, the reduced cofactor F_{420} is used by nitroreductases such as Ddn to reductively activate different nitro prodrugs into antimycobacterial metabolites[2, 3, 6, 7, 15, 17, 35]. Intriguingly, our forward genetic selection did not give rise to the disruption of any nitroreductase-coding gene in Mab. We reasoned this might be similar to what we observed for Mtb where only selection at a low concentration of HC2210 gave rise to mutations in *ddn*, with mutations in *ddn* not being isolated at a higher selection concentration[15]. Therefore, we repeated our forward genetic selection by plating Mab cells onto 7H10 agar plates containing lower concentrations of HC2210 (20 μM and 10 μM). However, the resistant mutants that developed at this lower selection pressure also did not harbor mutations in any nitroreductase-coding gene (**Figure A.3.2, Table A.2.1**).

Table 3.3. Mutations in HC2210-resistant mutants that were generated at a higher selection pressure of 80 μM or 200 μM HC2210

Mutant strain	SNP location (nt)	Genes (s)	Protein	Nucleotide change	Amino acid substitution
Mab_1	3,325,718	*[MAB_3287c]-[MAB_3290]*	CofC	Δ3,264 bp	
Mab_7	3,325,718	*[MAB_3287c]-[MAB_3290]*	CofC	Δ3,264 bp	
Mab_17	3,327,607	*MAB_3289*	CofC	+G	coding (142/615 nt)
Mab_19	3,328,026	*MAB_3289*	CofC	GAC→GAA	D187E
Mab_30	3,327,896	*MAB_3289*	CofC	Δ1 bp	coding (431/615 nt)
Mab_32	3,328,026	*MAB_3289*	CofC	GAC→GAA	D187E
Mab_2	1,322,058	*MAB_1319*	CofGH	2 bp→AT	coding (2273-2274/2646 nt)
Mab_3	1,320,081	*MAB_1319*	CofGH	+G	coding (296/2646 nt)
Mab_5	1,320,294	*MAB_1319*	CofGH	2 bp→TT	coding (509-510/2646 nt)
Mab_6	1,322,377	*MAB_1319*	CofGH	Δ1 bp	coding (2592/2646 nt)
Mab_8	1,320,294	*MAB_1319*	CofGH	2 bp→TT	coding (509-510/2646 nt)
Mab_9	1,320,294	*MAB_1319*	CofGH	2 bp→TT	coding (509-510/2646 nt)
Mab_17	1,322,342	*MAB_1319*	CofGH	Δ37 bp	coding (2557-2593/2646 nt)
Mab_18	1,320,744	*MAB_1319*	CofGH	AAG→AGG	K320R
Mab_22	1,321,759	*MAB_1319*	CofGH	Δ1 bp	coding (1974/2646 nt)
Mab_27	1,320,917	*MAB_1319*	CofGH	GGC→TGC	G378C
Mab_31	1,321,110	*MAB_1319*	CofGH	+C	coding (1325/2646 nt)
Mab_37	1,320,162	*MAB_1319*	CofGH	Δ11 bp	coding (377-387/2646 nt)
Mab_41	1,322,041	*MAB_1319*	CofGH	+T	coding (2256/2646 nt)
Mab_42	1,321,658	*MAB_1319*	CofGH	CAG→TAG	Q625*
Mab_43	1,321,138	*MAB_1319*	CofGH	Δ2 bp	coding (1353-1354/2646 nt)
Mab_11	3,658,224 3,658,233	*MAB_3607*	CofD		coding (1039/1086nt) coding (1048/1086nt)
Mab_26	3,657,582	*MAB_3607*	CofD	Δ1 bp	coding (397/1086 nt)
Mab_28	3,657,582	*MAB_3607*	CofD	Δ1 bp	coding (397/1086 nt)
Mab_4	4,301,081	*MAB_4230c*	Fgd	+C	coding (66/1014 nt)
Mab_15	4,293,562	*[MAB_4225c] – [MAB_4231]*	Fgd	Δ8,336 bp	
Mab_38	379,197 379,199	*MAB_0382*	GlpK	GTC→GTT GAT→GTT	V413V D414V
Mab_39	378,913	*MAB_0382*	GlpK	CAG→TAG	Q319*
Mab_40	378,222	*MAB_0382*	GlpK	Δ1 bp	coding (264/1515nt)
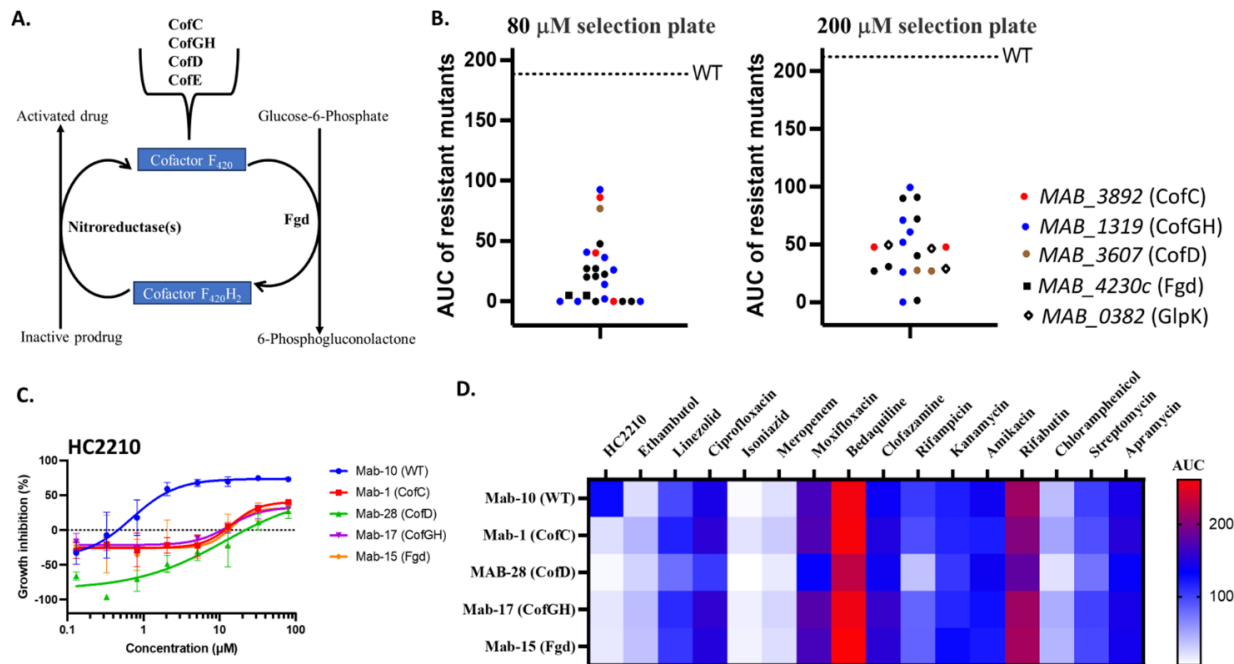
Figure 3.2. The activity of HC2210 in *M. abscessus* (Mab) is dependent on the cofactor F_{420} activation machinery. **A**. A model on how the genes discovered from the forward genetic screen work together in the activation of HC2210 in Mab. CofC, CofGH, CofD, and CofE are involved in the biosynthesis of cofactor F_{420}. The newly synthesized cofactor is in the oxidized form and is used by Fgd in the pentose phosphate pathway to oxidize glucose-6-phosphate into 6-phosphogluconolactone. This generates a reduced form of the cofactor that is used by an unknown nitroreductase(s) to reductively activate the nitro prodrug into metabolites that inhibit the growth of the bacteria. **B**. Resistant mutants and the disrupted genes identified from the forward genetic selection in agar plates containing 80 μM or 200 μM of HC2210. **C**. HC2210 shows reduced activity against all the tested mutants that are deficient in the biosynthesis or reduction of cofactor F_{420}. The error bars represent the standard deviations of at least two biological replicates. **D**. The resistance phenotype of the *fgd* or F_{420} mutants is restricted to HC2210. For **B** and **D**, the area under the curve (AUC) was used as a relative measure of the potency of the compounds across the tested mutants and was compared to that of the WT (wildtype).

The *fgd* and F_{420} biosynthesis mutants retain their susceptibility to common antimycobacterial drugs

Next, we examined if the *fgd* or F_{420} biosynthesis mutants have differing sensitivities to other antibiotics. To explore this, we collected four mutants that are representative of the genes involved in the biosynthesis or reduction of the F_{420} cofactor and reconfirmed their resistance to HC2210 (**Figure 3.2C**). Subsequently, the mutants were treated with different antibiotics in a

dose-response study. Compared to the wildtype, none of the mutants show any cross-resistance to the tested antibiotics (**Figure 3.2D**). This is expected since the cofactor F_{420} activation machinery is unique to nitro-containing compounds such as HC2210[2, 3, 6, 7, 15, 17, 35].

glpK mutants are resistant to HC2210 and other antimycobacterial drugs

The selection for HC2210-resistant mutants also gave rise to three mutants that harbored mutations in *MAB_0382*, a gene that codes for glycerol kinase (**GlpK**) (**Figure 3.2B, Table 3.2**). This gene has been implicated in clofazimine resistance in Mab[135], and *glpK* mutants in Mtb are known to be tolerant to several drugs[48, 141, 142]. GlpK catalyzes the first committal step of glycerol catabolism where it phosphorylates glycerol to glycerol-3-phosphate using ATP[48, 141-143]. The phosphorylated glycerol can then be utilized in downstream pathways to support bacterial growth (**Figure 3.3A**). Since GlpK is needed for glycerol metabolism, we reasoned that the *glpK* mutants can easily be confirmed to be deficient in glycerol assimilation by growing them in a minimal medium containing glycerol as the sole carbon source and comparing their growth in a glucose-containing media. While the *glpK* mutants grew as well as the wildtype in the glucose-containing media, they had a growth defect in the glycerol-containing media (**Figure 3.3B and 3.3C**), indicating their deficiency in the utilization of glycerol.
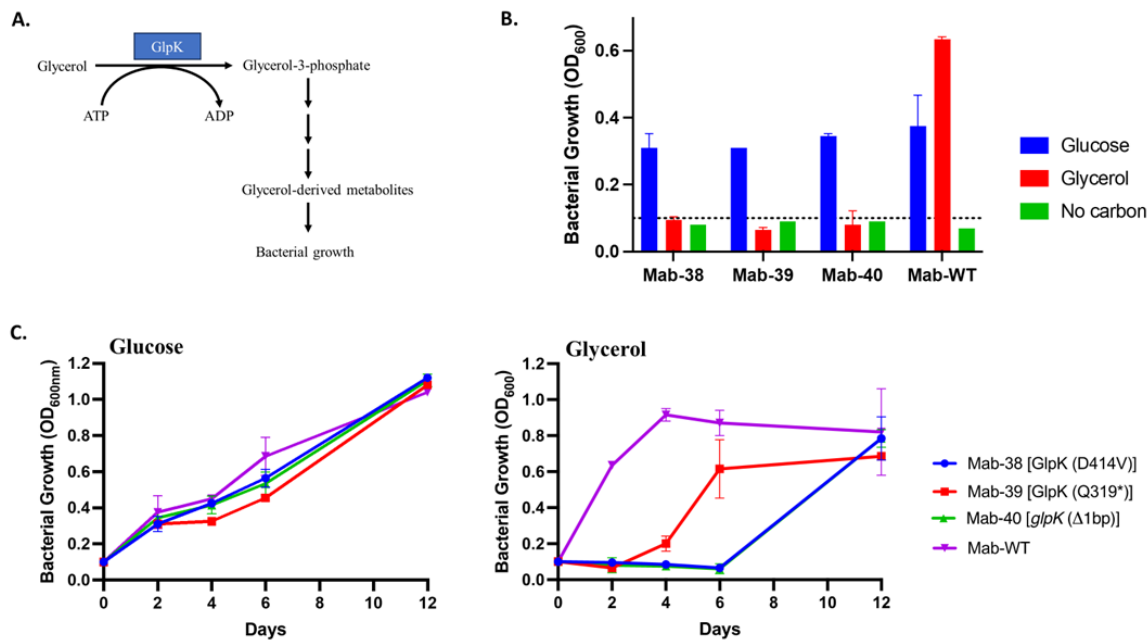
Figure 3.3. The *glpK* mutants are deficient in the utilization of glycerol as a sole carbon source. **A**. Schematic showing the role of GlpK (glycerol-3-kinase) in glycerol metabolism. GlpK uses ATP to phosphorylate glycerol, committing the lipid for downstream metabolism. **B**. The growth of the *glpK* mutants and WT after 48 hours or **C**. over a 12 day-period in minimal medium containing either glucose or glycerol as the sole carbon. The error bars represent the standard deviations of two biological replicates.

Next, we carried out cross-resistance profiling of the three *glpK* mutants against the other nitrofuranyl piperazines and observed resistance to the series (**Figure 3.4A**). We also examined the resistance of a *glpK* mutant to rifabutin, moxifloxacin, bedaquiline, and amikacin. While bedaquiline retained its potency against the *glpK* mutant, the other three antimycobacterial drugs had a modest reduction of activity (**Figure A.3.3**).
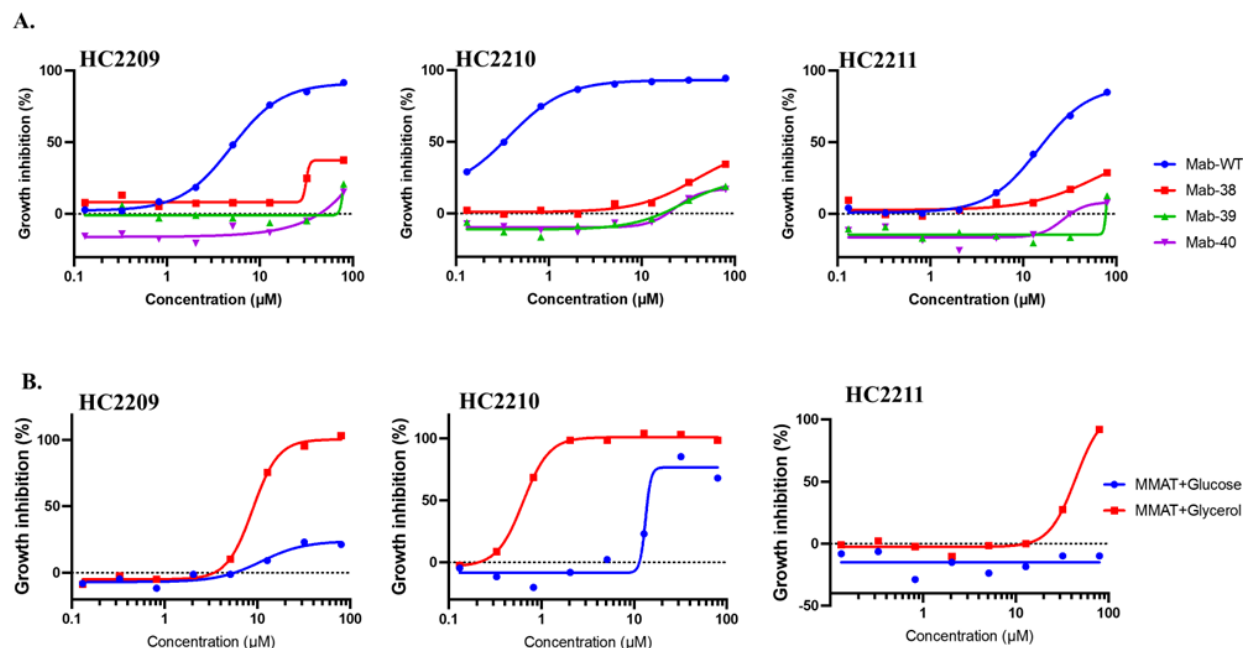
Figure 3.4. The nitofuranyl piperazines are resistant to the *glpK* mutants and their antimycobacterial activity against the WT is potentiated by glycerol. **A**. Cross-resistance screening of the nitrofuranyl piperazines against the *glpK* mutants. **B**. Enhanced activity of the compounds against the WT in minimal medium (MMAT) containing glycerol as the sole carbon source.

Glycerol potentiates the antimycobacterial activity of HC2209, HC2210, and HC2211

Having established that the *glpK* mutants are resistant to the nitrofuranyl piperazines, we hypothesized that glycerol may be potentiating the antimycobacterial activity of the compounds. To test this hypothesis, we conducted an *in vitro* dose-response study of HC2209, HC2210, and HC2211 against Mab in minimal medium containing either glucose or glycerol as the sole carbon source. In the glucose-containing minimal medium, HC2210 had an EC_{50} value of 13.3 μM, and this potency against Mab significantly increased by about 20X in glycerol-containing medium (EC_{50} = 0.635 μM) (**Figure 3.4B**). Similarly, HC2209 and HC2211 had poor activity against Mab in glucose-containing minimal medium but regain their potencies in glycerol-containing medium (**Figure 3.4B**). Overall, this data show that glycerol enhances the antimycobacterial activities of

the compounds against Mab, a similar finding that has been reported for some drugs against Mtb[141]. Notably, Mab grows more slowly in glucose than glycerol (**Figure 3.3C**) and it is possible that differences in potency of the bacteria in the different media are driven by carbon source-dependent differences in growth rate, or alternatively, an inhibitory mechanism that is specific to glycerol.

HC2210 impacts genes involved in lipid metabolism and oxidative stress in Mab

To gain further mechanistic insights into the activity of HC2210 against Mab, we conducted transcriptional profiling of HC2210-treated Mab cultures relative to DMSO treated control. Only 80 genes were differentially regulated by HC2210 treatment at the cutoff criteria of log fold change > |1.5| and false discovery rate q-value < 0.05 (**Figure 3.5A, Figure 3.5B, Dataset 3.1**). About 69% of the differentially expressed genes were upregulated, while the remaining were downregulated.
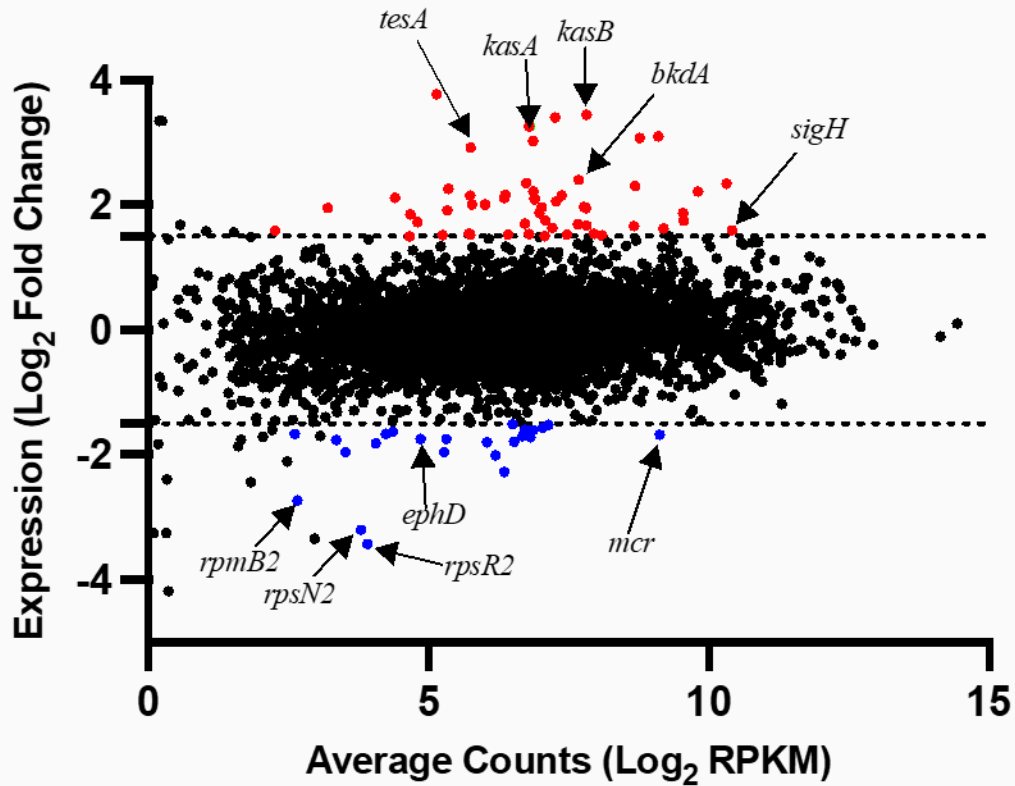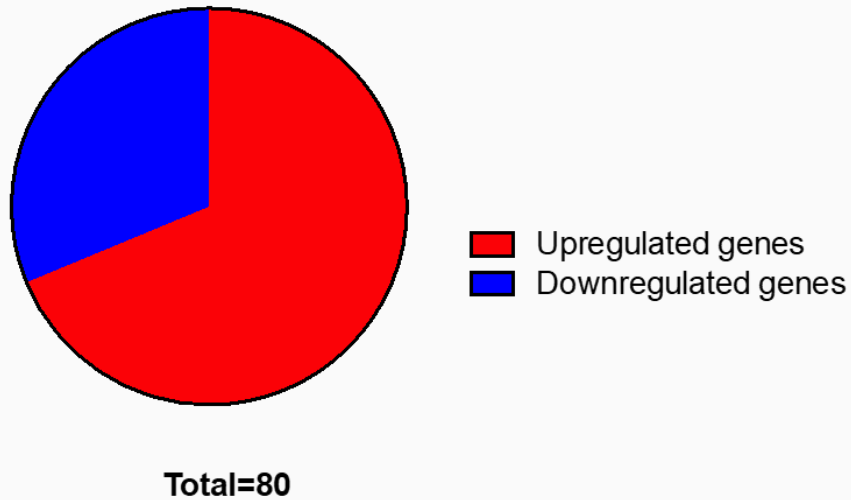
Figure 3.5. Transcriptional profiling of *M. abscessus* (Mab) cultures that were treated with HC2210 or DMSO control. **A.** Magnitude-amplitude plot of differentially expressed genes in HC2210-treated cultures relative to the DMSO control at a significance threshold of $q < 0.05$ and log fold change $> |1.5|$. The dotted line represents the $\log_2$ fold changes of 1.5 or -1.5. The red circles represent upregulated genes, while the blue circles represent downregulated genes.

Figure 3.5. (cont'd)
The black circles are genes that did not meet the significance threshold. **B.** Pie-chart depicting the total number of upregulated and downregulated genes (log2 fold change > |1.5| and q <0.05). **C.** Heatmap showing the differentially expressed genes in HC2210-treated Mab cultures. The *M. tuberculosis* H37Rv homolog and functional category of the genes are included.

M. abscessus Gene	HC2210	*M. tuberculosis* Orthologue	*M. tuberculosis* Protein	Functional Category
MAB_0331c		*Rv2055c*	RpsR2	Information pathways
MAB_0332c		*Rv2056c*	RpsN2	Information pathways
MAB_0334c		*Rv2058c*	RpmB2	Information pathways
MAB_0514		*Rv2214c*	EphD	Virulence, detoxification, adaptation
MAB_0659		*Rv0097*	Rv0097	Intermediary metabolism and respiration
MAB_0660		*Rv0098*	FcoT	Lipid metabolism
MAB_0661		*Rv0099*	FadD10	Lipid metabolism
MAB_0662		*Rv0100*	Rv0100	Conserved hypotheticals
MAB_0663		*Rv0101*	Nrp	Lipid metabolism
MAB_0761c		*Rv1715*	FadB3	Lipid metabolism
MAB_0894c		*Rv0462*	LpdC	Intermediary metabolism and respiration
MAB_0895c		*Rv2495c*	BkdC	Intermediary metabolism and respiration
MAB_0896c		*Rv2496c*	BkdB	Intermediary metabolism and respiration
MAB_0897c		*Rv2497c*	BkdA	Intermediary metabolism and respiration
MAB_0949c		*Rv1655*	ArgD	Intermediary metabolism and respiration
MAB_1053c		*Rv0948c*	Rv0948c	Intermediary metabolism and respiration
MAB_1182		*Rv1065*	Rv1065	Conserved hypotheticals
MAB_1339		*Rv3520c*	Rv3520c	Intermediary metabolism and respiration
MAB_1862		*Rv1143*	Mcr	Lipid metabolism
MAB_2028		*Rv2246*	KasB	Lipid metabolism
MAB_2030		*Rv2245*	KasA	Lipid metabolism
MAB_2032		*Rv0242c*	FabG4	Lipid metabolism
MAB_2033		*Rv2928*	TesA	Lipid metabolism
MAB_2034		*Rv2243*	FabD	Lipid metabolism
MAB_2035		*Rv2939*	PapA5	Lipid metabolism
MAB_2036		*Rv0677c*	MmpS5	Cell wall and cell processes
MAB_2263c		*Rv3476c*	KgtP	Cell wall and cell processes
MAB_2266c		*Rv2589*	GabT	Intermediary metabolism and respiration
MAB_2941		*Rv2971*	Rv2971	Intermediary metabolism and respiration
MAB_3543c		*Rv3223c*	SigH	Information pathways
MAB_3840		*Rv2323c*	Rv2323c	Conserved hypotheticals
MAB_3866c		*Rv1704c*	CycA	Cell wall and cell processes
MAB_3915		*Rv0564c*	GpdA1	Lipid metabolism
MAB_4346c		*Rv0753c*	MmsA	Intermediary metabolism and respiration
MAB_4353		*Rv1532c*	Rv1532c	Conserved hypotheticals
MAB_4418		*Rv2858c*	AldC	Intermediary metabolism and respiration
MAB_4514c		*Rv1968*	Mce3C	Virulence, detoxification, adaptation
MAB_4517c		*Rv1965*	YrbE3B	Virulence, detoxification, adaptation
MAB_4523		*Rv3645*	Rv3645	Cell wall and cell processes
MAB_4562		*Rv0179c*	LprO	Cell wall and cell processes
MAB_4635		*Rv1175c*	FadH	Lipid metabolism
MAB_4636		*Rv1871c*	Rv1871c	Conserved hypotheticals
MAB_4705c		*Rv0451c*	MmpS4	Cell wall and cell processes

Log Fold Change
3.5 2 1 0 -1 -2 -3.5

To classify the differentially regulated genes, we generated a heatmap of the differentially expressed genes, matching them with their Mtb orthologues and functional categories (obtained from Mycobrowser[144], **Figure 3.5C**). Several of the differentially regulated genes are in putative operons. For example, the ribosomal genes – *MAB_0331c* (RpsR2), *MAB_0332c* (RpsN2), and

MAB_0334c (RpmB2) – are expressed together from a single operon[145] and are repressed by HC2210. Also, *MAB_0659* (Rv0097), *MAB_0660* (FcoT), *MAB_0661* (FadD10), *MAB_0662* (Rv0100), and *MAB_0663* (Nrp) are part of a single operon[146] and are strongly upregulated by HC2210 treatment. The activities of FcoT, FadD10, Rv0100, and Nrp have been implicated in the biosynthesis of phthiocerol dimycocerosates (**PDIM**) and lipopeptides found in the mycobacterial cell envelope[146]. We also saw the upregulation of other genes such as *MAB_2033* (TesA) and *MAB_2035* (PapA5) that are involved in biosynthesis of PDIM and envelope-associated phenolic glycolipids in Mtb[147-150]. However, it is important to point out that Mab is not currently known to produce PDIMs or phenolic glycolipids[133], although research in this area for Mab is still at infancy. Interestingly, *MAB_0514* (EphD), an epoxide hydrolase that is involved in the metabolism of mycolic acids[151], was downregulated by HC2210. Consistent for what is known for the mechanism-of-action of cell wall inhibitors such as isoniazid and ethionamide and some nitro compounds such as pretomanid and JSF-2019 against Mtb[5, 9, 92, 152], HC2210 also led to the differential expression of some genes in the FAS-II pathway and these include *MAB_2028* (KasB), *MAB_2030* (KasA), and *MAB_2034* (FabD). Other HC2210-impacted genes that are involved in the metabolism of mycobacterial lipids include *MAB_0761c* (FadB3), *MAB_2032* (FabG4), *MAB_4635* (**FadH**), and *MAB_1862* (Mcr) amongst others[153-155]. Additionally, we observed the upregulation of different genes that are part of the defense system of the bacteria against oxidative stress. These include *MAB_3543* that codes for the stress response regulator, SigH[156], and *MAB_0462* (LpdC), a protein involved in the detoxification of reactive nitrogen species during infection[157]. Thus, SigH and LpdC may work as part of the intrinsic resistance system of Mab against HC2210.

Interestingly, when we transcriptionally profiled for the effect of HC2210 and pretomanid against Mtb, we observed that the compounds impacted the expression of 768 and 800 genes, respectively (Log$_2$ fold change > |1.5| and false discovery rate *q*-value < 0.05) (**Dataset 3.2**). The transcriptional profiles of HC2210 and pretomanid in Mtb were highly similar since a magnitude-

amplitude plot of the pretomanid-treated culture versus the HC2210-treated culture only gave rise to 15 differentially expressed genes (**Figure A.3.4**). We saw the downregulation of several ribosomal genes against Mtb (**Figure A.3.4; Dataset 3.2**), including the *rpsR2* homolog (*MAB_0331c*), *rpsN2* homolog (*MAB_0332c*), and *rpmB2* homolog (*MAB_0334c*) that we also observed in Mab (**Figure 3.5C**). Consistent with what we saw for Mab, we also observed the differential expression of several genes involved in lipid metabolism (**Figure A.3.4; Dataset 3.2**). Unlike what we observed for Mab where there was a significant upregulation of *sigH* and *lpdC*, genes involved in oxidative stress response[156, 157], we did not see any change for these genes in Mtb (**Dataset 3.2**). Another interesting difference between the transcriptional profile of HC2210 in Mab and Mtb is the expression of genes involved in respiration. While we saw the downregulation of genes that codes for the different subunits of the ATP synthase complex and those that make up the succinate dehydrogenase complex in Mtb (**Figure A.3.4; Dataset 3.2**), we did not see any significant movement in these genes or any other respiratory genes in Mab (**Figure A.3.4; Dataset 3.2**). Collectively, these data suggest that HC2210 may be inhibiting the growth of Mab by targeting the biosynthesis of envelope lipids and causing oxidative stress; while in Mtb, inhibition of lipid biosynthesis as well as respiration might be the major means by which the compound inhibits the growth of the pathogen.

Discussion:

This current study defines the antimycobacterial activity of HC2210 and related nitrofuranyl piperazines against Mab. Using forward genetic selection, we showed HC2210 depends on the cofactor F_{420} machinery, and presume that it acts as a prodrug that needs to be reductively activated, as similarly reported for the nitrofuranyl piperazines in Mtb[15]. The reductive activation of many nitro prodrugs is usually catalyzed by nitroreductases that utilize the reducing power of different cofactors. Ddn is a known nitroreductase that uses cofactor F_{420} to activate different nitro-containing compounds in Mtb[2, 3, 6, 7, 15, 17, 35]. In Mtb, we reported a partial resistance

of *ddn* mutants to the nitrofuranyl piperazines. There are at least 12 *ddn* orthologues in Mab (**Figure A.3.5**). Interestingly, the forward genetic selection in our current study did not give rise to mutations in any of the *ddn* orthologues in Mab. This suggests a possible redundancy in the activating nitroreductases, reducing the chance of selecting mutants in a single activating nitroreductase. Intriguingly, two F_{420}-dependent genes (*MAB_1339* and *MAB_4636*) were significantly upregulated by HC2210 treatment in Mab (**Figure 3.5C**). While none of these genes are *ddn* orthologues, they are annotated to have quinone reductase activity, thus having the possibility of serving as nitroreductases. Despite the logical candidacy of these genes as activators of HC2210, future studies in our lab will adopt an unbiased whole genome-based approach to decipher the nitroreductase(s) that activates HC2210 and other nitrofuranyl piperazines in Mab.

Selection of HC2210 resistant mutants also identified mutants in *glpK*. This gene has previously been shown to promote resistance to clofazimine in Mab[135]. The function of *glpK* in Mab physiology is poorly characterized, however, it is well studied in Mtb[141]. *glpK* mutants in Mtb are associated with small colony morphotypes[48], a phenotype that we also observed for our Mab *glpK* mutants (**Table 3.2**). In Mtb, *glpK* mutants are unable to grow well in glycerol, but over time, these mutants revert to the wildtype phenotype due to the homopolymeric nature of the gene[48, 141]. Mtb *glpK* mutants are also known to be tolerant to many antibiotics, including isoniazid, rifampicin, ethambutol, and moxifloxacin[48, 141]. We report the same for Mab, where the HC2210-derived *glpK* mutants exhibit strong resistance to HC2210 and more modest resistance to rifabutin, moxifloxacin, and amikacin. Lastly, glycerol potentiates the activity of many antimycobacterial compounds in Mtb[141], an observation that we replicated for HC2210 and analogs in Mab. Notably, glycerol is associated with more rapid growth in Mab, and we have yet to determine if the enhanced sensitivity to HC2210 in the presence of glycerol is due to differences in growth or a mechanism specific to glycerol metabolism. Future studies in our lab will be

dedicated towards understanding the role of GlpK and glycerol in the antimycobacterial activities of HC2210 against Mab.

Additionally, we showed that HC2210 had varying levels of potency against multidrug-resistant clinical isolates of Mab, and this is independent of the glycopeptidolipid-driven colony morphology[158]. A similar observation was made by another group for first-line drugs such as amikacin, clarithromycin, and cefoxitin that maintain similar activity against smooth and rough Mab morphotypes[159]. In the same study, tigecycline showed a morphotype-dependent activity against Mab[159], although the molecular basis was never worked out. While the activity of HC2210 is independent of the colony morphology, the varying potencies of the compound against the clinical strains warrants a detailed molecular examination to define the driving factors. This will aid in the design of HC2210 analogs that will retain their potency across different clinical isolates of Mab.

In Mtb, nitro-containing drugs are proposed to act by targeting the biosynthesis of envelope lipids and respiration, with the latter being the predominant antimycobacterial activity in anaerobic conditions. However, our transcriptional profiling of HC2210-treated Mab shows that none of the respiratory cytochromes or dehydrogenases were impacted by HC2210, suggesting that the compound may not be targeting respiration in Mab. This hypothesis is supported by observed bacteriostatic activity of HC2210, whereas inhibitors of respiration in Mtb are usually cidal. The transcriptional signature of HC2210 in Mab is mostly composed of genes involved in lipid metabolism, indicating that the compound primarily inhibits the bacteria by targeting the biosynthesis of different cell envelope lipids. This leaves open the question of how the lipid composition of the mycobacterial envelope is impacted by HC2210. In Mtb, pretomanid is known to deplete the level of ketomycolates, leading to the accumulation of the hydroxmycolates precursors[23, 40]. Future studies in our lab will use thin layer chromatography and mass spectrometry to profile the lipid composition of HC2210-treated Mab and Mtb cultures. Studies

will also be prioritized to understand why the expression of respiratory genes in Mab do not move in response to the hypothetical release of the nitric oxide electron sink by HC2210. It is possible that the inability of HC2210 to inhibit respiration in Mab compared to Mtb is responsible for the bacteriostatic versus the bactericidal activities of the compound seen in each species, respectively.

Additionally, the activation of nitro prodrugs is usually associated with the release of nitric acid radicals that inhibit the growth of the bacteria. In return, the bacteria protect itself against these radicals through the activities of its antioxidant systems. Not surprisingly, genes linked to resistance against oxidative stress were also significantly upregulated by HC2210 in Mab. In Mtb, SigH is known to control a regulon of genes that enables the bacteria to survive different harsh conditions including oxidative stress[62, 160]. However, this gene was not impacted by HC2210 or pretomanid treatment in Mtb, and the reason for this discrepancy is yet to be determined. In any case, the increased expression of *sigH* in Mab has been associated with the resistance of Mab against tigecycline[156, 161]. It is possible that HC2210 will cause Mab to become less sensitive to tigecycline. Therefore, the *in vitro* pharmacodynamic interaction of HC2210 with other drugs need to be properly studied through a comprehensive drug-drug combination study. Overall, we have provided initial mechanistic insights into the activities of HC2210 against Mab that support possible development of this series as drugs for Mab infections.

Materials and Method:

Culture conditions, strains, and compounds

Unless otherwise specified, *Mycobacterium abscessus* (Mab) ATCC 19977 was used in this study and was grown shaking in 7H9 Middlebrook medium supplemented with 10% oleic acid-albumin-dextrose-catalase (**OADC**), 0.05% Tween 80, and with or without 0.2% cycloheximide at 35°C – 37°C. Streptomycin-resistant CDC1551 *M. tuberculosis* (Mtb) culture was grown in standing vented flasks of 7H9/OADC media at 37°C and 5% CO_2.

In vitro dose response study of the compounds

Mab cultures were aliquoted (0.2 mL) into 96-well assay plates to an initial optical density (**OD**) of 0.1. Starting at 80 µM, the cultures were treated with an 8-point (2.5-fold) dilution series of the nitrofuranyl piperazines (HC2209, HC2210, HC2211) or other drugs such as bedaquiline, rifabutin, amikacin amongst others. For comparative study of some of the most potent compounds, an 11-point (2.5-fold dilutions) starting from 40 µM was used. The treated cultures were incubated for 3 days at 37°C. After incubation, the optical density (OD) of the cultures was measured in a plate reader (PerkinElmer Enspire) at 595nm, and the growth of the cultures was normalized based on the OD relative to a amikacin-positive control (100% growth inhibition) and a DMSO-negative control (0% growth inhibition). The half-maximal effective concentrations (EC_{50s}) of each compound were determined by fitting the normalized data to a four-parameter logistic equation using GraphPad Prism software package.

Dose-dependent killing assay

The Mab culture was first diluted to an initial OD of 0.1 OD and dispensed in 5 mL aliquots into T25 vented flasks. The culture was treated with five different concentrations of HC2210 (80 µM, 32 µM, 12.8 µM, 5.2 µM, and 0.08 µM), a single concentration of amikacin (20 µM) as positive control, and an equivalent volume of DMSO as a negative control. After 4 days of incubation at 35°C (200 rpm), the cultures were diluted serially in phosphate-buffered saline-Tween-80 solution and plated for colony forming units (CFU) in 7H10/OADC agar quadrant plates. The bactericidal activity was determined by comparing the CFU of the initial inoculum to the bacterial CFU after treatment.

Isolation of resistant mutants

The isolation and confirmation of resistant mutants were done as previously described with slight modifications[130]. Briefly, different volumes (0.05 mL, 0.1 mL, and 0.2 mL) of a growing Mab culture (OD = 0.1) were inoculated onto 7H10/OADC agar plates containing 80 µM and 200

µM of HC2210, or 0.25 mL of Mab culture (OD = 0.1) on 10 µM and 20 µM of HC2210. The plates were incubated at 37°C until colonies appeared. Colonies were randomly picked from each plate and grown in 7H9/OADC broths. The broth cultures were subjected to a dose-response study using HC2210 as previously described above. Resistance was confirmed by an increase in the EC_{50s} of the mutants when compared to that of the Mab WT culture.

Whole-genome sequencing and analysis

The genomic DNAs of the confirmed resistant mutants and the Mab WT control were extracted and submitted for Illumina-based whole-genome sequencing. The breseq computational pipeline was used to analyze the sequence reads and identify single-nucleotide variations [131, 132]. Mab ATCC 19977 reference genome was used in the analysis. After subtracting the mutations shared by the resistant mutants with the Mab WT control, all the unique mutations in the resistant mutant strains were identified.

Growth of *glpK* mutants

In order to confirm that the *glpK* Mab mutants are unable to utilize glycerol, the mutants and the WT cultures grown in 7H9OADC media were harvested by centrifugation and washed to remove residual 7H9OADC. This was followed by the resuspension of the pellets in minimal media containing either 10 mM of glycerol or glucose as the sole carbon source to a fixed starting OD of 0.1 in T25 flasks. The cultures were incubated shaking at 37°C and the optical density is monitored over the span of 12 days.

Transcriptional profiling

Mab cultures were treated in two biological replicates with 10 µM of HC2210 and an equivalent volume of DMSO for 24 hours at T25 standing flasks in 37°C incubator (without 5% CO_2). The same is done for Mtb cultures except that 2 µM of HC2210 is used and cultures were incubated in T25 standing flasks at 37°C, 5% CO_2 for 24 hours. After treatment, the pellets were harvested, and the bacterial RNA was extracted using the TRIzol-based protocol as previously

described[162]. The sequencing reads were analyzed using the commercially licensed CLC Genomics Suite and are presented in Dataset 3.1 (for Mab) and Dataset 3.2 (for Mtb).

CHAPTER FOUR: HC2250 is a putative DprE1 inhibitor with a secondary mechanism of action and *in vivo* efficacy in a murine model of tuberculosis

This work is in preparation for journal submission as a Brief Report. The authors and their affiliations are listed below:

Ifeanyichukwu E. Eke[1], Bassel Abdalla[1], Veronica Albrecht[1], Adam Kibiloski[1], Heather Murdoch[1], Alexandria Oviatt[1], Matthew Giletto[2], Edmund Ellsworth[2], and Robert B. Abramovitch[1]*

[1]Department of Microbiology, Genetics, and Immunology, and [2]Department of Pharmacology and Toxicology, Michigan State University, East Lansing, Michigan, 48824, United States.

Contributions:

I.E.E. and R.B.A. conceived and designed the studies. **I.E.E.** conducted the *in vitro* and genetic characterization studies. **I.E.E.,** B.A., V.J.A., A.K., H.M.M., and A.O. conducted the *in vivo* efficacy study. M.G. and E.E. synthesized the compound. **I.E.E.** and R.B.A. wrote the manuscript.

Abstract:

The decaprenylphosphoryl-D-ribose epimerase complex (**DprE1/DprE2**) participates in an epimerization reaction, forming arabinofuranosyl donors that are used in the biosynthesis of important cell wall components such as arabinogalactan and lipoarabinomannan. Owing to the essential role of this reaction in *Mycobacterium tuberculosis* (**Mtb**), inhibitors that target the complex have been prioritized in tuberculosis (**TB**) drug discovery. We have previously reported HC2250 as a putative DprE1 inhibitor. In this current study, we show that HC2250 has DprE1-independent activity in hypoxic conditions, exhibiting a dose-dependent bactericidal activity against dormant Mtb. We also showed that resistant mutants against HC2250 can only be generated in a *dprE1* mutant background, further highlighting that the compound has a secondary mechanism-of-action. Genome-wide transcriptional profiling of HC2250-treated cells revealed that the compound impacts genes that are involved in respiration, lipid metabolism, and stress response. About 50% of the transcriptional profile of HC2250 overlaps with that of a known DprE1 inhibitor, providing additional evidence that HC2250 is a putative DprE1 inhibitor with a secondary activity. In an acute murine model of TB infection, HC2250 was effective in reducing the mycobacterial burden of the lungs of the infected mice by ~0.8 log, supporting further development of the compound as a potential TB drug.

Introduction:

The *Mycobacterium tuberculosis* (**Mtb**) decaprenylphosphoryl-β-D-ribose oxidase (**DprE1**) and decaprenylphosphoryl-D-2-keto-ribose reductase (**DprE2**) proteins form a heteromeric epimerase complex involved in the production of decaprenylphosphoryl-D-arabinose, the only known source of arabinofuranosyl moieties used in the biosynthesis of arabinogalactan and lipoarabinomannan[10, 11, 44, 45, 49, 50, 52-59]. This epimerization reaction is proposed to occur at the periplasmic region of the bacterial cell envelope[55], highlighting the vulnerability of the complex as a therapeutic target. Indeed, many nitro-containing scaffolds that target DprE1 has been discovered, and they include nitrobenzothiazinones, dinitrobenzamides, trinitroxanthones, nitrobenzoquinoxalines, nitrotriazoles, and nitrobenzothiazoles [11, 12, 15, 45, 50, 52, 55, 60, 61]. Recently, we have reported HC2250, a nitrofuranyl hydrazide, as a putative DprE1 inhibitor[15]. Unlike other DprE1 inhibitors that lose their activity against **Mtb** in a non-replicating persistent (**NRP**) state, HC2250 retains its activity against the dormant bacteria[15].

In this chapter, we show that the bactericidal activity of HC2250 against dormant Mtb is independent of DprE1. We also demonstrate that resistant mutants against HC2250 can be selected for in a *dprE1* mutant (C384S) background, but not with WT Mtb, further highlighting that the compound likely has a secondary, DprE1-independent activity. Using RNA sequencing, we profiled the transcriptome of HC2250-treated Mtb and show that the compound impacts the expression of genes involved in respiration, lipid metabolism, and stress response. About 50% of the differentially expressed genes in the HC2250-treated cultures included those that are regulated by an unrelated DprE1 inhibitor, HC2238, supporting the possibility that part of its antimycobacterial activity is driven by DprE1 inhibition. However, a unique profile of HC2250, not shared by HC2238, supports a secondary activity that involves the modulation of genes involved in oxidative stress response. Lastly, we show that HC2250 is active against Mtb when delivered once daily and orally in an acute murine model of tuberculosis (**TB**), highlighting the possibility of

further developing this series as a potential TB drug. The ability of HC2250 to kill dormant Mtb, with potential multiple targets and a very low frequency of resistance, demonstrates potential functional advantages of HC2250 over other DprE1 inhibitors.

Results:

HC2250 has a DprE1-independent activity against non-replicating persistent Mtb

Covalent DprE1 inhibitors are known to lose their activity in the absence of a critical cysteine residue (C384) at the active site of the enzyme[10, 11, 45, 49, 52, 53, 57]. Generally, these inhibitors have a nitro group that is reductively activated into an electrophilic nitroso intermediate through the reducing activity of the FAD coenzyme of DprE1. Subsequently, a covalent bond is formed between the nucleophilic thiol group of C384 and the nitroso intermediate of the compound, inhibiting the enzyme[10, 11, 45, 49, 52, 53, 57]. Based on the loss of activity of HC2250 against a *dprE1* mutant (C384S) in replicating conditions, we have previously classified it as a covalent DprE1 inhibitor[15]. However, we also showed that HC2250 differed from other known DprE1 inhibitors in its ability to kill NRP Mtb, suggesting an additional mechanism-of-action[15]. Given this difference, we hypothesized that HC2250 will have a DprE1-independent bactericidal activity against NRP Mtb. To test this hypothesis, we used a hypoxic shift-down assay[120] and treated a spontaneous *dprE1* mutant (C384S) with different concentrations of HC2250 and compared its activity to a WT culture. This mutant also carries a mutation in the *fgd* gene that is required for activation of F_{420}-dependent nitro-containing compounds such as HC2210, pretomanid and delamanid[15]. However, we have previously shown that the Fgd does not contribute to the antimycobacterial activity of HC2250[15]. As expected, HC2250 showed a dose-dependent bactericidal activity against both the WT and the mutant (**Figure 4.1**), giving credence to our hypothesis of a secondary mechanism-of-action during hypoxia. We included dintrobenzamides (HC2226 and HC338), well-established DprE1 inhibitors, as controls in the study and confirmed that they do not have any activity against the NRP bacteria (**Figure 4.1**). Overall, this shows

HC2250 as a putative DprE1 inhibitor that acts independent of the protein under hypoxia and against non-replicating Mtb.
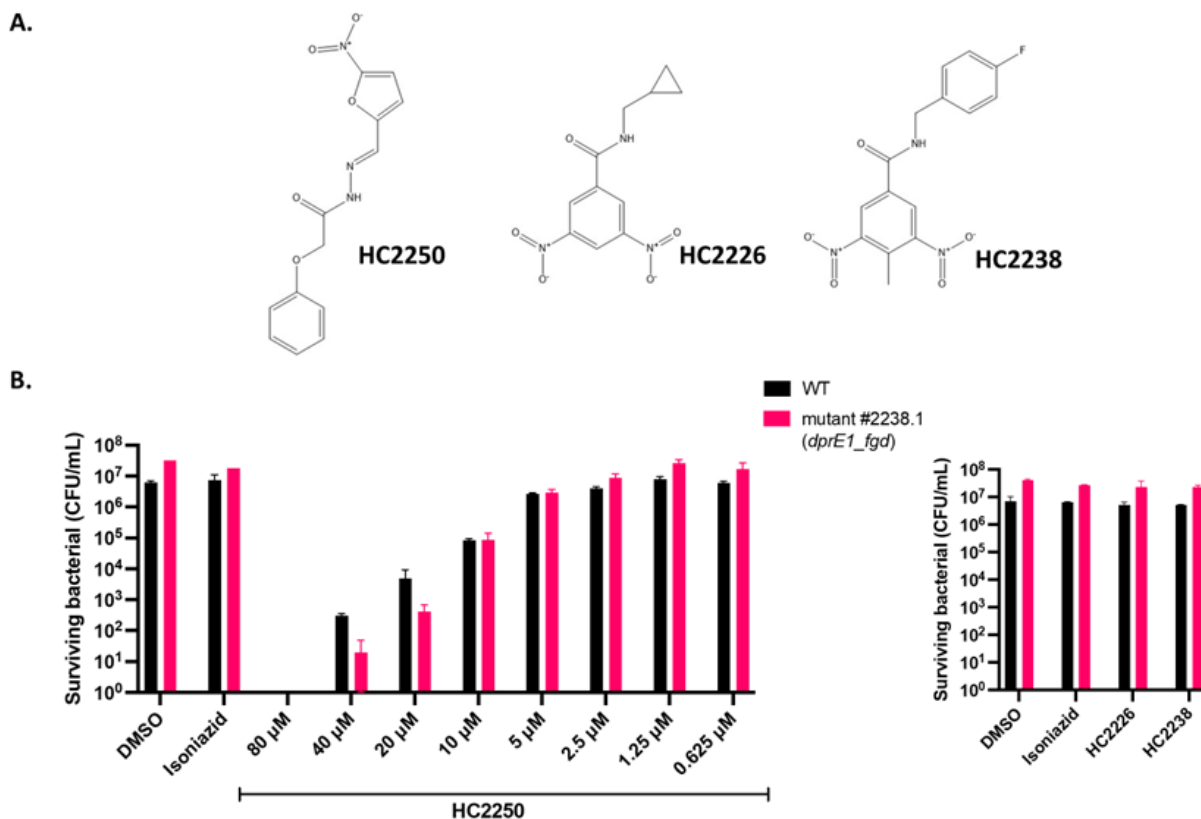
Figure 4.1. HC2250 acts independent of DprE1 in hypoxic conditions against non-replicating persistent (NRP) *M. tuberculosis* **(Mtb). A**. Chemical structures of HC2250 and two dintrobenzamide-based DprE1 inhibitors, HC2226 and HC2238. **B**. HC2250 shows a dose-dependent bactericidal activity against NRP Mtb, while the dintrobenzamides are inactive against the dormant bacteria. The error bars represent standard deviations of two biological replicates.

HC2250 resistant mutants can only be generated in a *dprE1* background

Apart from its high bactericidal activity against dormant Mtb in a hypoxic shift-down assay, our earlier work demonstrated that HC2250 also differs from other DprE1 inhibitors in the pattern of its potency loss against the spontaneous *dprE1* mutant (C384S) in replicating conditions[15]. While classical DprE1 inhibitors such as the dintrobenzamides completely lose their activity against the mutant at all the tested concentrations (80 μM – 0.131 μM), HC2250 retained its

antimycobacterial activity against the mutant at 80 μM and loses activity at lower concentrations[15].

This reinforced our initial suspicion that HC2250 might have an additional target(s). Therefore, in our bid to uncover other targets of HC2250, we used a forward genetic selection approach where we plated 1 x 10^9 CFU of WT Mtb onto 7H10 agar containing different concentrations (20 μM, 40 μM, and 100 μM) of HC2250 and allowed for resistant mutants to develop. However, this initially proved unsuccessful for HC2250 since we could not generate any resistant colonies, suggesting the frequency of resistance for the compound is less than 1 x 10^{-9}. Interestingly, when we repeated the same selection with a *dprE1* C384S resistant mutant and at higher concentrations of 100 μM and 500 μM of HC2250, resistant colonies emerged at a resistance frequency of 2.64 x 10^{-7} and 6.58 x 10^{-8}, respectively. Efforts are underway to confirm and characterize the resistant mutants. Nevertheless, the low frequency of resistance against WT Mtb and the isolation of resistant mutants in the *dprE1* mutant, are further supportive of HC2250 having a secondary mechanism of action, in addition to DprE1 inhibition.

HC2250 modulates genes involved in respiration and general stress response

Next, we conducted RNA-seq transcriptional profiling of HC2250-treated cells to decipher the cellular pathways impacted by the compound. Relative to the DMSO control and at a significance threshold of fold change > |1.5| and a false discovery rate p-value < 0.05, HC2250 impacted the expression of 223 genes (**Dataset 4.1, Figure 4.2**). Out of these significantly expressed genes, 80 were upregulated, while the remaining were downregulated. *iniB*, part of the *iniBAC* operon that is a prominent marker of cell envelope stress[5, 9, 92], was significantly upregulated, suggesting that HC2250 might be targeting the cell envelope. Indeed, we also observed the upregulation of regulatory genes that are commonly associated as part of the cellular response to envelope stress. They include *mprB*, of the MprA-MprB two-component system, and the sigma factors, *sigE* and *sigB*. MprAB is a known master regulator that induces the expression of *sigB* and *sigE* in Mtb[163]. Predictably, this will also lead to the modulation of

downstream stress-responsive genes in the bacteria as we also observed in this study (**Figure 4.2B**). Some of these stress-response genes are involved in lipid metabolism, and they include *ppe51*, *pks2*, *fadD23*, *papA1*, *fadD30*, pks6, and *lppX* amongst others[163-166]. The modulation of these genes by the HC2250 treatment suggests that the remodeling of the mycobacterial envelope lipids is part of the bacterial response to HC2250. Interestingly, *clpB*, an ATP-dependent molecular chaperone that is known as part of the mycobacterial general stress response[167, 168], was significantly upregulated by HC2250. Other oxidative stress-responsive genes that were upregulated in the study include *furA*, a ferric uptake regulator, and *trxB1*, a thioredoxin reductase. FurA and TrxB1 help in maintaining the redox balance of the bacteria in response to oxidative stress[169-171]. Thus, HC2250 might also be acting by disrupting the redox homeostasis of the cell.

To add to the mechanistic complexity of HC2250, we also saw the downregulation of genes that are part of the respiratory apparatus of the bacteria. These include the ATP synthase complex (*atpB*, *atpE*, *atpF*, *atpH*, *atpA*, *atpG*, and *atpC*) and the NADH dehydrogenase I (*nuoA*, *nuoA*, and *nuoK*). Others are *sdhC*, a member of the succinate dehydrogenase complex; *cydB*, a subunit of the oxygen high-affinity terminal cytochrome *bd* oxidase; and members of the mycobacterial cytochrome P_{450} system such as *cyp128* and *cyp121*. The downregulation of these respiratory genes is a transcriptional hallmark of most nitro-containing compounds [5, 9, 40, 92], and is not surprising that we also observed it with HC2250. Interestingly, *menE*, a gene involved in the biosynthesis of menaquinone, was upregulated. In addition to its role as an electron carrier during respiratory cycle, menaquinone can also serve as part of the bacterial resistome against oxidative stress[18], explaining for its upregulation in our study.
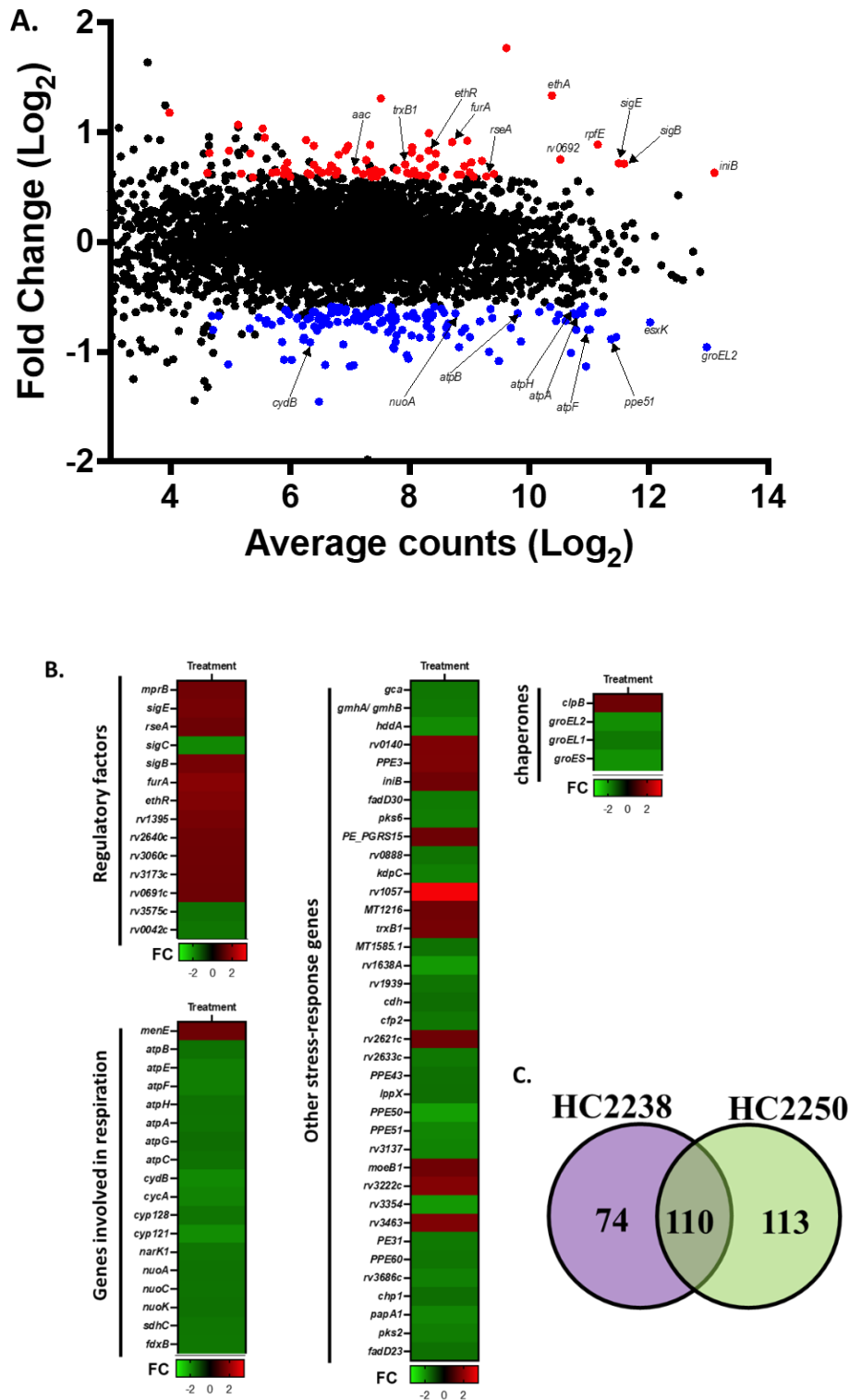
Figure 4.2. Transcriptional profiling of _M. tuberculosis_ (Mtb) cultures that were treated with HC2250 or DMSO control. **A.** Magnitude-amplitude plot of differentially expressed genes in HC2250-treated cultures relative to the DMSO control at a significance threshold of q < 0.05 and fold change > |1.5|.

Figure 4.2. (cont'd)
The red circles indicate the upregulated genes while the blue circles are the downregulated genes. **B.** Heatmap of some differentially expressed genes in the HC2250-treated Mtb cultures at a significance fold change > |1.5| and q < 0.05. **C.** Pie-chart of the differentially expressed genes in HC2238- and HC2250-treated cultures (fold change > |1.5| and q < 0.05).

Going further, we decide to determine the transcriptional profile of cultures treated with HC2238, a putative DprE1 inhibitor that is inactive against NRP Mtb (**Figure 4.1B**) and compare it to the HC2250-treated Mtb. At the significance threshold of fold change > |1.5| and a false discovery rate p-value < 0.05, HC2238 impacted the expression of 184 genes. When we compare to the transcriptional profile of the HC2250-treated Mtb, 110 genes were found to overlap in both treatments (**Figure 4.2C, Dataset 4.1**). This represents ~50% of the transcriptional profile of HC2250 treatment and ~60% of the HC2238-impacted genes. A closer examination at these overlapping genes showed that they include genes involved in lipid metabolism (*ppe51*, *pks2*, *fadD23*, *papA1*, *fadD30*, pks6); respiration (*atpE*, *atpF*, *atpH*, *atpC*, *nuoA*, *nuoC*, *nuoK*; *cydB*), and transcriptional factors such as *mprB* and *sigB*, all of which we have previously observed for HC2250 (**Dataset 4.1**). This further lends credence to the fact that HC2250 is a putative DprE1 inhibitor. However, genes such as *sigH*, *furA*, *clpB*, and *trxB1* did not meet the statistical cutoff in the HC2238-treated cells, an important difference from the HC2250-treated cells where these four genes were significantly upregulated. This suggests that HC2250 might be playing greater roles in causing oxidative stress since these genes are involved as part of the bacterial response to this stress[167-171]. Overall, HC2250 impacts the expression of genes involved in the general stress response of the bacteria as well as those linked to respiration and lipid metabolism.

HC2250 has *in vivo* efficacy in an acute murine model of tuberculosis

Given the unique mechanism of HC2250 as a scaffold that putatively targets DprE1 and still retains antimycobacterial activities against dormant Mtb, we conducted a preliminary study to determine its *in vivo* efficacy. We used an acute murine model of tuberculosis where C57BL/6 mice were first infected with a low dose of Mtb Erdman (200 CFUs) through an aerosol delivery system. After one day of infection, we initiated a once-daily treatment through oral gavage with 75 mg/kg HC2250, 25 mg/kg isoniazid as a positive control, or a vehicle control (corn oil). Treatment proceeded daily for two weeks. No colonies were found from lung homogenates of isoniazid-treated mice (**Figure 4.3**), demonstrating the already known sterilizing effect of isoniazid in acute murine model of tuberculosis[172]. Compared to the vehicle control, the HC2250 treatment significantly reduced the bacterial burden of the lungs of the infected mice by about 0.83 log (*p-value* 0.006). Together, these data show HC2250 to be an orally bioavailable compound that has *in vivo* efficacy and supports its further development as a potential TB drug.
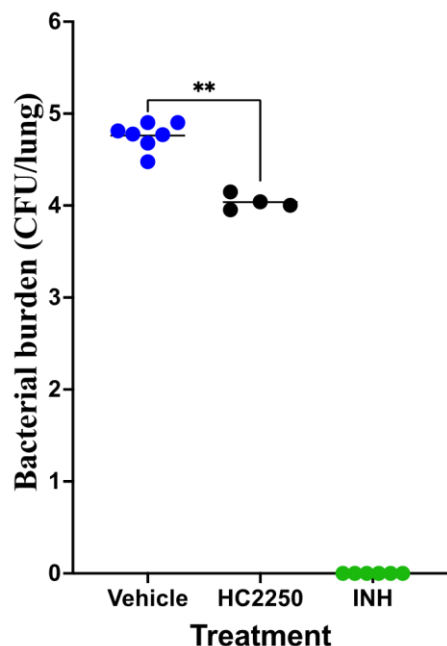
Figure 4.3. HC2250 significantly reduces the mycobacterial burden of the lungs of infected mice in an acute murine model of tuberculosis. The infected C57BL/6 mice were treated for two weeks with a corn oil/DMSO mixture as a vehicular control, 25 mg/kg isoniazid as a positive control, and 75 mg/kg HC2250. This was followed by assessing the lung mycobacterial burden of the treated mice. The bacterial burden of the isoniazid-treated mice falls below the limit of detection, indicating a sterilizing activity. When compared to the vehicular control in a non-parametric Mann-Whitney U test, HC2250 significantly reduced the mycobacterial burden of the mice by ~0.8 log (**p < 0.05).

Discussion:

TB pathogenesis is usually characterized by the formation of the granuloma, a pathological structure that is characterized by a low oxygen tension[173, 174]. Mtb, a strictly aerobic pathogen, normally responds to this hypoxic environment by remodeling its physiology to a non-replicating persistent state that is non-responsive to many antibiotics[173, 174]. Since DprE1 is involved in cell wall biosynthesis only during replication, it makes sense that DprE1 inhibitors are inactive against dormant Mtb[15]. We observed this in our earlier report for dintrobenzamides, but also pointed out that HC2250, a nitrofuran-based putative DprE1 inhibitor, is bactericidal against dormant Mtb[15]. In this current study, we showed that the bactericidal activity of HC2250 against NRP Mtb is independent of the DprE1 target. The molecular details for the activity of HC2250

against the *dprE1* mutant (C384S) in hypoxic conditions remain unknown. The secondary mechanism-of-action of HC2250 will probably become clearer when we follow up with the resistant mutants that we have raised against the compound.

Adding to the possibility that HC2250 has a secondary target is our inability to generate resistant mutants to the compound in a WT background. We could only raise mutants when we used a *dprE1* mutant. It is notable that HC2250 has a very low frequency of resistance since this could translate to a higher clinical longevity and efficiency. However, we call for caution until all the genes that may be driving the resistance are characterized. This is due to the possibility that the resistance to the compound might be driven by an efflux-pump mechanism, conferring cross-resistance to other drugs[175].

Our transcriptional profiling of HC2250-treated cultures shows that the compound impacts respiration, lipid metabolism, and induces the stress response network of the bacteria. Biochemical assays involving the measurement of the ATP levels of HC2250-treated cells, membrane potential, reactive oxygen species, as well as membrane lipid profiling are needed to validate this observation.

The observed *in vivo* efficacy for HC2250, although modest, is surprising given the relatively low potency against replicating Mtb *in vitro* (EC_{50} of 5 µM)[15]. Notably, in infected macrophages, HC2250 had an EC_{50} of < 330 nM[15], supporting the possibility that host immune pressures may sensitize Mtb to killing by HC2250. It is also possible that HC2250 has favorable pharmacokinetic properties that translate to high levels or long periods of exposure to Mtb in the lungs. Further preclinical development studies are required to optimize HC2250. This might include structure-activity relationship studies to develop new analogs with the goal of achieving higher potency, metabolic stability, and desirable pharmacokinetic parameters. Additionally, given the ability of HC2250 to kill NRP Mtb, it will be important to examine efficacy in animal models that generate hypoxic granulomas, such as C3HeB/FeJ mice[176-178]. Nevertheless, the *in vivo*

efficacy of HC2250 provides proof-of-concept that the series is a strong starting point for such studies. Overall, given the activity of HC2250 against NRP Mtb, the low frequency of resistance and its oral-bioavailability and *in vivo* efficacy, these findings support further development of HC2250 as a potential TB drug.

Materials and Methods:

Culture conditions, strains, and compounds

Unless otherwise specified, streptomycin-resistant or wild type Erdman and CDC1551 Mtb strains were used. The strains were maintained in 7H9 Middlebrook medium supplemented with 10% oleic acid-albumin-dextrose-catalase (**OADC**), 0.05% Tween 80, and with or without 0.2% cycloheximide and were incubated at 37°C and 5% CO_2 in standing vented flasks.

Hypoxic shift-down assay to test activity against NRP Mtb

The hypoxic shift-down assay [120] was used to generate NRP bacilli and was performed as previously described with slight modifications [113]. Briefly, 0.2 mL aliquots of Streptomycin-resistant Erdman *dprE1*/*fgd* mutant culture in 7H9/OADC medium was dispensed into 96-well assay plates to an initial OD of 0.25. A WT CDC1551 was used as a control. The cultures were incubated at 37°C in an anaerobic chamber (BD GasPak). At 4 days of incubation, cultures have become completely anaerobic as indicated by the methylene blue indicator becoming colorless. This was considered to be the first day of anaerobiosis. Subsequently, different concentrations of HC2250 were added to the cultures and incubated for 10 days in the anaerobic chamber. Isoniazid, DMSO, HC2226, and HC2238 were included as controls in the study. The surviving bacterial CFU at different treatments was enumerated at day 10 by plating onto 7H10/OADC agar.

Isolation of resistant mutants

The isolation and confirmation of resistant mutants were done as previously described [130]. Briefly, 1×10^9 CFU of WT culture or *dprE1* mutant was plated onto 7H10/OADC agar plates containing different concentrations of HC2250. The plates were incubated at 37°C for more than

8 weeks or until colonies appeared. After counting the colonies, the plates were stored in the fridge (4°C) until needed.

Transcriptional profiling

CDC155 Mtb WT cultures were resuspended in 10 mL 7H9OADC at an optical density of 0.4. The cultures were treated in two biological replicates with 2 µM of HC2250 and an equivalent volume of DMSO for 24 hours at 37°C, 5% CO_2 in T25 standing flasks. The same is done for HC2238. After treatment, the pellets were harvested, and the bacterial RNA was extracted using the TRIzol-based protocol as previously described[162]. The sequencing reads were analyzed using the commercially licensed CLC Genomics Suite and are presented in Dataset 4.1.

Evaluation of the efficacy of HC2250 is an acute murine TB infection model

All animal studies were approved by the Michigan State University Institutional Animal Care and Use Committee. Female, ~8-week-old C57BL/6 mice purchased from Jackson Laboratories were used in this study. Low dose infection was initiated by aerosol exposure to 200 CFU of *M. tuberculosis* Erdman strain using a Glas-Col aerosol inhalation exposure device. Treatment was initiated one day after infection by administering the mice with oral doses of the vehicle (corn oil/5% DMSO), 75mg/kg of HC2250, or 25mg/kg isoniazid through oral gavage. The mice were dose once daily for 14 days, followed by euthanasia to harvest the lungs. The harvested lungs were homogenized, and the mycobacterial burdens of the lungs were assessed by enumerating CFUs. The mean differences between the groups were compared in the non-parametric Mann-Whitney U test.

CHAPTER FIVE: Functional Characterizations of *Mycobacterium tuberculosis* inhibitors discovered in the Molecular Libraries Small Molecule Repository

This work is in preparation for journal submission, and the authors and their contributions are listed below:

Ifeanyichukwu E. Eke[1], John T. Williams[1], Robert B. Abramovitch*

Department of Microbiology, Genetics and Immunology, Michigan State University, East Lansing, Michigan, 48824, United States.

[1]*Authors contributed equally to this study.*

I.E.E., J.T.W., and R.B.A. conceived and designed the studies. J.T.W. conducted the targeted mutant screening and prioritization studies including the eukaryotic cytotoxicity and *ex vivo* assay; **I.E.E.** conducted the cheminformatic analyses and Pks13 studies. I.E.E. J.T.W., and R.B.A. wrote the manuscript.

Abstract:

High-throughput screening (**HTS**) of small molecules is a starting point for many drug development pipelines, including tuberculosis. These screens normally result in multiple hits whose mechanisms-of-action remain unknown. From our initial HTS of the Molecular Libraries Small Molecule Repository (**MLSMR**), we cherry-picked 935 compounds that inhibited the growth of *Mycobacterium tuberculosis* and set out to provide an early assessment of their mechanism-of-action. To characterize the MLSMR Mtb growth inhibitors, our approach involves a combination of cheminformatics and targeted mutant screening against mutants in *katG*, *hadAB*, and a mixed pool of *mmpL3* mutants. As a validation of this approach, we identified 101 isoniazid analogs that predictably lose all their antimycobacterial activities against the *katG* mutant. Interestingly, 8 isoniazid analogs retain part of their activity against the mutant, suggesting an alternative KatG-independent mechanism. Our method also identified new compounds belonging to already known scaffolds that target HadAB or MmpL3. Additionally, we explored the nitro-containing compounds in our dataset and discovered nitrofuranyl benzothiazoles that show enhanced activity against the *mmpL3* and *katG* mutants, a phenomenon known as collateral sensitivity. Overall, this study will serve as an important resource for further follow-up studies of antitubercular small molecules in the MLSMR library and provide a well-characterized training set for artificial intelligence-driven antimycobacterial drug discovery.

Introduction:

The rising incidence of drug-resistant tuberculosis (**TB**) demands the development of new TB drugs[179]. Central to this effort are high-throughput screening (**HTS**) campaigns of different molecular libraries for agents that inhibit the growth *of Mycobacterium tuberculosis* (**Mtb**), followed by preclinical secondary assays to prioritize hits, and mechanism-of-action studies to decipher the molecular targets of prioritized hits.

We previously conducted a HTS of a collection of ~340,000 compounds from the National Institutes of Health Molecular Libraries Small Molecule Repository (**MLSMR**) to identify inhibitors of the DosRST two component regulatory system[113]. This screen was conducted using the Mtb CDC1551(*hspX'::GFP*) reporter strain that exhibits hypoxia-inducible, DosRST-dependent fluorescence. In this screen, we identified several distinct classes of inhibitors that selectively inhibited fluorescence, but not growth. These inhibitors directly targeted the DosS and DosT sensor kinases or the DosR response regulator to inhibit the signaling pathway[113, 180]. However, the screen also identified numerous compounds that inhibited Mtb growth, presumably independent of DosRST. Since the DosRST signaling pathway is not required for growth under the screening conditions, these compounds potentially represent new Mtb growth inhibitors. Notably, a subset of these compounds was previously screened for growth inhibition of Mtb under different conditions[181, 182].

In the current study, we sought to characterize 935 Mtb growth-inhibiting compounds identified from the HTS. Cherry-picked samples of these 935 inhibitors were subjected to functional and chemoinformatic characterizations and are henceforth referred to as the MLSMR Mtb inhibitors. To functionally characterize the MSLMR dataset, the compounds were initially examined in a series of dose-response secondary assays for *in vitro* potency against Mtb; *ex vivo* activity against Mtb in macrophages; and cytotoxicity in macrophages. Next, we sought to characterize the mechanisms-of-action of the compounds. Forward genetic selection is commonly

used to identify the molecular targets of antimycobacterial compounds. However, this method is limited by the slow-growing nature of Mtb, with resistant colonies taking several weeks to develop[183]. With the large number of MLSMR Mtb inhibitors, it is laborious to use forward genetic selection to characterize their molecular targets. Previously, we successfully used a targeted mutant screening approach to identify inhibitors that target MmpL3, an essential mycobacterial protein[130]. This method is amenable to HTS and involves the simultaneous screening of prioritized hits against a wildtype (**WT**) Mtb culture and a pooled mutant library of a specific gene. After screening, the potency of the hits against the WT and mutant library is compared. The working principle of this approach is that the mutant pool will be cross-resistant to the molecules that target the disrupted gene but will retain its susceptibility against other molecules. Due to the success of this method in revalidating already known MmpL3 inhibitors and discovering new scaffolds[130], we extended this approach to functionally characterize the MLSMR Mtb inhibitors.

Using an 8-point dose-response, we tested the MLSMR Mtb inhibitors for activity against an *mmpL3* mutant pool, *katG* transposon mutant, and *hadAB* mutants, and compared the potency of the compounds with that against the WT. This approach, coupled with cheminformatic analyses, provided an early mechanism-of-action assessment of some compounds in the dataset, *vis-à-vis* putative MmpL3 inhibitors, isoniazid-like compounds, and putative HadAB inhibitors. For instance, it identified already known scaffolds that target MmpL3 or HadAB, or that depend on KatG for activation, establishing the reproducibility of the approach. It also uncovered new scaffolds that putatively target MmpL3 or HadAB, or that depend on KatG for activation. We also identified compounds that exhibited enhanced activity against the mutants, a phenomenon known as collateral sensitivity. Lastly, given their proven utility as TB drugs, we provide a detailed analyses of some nitro-containing scaffolds in the dataset. Overall, this study will serve as an important resource for further prioritization and follow-up studies of MLSMR Mtb inhibitors. Additionally, this well-characterized resource should prove useful as a training set for artificial intelligence-driven antimycobacterial drug discovery.

Results and Discussion:

In vitro and _ex vivo_ efficacy of the MLSMR Mtb inhibitors and eukaryotic cytotoxicity

Our previous single-dose HTS of the ~ 340,000-compound NIH's MLSMR library resulted in about 15,000 compounds that showed >50% inhibition of the growth of Mtb[113]. Full screening results are publicly available at the PubChem database accession AID 1159583. From these ~15,000 growth inhibitors, we cherry-picked 935 compounds and henceforth referred to them as the MLSMR Mtb inhibitors (**Dataset 5.1**). To confirm the efficacy of these compounds, we examined Mtb growth inhibition, using an 8-point dose response, against extracellular and Mtb growing in infected primary bone marrow-derived macrophages. The growth inhibition values of some of the compounds could not be fitted into the four-parameter logistic equation that is normally used in calculating the half-maximal effective concentration (EC_{50}); therefore, we opted to use the area under the curve (**AUC**) as a relative measure of the potency of the compounds. We had previously used this approach to compare the potency of MmpL3 inhibitors against WT and _mmpL3_ resistant mutant pool, with the MmpL3 inhibitors having a large AUC when tested against the WT and a smaller AUC against the mutant pool[130]. Therefore, it follows that compounds with lower EC_{50} values will normally give rise to larger AUC values. However, care should be taken with this interpretation since this is only a relative measure of potency, and the EC_{50} remains the standard potency measure of a compound.

Using an arbitrary AUC cutoff of 25 for classification, 83% (n = 761) of the MLSMR Mtb inhibitor cherry-picks confirmed as growth inhibitors of extracellular Mtb (**Dataset 5.1**). This high confirmation rate is consistent with the high Z-factor (0.9) of the primary HTS[113]. When we analyzed for the inhibition of intracellular Mtb in bone marrow-derived macrophages, 94.4% (n = 883) crossed the 25 AUC cutoff (**Dataset 5.1**), suggesting some compounds may have higher activity in macrophages as compared to _in vitro_. To highlight some of these compounds, we divided the _ex vivo_ AUC of each of the compounds by their _in vitro_ values and plotted these ratios

against the *ex vivo* AUC values (**Figure 5.1A, Dataset 5.1**). This approach identified 58 compounds that showed higher activity against intracellular Mtb. Examination of the structures of some of these compounds showed the presence of groups that can explain for their bias towards a higher intracellular activity. For instance, **218**, shares a pyrazine ring as well as a carbonyl group like pyrazinamide, a first-line TB drug that is only active against intracellular Mtb[184, 185]. While this confirms the validity of our approach in identifying compounds with higher *ex vivo* activity, follow-up studies need to be done especially for compounds that do not have a pyrazinamide-like structure.   Next, we tested for the eukaryotic cytotoxicity of the MLSMR dataset in bone marrow-derived macrophages. About 48% (n = 445) of the tested compounds did not cross the 25 AUC cutoff, indicating limited cytotoxicity. Additionally, when we calculated the selectivity index of the compounds using the AUC values, we observed that the index values of most of the compounds (n = 812) was greater than one, indicating higher *ex vivo* activity compared to cytotoxicity (**Dataset 5.1**).
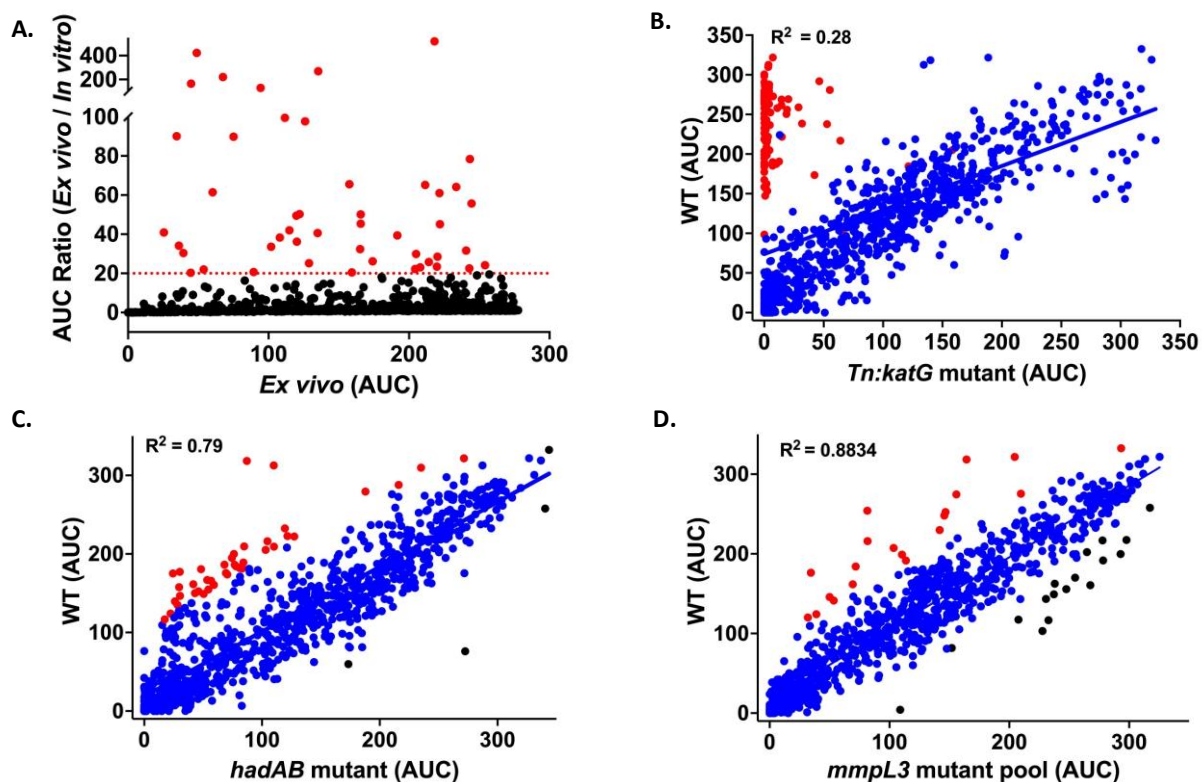
Figure 5.1. Targeted high throughput screening of the MLSMR dataset. **A.** Identification of compounds from the MLSMR dataset that have more *ex vivo* activity compared to *in vitro* activity. The AUC ratio for each compound was calculated by dividing its *ex vivo* AUC value by the *in vitro* AUC value. Those that do not cross the 20 AUC ratio cutoff are represented in black, while red indicates those that crossed the cutoff. 11 compounds are not represented here since their AUC ratio cannot be calculated (*in vitro* AUC is 0), but they can be seen in Dataset 5.1. **B.** Comparison of the activity of the compounds in the MLSMR dataset against the WT and *Tn:KatG* mutant. Those in red are isoniazid analogs, while blue represents other compounds in the MLSMR dataset. **C.** Comparison of the activity of the compounds in the MLSMR dataset against the WT and *hadAB* mutant. HadAB inhibitors are marked in red from the Mahalanobis outlier analysis, and hits that show enhanced activity against the mutant are represented in black (p value < 0.05). The rest of the MLSMR dataset are in blue. **D**. Comparison of the activity of the compounds in the MLSMR dataset against the WT and *mmpL3* mutant pool. MmpL3 inhibitors are marked in red from the Mahalanobis outlier analysis, and hits that show enhanced activity against the mutant are represented in black (p value < 0.05). The rest of the MLSMR dataset are in blue.

Targeted mutant screening and analyses

To decipher the biological activity of the MLSMR Mtb inhibitors, we screened the compounds in a dose-response against an *mmpL3* mutant pool (composed of 24 separate *mmpL3* mutants)[130], a *katG* transposon mutant that is resistant to isoniazid, and a *hadAB* mutant. By comparing the potency of the compounds against each of the mutants (**Dataset 5.2**, **Figure 5.1**), we identified outliers with significantly decreased or enhanced potency as compared to the WT.

Isoniazid and isoniazid-based compounds

When we compared the activities of the MLSMR Mtb inhibitors against the WT and the *katG Tn* mutant, we identified a distinct cluster of compounds that completely lose their potency against the *katG Tn* mutant (**Figure 5.1B**). We hypothesized that these compounds are enriched in isoniazid analogs since isoniazid is a prodrug that depends on KatG for activation into an antimycobacterial metabolite[186, 187]. It follows that without a functional *katG* gene, isoniazid will not inhibit the growth of Mtb. Indeed, a substructure similarity search identified 109 isoniazid analogs (**Dataset 5.2; Figure 5.2**), with most of them (n = 101) completely losing their activity against the *katG Tn* mutant. However, we saw some isoniazid analogs (n = 8) that retain part of their antimycobacterial activity against the transposon mutant, suggesting an additional KatG-independent system for inhibiting the growth of Mtb. These potentially multitarget compounds could be useful agents that limit the evolution of resistance. Additionally, all the 109 isoniazid analogs retain their activities against the other tested mutants (**Figure 5.2**).

A.

	WT(AUC)	mmpL3(AUC)	hadAB(AUC)	Tn:katG(AUC)
55	226.40	263.00	249.90	0.00
64	167.40	158.30	190.80	0.00
66	203.50	227.50	222.30	0.00
71	237.80	269.90	259.70	3.10
72	183.90	208.00	213.40	0.00
78	215.20	245.60	241.40	2.19
87	243.10	259.20	277.40	1.84
97	239.10	206.00	234.30	0.16
138	187.10	217.00	220.90	0.72
152	250.80	282.50	265.20	0.00
155	286.10	291.10	299.20	0.30
181	290.40	305.30	305.00	0.00
184	199.40	253.40	238.50	0.00
191	269.50	258.50	298.30	0.00
192	257.90	268.10	269.90	10.93
196	266.70	290.00	293.00	0.00
201	268.80	293.50	262.30	14.56
202	273.30	288.90	290.40	0.65
213	271.40	289.30	281.50	2.28
232	269.70	284.10	262.30	3.10
234	218.90	242.50	244.00	1.42
236	268.30	289.40	303.50	0.79
255	271.60	268.90	312.40	0.00
265	221.90	236.40	226.20	0.66
266	194.90	256.10	255.90	0.00
286	279.60	302.10	307.00	3.95
294	279.50	289.80	299.80	0.00
312	187.50	222.40	221.70	10.05
351	284.00	264.40	319.80	3.95
352	272.70	267.10	215.90	0.00
361	198.60	235.90	210.60	2.06
374	264.80	289.60	294.30	0.00
389	238.50	288.70	289.90	31.73
407	275.80	289.80	257.90	2.64
414	267.80	245.20	300.30	0.62
415	221.80	228.60	184.10	14.79
422	226.40	241.40	253.40	0.61
434	189.20	195.50	226.20	0.00
441	263.90	278.60	275.70	0.00
453	236.60	262.90	192.40	4.61
457	153.40	201.80	163.20	2.55
459	185.40	193.70	159.40	7.03
460	269.40	238.20	284.40	1.94
463	189.80	191.20	162.40	7.13
516	267.70	288.40	291.30	0.00
535	187.40	195.10	197.70	0.24
545	276.70	299.10	272.30	0.00
562	263.30	277.50	289.80	0.00
564	250.50	277.30	281.20	18.69
* 569	204.90	208.10	177.50	158.20
583	201.00	213.70	233.30	2.19
608	309.80	300.10	235.10	3.29
611	272.80	297.80	270.00	7.39
* 622	184.60	144.90	217.20	121.30
626	186.70	222.30	242.00	0.00

	WT(AUC)	mmpL3(AUC)	hadAB(AUC)	Tn:katG(AUC)
627	258.10	283.70	288.80	1.69
628	217.00	238.40	248.10	2.45
632	271.80	276.00	288.80	0.40
634	232.70	272.10	294.60	0.00
659	218.90	259.70	256.40	0.00
663	190.50	237.70	240.50	12.40
665	263.20	281.90	302.80	4.03
672	321.80	325.50	326.80	7.15
678	277.00	287.70	298.30	0.00
698	300.60	311.80	331.20	0.00
702	257.80	317.40	340.50	0.00
711	50.15	16.28	38.03	1.91
713	204.80	244.90	250.40	4.38
721	221.90	235.90	249.90	3.10
722	272.50	284.50	257.80	0.00
724	218.60	223.70	241.70	0.00
726	252.40	262.10	233.10	5.08
737	242.80	234.70	248.40	1.17
739	245.40	256.20	251.30	0.00
756	98.39	120.90	168.30	0.00
760	230.70	261.50	250.00	1.21
763	47.90	45.06	101.60	8.13
776	177.40	219.30	205.10	0.00
778	162.50	238.00	244.00	1.95
803	276.00	273.50	210.40	1.25
811	216.10	199.40	186.70	1.08
822	278.30	279.40	282.30	0.13
823	256.00	252.80	240.80	0.99
848	298.30	292.70	272.00	0.00
863	312.60	309.10	287.30	3.49
864	279.40	236.20	187.90	3.05
869	147.30	157.90	155.70	0.78
871	156.30	149.30	210.30	1.32
873	158.50	140.90	182.20	0.00
886	287.30	269.70	262.70	0.50
901	218.50	243.70	251.80	0.00
924	258.90	271.40	213.20	28.80
929	244.80	232.70	263.30	0.00
947	274.30	279.70	250.00	0.17
958	274.40	291.60	277.90	0.00
961	269.30	287.20	261.00	20.29
973	268.90	297.20	262.30	0.00
1022	287.80	301.80	216.10	4.19
1036	251.00	257.90	268.40	0.00
1044	208.60	204.10	220.00	1.83
1054	245.00	220.40	250.90	0.00
* 1061	237.70	288.20	285.50	52.81
* 1063	173.50	159.30	220.90	42.27
* 1071	103.10	227.70	181.80	65.39
1078	256.00	280.50	299.00	19.13
* 1079	291.80	243.50	298.10	46.33
* 1087	280.80	271.00	304.90	55.22
* 1101	216.80	277.80	273.60	63.99
1104	261.50	268.40	304.40	14.41

B.

569   622   1061   1063

1071   1079   1087   1101

Figure 5.2. Activity of isoniazid analogs in the MLSMR dataset against the three mutants and some representative structures. A. The activities of the isoniazid analogs in the MLSMR
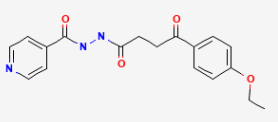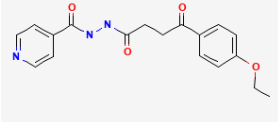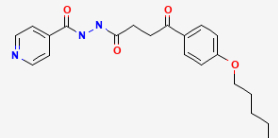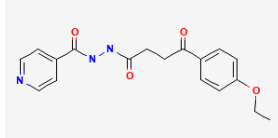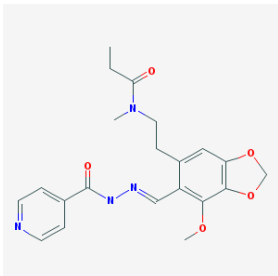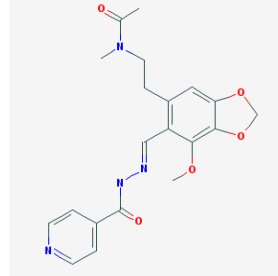
113

Figure 5.2. (cont'd)
dataset against the three mutant backgrounds. **B**. Structures of isoniazid analogs that do not completely loss their activity against the *Tn:katG* mutant (They have AUC > 40 against the *Tn:katG* mutant).

Next, we explored the structure-activity relationships of the isoniazid analogs in an activity cliff analysis. We used the Skelphere molecular descriptor of the analogs as a measure of their structural similarities, and the AUC of the analogs against the WT as a measure of the activity or potency. This activity cliff analysis gave rise to defined clusters of the analogs based on their structure-activity landscape index (**SALI**), values that are calculated from the chemical similarities of the compounds as well as their antimycobacterial activities[188]. The higher the SALI value, the more significant the change in the activity of the analogs when a minor structural modification is made. As shown in **Figure A.4.1** and **Dataset 5.3**, most of the analogs have a small SALI (<1000), indicating nonsignificant potency changes resulting from the structural modifications. However, there are some analogs that have large SALI values (>1000). These represent modifications that can be pursued by medicinal chemists to further optimize the analogs. As an example, we will discuss few pairwise comparisons here (**Table 5.1**), but all the 288 pairwise comparisons that resulted from the activity cliff analysis of the 106 isoniazid analogs can be seen in **Dataset 5.3**.
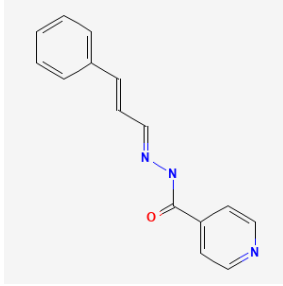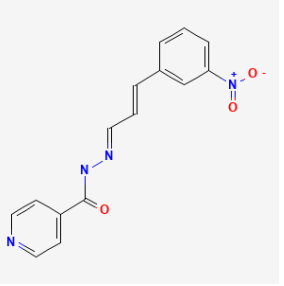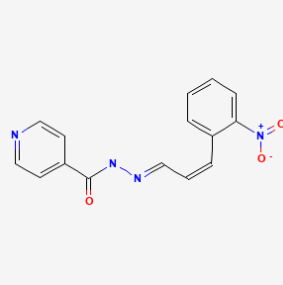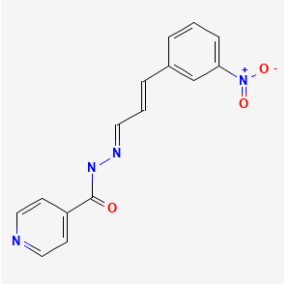
Compounds **152** and **1071** have a 97% structural similarity; however, shortening the length of the alkyl group that is linked to the phenyloxy group of the latter significantly reduced its activity (**Table 5.1**). This same pattern can also be seen for **213** and **1071**; as well as **192** and **1071**, where longer-chained alkyl groups attached to the terminal phenyl or phenyloxy groups consistently led to a higher activity against the WT. **871** and **1036** have a 96% similarity and differ only in the presence of a terminal propionamide group in the former and an acetamide group in the latter. However, **871** had a substantially higher activity than **1036**, illustrating the detrimental nature of the acetamide group. Lastly, **763** and **864** are highly similar to each other (89%) and only differ based on the position of the nitro group in their shared nitrophenyl moiety. While **864** has a 2-nitrophenyl group and had a higher activity, **763** has a 3-nitrophenyl group that is

antithetical to its antimycobacterial activity. This point is further illustrated in **71** and **763**; as well as **415** and **763** (**Table 5.1**). Notably, although beyond the scope of this study, it is possible to extend this analysis from the collection of cherry-pick compounds to all of the compounds in the MLSMR collection to identify modifications impacting activity.

Table 5.1. Pairwise comparison of some isoniazid analogs for structure-activity relationship study

Structure 1	Structure 2	Similarity	AUC 1	AUC 2	Delta Activity	SALI
152	**1071**	0.96775	250.8	103.1	147.7	4580.3
213	**1071**	0.9594	271.4	103.1	168.3	4144.9
192	**1071**	0.94314	257.9	103.1	154.8	2722.4
871	**1036**	0.9561	156.3	251	94.7	2157.2

Table 5.1. (cont'd)
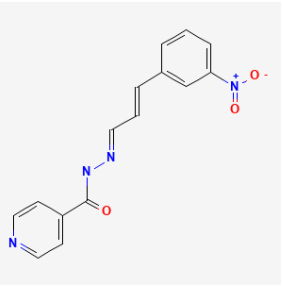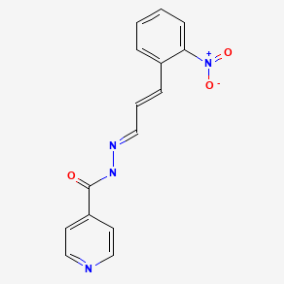
763	**864**	0.89253	47.9	279.4	231.5	2154.1
71	**763**	0.86146	237.8	47.9	189.9	1370.8
415	**763**	0.85377	221.8	47.9	173.9	1189.2

AUC 1 = Activity of compound 1 against the WT, while AUC 2 = Activity of compound 2 against the WT. Delta activity = difference in the AUC values of the two compounds. SALI = structure-activity landscape index.
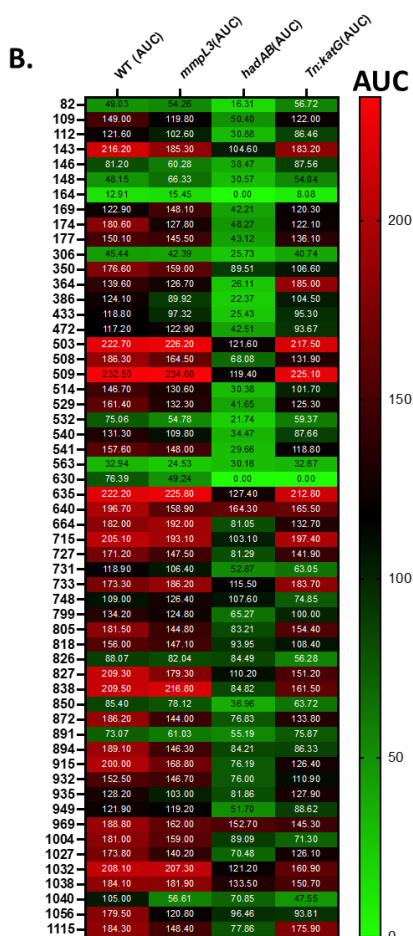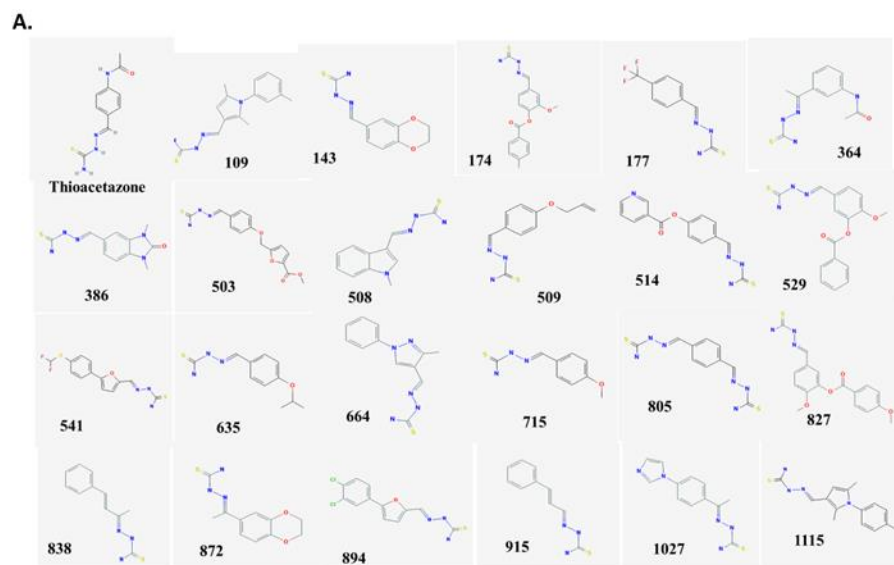
Thiosemicarbazone-containing compounds

Thioacetazone (**TAC**) is a well-known thiosemicarbazone-based bacteriostatic prodrug that had been used for TB treatment. The activating mycobacterial protein for TAC is EthA, a FAD-containing monooxygenase, and this protein also serves as the activator for ethionamide[189]. When activated, both TAC and ethionamide inhibit mycolic acid biosynthesis, targeting different proteins that are involved in the FAS-II pathway of mycolic acid biosynthesis. Ethionamide shares the

same target with isoniazid, both targeting InhA of the FAS-II pathway. On the other hand, TAC targets the HadAB or HadBC dehydratase complex of the FAS-II pathway[190-192].

Many analogs of TAC have been shown to inhibit mycolic acid synthesis[189, 192]. Therefore, it is not surprising that our outlier analysis resulted into 23 thiosemicarbazone-based compounds that showed a statistically significant reduction in their antimycobacterial activity against the *hadAB* mutant (**Figure 5.1C, Figure 5.3A, Dataset 5.2**). Reasoning that there might be other thiosemicarbazone-based compounds that have been overlooked by our stringent statistical approach, we used thiosemicarbazone as a query in a substructure similarity search of the MLSMR dataset. This resulted in an additional 33 thiosemicarbazone-containing compounds, with all of them showing reduced activity against the *hadAB* mutants (**Figure 5.3B, Dataset 5.2**). Together, our data suggests these thiosemicarbazones as putative HadAB inhibitors, although further validation is needed.

We also identified two thiazole hydrazine-based compounds (**84** and **188**) as outliers in the *hadAB* resistant mutant screen and that may be putative HadAB inhibitors (**Figure A.4.2, Dataset 5.2**). Substructure similarity search of the MLSMR dataset revealed 7 more thiazole hydrazine-based compounds that might be putative HadAB inhibitors (**Figure A.4.2B**). Additionally, **490**, a thioxo triazine, came out from our outlier analysis as a novel scaffold with less activity in the *hadAB* mutant (**Figure A.4.2, Dataset 5.2**). There are two other thioxo triazines in our dataset, but only one (**594**) showed reduced activity against the *hadAB* mutant (**Figure A.4.2B**).

Figure 5.3. Identification of thioacetazone-like compounds as putative hadAB inhibitors. **A.** Thiosemicarbazone-based compounds identified from the outlier analysis of the *hadAB* screen. The structure of the antitubercular drug, thiacetazone, is included here for comparison.
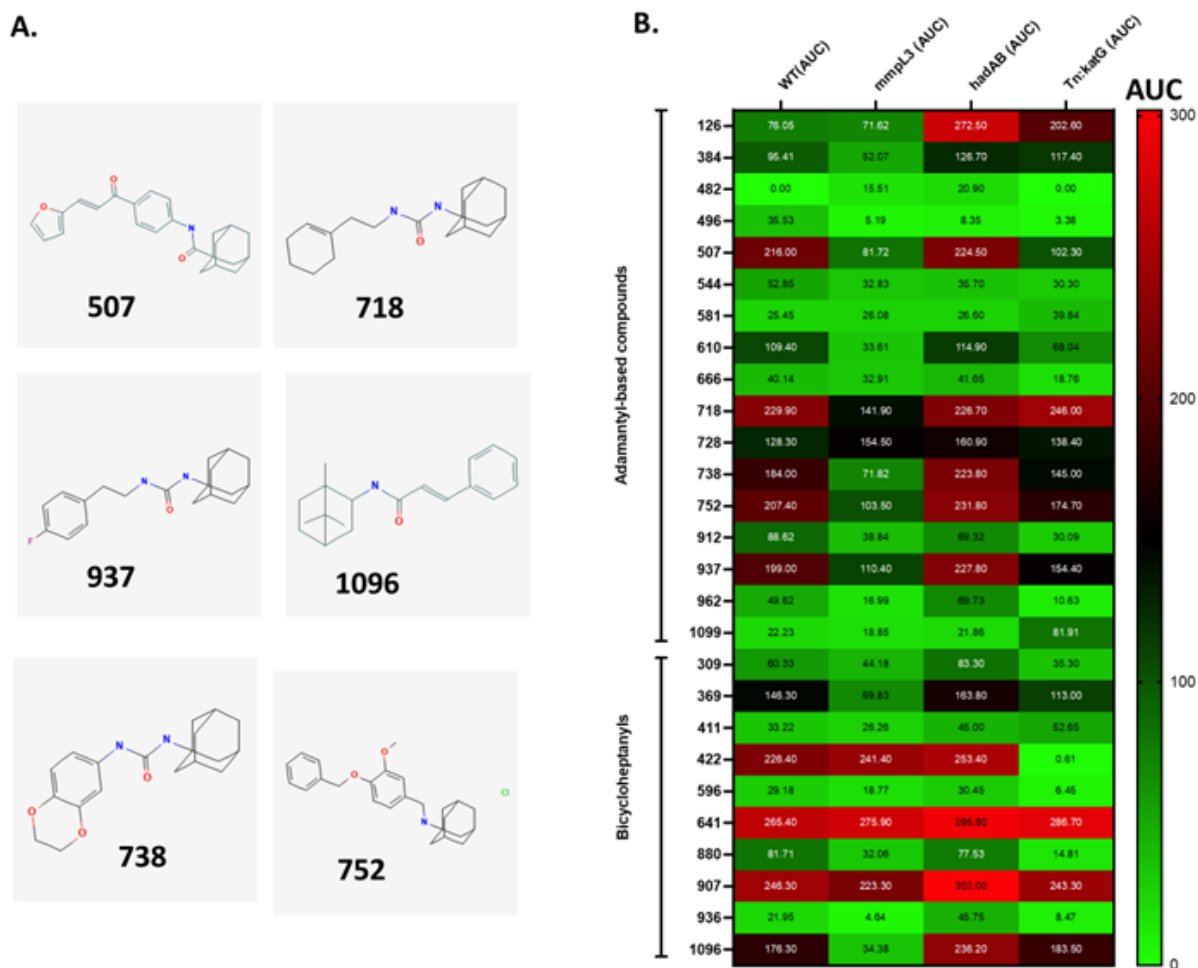
B. The activities of all the thiosemicarbazone-based compounds in the MLSMR dataset against the three mutant backgrounds.

Adamantyl-based and related compounds with resistance in the *mmpL3* mutant pool

Five adamantyl-based compounds were among the outliers that came out from our analysis of the activities of the MLSMR dataset against the WT and *mmpL3* mutant pool (**Dataset 5.2, Figure 5.4**). They are adamantyl ureas (**718**, **738**, and **937**), adamantyl carboxamide (**507**), and adamantyl amine (**752**) compounds. This is in line with numerous studies that have genetically and biochemically confirmed these adamantyl-based scaffolds as MmpL3 inhibitors[130, 183]. To identify other adamantyl-containing compounds in our dataset, we did a substructure similarity search with adamantyl as the query substructure. This gave rise to 14 additional adamantyl-based analogs (**Dataset 5.2**). However, two of these compounds contained an isoniazid backbone (**863** and **961**) and were described in the previous section as KatG-dependent (**Figure 5.2A**). Hence, we did not include **863** and **931** when we generated a heatmap of all the adamantyl-based compounds against the WT and the three mutant pools (**Figure 5.4**). In addition to the five compounds that were identified from the outlier analysis, we saw other adamantyl-based compounds that showed reduced activity against the *mmpL3* mutant. They include **384**, **496**, **544**, **610**, and **912** amongst others. Interestingly, **126**, an adamantyl thiourea, had an insignificant potency loss against the *mmpL3* pool, but showed enhanced antimycobacterial activity against the *hadAB* and *Tn:katG* mutants. This may be an example of collateral sensitivity where a compound shows enhanced activity against resistant mutants, although additional studies are required to confirm this observation. Overall, adamantyl-based scaffolds represent a rich source for MmpL3 inhibitors.

Consistent with a previous study from our lab[130], our outlier analysis also identified **1096**, a bicycloheptanyl carboxamide, as a putative MmpL3 inhibitor (**Figure 5.4**). There are other bicycloheptanyls in our dataset (**Dataset 5.2**), including those linked to a dintrobenzamide (**641**),

isoniazid (**422**), or a fluoroquinolone (**907**). As expected, **641**, **422**, and **907** are highly potent and retain their activity against the *mmpL3* mutant pool, while all bicycloheptanyl carboxamides in our dataset loses their activity against the *mmpL3* mutant (**Figure 5.4**).

A.

507 718

937 1096

738 752

B.

	WT (AUC)	mmpL3 (AUC)	hadAB (AUC)	Tn:katG (AUC)
Adamantyl-based compounds				
126	76.05	71.82	272.50	202.60
384	95.41	52.07	126.70	117.40
482	0.00	15.51	20.90	0.00
496	35.53	5.19	8.35	3.38
507	216.00	81.72	224.50	102.30
544	52.85	32.83	35.70	30.30
581	25.45	26.08	26.60	39.84
610	109.40	33.61	114.90	68.04
666	40.14	32.91	41.65	18.76
718	229.90	141.90	226.70	246.00
728	128.30	154.50	160.90	138.40
738	184.00	71.82	223.80	145.00
752	207.40	103.50	231.80	174.70
912	88.62	38.84	69.32	30.09
937	199.00	110.40	227.80	154.40
962	49.62	16.99	69.73	10.63
1099	22.23	18.85	21.86	81.91
Bicycloheptanyls				
309	60.33	44.18	83.30	35.30
369	146.30	69.83	163.80	113.00
411	33.22	26.26	45.00	52.65
422	226.40	241.40	253.40	0.61
596	29.18	18.77	30.45	6.45
641	265.40	275.90	295.80	286.70
880	81.71	32.06	77.53	14.81
907	246.30	223.30	302.00	243.30
936	21.95	4.64	46.75	8.47
1096	176.30	34.38	236.20	183.50

AUC
300
200
100
0

Figure 5.4. Adamantyl-based compounds as putative mmpL3 inhibitors. **A.** The adamantyl-based compounds and the bicycloheptanyl-based compound identified from the outlier analysis of the *mmpL3* mutant screen. **B.** Activities of the adamantyl- and bicycloheptanyl-based compounds in the MLSMR dataset against the three mutant backgrounds.

121

Cyclooctyl ureas and related compounds with resistance in the *mmpL3* mutant pool

Our lab previously characterized a cyclooctyl piperazine (HC2178) and a cyclohexyl urea (HC2138) as MmpL3 inhibitors[130]. In this current study, we followed up by identifying new cycloctyl-based compounds as putative MmpL3 inhibitors. Our statistical analysis of outliers in the *mmpL3* mutant screening data identified one cyclooctyl carboxamide (**585**) and six cyclooctyl ureas (**623**, **655**, **878**, **939**, **941**, and **1042**) as potential MmpL3 inhibitors (**Figure A.4.3**). Using substructure similarity search as a complementary method, other cyclooctyl-based compounds in the MLSMR dataset were identified as putative MmpL3 inhibitors (**Dataset 5.2, Figure A.4.3**). These include **12**, **154**, **867**, and **874**. Our outlier analysis also showed a cyclohexyl amine (**862**) and a cyclopropyl urea (**673**) significantly lose their antimycobacterial activity against the *mmpL3* mutant (**Figure A.4.3**) Overall, these compounds represent new additions to the increasing portfolio of MmpL3 inhibitors and need to be further studied.

Nitro-containing compounds:

Nitrofuranyl piperazine benzene-based compounds

In our previous study, we have showed three nitrofuranyl piperazine benzene-based compounds (HC2209, HC2210, HC2211) from the MLSMR Mtb inhibitors are antimycobacterial prodrugs that depend on the mycobacterial deazaflavin machinery and its attendant nitroreductase(s) for activation into possible toxic metabolites[15]. In our bid to identify other analogs in the MLSMR dataset, we used the nitrofuranyl-piperazine-benzene parent structure as a query in a substructure similarity search. This analysis identified seven analogs including the already described HC2209, HC2210, and HC2211 (**Dataset 5.4**). As a complementary chemoinformatic approach, we clustered the whole MLSMR Mtb inhibitor collection using the Skelphere molecular descriptor. Predictably, the seven analogs clustered together, suggesting that we did not miss any related analogs in the collection (**Figure 5.5**).
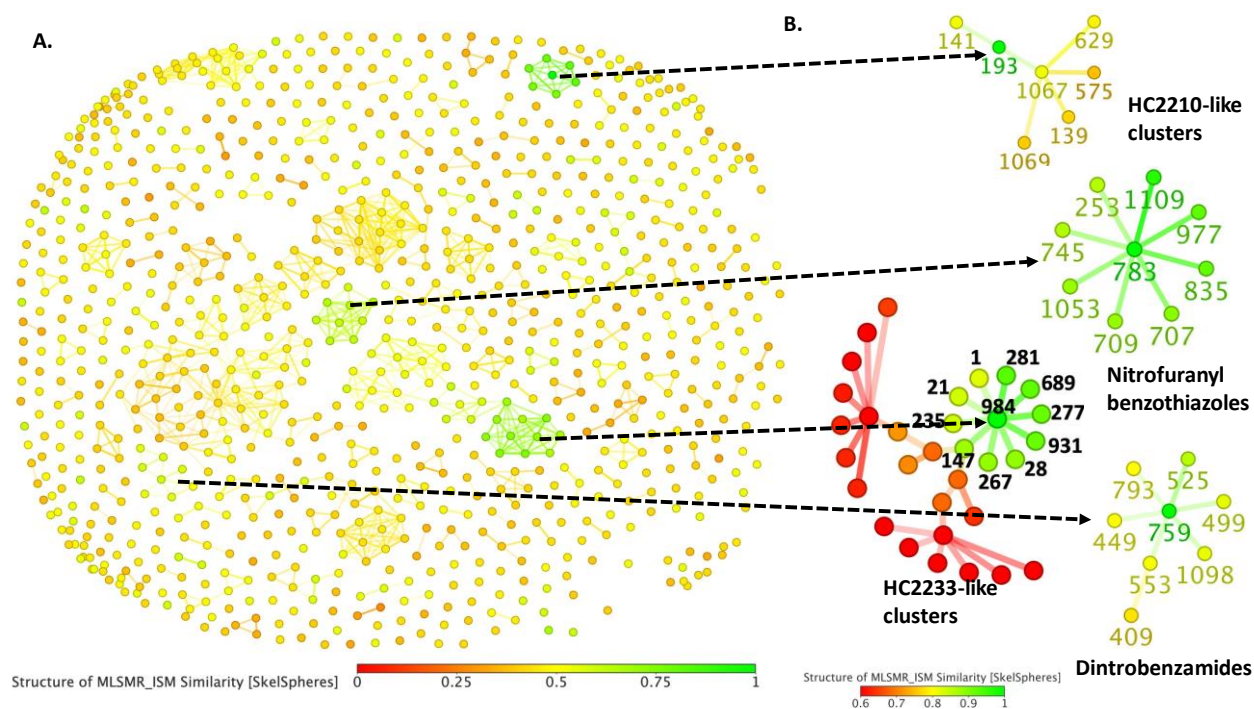
Figure 5.5. Chemical similarity clustering of all the compounds in the MLSMR dataset. **A**. Similarity skelsphere of the MLSMR clusters and **B.** neighborhood tree visualization of different nitro scaffolds that cluster together.

Next, we characterized the inhibitory activities of these analogs by comparing their potencies, as defined by the AUC, against the WT and the tested mutants (**Figure 5.6A; Figure 5.7A**). While the number of analogs is too small for a comprehensive SAR study, HC2210 is the most potent analog against the WT (AUC = 287.2). We have so far confirmed HC2210 to have a drug-like EC_{50} of 50 nm *in* vitro and to be effective in a chronic murine model of tuberculosis when delivered once daily and orally at 75 mg/kg[15]. In contrast, **575** had the lowest potency against the WT (AUC = 28.79). This is surprising since **1067**, the closely related analog of **575**, maintained a high potency against the WT (AUC = 221.3). The two analogs differ only in the position of the substituted chlorine group in the benzene moiety. **139** and **1069** are also closely related analogs, with the latter having a dimethyl group attached to the benzene ring and the former having a methyl group. These compounds have similar potencies against the WT, suggesting that the

methyl-based substitutions do not impact their inhibitory activities. **139** and **1069** also differ in terms of their activities against the mutants. While **139** loses some of its activities against the *mmpL3* mutant pool and *Tn:katG* mutant, **1069** retains its activities against the mutants. HC2209, HC2210, HC2211, and **1067** showed slightly enhanced potencies against the three mutants, although further studies are needed to confirm the possibility of a collateral sensitivity.
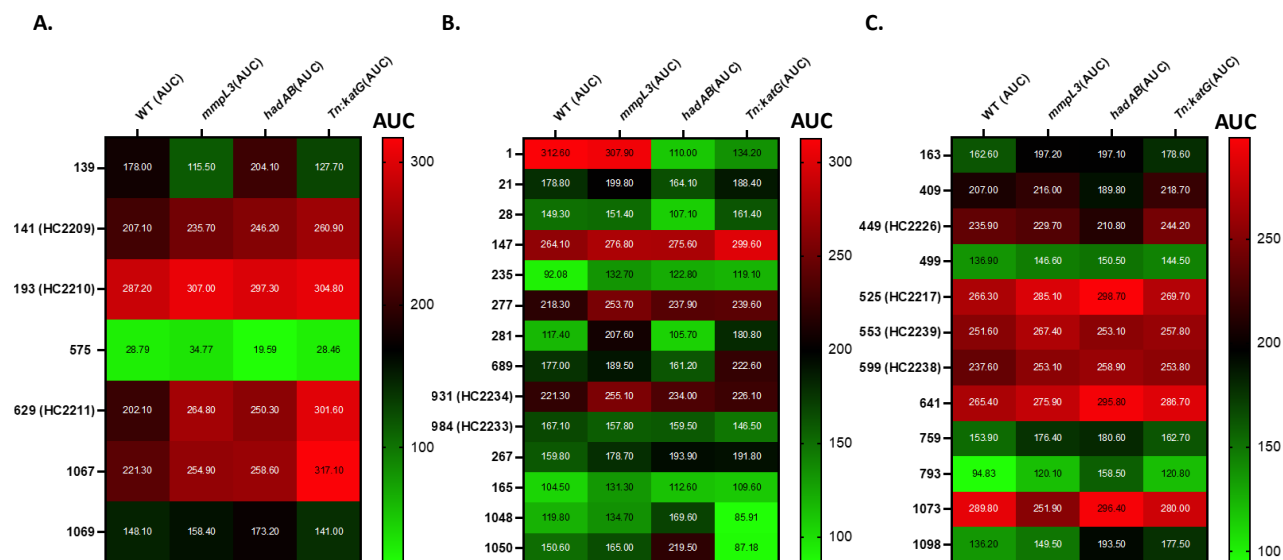
Figure 5.6. Activity of some nitro scaffolds against the three mutants that were tested in the study. **A**. Activity of the HC2210-like compounds (nitrofuranyl piperazines). **B.** Activity of the nitrofuranyl carboxamides. **C.** Activity of the dinitrobenzamides.
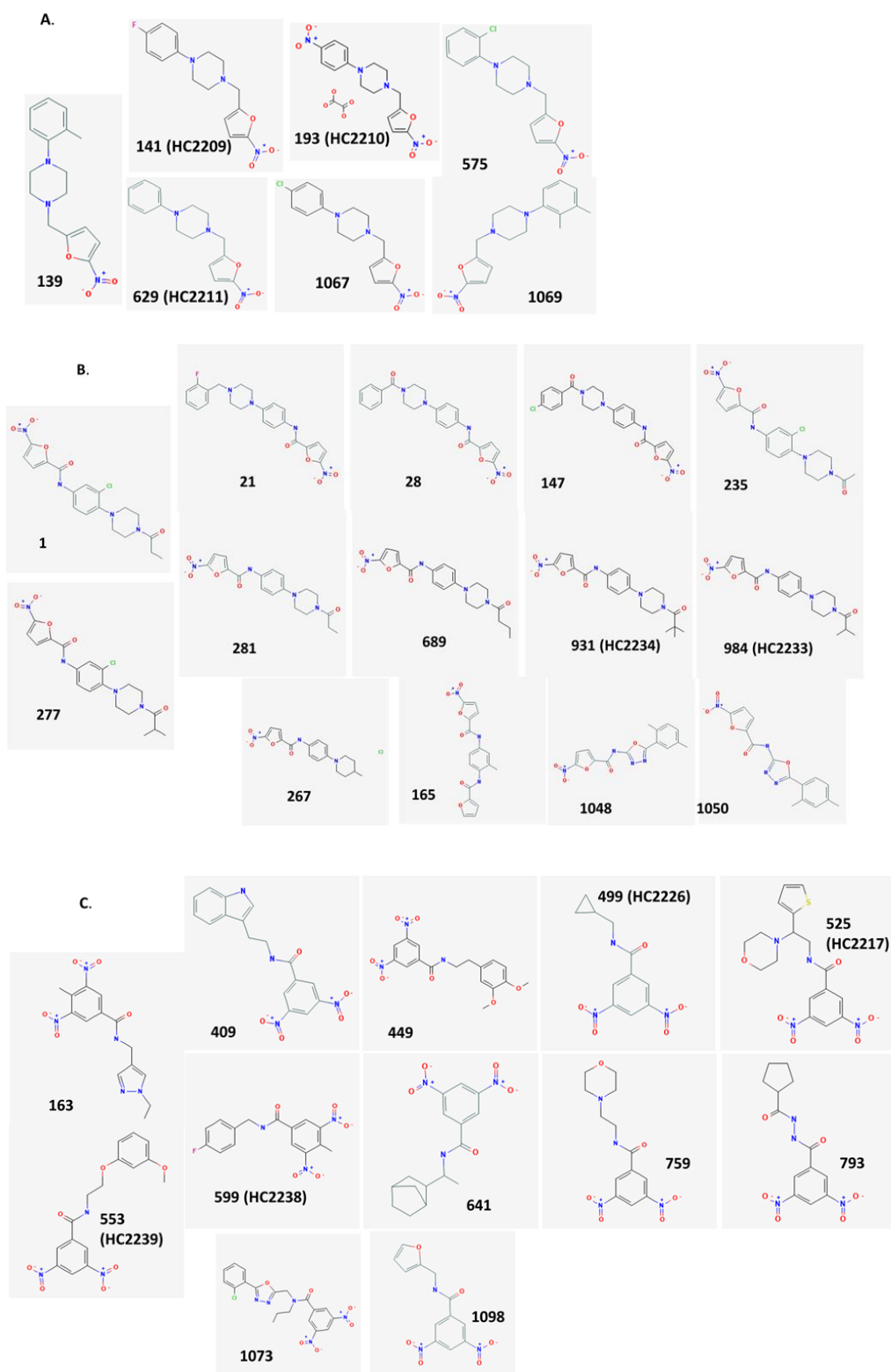
Figure 5.7. Structures of the A. HC2210-like compounds (nitrofuranyl piperazines) **B.** nitrofuranyl carboxamides, and **C.** dintrobenzamides identified in **Figure 5.5** and **Figure 5.6**.

Nitrofuranyl carboxamides

Following the drug discovery efforts of Lee and colleagues[193, 194], nitrofuranyl carboxamides have emerged as important antimycobacterial compounds[15, 181, 182]. Our group recently characterized two nitrofuranyl carboxamides – HC2233 (compound **984**) and HC2234 (compound **931**) – from the MLSMR Mtb inhibitors to be active against replicating and non-replicating Mtb[15]. These compounds are active in both *ddn* and *fgd* mutants supporting that they do not require the cofactor F_{420}-dependent activation mechanism. Due to the potent activity of this series against non-replicating persistent Mtb, we were interested in identifying other analogs in the MLSMR dataset using chemical similarity clustering. This approach gave rise to 9 analogs that clustered closely with HC2233 and HC2234 (**Figure 5.5**). Among these series, **1**, with a substituted 3-chlorophenyl and 4-propanoylpiperazine rings had the highest potency against the WT (**Figure 5.6B, Figure 5.7B**). It has two close relatives (**235** and **277**) that only differ from each other in terms of the length of the alkyl group attached to the terminal carbonyl group. **1** has an ethyl group attached to the terminal carbonyl group, while **235** has an acetyl group, and **277** has an isopropyl group. Interestingly, **1** and **277** showed similar potencies against the WT. However, **235** was different from the two compounds in terms of its lower potency against the WT, suggesting a negative impact of the substituted acetyl group on the antimycobacterial activity of the compound. Also, of interest, **1** and **281,** only differ by a chloro-group on the phenyl ring, with the chloro-substitution resulting in an almost 3-fold increase in AUC.

Examining the activities of this series against the mutants showed that most of the analogs retained their inhibitory activities against the tested strains (**Figure 5.6B**). Additionally, we queried the MLSMR Mtb inhibitors in a substructure similarity search for analogs of 5-nitrofuran-2-carboxamide. This uncovered 14 nitrofuranyl carboxamide-containing molecules, including the 11 benzyl piperazine/piperidine-linked molecules that clustered closely with HC2233 and HC2234

(**Figure 5.7B, Dataset 5.4).** The other three compounds are either conjugated with an oxadiazole benzene group (**1048** and **1050**) or a benzene carboxamide furanyl ring (**165**).

Dintrobenzamides

We have recently characterized four dinitrobenzamides (HC2217, HC2226, HC2238, and HC2239) from the MLSMR Mtb inhibitors as putative DprE1 inhibitors[15]. This is in line with previous studies that have genetically and biochemically established dinitrobenzamides as DprE1 inhibitors[45, 50]. To uncover other dintrobenzamides in the MLSMR dataset, we carried out a substructure similarity query of the dataset. This resulted in 12 dinitrobenzamide analogs, including the already described four compounds (**Figure 5.7C, Dataset 5.4**). Structural similarity clustering showed that eight of the identified analogs clustered together (**Figure 5.5**), while the other four compounds are found either in singletons or pairs. A look at the activity of the compounds against the WT showed that they maintained relatively high potency against the WT, although **793** and **499** exhibited relatively moderate activity (**Figure 5.6C**). When we extended the investigation to the mutant strains, we also observed that all the dintrobenzamides maintained their activities against the mutants. This is predictable since the target proteins are involved in synthesizing different components of the cell wall. DprE1 is involved in the synthesis of arabinogalactan, while MmpL3 and HadAB are catalyzing different steps in mycolic acid synthesis. Additionally, dinitrobenzamides are mechanism-based DprE1 inhibitors and do not primarily work through production of reactive oxygen species. Thus, disruption of the *katG* gene should not have any effect on the activity of the compounds.

Nitrofuranyl hydrazides

Recent work by Batt and group[59] identified two 5-nitrofuran-2-carbohydrazides as DprE2 inhibitors that possibly depend on the deazaflavin system for activation into active metabolites. Their report was closely followed by ours which characterized a 5-nitrofuran methylidene hydrazide (HC2250) from the MLSMR dataset as a putative DprE1 inhibitor[15]. However, we

showed that HC2250 does not depend on the deazaflavin activation machinery. Together, these two reports represent the first characterization of nitrofurans as inhibitors of the DprE1/E2 complex. To uncover other putative DprE1/E2-targeting nitrofuranyl hydrazide analogs, we used 5-nitrofuran-2-methylidene hydrazide and 5-nitrofuran-2-carbohydrazide substructures to query the MLSMR dataset. The latter did not yield any analog, while the former resulted to 5 analogs, including the already described HC2250 (**Dataset 5.4, Figure A.4.4**). The analogs maintained a high inhibitory activity against the WT and the mutants.

5-nitrofuran-2-methanone piperazinyl benzothiazoles

Our statistical outlier analysis of the *mmpL3* mutant screen showed that the mutant pool exhibited enhanced sensitivity to some compounds (**Dataset 5.4, Figure 5.1**). These include 7 analogs of nitrofuranyl/nitrothiophenyl benzothiazoles amongst others (**Figure 5.8**). In the structural similarity clustering of these analogs, two additional analogs (**977** and **1109)** were also identified (**Figure 5.5, Figure 5.8**). Substructure similarity search of the dataset did not reveal any additional analogs, indicating that all the analogs are well represented in the cluster. A side-by-side comparison of the potency of the analogs against the WT and the mutants revealed interesting trends (**Figure 5.8**). First, modifications at different positions of the benzothiazole ring did not impact the activities of the analogs against the WT. Second, all the analogs exhibited enhanced activity against the mixed *mmpL3* mutant pool. This collateral sensitivity also extended to the *katG* transposon mutant but does not extend to the *hadAB* mutant. Since the scaffold contains a nitro group that can easily form reactive species, we can explain the enhanced activity in the *katG* mutant background may to be due to the absence of KatG, an oxidoreductase that normally removes the toxic reactive oxygen species. The collateral sensitivity in the *mmpL3* background may be explained by the increased cellular entry of the compounds, although these hypotheses need to be tested. In any case, this scaffold may represent a component of future combination regimens that contain either isoniazid or MmpL3 inhibitors.
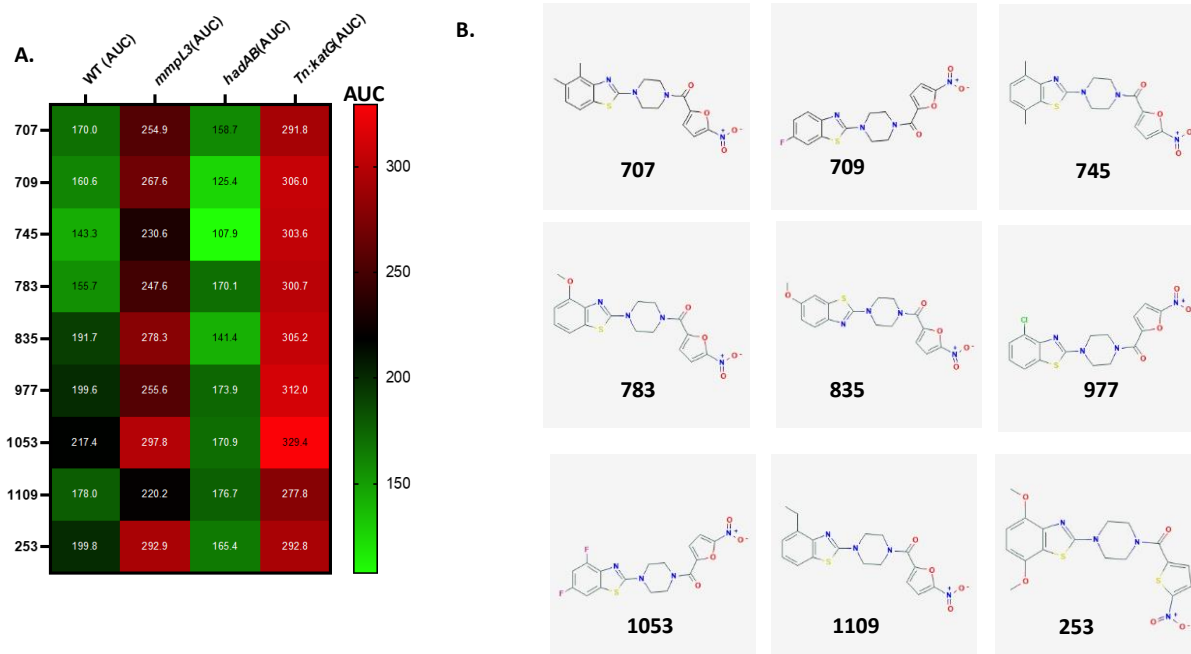
Figure 5.8. Nitro-containing benzothiazoles have enhanced activity against the *mmpL3* and *Tn:katG* mutants. **A**. Activity of the compounds against the three tested mutants. **B**. Structures of the compounds.

Pks13 Inhibitors:

One class of Pks13 inhibitors includes scaffolds that have a thiophene group linked to a pentafluorobenzyl carboxamate scaffold[195, 196]. Since Pks13 is an essential enzyme involved in mycolic acid biosynthesis, we decided to explore the MLSMR Mtb inhibitors for other putative pks13 inhibitors that have a pentafluorobenzyl carboxamate scaffold. When we queried our MLSMR Mtb inhibitor colleciton, only three compounds – **75**, **284**, and **904** had this scaffold. However, when we used only pentafluorobenzyl as the structure query, we saw that a total of six compounds in our collection (**75**, **284**, **382**, **394**, **904**, and **1052**) had the substructure. To confirm if these compounds are Pks13 inhibitors, we purchased fresh powders of **75**, **284**, and **394**, renaming them as HC2258, HC2259, and HC2260, respectively. In a dose-response study, we

reconfirmed that these compounds are active against Mtb, with HC2259 being the most potent compound (**Figure 5.9A**). We followed up our study by generating mutants that are resistant to HC2259 (**Figure A.4.5**) and sequencing to confirm resistance. A relatively low frequency of resistance (1 x 10^{-8}) was observed for HC2259, agreeing with what has been reported for other Pks13 inhibitors[197]. Predictably, all the resistant mutants had genetic changes in *pks13*, mostly point mutations, implicating the gene as a possible target of the compound. In a cross-resistance screen, all the tested mutants were also resistant to HC2258 and HC2259, suggesting Pks13 as a shared common target (**Figure 5.9B, Figure A.4.5**). Moreover, in agreement with previous studies[195, 197], TB drugs such as isoniazid and ethambutol that target mycolic acid biosynthesis retained their activity against the mutants (**Figure 5.9B, Figure A.4.5**). Overall, HC2258, HC2259, and HC2260 are putative Pks13 inhibitors, although biochemical data to this effect need to be provided.
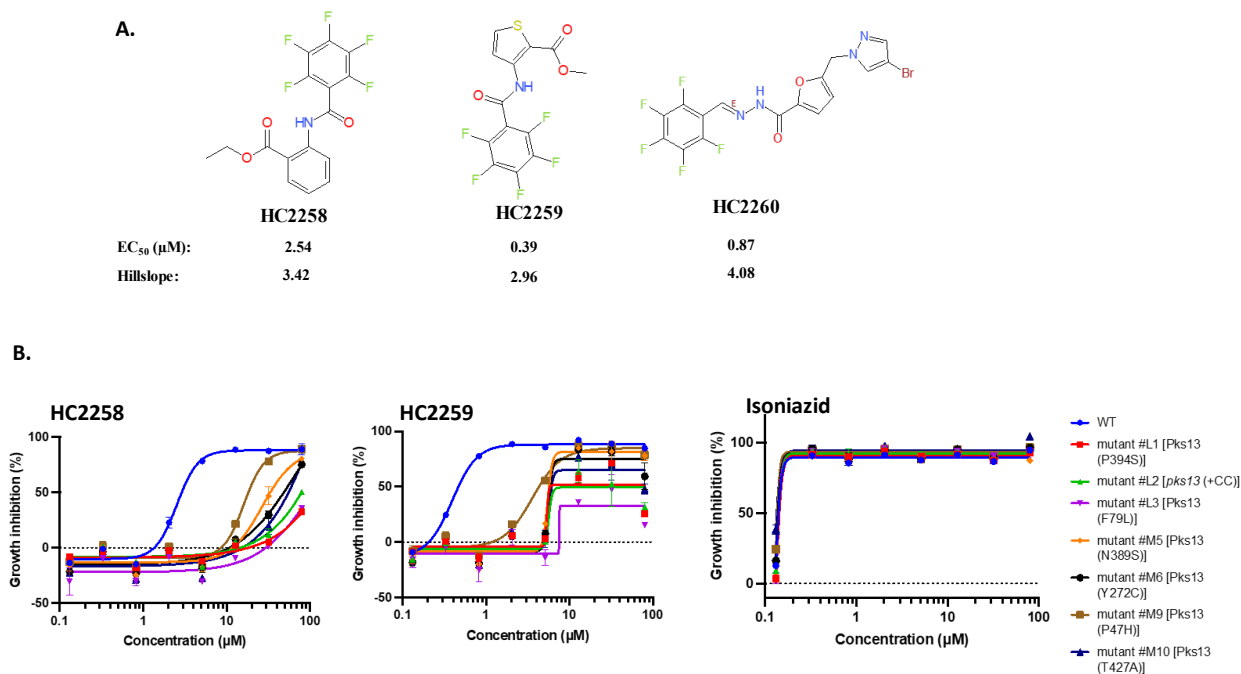
Figure 5.9. Identification of Pks13 inhibitors from follow-up studies. A. Structures of the Pks13 inhibitors that were studied. **B.** Cross-resistance screening of the *pks13* mutants.

Concluding Remarks:

Our study has used a combination of genetic and cheminformatic tools to provide an early mechanistic insight into the antimycobacterial activities of some compounds from the MLSMR library. These insights can guide further studies, especially using biochemical approaches, to confirm the mechanisms-of-action of these compounds. Our study has provided a prioritization pipeline for some antimycobacterial hits from the MLSMR library. For instance, the isoniazid analogs that have a KatG-independent antimycobacterial activity needs to be prioritized for possible development as TB drugs. The nitrofuranyl benzothiazoles have the possibility of being included in combination regimens for TB treatment with MmpL3 drugs such as SQ109 or the KatG-dependent drug, isoniazid. In any case, these possibilities support more detailed follow-up studies from different groups. Additionally, the new compounds that we identified from our screen as putative MmpL3 or HadAB inhibitors can serve as training sets for machine learning

possibilities in the TB drug development. A limitation of this study is that the relative activities of the cherry-pick compounds, which have been subject to multiple freeze-thaw cycle, may not translate to what may be obtained using fresh powders. Additionally, without resynthesis and confirmation of the activity, it is possible some chemical identities may be incorrect. Interpretation of the findings needs to be considered with this caveat and resynthesis of key analogs is required prior to more extensive studies.

In recent years, artificial intelligence-based approaches are emerging for the discovery of new drugs[198]. Machine learning algorithms are dependent on high-quality, feature-rich datasets on which to train models. It is our hope that the functional characterizations in our study can be used to enrich training models and this resource will spur artificial intelligence-driven drug discovery and development for Mtb. Overall, this resource should serve as a valuable source of information for antimycobacterial compounds that can be studied to further understand mycobacterial physiology and develop new TB drugs.

Materials and Method:

Culture conditions

Unless otherwise indicated, the different *Mycobacterium tuberculosis* (Mtb) strains used in this study were cultured and maintained in 100 mL 7H9 OADC with glycerol and tween-80, and the media was buffered to pH 7.0 with 100 mM MOPS. The cultures were allowed to grow at 37°C in 5.0% CO_2.

Targeted high throughput mutant screening

Previously described methods were adapted in the targeted high throughput screening [113, 130, 180]. Briefly described, the 935 cherry-pick hits from the MLSMR library were diluted 2.5-fold starting at 8mM and used in an 8-dose response study to test the cultures. For the screening, Mtb CDC1551 *hspX'*::GFP reporter strain (WT) and the different mutants (*mmpL3* mutant pool; *hadAB* mutant; *Tn:KatG* mutant) were cultured to mid-log phase (OD_{600} ~0.6) in 7H9 medium. This was

followed by aliquoting the 50 uL of the cultures into 384-well plates at an initial inoculum of OD_{600} = 0.05. Treatment was initiated by adding 0.5 µL of each compound, giving rise to a final concentration of 80 – 0.13 µM. DMSO and rifampicin were used as negative and positive controls, respectively. Plates were incubated with wet paper towel for six days at 37°C in 5% CO_2 Incubator. The absorbance (OD_{600}) of the cultures was then read on a Perkin Elmer plate reader, and the percent growth inhibition was calculated relative to controls. The area under the curve of the dose-response was used as a relative measure of potency and was calculated in GraphPad Prism (version 10). The Mahalanobis outlier method was used to identify outliers in the WT vs *hadAB* screen, as well as WT vs *mmpL3* and this was done with the statistical package, SPSS.

Eukaryotic cytotoxicity assay

Primary bone marrow-derived macrophages (BMDM) were obtained and cultured using a previously described protocol[199]. This was followed by seeding 384-well opaque plates with the macrophage cells and treating with different concentrations of the compounds as described in the targeted mutant screening above. DMSO and 4% triton X-100 were included as negative and positive control, respectively. The macrophage plates were then incubated with wet paper towel at 37°C and 5% CO_2. After six days of treatment, cell viability was assessed using the cell titer glow assay (Promega) and percent cytotoxicity was calculated relative to DMSO and 4% triton x-100 controls. The area under the curve of the dose-response was calculated in GraphPad Prism (version 10).

Intracellular Mtb Growth Inhibition

BMDM were obtained and seeded into 384-well opaque plates as previously described[199]. After 24 hours of seeding, the macrophages were infected with a Mtb CDC1551 strain expressing firefly luciferase at an MOI of 1[199]. Infection was allowed to proceed for 1 hour at 37°C, followed by treatment with the compounds in a dose-response study as described above. After six days of treatment, the bright glow luciferin assay (Promega) protocol was used to assess the growth of

the intracellular Mtb. Due to an edge effect, DMSO treated cells could not be used a negative-controls, and percent intracellular growth was instead measured relative to rifampicin and the average bacterial growth of Mtb treated with the lowest concentrations tested as the negative control.

Similarity Clustering and activity cliff analysis in DataWarrior

SDF files for each compound were provided by the NIH and were inputted into Datawarrior software. The Skelphere molecular descriptor of the compounds was calculated and used for clustering similar compounds in DataWarrior under default settings. The Skelphere descriptor was also used in the activity cliff analysis, with the area under the curve of the compounds against the WT used as a measure of their activity.

Isolation and characterization of Pks13 resistant mutants

The isolation and confirmation of resistant mutants were done as previously described [130]. Briefly, $1x10^9$ CFU of CDC155 Mtb cultures was plated onto 7H10/OADC agar plates amended with HC2259. The plates were incubated at 37°C until colonies appeared. The colonies were regrown in 7H9OADC and reconfirmed for resistance in a dose-response study. This was followed by whole-genome sequencing of the mutants and comparing the changes with that of the WT to identify the resistance gene.

CHAPTER SIX: Conclusions and future plans

Summary of key findings:

The approval of pretomanid and delamanid for tuberculosis (**TB**) treatment has reignited interest in the development of new nitro-containing scaffolds for TB chemotherapy. Generally, nitro-containing compounds have a number of advantages over other TB drugs. They are prodrugs that depend on different mycobacterial nitroreductases, highlighting their specificity for mycobacterial species[6, 15, 16]. Thus, the composition of the normal flora should hypothetically remain unchanged from treatment with these nitro-based compounds, and the drugs should have minimal toxicity on eukaryotic cells. Second, they usually target multiple cellular pathways in the pathogen, and have demonstrated utility in the treatment of multidrug-resistant (**MDR**) and extensively drug-resistant (**XDR**) TB cases. For instance, pretomanid is included in combination regimens such as the bedaquiline-pretomanid-linezolid regimen for the treatment of MDR and XDR cases that are resistant to several drugs[200, 201]. Lastly, these compounds maintain their activity against non-replicating persistent *Mycobacterium tuberculosis* (**Mtb**), perhaps through their ability to target respiration in the bacteria[5, 7, 9, 15, 51, 92] and can be used in the treatment of latent TB or in shorter treatment regimens[202, 203].

In this dissertation, I have characterized the mechanisms-of-action of novel nitro-containing compounds against Mtb and *M. abscessus* (**Mab**). I have demonstrated these compounds as potential drugs that can be developed for treatment of TB and non-tuberculous mycobacterial infections (**NTMIs**). I have also used these compounds to provide novel insights into the physiology and functions of different mycobacterial proteins. I will now provide a summary of key findings in each chapter.

In <u>Chapter One</u>, I set the stage for the works discussed in this dissertation by summarizing the prodrug-activating activities and native functions of different mycobacterial nitroreductases that have reported in literature. Some of these nitroreductases include Acg, NfnB, Rv3131, Rv3368c, DsbA, DprE1 and Ddn, with the latter two being the subject of the latter chapters of this

dissertation. These enzymes use different cofactors for the reductive activation of their nitro-containing substrates. For instance, Ddn uses the reduced form of cofactor F_{420} that is generated by Fgd, while DprE1 uses $FADH_2$.

In Chapter Two, I followed up with the characterization of the mechanisms-of-action of 10 nitro-containing compounds[15] that we previously identified from our high-throughput screening of the National Institutes of Health's Molecular Libraries Small Molecules Repository (**MLSMR**) (see Chapter Five). I showed through a forward genetic selection that three of these compounds, nitrofuranyl piperazines (HC2209, HC2210, and HC2211), depend on the cofactor F_{420} activation machinery of Mtb for possible activation into antimycobacterial metabolites. I also included pretomanid as probe-based confirmation of the *ddn* and *fgd* spontaneous mutants and showed, in agreement with what has been reported in literature[1, 3, 6, 7], that the drug completely loses its activity against the mutants. Interestingly, the three nitrofuranyl piperazines retain part of their inhibitory activity against the *ddn* mutants, but completely loses it against the *fgd* mutants, pointing to a secondary F_{420}-dependent nitroreductase. Additionally, these nitrofurans differ from pretomanid in their activity against *M. abscessus* (see Chapter Three). Additionally, I showed four new dinitrobenzamides (HC2217, HC2226, HC2238, and HC2239) as putative DprE1 inhibitors since they lose their activity against a *dprE1* mutant. This is in line with what has been reported in previous studies about the DprE1-targeting activity of compounds that contains this scaffold[45, 50]. Interestingly, HC2250, a nitrofuranyl hydrazide, also loses its activity against the *dprE1* mutant. This represents the first mention of a nitrofuran as a putative DprE1 inhibitor[15], and closely follows a recent report of nitrofuran-based compounds as DprE2 inhibitors[59]. Given the novelty of HC2250 as a putative DprE1 inhibitor, I followed up with studies of the compound (see Chapter Four). Finally, in Chapter Two, I demonstrated that HC2210 has *in vivo* efficacy in a chronic murine model of tuberculosis, reducing the mycobacterial burden of the lungs and spleens of the infected mice by ~1 log. This shows the promise of developing HC2210 as a potential TB drug.

In <u>Chapter Three</u>, I showed that HC2210 is a bacteriostatic compound against Mab. This differs from what I have previously reported about the bactericidal activity of the compound against Mtb (see <u>Chapter Two</u>). This difference may come down to the different transcriptional impact of the compound on the two mycobacterial species. In Mtb, I showed that HC2210 affects the expression of genes involved in respiration and cell envelope biosynthesis, a transcriptional trademark of many nitro-containing compounds against Mtb[5, 9, 92]. However, in Mab, genes involved in respiration were not affected. Only genes involved in oxidative stress response and lipid metabolism were affected by the compound in Mab. Additionally, forward genetic selection studies identified important differences in the activation of HC2210 in both species. Similar to what I reported for the activation of the compound in Mtb (see <u>Chapter Two</u>), HC2210 also depends on the cofactor F_{420} activation machinery of Mab. However, the genetic selection could not identify any nitroreductase in Mab as the activating enzyme. This differs from Mtb where the selection study implicated Ddn as a primary nitroreductase for the compound[15] (see <u>Chapter Two</u>). The genetic selection study also showed that the disruption of glycerol kinase (**GlpK**), an enzyme involved in the first committal step of glycerol utilization, led to the loss of activity of HC2210 and other antimycobacterial drugs. This represents one of the few mentions of this gene in the resistance mechanism of Mab[135], although much is known about its role in Mtb[48, 141, 142]. Finally, in <u>Chapter Three</u>, I showed that HC2210 is about 5X more potent than amikacin, one of the standard-of-care drugs for Mab-caused NTMIs and has varying activity against different clinical isolates of Mab. This represents the potential clinical utility of this scaffold for the treatment of Mab infections.

In <u>Chapter Four</u>, I followed up with an initial observation that HC2250 is active against non-replicating persistent (NRP) Mtb while other DprE1 inhibitors are expectedly inactive[15] (see <u>Chapter Two</u>), and showed that the bactericidal activity of HC2250 against NRP Mtb is independent of the DprE1 mechanism-based activator in a hypoxic shift-down assay. Transcriptional profiling of HC2250-treated cells revealed that genes involved in respiration, lipid

metabolism, and stress response are impacted by the compound. Additionally, about 50% of the impacted genes in HC2210-treated cultures overlapped with genes impacted by a known DprE1 inhibitor scaffold, demonstrating that HC2250 is a putative DprE1 inhibitor with a secondary activity. HC2250 was also active in an acute murine model of TB infection, reducing the mycobacterial burden of the lungs of the infected mice by ~0.8 log. This supports the further development of this compound as a potential TB drug.

Lastly, in <u>Chapter Five</u>, targeted mutant screening and cheminformatics was used to explore the mechanisms-of-action of 935 growth inhibitors that we cherry-picked from our previous high throughput screening of the MLSMR library. As a validation, this approach identified 101 isoniazid analogs that completely lose their activity against a *Tn:katG* mutant. Interestingly, I observed 8 isoniazid analogs that retain some of their antimycobacterial activity against the mutant, suggesting a secondary KatG-independent mechanism-of-action. This approach also identified scaffolds that are known HadAB or MmpL3 inhibitors, serving as a further validation. Additionally, when I compared the *in vitro* and *ex vivo* activity of the compounds, I discovered 58 compounds that have higher activity against intracellular Mtb. One of these compounds is structurally similar to pyrazinamide, a first-line TB drug that is known to be active against intracellular Mtb and inactive against extracellular Mtb under normal laboratory conditions[184, 185]. Next, I used cheminformatic tools to further explore the MLSMR cherry-picks and I reported several nitro-containing compounds in the collection, including members belonging to the nitrofuranyl piperazines, nitrofuranyl carboxamides, nitrofuranyl hydrazides, nitrofuranyl benzothiazoles, and the dinitrobenzamides. Some of these hits have previously been characterized[15] (see <u>Chapter Two</u>). Interestingly, I discovered that the nitrofuranyl benzothiazoles showed enhanced antimycobacterial activity against the *mmpL3* and *katG* mutants, a phenomenon known as collateral sensitivity. Upon further study, this scaffold might prove effective for possible inclusion in TB drug regimens that contain a KatG-dependent drug or an MmpL3 inhibitor. I also use forward genetic selection to characterize some Pks13 inhibitors in the dataset.

Overall, this early assessment of the mechanisms-of-action of antitubercular hits from the MLSMR dataset might prove effective for prioritization studies and might serve as an important training set for artificial intelligence-driven drug development.

Remarks on future studies:

This dissertation has opened interesting lines of enquiry that need to be pursued in future studies. One of these is the question of the secondary F_{420}-dependent nitroreductase that is involved in the activation of the nitrofuranyl piperazines in Mtb. I propose the use of an unbiased whole-genome screening approach such as transposon mutagenesis or CRISPR screen to identify this nitroreductase gene(s). Alternatively, a biased approach can also be used to identify the nitroreductase. This first involves the phylogenetic identification of *ddn* homologs in Mtb, followed by the disruption or overexpression of the genes and testing for their impact on the activity of the compounds. Another question is why these nitrofuranyl piperazines are active against Mab, while pretomanid is inactive? This might come down to genetic polymorphism of the activating enzyme, efflux-driven resistance, or limited cellular entry of pretomanid into Mab. The latter two might not be reason since a previous study from another group has shown pretomanid is inactive against Mab even at a high concentration of 2 mM[204]. This is about 25X the highest concentration of pretomanid tested here. In any case, well-designed experiments can be used to answer these questions. For instance, the *ddn* homolog of Mtb can be cloned and expressed in Mab, followed by treatment with pretomanid to examine its effect on the bacteria. Taken together, these studies should be able to decipher the reason for the inactivity of pretomanid in Mab.

While I have shown that the nitrofuranyl piperazines and nitrofuranyl carboxamides are active against Mab[15], it will be interesting to explore their activities against other mycobacterial species such as *M. avium* complex, *M. ulcerans*, *M. chelonae*, *M. intracellulare* amongst others. This is especially needed since these species are important etiologic agents of different clinical manifestations of NTMIs. Additionally, it will be interesting to know if the *in vitro* activity of the

nitrofurans against Mab translates to *in vivo* efficacy in murine model of Mab infections. Studies in this direction are currently planned in the lab. Moreover, given that HC2210 and HC2250 have been demonstrated to have *in vivo* efficacy in a murine model of TB, it will also be interesting to see their efficacy in other animal model of TB infections. Monotherapy is an exception rather than the norm in TB treatment. Most TB chemotherapy involves a minimum of two drugs that have different targets, reducing the chances of developing resistance to both drugs. Some drugs might be antagonistic to each other, while others might be synergistic, and others might be indifferent to each other[205-207]. Therefore, part of the preclinical development of the nitro-containing compounds as potential drugs should include both *in vitro* and *in vivo* combination-based assays with commonly available TB drugs to determine how the compounds interact with the drugs.

Apart from the *in vivo* pharmacodynamics studies, the nitro-containing compounds in this dissertation needs to be characterized for their pharmacokinetic properties. This can include studies such as the Ames' test to decipher their mutagenic potential; mammalian cytochrome P_{450} induction or inhibition; microsomal stability; and *in vivo* pharmacokinetic studies to decipher the therapeutic exposure, bioavailability, distribution, and metabolism of the compounds. Additionally, these studies can drive the generation of analogs with more effective activities against bacteria or a better pharmacokinetic property. Progress in this direction has already been made in our lab, but they are sufficiently preliminary that they were not included in the main body of this dissertation. As an example, we collaborated with Dr. Edmund Ellsworth and his medicinal chemistry team at Michigan State University to test 99 analogs of HC2210 against Mab and Mtb. This gave rise to MSU-45598 as a compound that is 12X more potent than the parent compound against Mtb and Mab (**Figure A.5.1**). Additionally, when I tested the analogs against *ddn* and *fgd* mutants, I observed three broad categories of HC2210 analogs in our collection (**Figure A.5.2**). The first group are analogs that are activated like the parent compound, where they show a partial loss in activity against the *ddn* mutant, and a complete loss against the *fgd* mutant. Then, there are analogs that partially lose their activity against both mutants. This indicates that they require

the F_{420}-dependent (Ddn) and an F_{420}-independent activation machinery. The last group are those that do not lose their activity against both mutants, suggesting a complete F_{420}-independence and a drift of these analogs towards a different target. The structures of these analogs have been withheld until a patent is filed, but they represent a rich source of chemical biology data to explore the interactions of the nitrofuran with its target or nitroreductase.

From my genetic studies, I have proposed HC2250 as a DprE1 inhibitor, but a biochemical validation of this classification is needed. To this end, efforts should be made towards expressing the DprE1/E2 complex and investigating the effects of the nitrofuran on the catalytic activities of the proteins. The same should also be done for the Ddn-dependent compounds that I have been identified in this study. Though historical antecedent on the mechanisms-of-action of nitro-containing compounds[5, 7, 40, 92, 146] and the transcriptional profiling in this dissertation suggests that the nitro compounds are modulating respiration, lipid metabolism, and causing oxidative stress, biochemical data to this effect needs to be provided for the compounds. This might include assays that determine the ATP levels, membrane potential, reactive oxygen species, and lipid composition of treated cells and comparing them with that of the untreated cells. Additionally, well-designed, and timed mass spectrometry-based methods can be used to identify the reactive nitrogen species and metabolites that are produced from the activation of the nitro prodrugs. This will aid in future drug design studies in developing more effective antimycobacterial drugs.

Lastly, the works presented in Chapter Five of this dissertation represent a rich avenue for many follow-up studies. For instance, the collateral sensitivity of the *mmpL3* and *hadAB* mutants against the nitrofuranyl benzothiazoles needs to be further investigated. The isoniazid analogs that do not completely lose their activity against the *Tn:katG* also need to be studied. The same can also be said for the compounds that show a pyrazinamide-like behavior where they show higher activity against intracellular Mtb than extracellular Mtb. Additionally, the resource datasets

attached to the dissertation can be used in designing machine learning algorithms for predicting compounds that will lose or retain their activity against a *Tn:katG*, *mmpL3*, or *hadAB* mutant.

Overall, my dissertation has used a chemical-genetic approach to characterize the mechanisms-of-action of nitro-containing compounds against Mtb and Mab. It is my hope that these compounds can prove to be more effective drugs for TB and Mab infections.

REFERENCES

1.   Cellitti SE, Shaffer J, Jones DH, Mukherjee T, Gurumurthy M, Bursulaya B, Boshoff HI, Choi I, Nayyar A, Lee YS, Cherian J, Niyomrattanakit P, Dick T, Manjunatha UH, Barry CE, 3rd, Spraggon G, Geierstanger BH. 2012. Structure of Ddn, the deazaflavin-dependent nitroreductase from Mycobacterium tuberculosis involved in bioreductive activation of PA-824. Structure 20:101-12.

2.   Gurumurthy M, Mukherjee T, Dowd CS, Singh R, Niyomrattanakit P, Tay JA, Nayyar A, Lee YS, Cherian J, Boshoff HI, Dick T, Barry CE, 3rd, Manjunatha UH. 2012. Substrate specificity of the deazaflavin-dependent nitroreductase from Mycobacterium tuberculosis responsible for the bioreductive activation of bicyclic nitroimidazoles. FEBS J 279:113-25.

3.   Rifat D, Li SY, Ioerger T, Shah K, Lanoix JP, Lee J, Bashiri G, Sacchettini J, Nuermberger E. 2020. Mutations in fbiD (Rv2983) as a Novel Determinant of Resistance to Pretomanid and Delamanid in Mycobacterium tuberculosis. Antimicrob Agents Chemother 65.

4.   Matsumoto M, Hashizume H, Tomishige T, Kawasaki M, Tsubouchi H, Sasaki H, Shimokawa Y, Komatsu M. 2006. OPC-67683, a nitro-dihydro-imidazooxazole derivative with promising action against tuberculosis in vitro and in mice. PLoS Med 3:e466.

5.   Manjunatha U, Boshoff HI, Barry CE. 2009. The mechanism of action of PA-824: Novel insights from transcriptional profiling. Commun Integr Biol 2:215-8.

6.   Manjunatha UH, Boshoff H, Dowd CS, Zhang L, Albert TJ, Norton JE, Daniels L, Dick T, Pang SS, Barry CE, 3rd. 2006. Identification of a nitroimidazo-oxazine-specific protein involved in PA-824 resistance in Mycobacterium tuberculosis. Proc Natl Acad Sci U S A 103:431-6.

7.   Singh R, Manjunatha U, Boshoff HI, Ha YH, Niyomrattanakit P, Ledwidge R, Dowd CS, Lee IY, Kim P, Zhang L, Kang S, Keller TH, Jiricek J, Barry CE, 3rd. 2008. PA-824 kills nonreplicating Mycobacterium tuberculosis by intracellular NO release. Science 322:1392-5.

8.   Fujiwara M, Kawasaki M, Hariguchi N, Liu Y, Matsumoto M. 2018. Mechanisms of resistance to delamanid, a drug for Mycobacterium tuberculosis. Tuberculosis (Edinb) 108:186-194.

9.   Wang X, Inoyama D, Russo R, Li SG, Jadhav R, Stratton TP, Mittal N, Bilotta JA, Singleton E, Kim T, Paget SD, Pottorf RS, Ahn YM, Davila-Pagan A, Kandasamy S, Grady C, Hussain S, Soteropoulos P, Zimmerman MD, Ho HP, Park S, Dartois V, Ekins S, Connell N, Kumar P, Freundlich JS. 2020. Antitubercular Triazines: Optimization and Intrabacterial Metabolism. Cell Chem Biol 27:172-185 e11.

10.   Makarov V, Manina G, Mikusova K, Mollmann U, Ryabova O, Saint-Joanis B, Dhar N, Pasca MR, Buroni S, Lucarelli AP, Milano A, De Rossi E, Belanova M, Bobovska A, Dianiskova P, Kordulakova J, Sala C, Fullam E, Schneider P, McKinney JD, Brodin P, Christophe T, Waddell S, Butcher P, Albrethsen J, Rosenkrands I, Brosch R, Nandi V,

Bharath S, Gaonkar S, Shandil RK, Balasubramanian V, Balganesh T, Tyagi S, Grosset J, Riccardi G, Cole ST. 2009. Benzothiazinones kill Mycobacterium tuberculosis by blocking arabinan synthesis. Science 324:801-4.

11. Neres J, Pojer F, Molteni E, Chiarelli LR, Dhar N, Boy-Rottger S, Buroni S, Fullam E, Degiacomi G, Lucarelli AP, Read RJ, Zanoni G, Edmondson DE, De Rossi E, Pasca MR, McKinney JD, Dyson PJ, Riccardi G, Mattevi A, Cole ST, Binda C. 2012. Structural basis for benzothiazinone-mediated killing of Mycobacterium tuberculosis. Sci Transl Med 4:150ra121.

12. Landge S, Mullick AB, Nagalapur K, Neres J, Subbulakshmi V, Murugan K, Ghosh A, Sadler C, Fellows MD, Humnabadkar V, Mahadevaswamy J, Vachaspati P, Sharma S, Kaur P, Mallya M, Rudrapatna S, Awasthy D, Sambandamurthy VK, Pojer F, Cole ST, Balganesh TS, Ugarkar BG, Balasubramanian V, Bandodkar BS, Panda M, Ramachandran V. 2015. Discovery of benzothiazoles as antimycobacterial agents: Synthesis, structure-activity relationships and binding studies with Mycobacterium tuberculosis decaprenylphosphoryl-beta-D-ribose 2'-oxidase. Bioorg Med Chem 23:7694-710.

13. Rich EA, Torres M, Sada E, Finegan CK, Hamilton BD, Toossi Z. 1997. Mycobacterium tuberculosis (MTB)-stimulated production of nitric oxide by human alveolar macrophages and relationship of nitric oxide production to growth inhibition of MTB. Tuber Lung Dis 78:247-55.

14. Negri A, Javidnia P, Mu R, Zhang X, Vendome J, Gold B, Roberts J, Barman D, Ioerger T, Sacchettini JC, Jiang X, Burns-Huang K, Warrier T, Ling Y, Warren JD, Oren DA, Beuming T, Wang H, Wu J, Li H, Rhee KY, Nathan CF, Liu G, Somersan-Karakaya S. 2018. Identification of a Mycothiol-Dependent Nitroreductase from Mycobacterium tuberculosis. ACS Infect Dis 4:771-787.

15. Eke IE, Williams JT, Haiderer ER, Albrecht VJ, Murdoch HM, Abdalla BJ, Abramovitch RB. 2023. Discovery and characterization of antimycobacterial nitro-containing compounds with distinct mechanisms of action and in vivo efficacy. Antimicrob Agents Chemother 67:e0047423.

16. Hurdle JG, Lee RB, Budha NR, Carson EI, Qi J, Scherman MS, Cho SH, McNeil MR, Lenaerts AJ, Franzblau SG, Meibohm B, Lee RE. 2008. A microbiological assessment of novel nitrofuranylamides as anti-tuberculosis agents. J Antimicrob Chemother 62:1037-45.

17. Lee BM, Harold LK, Almeida DV, Afriat-Jurnou L, Aung HL, Forde BM, Hards K, Pidot SJ, Ahmed FH, Mohamed AE, Taylor MC, West NP, Stinear TP, Greening C, Beatson SA, Nuermberger EL, Cook GM, Jackson CJ. 2020. Predicting nitroimidazole antibiotic resistance mutations in Mycobacterium tuberculosis with protein engineering. PLoS Pathog 16:e1008287.

18. Gurumurthy M, Rao M, Mukherjee T, Rao SP, Boshoff HI, Dick T, Barry CE, 3rd, Manjunatha UH. 2013. A novel F(420) -dependent anti-oxidant mechanism protects

Mycobacterium tuberculosis against oxidative stress and bactericidal agents. Mol Microbiol 87:744-55.

19.   Bahuguna A, Rawat S, Rawat DS. 2021. QcrB in Mycobacterium tuberculosis: The new drug target of antitubercular agents. Med Res Rev 41:2565-2581.

20.   Shi L, Sohaskey CD, Kana BD, Dawes S, North RJ, Mizrahi V, Gennaro ML. 2005. Changes in energy metabolism of Mycobacterium tuberculosis in mouse lung and under in vitro conditions affecting aerobic respiration. Proc Natl Acad Sci U S A 102:15629-34.

21.   Guerra-Lopez D, Daniels L, Rawat M. 2007. Mycobacterium smegmatis mc2 155 fbiC and MSMEG_2392 are involved in triphenylmethane dye decolorization and coenzyme F420 biosynthesis. Microbiology (Reading) 153:2724-2732.

22.   Hasan MR, Rahman M, Jaques S, Purwantini E, Daniels L. 2010. Glucose 6-phosphate accumulation in mycobacteria: implications for a novel F420-dependent anti-oxidant defense system. J Biol Chem 285:19135-44.

23.   Purwantini E, Mukhopadhyay B. 2013. Rv0132c of Mycobacterium tuberculosis encodes a coenzyme F420-dependent hydroxymycolic acid dehydrogenase. PLoS One 8:e81985.

24.   Bashiri G, Perkowski EF, Turner AP, Feltcher ME, Braunstein M, Baker EN. 2012. Tat-dependent translocation of an F420-binding protein of Mycobacterium tuberculosis. PLoS One 7:e45003.

25.   Purwantini E, Daniels L, Mukhopadhyay B. 2016. F420H2 Is Required for Phthiocerol Dimycocerosate Synthesis in Mycobacteria. J Bacteriol 198:2020-8.

26.   Ahmed FH, Mohamed AE, Carr PD, Lee BM, Condic-Jurkic K, O'Mara ML, Jackson CJ. 2016. Rv2074 is a novel F420 H2 -dependent biliverdin reductase in Mycobacterium tuberculosis. Protein Sci 25:1692-709.

27.   Malen H, Pathak S, Softeland T, de Souza GA, Wiker HG. 2010. Definition of novel cell envelope associated proteins in Triton X-114 extracts of Mycobacterium tuberculosis H37Rv. BMC Microbiol 10:132.

28.   Sinha S, Arora S, Kosalai K, Namane A, Pym AS, Cole ST. 2002. Proteome analysis of the plasma membrane of Mycobacterium tuberculosis. Comp Funct Genomics 3:470-83.

29.   Park SH, Opella SJ. 2010. Triton X-100 as the "short-chain lipid" improves the magnetic alignment and stability of membrane proteins in phosphatidylcholine bilayers for oriented-sample solid-state NMR spectroscopy. J Am Chem Soc 132:12552-3.

30.   de Cock H, van Blokland S, Tommassen J. 1996. In vitro insertion and assembly of outer membrane protein PhoE of Escherichia coli K-12 into the outer membrane. Role of Triton X-100. J Biol Chem 271:12885-90.

31.   Helenius A, Simons K. 1972. The binding of detergents to lipophilic and hydrophilic proteins. J Biol Chem 247:3656-61.

32.   Makino S, Reynolds JA, Tanford C. 1973. The binding of deoxycholate and Triton X-100 to proteins. J Biol Chem 248:4926-32.

33.   Kyte J, Doolittle RF. 1982. A simple method for displaying the hydropathic character of a protein. J Mol Biol 157:105-32.

34.   Sinha S, Kosalai K, Arora S, Namane A, Sharma P, Gaikwad AN, Brodin P, Cole ST. 2005. Immunogenic membrane-associated proteins of Mycobacterium tuberculosis revealed by proteomics. Microbiology (Reading) 151:2411-2419.

35.   Haver HL, Chua A, Ghode P, Lakshminarayana SB, Singhal A, Mathema B, Wintjens R, Bifani P. 2015. Mutations in genes for the F420 biosynthetic pathway and a nitroreductase enzyme are the primary resistance determinants in spontaneous in vitro-selected PA-824-resistant mutants of Mycobacterium tuberculosis. Antimicrob Agents Chemother 59:5316-23.

36.   Mohamed AE, Ahmed FH, Arulmozhiraja S, Lin CY, Taylor MC, Krausz ER, Jackson CJ, Coote ML. 2016. Protonation state of F420H2 in the prodrug-activating deazaflavin dependent nitroreductase (Ddn) from Mycobacterium tuberculosis. Mol Biosyst 12:1110-3.

37.   Greening C, Ahmed FH, Mohamed AE, Lee BM, Pandey G, Warden AC, Scott C, Oakeshott JG, Taylor MC, Jackson CJ. 2016. Physiology, Biochemistry, and Applications of F420- and Fo-Dependent Redox Reactions. Microbiol Mol Biol Rev 80:451-93.

38.   Zheng L, Qi X, Zhang W, Wang H, Fu L, Wang B, Chen X, Chen X, Lu Y. 2023. Efficacy of PBTZ169 and pretomanid against Mycobacterium avium, Mycobacterium abscessus, Mycobacterium chelonae, and Mycobacterium fortuitum in BALB/c mice models. Front Cell Infect Microbiol 13:1115530.

39.   Zhang F, Li S, Wen S, Zhang T, Shang Y, Huo F, Xue Y, Li L, Pang Y. 2020. Comparison of in vitro Susceptibility of Mycobacteria Against PA-824 to Identify Key Residues of Ddn, the Deazoflavin-Dependent Nitroreductase from Mycobacterium tuberculosis. Infect Drug Resist 13:815-822.

40.   Stover CK, Warrener P, VanDevanter DR, Sherman DR, Arain TM, Langhorne MH, Anderson SW, Towell JA, Yuan Y, McMurray DN, Kreiswirth BN, Barry CE, Baker WR. 2000. A small-molecule nitroimidazopyran drug candidate for the treatment of tuberculosis. Nature 405:962-6.

41.   Grinter R, Greening C. 2021. Cofactor F420: an expanded view of its distribution, biosynthesis and roles in bacteria and archaea. FEMS Microbiol Rev 45.

42. Bashiri G, Antoney J, Jirgis ENM, Shah MV, Ney B, Copp J, Stuteley SM, Sreebhavan S, Palmer B, Middleditch M, Tokuriki N, Greening C, Scott C, Baker EN, Jackson CJ. 2019. A revised biosynthetic pathway for the cofactor F(420) in prokaryotes. Nat Commun 10:1558.

43. Kim SH, Park S, Park E, Kim JH, Ghatge S, Hur HG, Rhee S. 2021. Structure and substrate specificity determinants of NfnB, a dinitroaniline herbicide-catabolizing nitroreductase from Sphingopyxis sp. strain HMH. J Biol Chem 297:101143.

44. Manina G, Bellinzoni M, Pasca MR, Neres J, Milano A, Ribeiro AL, Buroni S, Skovierova H, Dianiskova P, Mikusova K, Marak J, Makarov V, Giganti D, Haouz A, Lucarelli AP, Degiacomi G, Piazza A, Chiarelli LR, De Rossi E, Salina E, Cole ST, Alzari PM, Riccardi G. 2010. Biological and structural characterization of the Mycobacterium smegmatis nitroreductase NfnB, and its role in benzothiazinone resistance. Mol Microbiol 77:1172-85.

45. Ribeiro AL, Degiacomi G, Ewann F, Buroni S, Incandela ML, Chiarelli LR, Mori G, Kim J, Contreras-Dominguez M, Park YS, Han SJ, Brodin P, Valentini G, Rizzi M, Riccardi G, Pasca MR. 2011. Analogous mechanisms of resistance to benzothiazinones and dinitrobenzamides in Mycobacterium smegmatis. PLoS One 6:e26675.

46. Buchieri MV, Cimino M, Rebollo-Ramirez S, Beauvineau C, Cascioferro A, Favre-Rochex S, Helynck O, Naud-Martin D, Larrouy-Maumus G, Munier-Lehmann H, Gicquel B. 2017. Nitazoxanide Analogs Require Nitroreduction for Antimicrobial Activity in Mycobacterium smegmatis. J Med Chem 60:7425-7433.

47. van der Woude MW, Baumler AJ. 2004. Phase and antigenic variation in bacteria. Clin Microbiol Rev 17:581-611, table of contents.

48. Safi H, Gopal P, Lingaraju S, Ma S, Levine C, Dartois V, Yee M, Li L, Blanc L, Ho Liang HP, Husain S, Hoque M, Soteropoulos P, Rustad T, Sherman DR, Dick T, Alland D. 2019. Phase variation in Mycobacterium tuberculosis glpK produces transiently heritable drug tolerance. Proc Natl Acad Sci U S A 116:19665-19674.

49. Makarov V, Lechartier B, Zhang M, Neres J, van der Sar AM, Raadsen SA, Hartkoorn RC, Ryabova OB, Vocat A, Decosterd LA, Widmer N, Buclin T, Bitter W, Andries K, Pojer F, Dyson PJ, Cole ST. 2014. Towards a new combination therapy for tuberculosis with next generation benzothiazinones. EMBO Mol Med 6:372-83.

50. Christophe T, Jackson M, Jeon HK, Fenistein D, Contreras-Dominguez M, Kim J, Genovesio A, Carralot JP, Ewann F, Kim EH, Lee SY, Kang S, Seo MJ, Park EJ, Skovierova H, Pham H, Riccardi G, Nam JY, Marsollier L, Kempf M, Joly-Guillou ML, Oh T, Shin WK, No Z, Nehrbass U, Brosch R, Cole ST, Brodin P. 2009. High content screening identifies decaprenyl-phosphoribose 2' epimerase as a target for intracellular antimycobacterial inhibitors. PLoS Pathog 5:e1000645.

51. Albesa-Jove D, Chiarelli LR, Makarov V, Pasca MR, Urresti S, Mori G, Salina E, Vocat A, Comino N, Mohorko E, Ryabova S, Pfeiffer B, Lopes Ribeiro AL, Rodrigo-Unzueta A,

Tersa M, Zanoni G, Buroni S, Altmann KH, Hartkoorn RC, Glockshuber R, Cole ST, Riccardi G, Guerin ME. 2014. Rv2466c mediates the activation of TP053 to kill replicating and non-replicating Mycobacterium tuberculosis. ACS Chem Biol 9:1567-75.

52. Trefzer C, Rengifo-Gonzalez M, Hinner MJ, Schneider P, Makarov V, Cole ST, Johnsson K. 2010. Benzothiazinones: prodrugs that covalently modify the decaprenylphosphoryl-beta-D-ribose 2'-epimerase DprE1 of Mycobacterium tuberculosis. J Am Chem Soc 132:13663-5.

53. Riccardi G, Pasca MR, Chiarelli LR, Manina G, Mattevi A, Binda C. 2013. The DprE1 enzyme, one of the most vulnerable targets of Mycobacterium tuberculosis. Appl Microbiol Biotechnol 97:8841-8.

54. Wolucka BA. 2008. Biosynthesis of D-arabinose in mycobacteria - a novel bacterial pathway with implications for antimycobacterial therapy. FEBS J 275:2691-711.

55. Piton J, Foo CS, Cole ST. 2017. Structural studies of Mycobacterium tuberculosis DprE1 interacting with its inhibitors. Drug Discov Today 22:526-533.

56. Mikusova K, Huang H, Yagi T, Holsters M, Vereecke D, D'Haeze W, Scherman MS, Brennan PJ, McNeil MR, Crick DC. 2005. Decaprenylphosphoryl arabinofuranose, the donor of the D-arabinofuranosyl residues of mycobacterial arabinan, is formed via a two-step epimerization of decaprenylphosphoryl ribose. J Bacteriol 187:8020-5.

57. Trefzer C, Skovierova H, Buroni S, Bobovska A, Nenci S, Molteni E, Pojer F, Pasca MR, Makarov V, Cole ST, Riccardi G, Mikusova K, Johnsson K. 2012. Benzothiazinones are suicide inhibitors of mycobacterial decaprenylphosphoryl-beta-D-ribofuranose 2'-oxidase DprE1. J Am Chem Soc 134:912-5.

58. Abrahams KA, Batt SM, Gurcha SS, Veerapen N, Bashiri G, Besra GS. 2023. DprE2 is a molecular target of the anti-tubercular nitroimidazole compounds pretomanid and delamanid. Nat Commun 14:3828.

59. Batt SM, Toth S, Rodriguez B, Abrahams KA, Veerapen N, Chiodarelli G, Cox LR, Moynihan PJ, Lelievre J, Futterer K, Besra GS. 2023. Assay development and inhibition of the Mt-DprE2 essential reductase from Mycobacterium tuberculosis. Microbiology (Reading) 169.

60. Stanley SA, Grant SS, Kawate T, Iwase N, Shimizu M, Wivagg C, Silvis M, Kazyanskaya E, Aquadro J, Golas A, Fitzgerald M, Dai H, Zhang L, Hung DT. 2012. Identification of novel inhibitors of M. tuberculosis growth using whole cell based high-throughput screening. ACS Chem Biol 7:1377-84.

61. Imran M, Khan SA, Asdaq SMB, Almehmadi M, Abdulaziz O, Kamal M, Alshammari MK, Alsubaihi LI, Hussain KH, Alharbi AS, Alzahrani AK. 2022. An insight into the discovery, clinical studies, compositions, and patents of macozinone: A drug targeting the DprE1 enzyme of Mycobacterium tuberculosis. J Infect Public Health 15:1097-1107.

62.   Raman S, Song T, Puyang X, Bardarov S, Jacobs WR, Jr., Husson RN. 2001. The alternative sigma factor SigH regulates major components of oxidative and heat stress responses in Mycobacterium tuberculosis. J Bacteriol 183:6119-25.

63.   Albesa-Jove D, Comino N, Tersa M, Mohorko E, Urresti S, Dainese E, Chiarelli LR, Pasca MR, Manganelli R, Makarov V, Riccardi G, Svergun DI, Glockshuber R, Guerin ME. 2015. The Redox State Regulates the Conformation of Rv2466c to Activate the Antitubercular Prodrug TP053. J Biol Chem 290:31077-89.

64.   Rosado LA, Wahni K, Degiacomi G, Pedre B, Young D, de la Rubia AG, Boldrin F, Martens E, Marcos-Pascual L, Sancho-Vaello E, Albesa-Jove D, Provvedi R, Martin C, Makarov V, Versees W, Verniest G, Guerin ME, Mateos LM, Manganelli R, Messens J. 2017. The antibacterial prodrug activator Rv2466c is a mycothiol-dependent reductase in the oxidative stress response of Mycobacterium tuberculosis. J Biol Chem 292:13097-13110.

65.   Rawat M, Johnson C, Cadiz V, Av-Gay Y. 2007. Comparative analysis of mutants in the mycothiol biosynthesis pathway in Mycobacterium smegmatis. Biochem Biophys Res Commun 363:71-6.

66.   Newton GL, Buchmeier N, Fahey RC. 2008. Biosynthesis and functions of mycothiol, the unique protective thiol of Actinobacteria. Microbiol Mol Biol Rev 72:471-94.

67.   Sareen D, Newton GL, Fahey RC, Buchmeier NA. 2003. Mycothiol is essential for growth of Mycobacterium tuberculosis Erdman. J Bacteriol 185:6736-40.

68.   Chiarelli LR, Salina EG, Mori G, Azhikina T, Riabova O, Lepioshkin A, Grigorov A, Forbak M, Madacki J, Orena BS, Manfredi M, Gosetti F, Buzzi A, Degiacomi G, Sammartino JC, Marengo E, Kordulakova J, Riccardi G, Mikusova K, Makarov V, Pasca MR. 2020. New Insights into the Mechanism of Action of the Thienopyrimidine Antitubercular Prodrug TP053. ACS Infect Dis 6:313-323.

69.   Mori G, Orena BS, Chiarelli LR, Degiacomi G, Riabova O, Sammartino JC, Makarov V, Riccardi G, Pasca MR. 2020. Rv0579 Is Involved in the Resistance to the TP053 Antitubercular Prodrug. Front Microbiol 11:292.

70.   Mu R, Kong C, Yu W, Wang H, Ma Y, Li X, Wu J, Somersan-Karakaya S, Li H, Sun Z, Liu G. 2019. Nitrooxidoreductase Rv2466c-Dependent Fluorescent Probe for Mycobacterium tuberculosis Diagnosis and Drug Susceptibility Testing. ACS Infect Dis 5:949-961.

71.   Li X, Geng P, Hong X, Sun Z, Liu G. 2021. Detecting Mycobacterium Tuberculosis using a nitrofuranyl calanolide-trehalose probe based on nitroreductase Rv2466c. Chem Commun (Camb) 57:13174-13177.

72.   Zheng P, Somersan-Karakaya S, Lu S, Roberts J, Pingle M, Warrier T, Little D, Guo X, Brickner SJ, Nathan CF, Gold B, Liu G. 2014. Synthetic calanolides with bactericidal activity against replicating and nonreplicating Mycobacterium tuberculosis. J Med Chem 57:3755-72.

73. Geng P, Hong X, Li X, Ni D, Liu G. 2022. Optimization of nitrofuranyl calanolides for the fluorescent detection of Mycobacterium tuberculosis. Eur J Med Chem 244:114835.

74. Grimm JB, Heckman LM, Lavis LD. 2013. The chemistry of small-molecule fluorogenic probes. Prog Mol Biol Transl Sci 113:1-34.

75. Murugasu-Oei B, Tay A, Dick T. 1999. Upregulation of stress response genes and ABC transporters in anaerobic stationary-phase Mycobacterium smegmatis. Mol Gen Genet 262:677-82.

76. Hong X, Geng P, Tian N, Li X, Gao M, Nie L, Sun Z, Liu G. 2024. From Bench to Clinic: A Nitroreductase Rv3368c-Responsive Cyanine-Based Probe for the Specific Detection of Live Mycobacterium tuberculosis. Anal Chem 96:1576-1586.

77. Chauhan S, Tyagi JS. 2009. Powerful induction of divergent tgs1-Rv3131 genes in Mycobacterium tuberculosis is mediated by DevR interaction with a high-affinity site and an adjacent cryptic low-affinity site. J Bacteriol 191:6075-81.

78. Shiraz M, Lata S, Kumar P, Shankar UN, Akif M. 2021. Immunoinformatics analysis of antigenic epitopes and designing of a multi-epitope peptide vaccine from putative nitro-reductases of Mycobacterium tuberculosis DosR. Infect Genet Evol 94:105017.

79. Purkayastha A, McCue LA, McDonough KA. 2002. Identification of a Mycobacterium tuberculosis putative classical nitroreductase gene whose expression is coregulated with that of the acr aene within macrophages, in standing versus shaking cultures, and under low oxygen conditions. Infect Immun 70:1518-29.

80. Peddireddy V, Doddam SN, Qureshi IA, Yerra P, Ahmed N. 2016. A putative nitroreductase from the DosR regulon of Mycobacterium tuberculosis induces pro-inflammatory cytokine expression via TLR2 signaling pathway. Sci Rep 6:24535.

81. Kwon KW, Kim WS, Kim H, Han SJ, Hahn MY, Lee JS, Nam KT, Cho SN, Shin SJ. 2017. Novel vaccine potential of Rv3131, a DosR regulon-encoded putative nitroreductase, against hyper-virulent Mycobacterium tuberculosis strain K. Sci Rep 7:44151.

82. Dong WZ, Shi J, Chu P, Liu RM, Wen SA, Zhang TT, Pang Y, Lu J. 2022. The putative NAD(P)H Nitroreductase, Rv3131, is the Probable Activating Enzyme for Metronidazole in Mycobacterium Tuberculosis. Biomed Environ Sci 35:652-656.

83. Khosla N, Thayil SM, Kaur R, Kesavan AK. 2021. MSMEG_3955 from Mycobacterium smegmatis is a FMN bounded homotrimeric NAD(P)H:Flavin mononucleotide (FMN) oxidoreductase. BMC Microbiol 21:319.

84. Hrdy I, Cammack R, Stopka P, Kulda J, Tachezy J. 2005. Alternative pathway of metronidazole activation in Trichomonas vaginalis hydrogenosomes. Antimicrob Agents Chemother 49:5033-6.

85.	Lofmark S, Edlund C, Nord CE. 2010. Metronidazole is still the drug of choice for treatment of anaerobic infections. Clin Infect Dis 50 Suppl 1:S16-23.

86.	Jenks PJ, Edwards DI. 2002. Metronidazole resistance in Helicobacter pylori. Int J Antimicrob Agents 19:1-7.

87.	Edwards DI. 1981. Mechanisms of cytotoxicity of nitroimidazole drugs. Prog Med Chem 18:87-116.

88.	Wayne LG, Sramek HA. 1994. Metronidazole is bactericidal to dormant cells of Mycobacterium tuberculosis. Antimicrob Agents Chemother 38:2054-8.

89.	Lin PL, Dartois V, Johnston PJ, Janssen C, Via L, Goodwin MB, Klein E, Barry CE, 3rd, Flynn JL. 2012. Metronidazole prevents reactivation of latent Mycobacterium tuberculosis infection in macaques. Proc Natl Acad Sci U S A 109:14188-93.

90.	Chauviac FX, Bommer M, Yan J, Parkin G, Daviter T, Lowden P, Raven EL, Thalassinos K, Keep NH. 2012. Crystal structure of reduced MsAcg, a putative nitroreductase from Mycobacterium smegmatis and a close homologue of Mycobacterium tuberculosis Acg. J Biol Chem 287:44372-83.

91.	Hu Y, Coates AR. 2011. Mycobacterium tuberculosis acg gene is required for growth and virulence in vivo. PLoS One 6:e20958.

92.	Van den Bossche A, Varet H, Sury A, Sismeiro O, Legendre R, Coppee JY, Mathys V, Ceyssens PJ. 2019. Transcriptional profiling of a laboratory and clinical Mycobacterium tuberculosis strain suggests respiratory poisoning upon exposure to delamanid. Tuberculosis (Edinb) 117:18-23.

93.	Ambroso JL, Dillberger J, Bruning-Barry R, Yang T. 2022. Assessment of the Carcinogenic Potential of Pretomanid in Transgenic Tg.rasH2 Mice. Int J Toxicol 41:367-379.

94.	Adil M, Iqbal W, Adnan F, Wazir S, Khan I, Khayam MU, Kamal MA, Ahmad S, Ahmed J, Khan IN. 2018. Association of Metronidazole with Cancer: A Potential Risk Factor or Inconsistent Deductions? Curr Drug Metab 19:902-909.

95.	Danielson DA, Hannan MT, Jick H. 1982. Metronidazole and cancer. JAMA 247:2498-9.

96.	AM AK, Fleiszer DM, Richards GK, Senterman MK, Brown RA. 1984. Effect of long-term metronidazole (MTZ) therapy on experimental colon cancer in rats. J Surg Res 36:547-52.

97.	Rustia M, Shubik P. 1972. Induction of lung tumors and malignant lymphomas in mice by metronidazole. J Natl Cancer Inst 48:721-9.

98.   Ashtekar DR, Costa-Perira R, Nagrajan K, Vishvanathan N, Bhatt AD, Rittel W. 1993. In vitro and in vivo activities of the nitroimidazole CGI 17341 against Mycobacterium tuberculosis. Antimicrob Agents Chemother 37:183-6.

99.   Mitchison D, Davies G. 2012. The chemotherapy of tuberculosis: past, present and future. Int J Tuberc Lung Dis 16:724-32.

100.   Goldstein BP. 2014. Resistance to rifampicin: a review. J Antibiot (Tokyo) 67:625-30.

101.   Manjunatha UH, SP SR, Kondreddi RR, Noble CG, Camacho LR, Tan BH, Ng SH, Ng PS, Ma NL, Lakshminarayana SB, Herve M, Barnes SW, Yu W, Kuhen K, Blasco F, Beer D, Walker JR, Tonge PJ, Glynne R, Smith PW, Diagana TT. 2015. Direct inhibitors of InhA are active against Mycobacterium tuberculosis. Sci Transl Med 7:269ra3.

102.   Pham DD, Fattal E, Tsapis N. 2015. Pulmonary drug delivery systems for tuberculosis treatment. Int J Pharm 478:517-29.

103.   Fan C, Eedara BB, Sinha S, Uddin MKM, Doyle C, Banu S, Das SC. 2024. Triple combination dry powder formulation of pretomanid, moxifloxacin, and pyrazinamide for treatment of multidrug-resistant tuberculosis. Int J Pharm 654:123984.

104.   Sung JC, Garcia-Contreras L, Verberkmoes JL, Peloquin CA, Elbert KJ, Hickey AJ, Edwards DA. 2009. Dry powder nitroimidazopyran antibiotic PA-824 aerosol for inhalation. Antimicrob Agents Chemother 53:1338-43.

105.   Garcia-Contreras L, Sung JC, Muttil P, Padilla D, Telko M, Verberkmoes JL, Elbert KJ, Hickey AJ, Edwards DA. 2010. Dry powder PA-824 aerosols for treatment of tuberculosis in guinea pigs. Antimicrob Agents Chemother 54:1436-42.

106.   Patil SM, Barji DS, Chavan T, Patel K, Collazo AJ, Prithipaul V, Muth A, Kunda NK. 2023. Solubility Enhancement and Inhalation Delivery of Cyclodextrin-Based Inclusion Complex of Delamanid for Pulmonary Tuberculosis Treatment. AAPS PharmSciTech 24:49.

107.   Patel A, Redinger N, Richter A, Woods A, Neumann PR, Keegan G, Childerhouse N, Imming P, Schaible UE, Forbes B, Dailey LA. 2020. In vitro and in vivo antitubercular activity of benzothiazinone-loaded human serum albumin nanocarriers designed for inhalation. J Control Release 328:339-349.

108.   Bagcchi S. 2023. WHO's Global Tuberculosis Report 2022. Lancet Microbe 4:e20.

109.   Edwards BD, Field SK. 2022. The Struggle to End a Millennia-Long Pandemic: Novel Candidate and Repurposed Drugs for the Treatment of Tuberculosis. Drugs 82:1695-1715.

110.   Scarim CB, Pavan FR. 2022. Recent advancement in drug development of nitro(NO(2))-heterocyclic compounds as lead scaffolds for the treatment of Mycobacterium tuberculosis. Drug Dev Res 83:842-858.

111.   Mudde SE, Upton AM, Lenaerts A, Bax HI, De Steenwinkel JEM. 2022. Delamanid or pretomanid? A Solomonic judgement! J Antimicrob Chemother 77:880-902.

112.   Gupta R, Geiter LJ, Hafkin J, Wells CD. 2015. Delamanid and QT prolongation in the treatment of multidrug-resistant tuberculosis. Int J Tuberc Lung Dis 19:1261-2.

113.   Zheng H, Colvin CJ, Johnson BK, Kirchhoff PD, Wilson M, Jorgensen-Muga K, Larsen SD, Abramovitch RB. 2017. Inhibitors of Mycobacterium tuberculosis DosRST signaling and persistence. Nat Chem Biol 13:218-225.

114.   Yempalla KR, Munagala G, Singh S, Magotra A, Kumar S, Rajput VS, Bharate SS, Tikoo M, Singh GD, Khan IA, Vishwakarma RA, Singh PP. 2015. Nitrofuranyl Methyl Piperazines as New Anti-TB Agents: Identification, Validation, Medicinal Chemistry, and PK Studies. ACS Med Chem Lett 6:1041-6.

115.   Pankey GA, Sabath LD. 2004. Clinical relevance of bacteriostatic versus bactericidal mechanisms of action in the treatment of Gram-positive bacterial infections. Clin Infect Dis 38:864-70.

116.   Wald-Dickler N, Holtom P, Spellberg B. 2018. Busting the Myth of "Static vs Cidal": A Systemic Literature Review. Clin Infect Dis 66:1470-1474.

117.   Boon C, Dick T. 2012. How Mycobacterium tuberculosis goes to sleep: the dormancy survival regulator DosR a decade later. Future Microbiol 7:513-8.

118.   Gengenbacher M, Kaufmann SH. 2012. Mycobacterium tuberculosis: success through dormancy. FEMS Microbiol Rev 36:514-32.

119.   Zheng H, Abramovitch RB. 2020. Inhibiting DosRST as a new approach to tuberculosis therapy. Future Med Chem 12:457-467.

120.   Mak PA, Rao SP, Ping Tan M, Lin X, Chyba J, Tay J, Ng SH, Tan BH, Cherian J, Duraiswamy J, Bifani P, Lim V, Lee BH, Ling Ma N, Beer D, Thayalan P, Kuhen K, Chatterjee A, Supek F, Glynne R, Zheng J, Boshoff HI, Barry CE, 3rd, Dick T, Pethe K, Camacho LR. 2012. A high-throughput screen to identify inhibitors of ATP homeostasis in non-replicating Mycobacterium tuberculosis. ACS Chem Biol 7:1190-7.

121.   Li L, Lv K, Yang Y, Sun J, Tao Z, Wang A, Wang B, Wang H, Geng Y, Liu M, Guo H, Lu Y. 2018. Identification of N-Benzyl 3,5-Dinitrobenzamides Derived from PBTZ169 as Antitubercular Agents. ACS Med Chem Lett 9:741-745.

122.   Brecik M, Centarova I, Mukherjee R, Kolly GS, Huszar S, Bobovska A, Kilacskova E, Mokosova V, Svetlikova Z, Sarkan M, Neres J, Kordulakova J, Cole ST, Mikusova K. 2015. DprE1 Is a Vulnerable Tuberculosis Drug Target Due to Its Cell Wall Localization. ACS Chem Biol 10:1631-6.

123. Gawad J, Bonde C. 2018. Decaprenyl-phosphoryl-ribose 2'-epimerase (DprE1): challenging target for antitubercular drug discovery. Chem Cent J 12:72.

124. Shi J, Lu J, Wen S, Zong Z, Huo F, Luo J, Liang Q, Li Y, Huang H, Pang Y. 2018. In Vitro Activity of PBTZ169 against Multiple Mycobacterium Species. Antimicrob Agents Chemother 62.

125. Ahmed FH, Carr PD, Lee BM, Afriat-Jurnou L, Mohamed AE, Hong NS, Flanagan J, Taylor MC, Greening C, Jackson CJ. 2015. Sequence-Structure-Function Classification of a Catalytically Diverse Oxidoreductase Superfamily in Mycobacteria. J Mol Biol 427:3554-3571.

126. Selengut JD, Haft DH. 2010. Unexpected abundance of coenzyme F(420)-dependent enzymes in Mycobacterium tuberculosis and other actinobacteria. J Bacteriol 192:5788-98.

127. Nessar R, Cambau E, Reyrat JM, Murray A, Gicquel B. 2012. Mycobacterium abscessus: a new antibiotic nightmare. J Antimicrob Chemother 67:810-8.

128. Incandela ML, Perrin E, Fondi M, de Jesus Lopes Ribeiro AL, Mori G, Moiana A, Gramegna M, Fani R, Riccardi G, Pasca MR. 2013. DprE1, a new taxonomic marker in mycobacteria. FEMS Microbiol Lett 348:66-73.

129. Poulton NC, Rock JM. 2022. Unraveling the mechanisms of intrinsic drug resistance in Mycobacterium tuberculosis. Front Cell Infect Microbiol 12:997283.

130. Williams JT, Haiderer ER, Coulson GB, Conner KN, Ellsworth E, Chen C, Alvarez-Cabrera N, Li W, Jackson M, Dick T, Abramovitch RB. 2019. Identification of New MmpL3 Inhibitors by Untargeted and Targeted Mutant Screens Defines MmpL3 Domains with Differential Resistance. Antimicrob Agents Chemother 63.

131. Barrick JE, Colburn G, Deatherage DE, Traverse CC, Strand MD, Borges JJ, Knoester DB, Reba A, Meyer AG. 2014. Identifying structural variation in haploid microbial genomes from short-read resequencing data using breseq. BMC Genomics 15:1039.

132. Deatherage DE, Barrick JE. 2014. Identification of mutations in laboratory-evolved microbes from next-generation sequencing data using breseq. Methods Mol Biol 1151:165-88.

133. Johansen MD, Herrmann JL, Kremer L. 2020. Non-tuberculous mycobacteria and the rise of Mycobacterium abscessus. Nat Rev Microbiol 18:392-407.

134. Ganapathy US, Dartois V, Dick T. 2019. Repositioning rifamycins for Mycobacterium abscessus lung disease. Expert Opin Drug Discov 14:867-878.

135.	Chen Y, Chen J, Zhang S, Shi W, Zhang W, Zhu M, Zhang Y. 2018. Novel Mutations Associated with Clofazimine Resistance in Mycobacterium abscessus. Antimicrob Agents Chemother 62.

136.	Aziz DB, Low JL, Wu ML, Gengenbacher M, Teo JWP, Dartois V, Dick T. 2017. Rifabutin Is Active against Mycobacterium abscessus Complex. Antimicrob Agents Chemother 61.

137.	Rominski A, Roditscheff A, Selchow P, Bottger EC, Sander P. 2017. Intrinsic rifamycin resistance of Mycobacterium abscessus is mediated by ADP-ribosyltransferase MAB_0591. J Antimicrob Chemother 72:376-384.

138.	Ganapathy US, Del Rio RG, Cacho-Izquierdo M, Ortega F, Lelievre J, Barros-Aguirre D, Aragaw WW, Zimmerman MD, Lindman M, Dartois V, Gengenbacher M, Dick T. 2021. A Mycobacterium tuberculosis NBTI DNA Gyrase Inhibitor Is Active against Mycobacterium abscessus. Antimicrob Agents Chemother 65:e0151421.

139.	Sarathy JP, Ganapathy US, Zimmerman MD, Dartois V, Gengenbacher M, Dick T. 2020. TBAJ-876, a 3,5-Dialkoxypyridine Analogue of Bedaquiline, Is Active against Mycobacterium abscessus. Antimicrob Agents Chemother 64.

140.	Ferro BE, van Ingen J, Wattenberg M, van Soolingen D, Mouton JW. 2015. Time-kill kinetics of antibiotics active against rapidly growing mycobacteria. J Antimicrob Chemother 70:811-7.

141.	Bellerose MM, Baek SH, Huang CC, Moss CE, Koh EI, Proulx MK, Smith CM, Baker RE, Lee JS, Eum S, Shin SJ, Cho SN, Murray M, Sassetti CM. 2019. Common Variants in the Glycerol Kinase Gene Reduce Tuberculosis Drug Efficacy. mBio 10.

142.	Pethe K, Sequeira PC, Agarwalla S, Rhee K, Kuhen K, Phong WY, Patel V, Beer D, Walker JR, Duraiswamy J, Jiricek J, Keller TH, Chatterjee A, Tan MP, Ujjini M, Rao SP, Camacho L, Bifani P, Mak PA, Ma I, Barnes SW, Chen Z, Plouffe D, Thayalan P, Ng SH, Au M, Lee BH, Tan BH, Ravindran S, Nanjundappa M, Lin X, Goh A, Lakshminarayana SB, Shoen C, Cynamon M, Kreiswirth B, Dartois V, Peters EC, Glynne R, Brenner S, Dick T. 2010. A chemical genetic screen in Mycobacterium tuberculosis identifies carbon-source-dependent growth inhibitors devoid of in vivo efficacy. Nat Commun 1:57.

143.	Poblete-Castro I, Wittmann C, Nikel PI. 2020. Biochemistry, genetics and biotechnology of glycerol utilization in Pseudomonas species. Microb Biotechnol 13:32-53.

144.	Kapopoulou A, Lew JM, Cole ST. 2011. The MycoBrowser portal: a comprehensive and manually annotated resource for mycobacterial genomes. Tuberculosis (Edinb) 91:8-13.

145.	Fan X, Tang X, Yan J, Xie J. 2014. Identification of idiosyncratic Mycobacterium tuberculosis ribosomal protein subunits with implications in extraribosomal function, persistence, and drug resistance based on transcriptome data. J Biomol Struct Dyn 32:1546-51.

146. Wang F, Langley R, Gulten G, Wang L, Sacchettini JC. 2007. Identification of a type III thioesterase reveals the function of an operon crucial for Mtb virulence. Chem Biol 14:543-51.

147. Waddell SJ, Chung GA, Gibson KJ, Everett MJ, Minnikin DE, Besra GS, Butcher PD. 2005. Inactivation of polyketide synthase and related genes results in the loss of complex lipids in Mycobacterium tuberculosis H37Rv. Lett Appl Microbiol 40:201-6.

148. Nguyen PC, Nguyen VS, Martin BP, Fourquet P, Camoin L, Spilling CD, Cavalier JF, Cambillau C, Canaan S. 2018. Biochemical and Structural Characterization of TesA, a Major Thioesterase Required for Outer-Envelope Lipid Biosynthesis in Mycobacterium tuberculosis. J Mol Biol 430:5120-5136.

149. Buglino J, Onwueme KC, Ferreras JA, Quadri LE, Lima CD. 2004. Crystal structure of PapA5, a phthiocerol dimycocerosyl transferase from Mycobacterium tuberculosis. J Biol Chem 279:30634-42.

150. Chavadi SS, Onwueme KC, Edupuganti UR, Jerome J, Chatterjee D, Soll CE, Quadri LEN. 2012. The mycobacterial acyltransferase PapA5 is required for biosynthesis of cell wall-associated phenolic glycolipids. Microbiology (Reading) 158:1379-1387.

151. Madacki J, Laval F, Grzegorzewicz A, Lemassu A, Zahorszka M, Arand M, McNeil M, Daffe M, Jackson M, Laneelle MA, Kordulakova J. 2018. Impact of the epoxide hydrolase EphD on the metabolism of mycolic acids in mycobacteria. J Biol Chem 293:5172-5184.

152. Wilson M, DeRisi J, Kristensen HH, Imboden P, Rane S, Brown PO, Schoolnik GK. 1999. Exploring drug-induced alterations in gene expression in Mycobacterium tuberculosis by microarray hybridization. Proc Natl Acad Sci U S A 96:12833-8.

153. Cox JAG, Taylor RC, Brown AK, Attoe S, Besra GS, Futterer K. 2019. Crystal structure of Mycobacterium tuberculosis FadB2 implicated in mycobacterial beta-oxidation. Acta Crystallogr D Struct Biol 75:101-108.

154. Dutta D. 2018. Advance in Research on Mycobacterium tuberculosis FabG4 and Its Inhibitor. Front Microbiol 9:1184.

155. Lu R, Schmitz W, Sampson NS. 2015. alpha-Methyl Acyl CoA Racemase Provides Mycobacterium tuberculosis Catabolic Access to Cholesterol Esters. Biochemistry 54:5669-72.

156. Lee CL, Ng HF, Ngeow YF, Thaw Z. 2021. A stop-gain mutation in sigma factor SigH (MAB_3543c) may be associated with tigecycline resistance in Mycobacteroides abscessus. J Med Microbiol 70.

157. Venugopal A, Bryk R, Shi S, Rhee K, Rath P, Schnappinger D, Ehrt S, Nathan C. 2011. Virulence of Mycobacterium tuberculosis depends on lipoamide dehydrogenase, a member of three multienzyme complexes. Cell Host Microbe 9:21-31.

158.   Roux AL, Viljoen A, Bah A, Simeone R, Bernut A, Laencina L, Deramaudt T, Rottman M, Gaillard JL, Majlessi L, Brosch R, Girard-Misguich F, Vergne I, de Chastellier C, Kremer L, Herrmann JL. 2016. The distinct fate of smooth and rough Mycobacterium abscessus variants inside macrophages. Open Biol 6.

159.   Ruger K, Hampel A, Billig S, Rucker N, Suerbaum S, Bange FC. 2014. Characterization of rough and smooth morphotypes of Mycobacterium abscessus isolates from clinical specimens. J Clin Microbiol 52:244-50.

160.   Sharp JD, Singh AK, Park ST, Lyubetskaya A, Peterson MW, Gomes AL, Potluri LP, Raman S, Galagan JE, Husson RN. 2016. Comprehensive Definition of the SigH Regulon of Mycobacterium tuberculosis Reveals Transcriptional Control of Diverse Stress Responses. PLoS One 11:e0152145.

161.   Ng HF, Tan JL, Zin T, Yap SF, Ngeow YF. 2018. A mutation in anti-sigma factor MAB_3542c may be responsible for tigecycline resistance in Mycobacterium abscessus. J Med Microbiol 67:1676-1681.

162.   Rohde KH, Abramovitch RB, Russell DG. 2007. Mycobacterium tuberculosis invasion of macrophages: linking bacterial gene expression to environmental cues. Cell Host Microbe 2:352-64.

163.   He H, Hovey R, Kane J, Singh V, Zahrt TC. 2006. MprAB is a stress-responsive two-component system that directly regulates expression of sigma factors SigB and SigE in Mycobacterium tuberculosis. J Bacteriol 188:2134-43.

164.   Yan M, Cao L, Zhao L, Zhou W, Liu X, Zhang W, Rao Z. 2023. The Key Roles of Mycobacterium tuberculosis FadD23 C-terminal Domain in Catalytic Mechanisms. Front Microbiol 14:1090534.

165.   Quadri LE. 2014. Biosynthesis of mycobacterial lipids by polyketide synthases and beyond. Crit Rev Biochem Mol Biol 49:179-211.

166.   Sulzenbacher G, Canaan S, Bordat Y, Neyrolles O, Stadthagen G, Roig-Zamboni V, Rauzier J, Maurin D, Laval F, Daffe M, Cambillau C, Gicquel B, Bourne Y, Jackson M. 2006. LppX is a lipoprotein required for the translocation of phthiocerol dimycocerosates to the surface of Mycobacterium tuberculosis. EMBO J 25:1436-44.

167.   Tripathi P, Singh LK, Kumari S, Hakiem OR, Batra JK. 2020. ClpB is an essential stress regulator of Mycobacterium tuberculosis and endows survival advantage to dormant bacilli. Int J Med Microbiol 310:151402.

168.   Vaubourgeix J, Lin G, Dhar N, Chenouard N, Jiang X, Botella H, Lupoli T, Mariani O, Yang G, Ouerfelli O, Unser M, Schnappinger D, McKinney J, Nathan C. 2015. Stressed mycobacteria use the chaperone ClpB to sequester irreversibly oxidized proteins asymmetrically within and between cells. Cell Host Microbe 17:178-90.

169. Lucarelli D, Vasil ML, Meyer-Klaucke W, Pohl E. 2008. The Metal-Dependent Regulators FurA and FurB from Mycobacterium Tuberculosis. Int J Mol Sci 9:1548-1560.

170. Lin K, O'Brien KM, Trujillo C, Wang R, Wallach JB, Schnappinger D, Ehrt S. 2016. Mycobacterium tuberculosis Thioredoxin Reductase Is Essential for Thiol Redox Homeostasis but Plays a Minor Role in Antioxidant Defense. PLoS Pathog 12:e1005675.

171. Bhat SA, Singh N, Trivedi A, Kansal P, Gupta P, Kumar A. 2012. The mechanism of redox sensing in Mycobacterium tuberculosis. Free Radic Biol Med 53:1625-41.

172. Williams JT, Giletto M, Haiderer ER, Aleiwi B, Krieger-Burke T, Ellsworth E, Abramovitch RB. 2024. The Mycobacterium tuberculosis MmpL3 inhibitor MSU-43085 is active in a mouse model of infection. Microbiol Spectr 12:e0367723.

173. Russell DG, Cardona PJ, Kim MJ, Allain S, Altare F. 2009. Foamy macrophages and the progression of the human tuberculosis granuloma. Nat Immunol 10:943-8.

174. Ehlers S, Schaible UE. 2012. The granuloma in tuberculosis: dynamics of a host-pathogen collusion. Front Immunol 3:411.

175. Kanji A, Hasan R, Hasan Z. 2019. Efflux pump as alternate mechanism for drug resistance in Mycobacterium tuberculosis. Indian J Tuberc 66:20-25.

176. Driver ER, Ryan GJ, Hoff DR, Irwin SM, Basaraba RJ, Kramnik I, Lenaerts AJ. 2012. Evaluation of a mouse model of necrotic granuloma formation using C3HeB/FeJ mice for testing of drugs against Mycobacterium tuberculosis. Antimicrob Agents Chemother 56:3181-95.

177. Irwin SM, Prideaux B, Lyon ER, Zimmerman MD, Brooks EJ, Schrupp CA, Chen C, Reichlen MJ, Asay BC, Voskuil MI, Nuermberger EL, Andries K, Lyons MA, Dartois V, Lenaerts AJ. 2016. Bedaquiline and Pyrazinamide Treatment Responses Are Affected by Pulmonary Lesion Heterogeneity in Mycobacterium tuberculosis Infected C3HeB/FeJ Mice. ACS Infect Dis 2:251-267.

178. Robertson GT, Ramey ME, Massoudi LM, Carter CL, Zimmerman M, Kaya F, Graham BG, Gruppo V, Hastings C, Woolhiser LK, Scott DWL, Asay BC, Eshun-Wilson F, Maidj E, Podell BK, Vasquez JJ, Lyons MA, Dartois V, Lenaerts AJ. 2021. Comparative Analysis of Pharmacodynamics in the C3HeB/FeJ Mouse Tuberculosis Model for DprE1 Inhibitors TBA-7371, PBTZ169, and OPC-167832. Antimicrob Agents Chemother 65:e0058321.

179. Khawbung JL, Nath D, Chakraborty S. 2021. Drug resistant Tuberculosis: A review. Comp Immunol Microbiol Infect Dis 74:101574.

180. Zheng H, Williams JT, Aleiwi B, Ellsworth E, Abramovitch RB. 2020. Inhibiting Mycobacterium tuberculosis DosRST Signaling by Targeting Response Regulator DNA Binding and Sensor Kinase Heme. ACS Chem Biol 15:52-62.

181.	Ananthan S, Faaleolea ER, Goldman RC, Hobrath JV, Kwong CD, Laughon BE, Maddry JA, Mehta A, Rasmussen L, Reynolds RC, Secrist JA, 3rd, Shindo N, Showe DN, Sosa MI, Suling WJ, White EL. 2009. High-throughput screening for inhibitors of Mycobacterium tuberculosis H37Rv. Tuberculosis (Edinb) 89:334-53.

182.	Maddry JA, Ananthan S, Goldman RC, Hobrath JV, Kwong CD, Maddox C, Rasmussen L, Reynolds RC, Secrist JA, 3rd, Sosa MI, White EL, Zhang W. 2009. Antituberculosis activity of the molecular libraries screening center network library. Tuberculosis (Edinb) 89:354-63.

183.	Williams JT, Abramovitch RB. 2023. Molecular Mechanisms of MmpL3 Function and Inhibition. Microb Drug Resist 29:190-212.

184.	Zhang Y, Shi W, Zhang W, Mitchison D. 2014. Mechanisms of Pyrazinamide Action and Resistance. Microbiol Spectr 2:MGM2-0023-2013.

185.	Shi W, Zhang X, Jiang X, Yuan H, Lee JS, Barry CE, 3rd, Wang H, Zhang W, Zhang Y. 2011. Pyrazinamide inhibits trans-translation in Mycobacterium tuberculosis. Science 333:1630-2.

186.	Zhang Y, Heym B, Allen B, Young D, Cole S. 1992. The catalase-peroxidase gene and isoniazid resistance of Mycobacterium tuberculosis. Nature 358:591-3.

187.	Lei B, Wei CJ, Tu SC. 2000. Action mechanism of antitubercular isoniazid. Activation by Mycobacterium tuberculosis KatG, isolation, and characterization of inha inhibitor. J Biol Chem 275:2520-6.

188.	Guha R, Van Drie JH. 2008. Structure--activity landscape index: identifying and quantifying activity cliffs. J Chem Inf Model 48:646-58.

189.	Dover LG, Alahari A, Gratraud P, Gomes JM, Bhowruth V, Reynolds RC, Besra GS, Kremer L. 2007. EthA, a common activator of thiocarbamide-containing drugs acting on different mycobacterial targets. Antimicrob Agents Chemother 51:1055-63.

190.	Qian L, Ortiz de Montellano PR. 2006. Oxidative activation of thiacetazone by the Mycobacterium tuberculosis flavin monooxygenase EtaA and human FMO1 and FMO3. Chem Res Toxicol 19:443-9.

191.	Singh BK, Singha M, Basak S, Biswas R, Das AK, Basak A. 2022. Fluorescently labelled thioacetazone for detecting the interaction with Mycobacterium dehydratases HadAB and HadBC. Org Biomol Chem 20:1444-1452.

192.	Alahari A, Trivelli X, Guerardel Y, Dover LG, Besra GS, Sacchettini JC, Reynolds RC, Coxon GD, Kremer L. 2007. Thiacetazone, an antitubercular drug that inhibits cyclopropanation of cell wall mycolic acids in mycobacteria. PLoS One 2:e1343.

193.   Tangallapally RP, Lee RE, Lenaerts AJ, Lee RE. 2006. Synthesis of new and potent analogues of anti-tuberculosis agent 5-nitro-furan-2-carboxylic acid 4-(4-benzyl-piperazin-1-yl)-benzylamide with improved bioavailability. Bioorg Med Chem Lett 16:2584-9.

194.   Tangallapally RP, Yendapally R, Lee RE, Hevener K, Jones VC, Lenaerts AJ, McNeil MR, Wang Y, Franzblau S, Lee RE. 2004. Synthesis and evaluation of nitrofuranylamides as novel antituberculosis agents. J Med Chem 47:5276-83.

195.   Wilson R, Kumar P, Parashar V, Vilcheze C, Veyron-Churlet R, Freundlich JS, Barnes SW, Walker JR, Szymonifka MJ, Marchiano E, Shenai S, Colangeli R, Jacobs WR, Jr., Neiditch MB, Kremer L, Alland D. 2013. Antituberculosis thiophenes define a requirement for Pks13 in mycolic acid biosynthesis. Nat Chem Biol 9:499-506.

196.   Xia F, Zhang H, Yang H, Zheng M, Min W, Sun C, Yuan K, Yang P. 2023. Targeting polyketide synthase 13 for the treatment of tuberculosis. Eur J Med Chem 259:115702.

197.   Aggarwal A, Parai MK, Shetty N, Wallis D, Woolhiser L, Hastings C, Dutta NK, Galaviz S, Dhakal RC, Shrestha R, Wakabayashi S, Walpole C, Matthews D, Floyd D, Scullion P, Riley J, Epemolu O, Norval S, Snavely T, Robertson GT, Rubin EJ, Ioerger TR, Sirgel FA, van der Merwe R, van Helden PD, Keller P, Bottger EC, Karakousis PC, Lenaerts AJ, Sacchettini JC. 2017. Development of a Novel Lead that Targets M. tuberculosis Polyketide Synthase 13. Cell 170:249-259 e25.

198.   Farghali H, Kutinova Canova N, Arora M. 2021. The potential applications of artificial intelligence in drug discovery and development. Physiol Res 70:S715-S722.

199.   Johnson BK, Abramovitch RB. 2015. Macrophage infection models for Mycobacterium tuberculosis. Methods Mol Biol 1285:329-41.

200.   Haley CA, Schechter MC, Ashkin D, Peloquin CA, Peter Cegielski J, Andrino BB, Burgos M, Caloia LA, Chen L, Colon-Semidey A, DeSilva MB, Dhanireddy S, Dorman SE, Dworkin FF, Hammond-Epstein H, Easton AV, Gaensbauer JT, Ghassemieh B, Gomez ME, Horne D, Jasuja S, Jones BA, Kaplan LJ, Khan AE, Kracen E, Labuda S, Landers KM, Lardizabal AA, Lasley MT, Letzer DM, Lopes VK, Lubelchek RJ, Patricia Macias C, Mihalyov A, Misch EA, Murray JA, Narita M, Nilsen DM, Ninneman MJ, Ogawa L, Oladele A, Overman M, Ray SM, Ritger KA, Rowlinson MC, Sabuwala N, Schiller TM, Schwartz LE, Spitters C, Thomson DB, et al. 2023. Implementation of Bedaquiline, Pretomanid, and Linezolid in the United States: Experience Using a Novel All-Oral Treatment Regimen for Treatment of Rifampin-Resistant or Rifampin-Intolerant Tuberculosis Disease. Clin Infect Dis 77:1053-1062.

201.   Conradie F, Bagdasaryan TR, Borisov S, Howell P, Mikiashvili L, Ngubane N, Samoilova A, Skornykova S, Tudor E, Variava E, Yablonskiy P, Everitt D, Wills GH, Sun E, Olugbosi M, Egizi E, Li M, Holsta A, Timm J, Bateson A, Crook AM, Fabiane SM, Hunt R, McHugh TD, Tweed CD, Foraida S, Mendel CM, Spigelman M, ZeNix Trial T. 2022. Bedaquiline-Pretomanid-Linezolid Regimens for Drug-Resistant Tuberculosis. N Engl J Med 387:810-823.

202.	Conradie F, Diacon AH, Ngubane N, Howell P, Everitt D, Crook AM, Mendel CM, Egizi E, Moreira J, Timm J, McHugh TD, Wills GH, Bateson A, Hunt R, Van Niekerk C, Li M, Olugbosi M, Spigelman M, Nix TBTT. 2020. Treatment of Highly Drug-Resistant Pulmonary Tuberculosis. N Engl J Med 382:893-902.

203.	Oelofse S, Esmail A, Diacon AH, Conradie F, Olayanju O, Ngubane N, Howell P, Everitt D, Crook AM, Mendel CM, Wills GH, Olugbosi M, Del Parigi A, Sun E, Calatroni A, Spigelman M, Dheda K. 2021. Pretomanid with bedaquiline and linezolid for drug-resistant TB: a comparison of prospective cohorts. Int J Tuberc Lung Dis 25:453-460.

204.	Mukherjee T, Boshoff H, Barry CE, 3rd. 2012. Comment on: Identification of antimicrobial activity among FDA-approved drugs for combating Mycobacterium abscessus and Mycobacterium chelonae. J Antimicrob Chemother 67:252-3.

205.	Rey-Jurado E, Tudo G, Martinez JA, Gonzalez-Martin J. 2012. Synergistic effect of two combinations of antituberculous drugs against Mycobacterium tuberculosis. Tuberculosis (Edinb) 92:260-3.

206.	Larkins-Ford J, Degefu YN, Van N, Sokolov A, Aldridge BB. 2022. Design principles to assemble drug combinations for effective tuberculosis therapy using interpretable pairwise drug response measurements. Cell Rep Med 3:100737.

207.	Larkins-Ford J, Greenstein T, Van N, Degefu YN, Olson MC, Sokolov A, Aldridge BB. 2021. Systematic measurement of combination-drug landscapes to predict in vivo treatment outcomes for tuberculosis. Cell Syst 12:1046-1063 e7.

Cofactor F$_{420}$H$_2$-dependent compounds
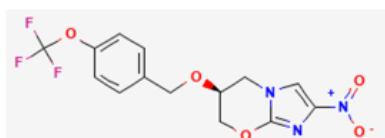
Pretomanid
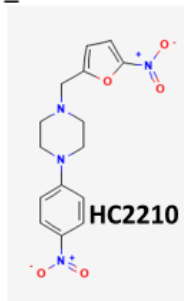
HC2210
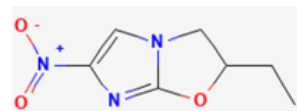
CGI-17341

DprE1 mechanism-based inhibitors
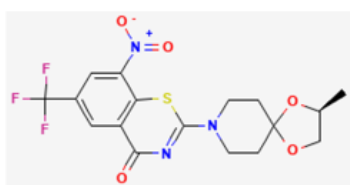
BTZ043
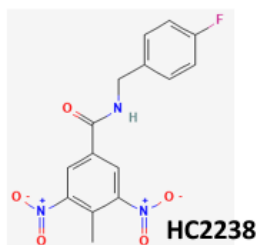
HC2238
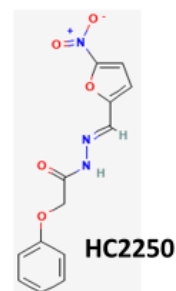
HC2250

Others
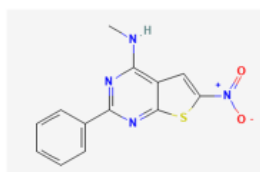
TP043
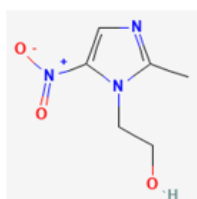
Metronidazole
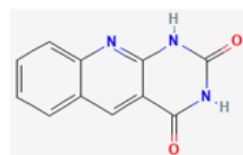
Cofactors

Deazaflavin
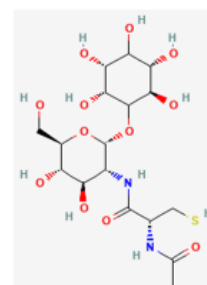
Mycothiol

Figure A.1.1. Different nitro-containing prodrugs and cofactors.
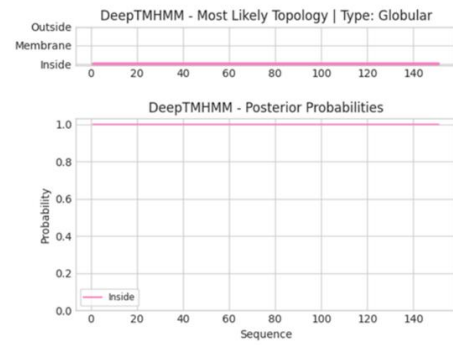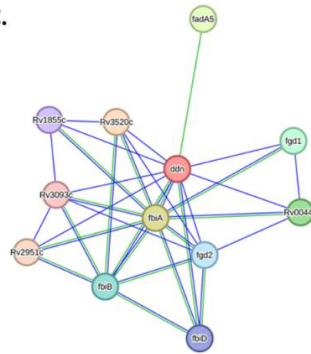
Figure A.1.2. The *in silico* prediction of the cellular localization of Ddn. **A.** The hydropathy plot of Ddn. **B.** DeepTMHMM transmembrane prediction for Ddn. **C.** The interaction network of Ddn as predicted from STRING.
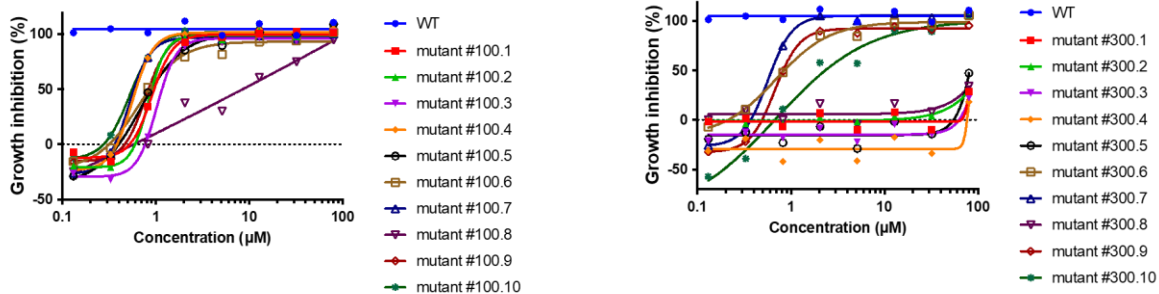
Figure A.2.1. Confirmation of spontaneous resistant mutants that were generated from plates containing either A. 100 nM or **B.** 300 nM of HC2210. The dotted lines represent the growth inhibition of the negative control (DMSO). All experiments were repeated twice with similar results.
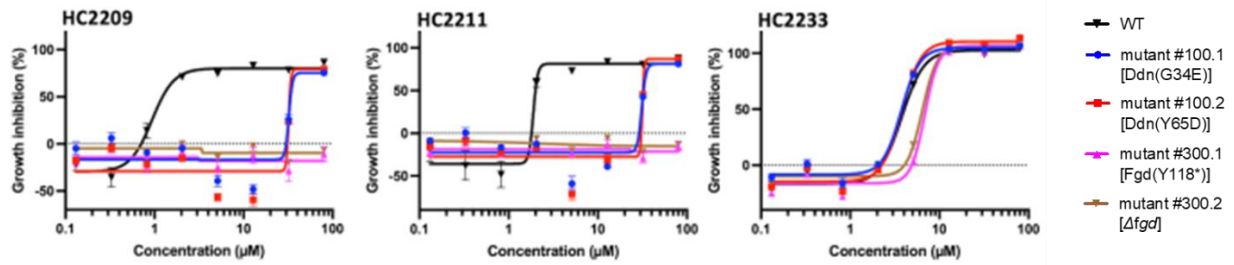
Figure A.2.2. Testing for the activity of the nitrofurans against the *ddn* and *fgd* spontaneous mutants. *fgd* mutants lead to full resistance to HC2209 and HC2211 and only a slight impact on susceptibility to HC2233. *ddn* mutants are partially resistant to HC2209 and HC2211, and fully susceptible to HC2233. The dotted lines represent the growth inhibition of the negative control (DMSO). The error bars represent the standard deviations of three biological replicates. All experiments were independently confirmed at least twice will similar results.
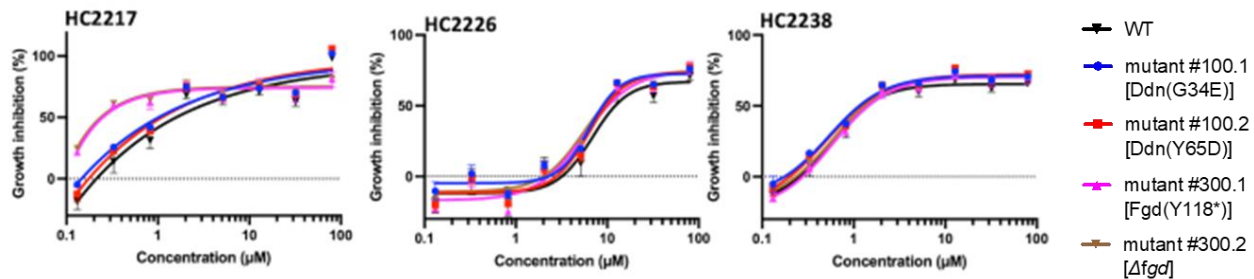
Figure A.2.3. Dinitrobenzamides do not depend on Ddn or Fgd for their activity. The dotted lines represent the growth inhibition of the negative control (DMSO). The error bars represent the standard deviations of three biological replicates. All experiments were repeated at least twice with similar results.
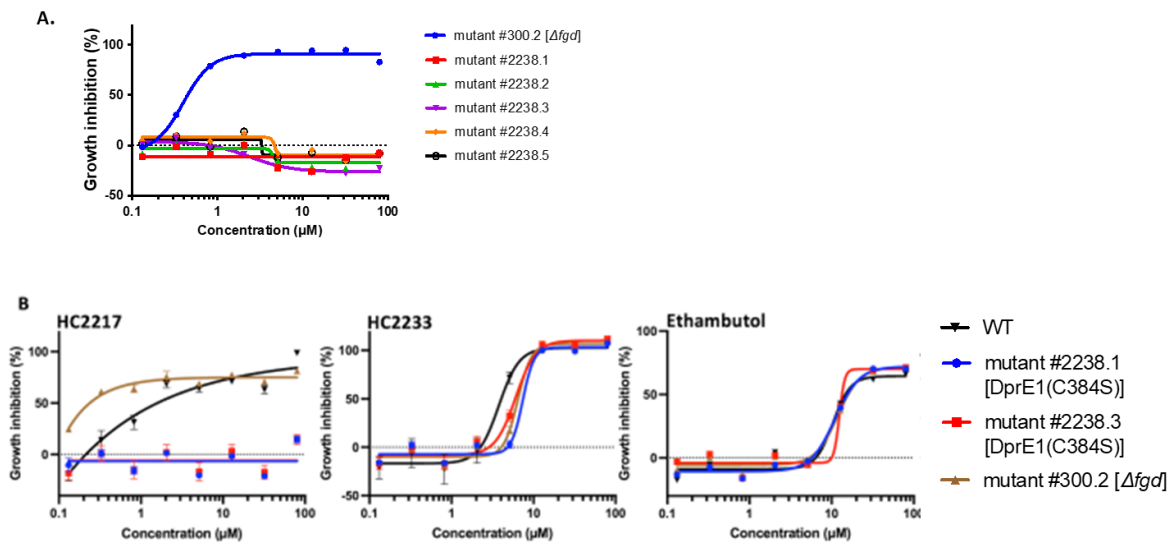
Figure A.2.4. Generation of *dprE1* resistant mutants and testing for the activity of other compounds in our collection against the mutants. **A.** Resistance screening of spontaneous mutants that were generated from 7H9/OADC plates containing HC2238 as a selection agent. **B.** DprE1 mutations confer resistance to HC2217, but not HC2233 or ethambutol. The dotted lines represent the growth inhibition of the negative control (DMSO). Dose responses in **B** were repeated twice with similar results and the error bars represent the standard deviations of three biological replicates.
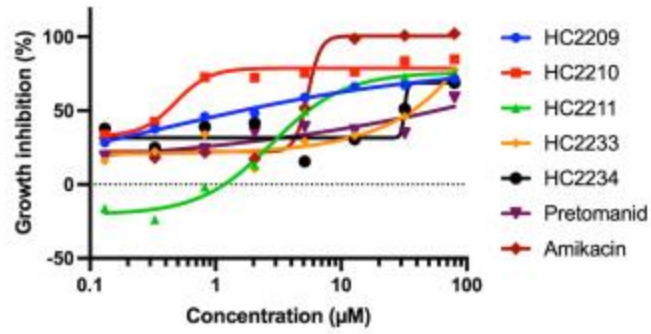
Figure A.2.5. Activity of the nitrofurans against *Mycobacterium abscessus*. The dose responses were repeated twice with similar results.
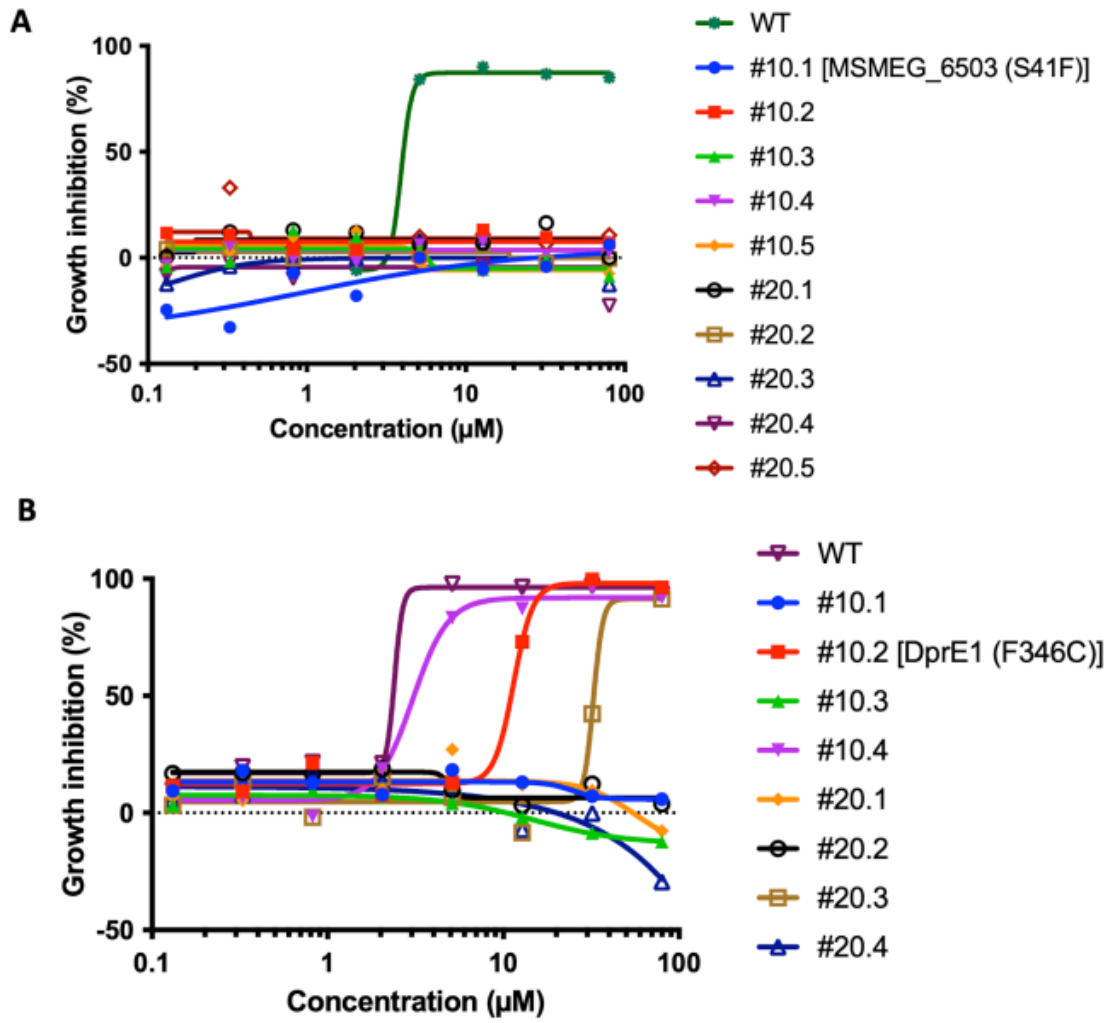
Figure A.2.6. Resistance screening of *Mycobacterium smegmatis* mutants against different dinitrobenzamides. **A.** Confirmation of mutants that were generated in selection plates containing HC2217. **B.** Confirmation of mutants that were generated in selection plates containing HC2238.
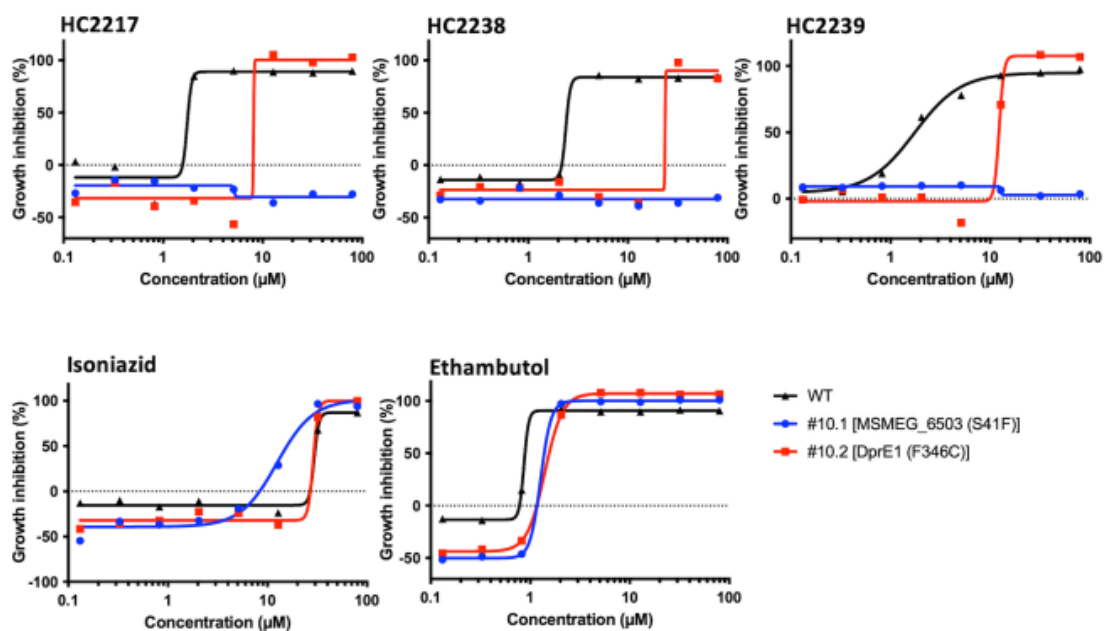
Figure A.2.7. Cross-resistance screening of *Mycobacterium smegmatis MSMEG_6503* and *dprE1* spontaneous mutants against HC2217, HC2238, HC2239. All three compounds have decreased potency against the spontaneous mutants.
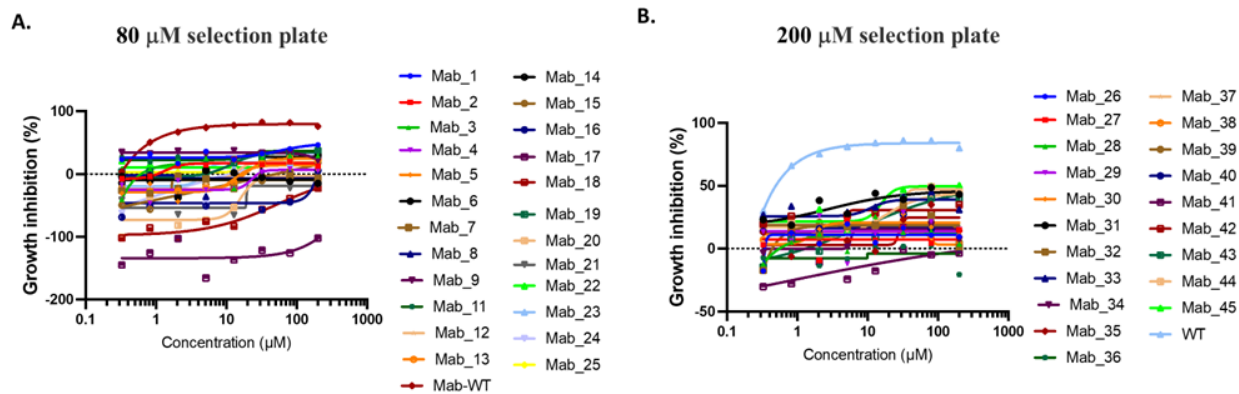
Figure A.3.1. Screening for HC2210-resistant mutants that were isolated from agar plates amended with either A. 80 μM or **B**. 200 μM of HC2210.
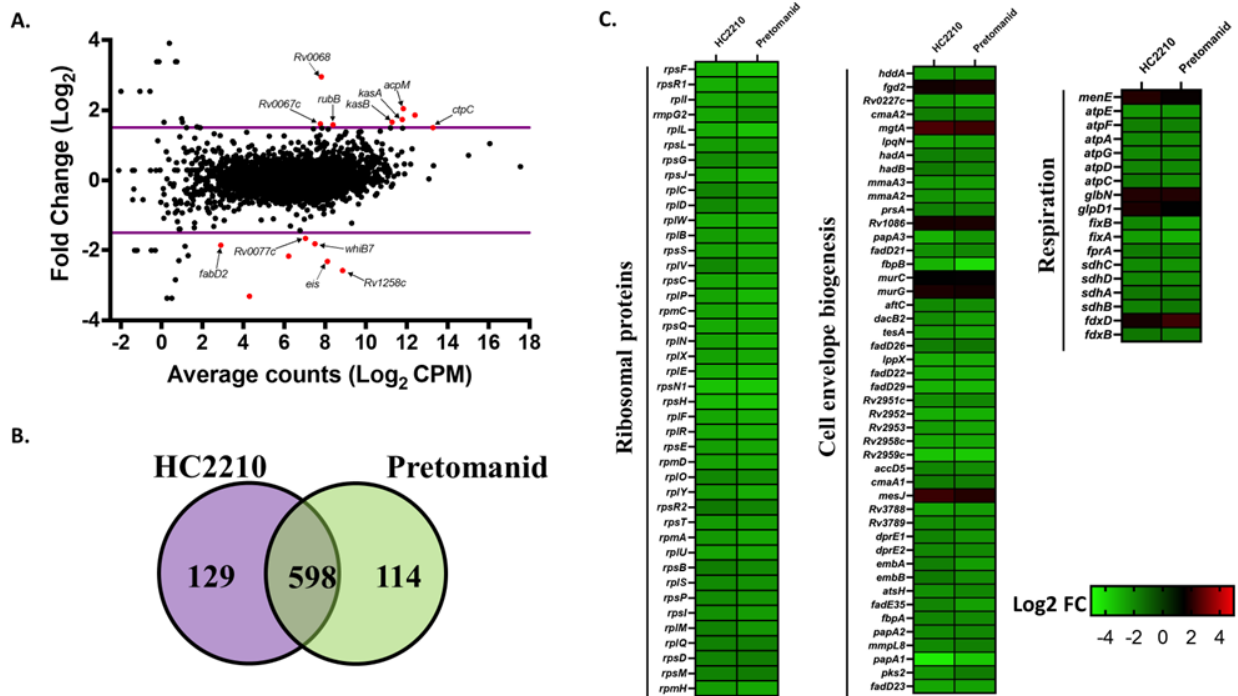
A. 10 μM selection plate
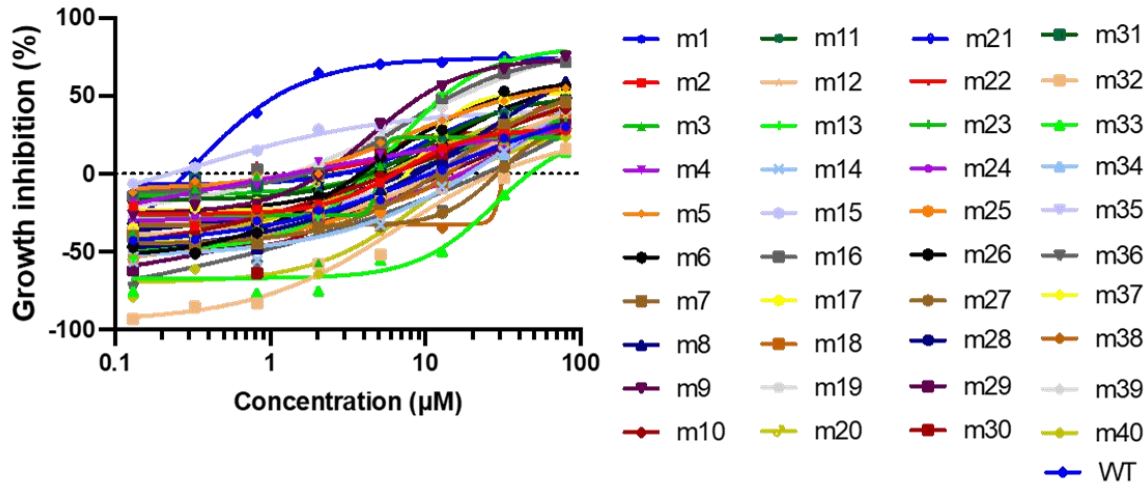
B. 20 μM selection plate
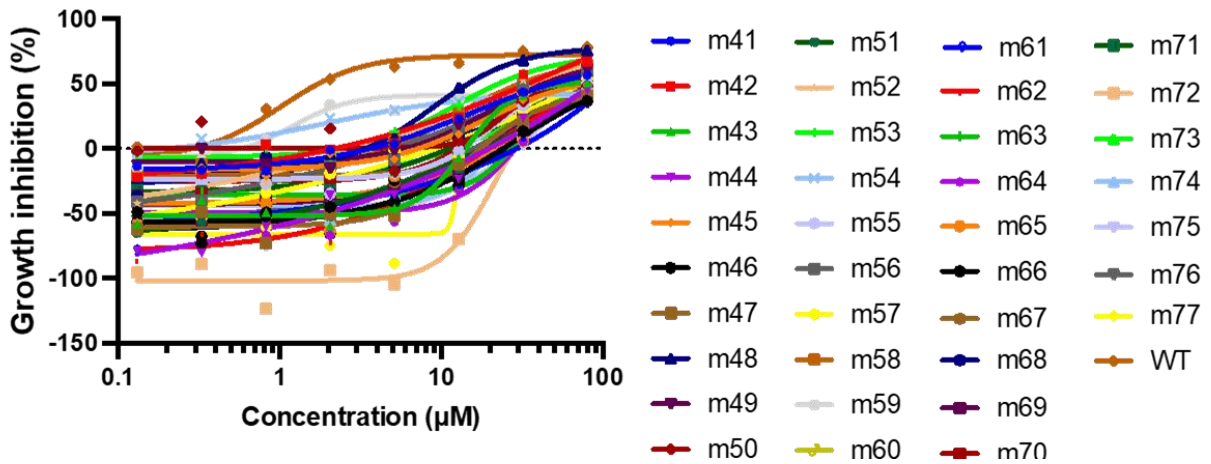
Figure A.3.2. Screening for HC2210-resistant mutants that were isolated from agar plates amended with either A. 10 μM or **B**. 20 μM of HC2210.
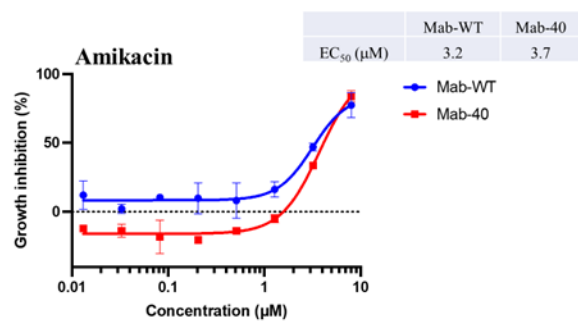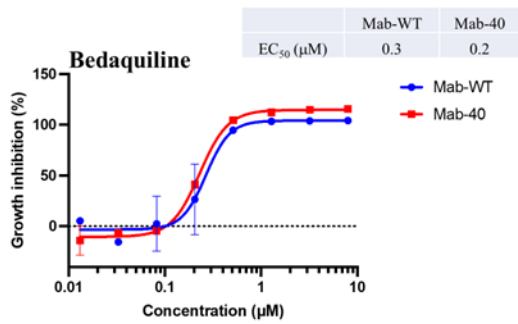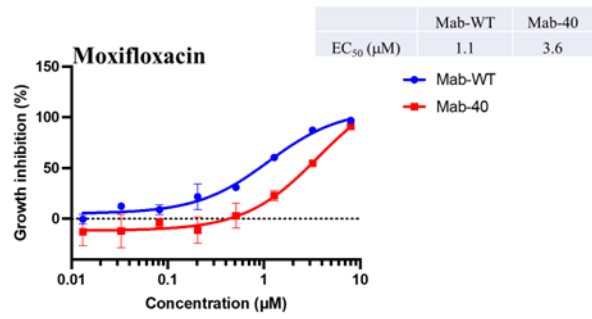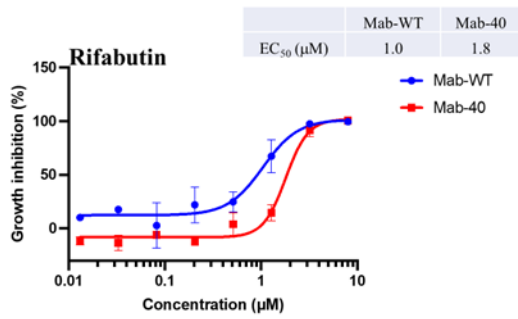
Figure A.3.3. Cross-resistance screening of the *glpK* mutant (Mab-40) against common antimycobacterial drugs.

Figure A.3.4. Transcriptional profiling of HC2210 and pretomanid. **A.** Magnitude-amplitude plot comparing the transcriptional profile of Pretomanid-treated *M. tuberculosis* (Mtb) cultures versus HC2210-treated Mtb cultures. At a significance threshold of q <0.05 and log$_2$ fold change >|1.5|, only 15 genes show significant difference between the two genes and they are indicated in red. Relative to DMSO, the compounds each differentially regulate >500 genes. **B**. Pie-chart showing that pretomanid and HC2210 share most of their differentially expressed genes at log$_2$ fold change >|1.5| and q <0.05. **C**. Relative to the DMSO-control, HC2210 and pretomanid affect genes involved in cell wall biosynthesis and respiration.
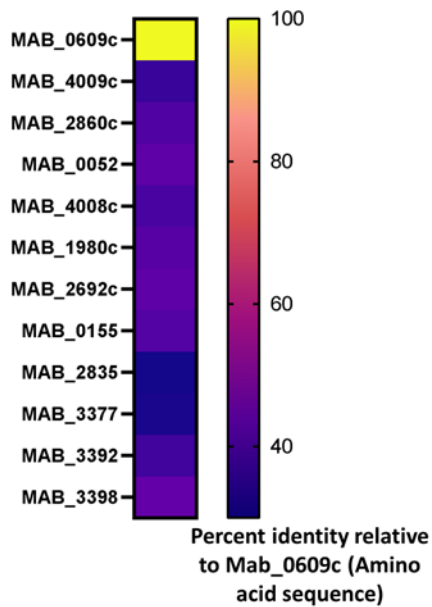
Gene	% identity (Amino acid sequence)
MAB_0609c	100
MAB_4009c	35.33
MAB_2860c	39.37
MAB_0052	41.67
MAB_4008c	38.19
MAB_1980c	40.48
MAB_2692c	41.67
MAB_0155	39.81
MAB_2835	30.66
MAB_3377	31.13
MAB_3392	36.73
MAB_3398	42.86

Figure A.3.5. Identification of *ddn* orthologs in *M. abscessus* when MAB_0609c (a homolog of Ddn in Mab) is used as the query in a BLASTp search with non-redundant protein sequence and *Mycobacterium abscessus* ATC19977 as the standard NCBI database and organism, respectively.
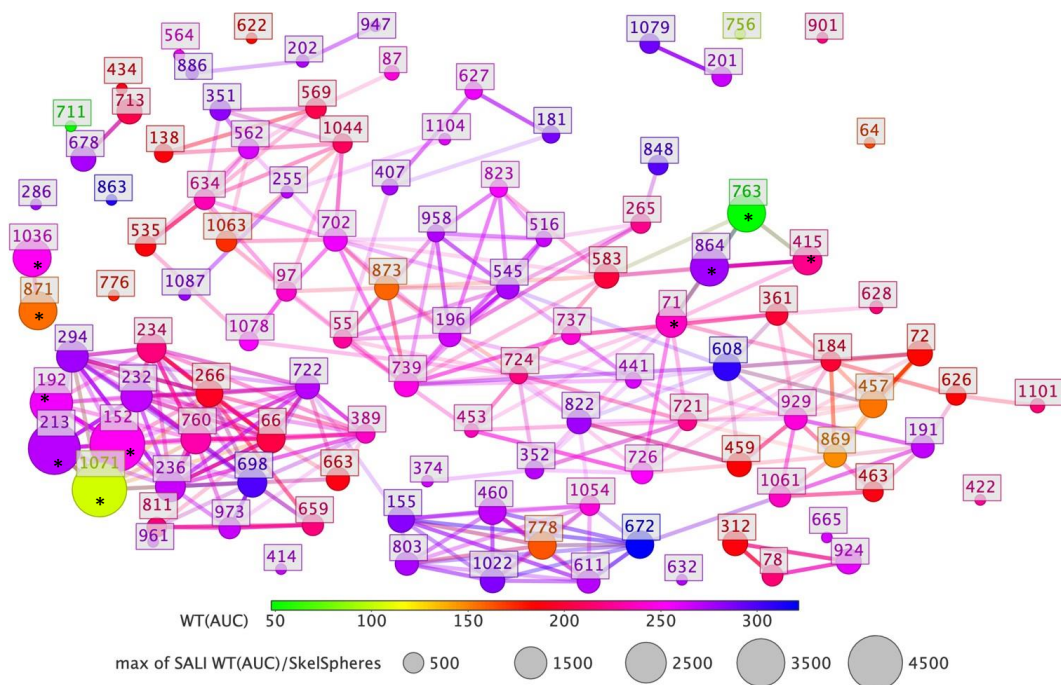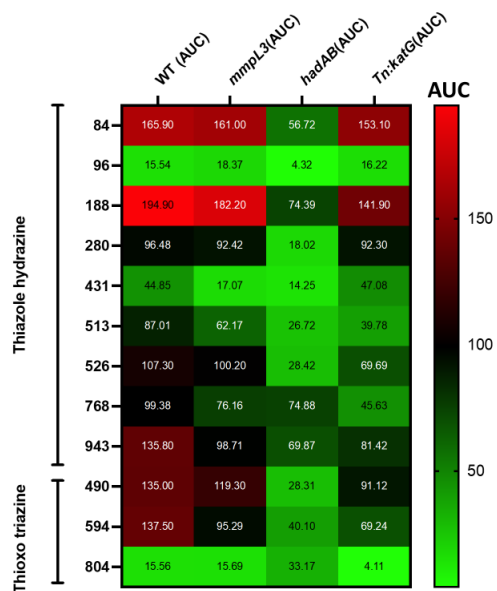
Figure A.4.1. Activity cliff analysis of the isoniazid analogs from the MLSMR dataset. The colors represent the AUC or activity of the analogs against the WT, while the size of the sphere indicates the value of the structure-activity landscape index (SALI). * = analogs that are compared in **Table 5.1**.
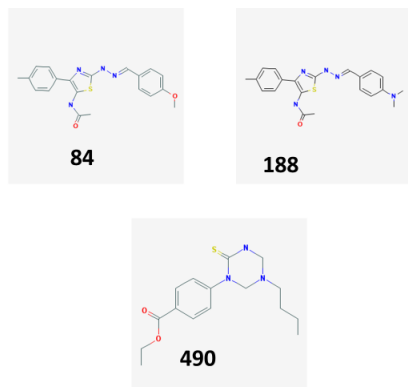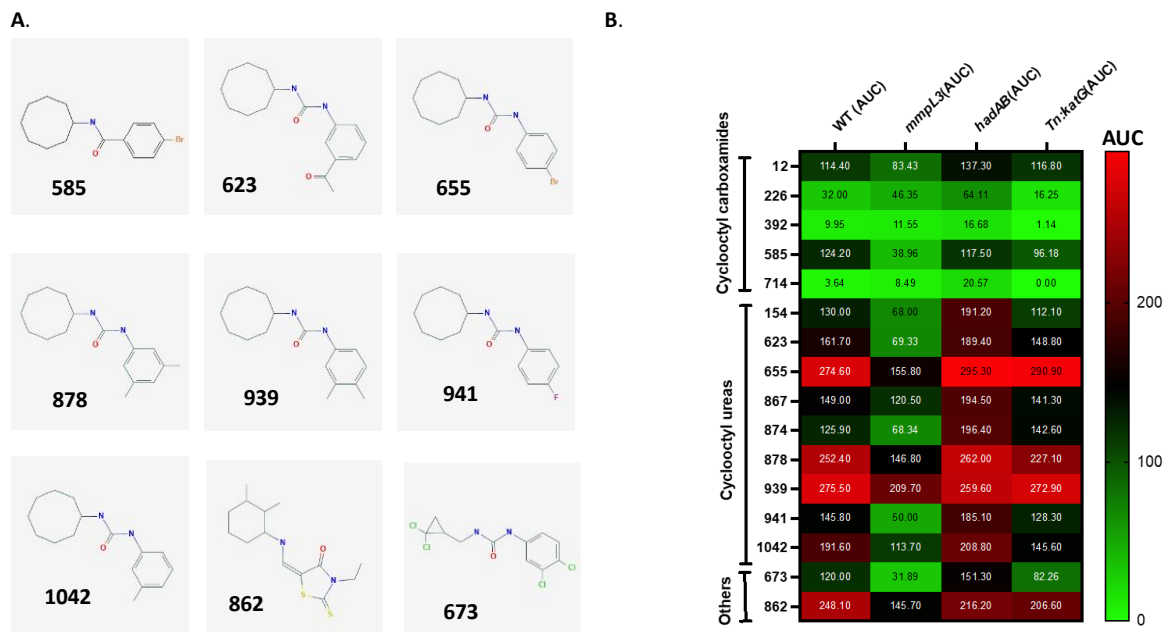
Figure A.4.2. Activity of the thiazole hydrazines in the MLSMR dataset against the three mutants. **A.** The thiazole hydrazine-based compounds and a thioxo triazine identified from the outlier analysis of the *hadAB* screen. **B.** Activities of all the thiazoles hyrdazines and thioxo triazines in the MLSMR dataset against the three mutants.

A.

585 | 623 | 655
878 | 939 | 941
1042 | 862 | 673

B.

	WT (AUC)	mmpL3 (AUC)	hadAB (AUC)	Tn:katG (AUC)
Cyclooctyl carboxamides				
12	114.40	83.43	137.30	116.80
226	32.00	46.35	64.11	16.25
392	9.95	11.55	16.68	1.14
585	124.20	38.96	117.50	96.18
714	3.64	8.49	20.57	0.00
Cyclooctyl ureas				
154	130.00	68.00	191.20	112.10
623	161.70	69.33	189.40	148.80
655	274.60	155.80	295.30	290.90
867	149.00	120.50	194.50	141.30
874	125.90	68.34	196.40	142.60
878	252.40	146.80	262.00	227.10
939	275.50	209.70	259.60	272.90
941	145.80	50.00	185.10	128.30
1042	191.60	113.70	208.80	145.60
Others				
673	120.00	31.89	151.30	82.26
862	248.10	145.70	216.20	206.60

Figure A.4.3. Cyclooctyl-based compounds from the MLSMR dataset as putative MmpL3 inhibitors. **A.** The cyclooctyl-based and related compounds identified from the outlier analysis of the *mmpL3* screen. **B.** Activities of all the cyclooctyl-based and related compounds in the MLSMR dataset against the three mutants.
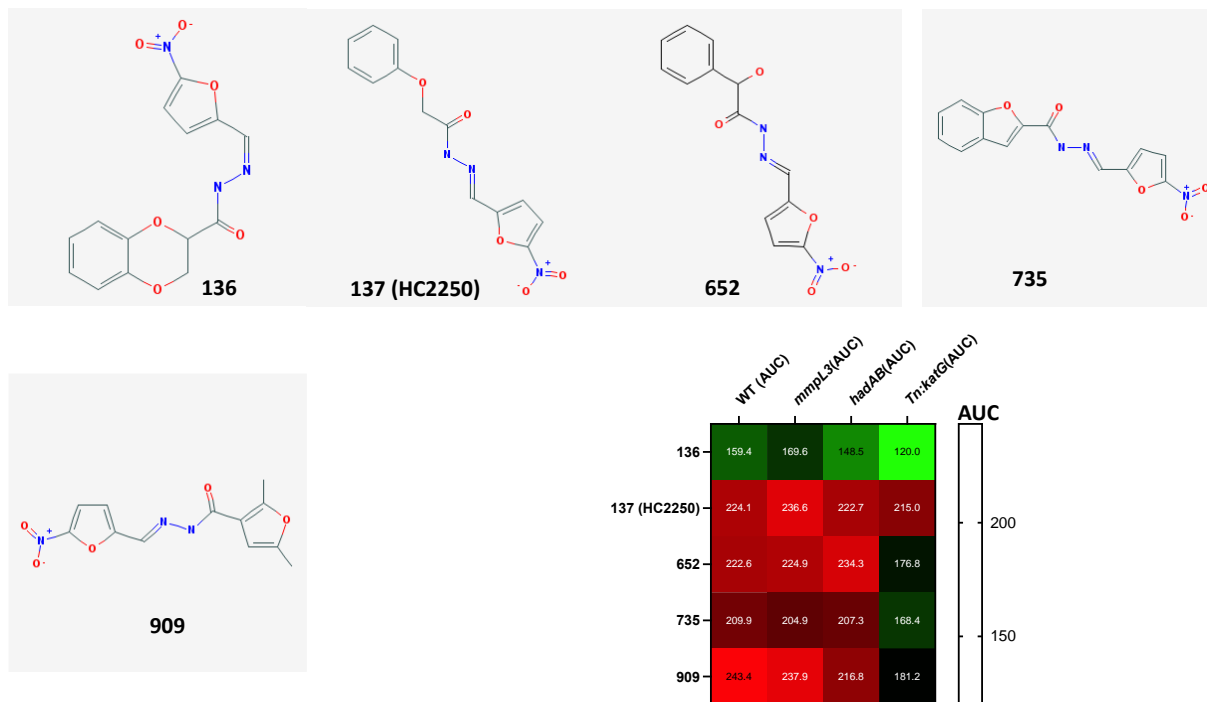
Figure A.4.4. The nitrofuranyl hydrazides identified in the MLSMR dataset and their activity against the three tested mutants.
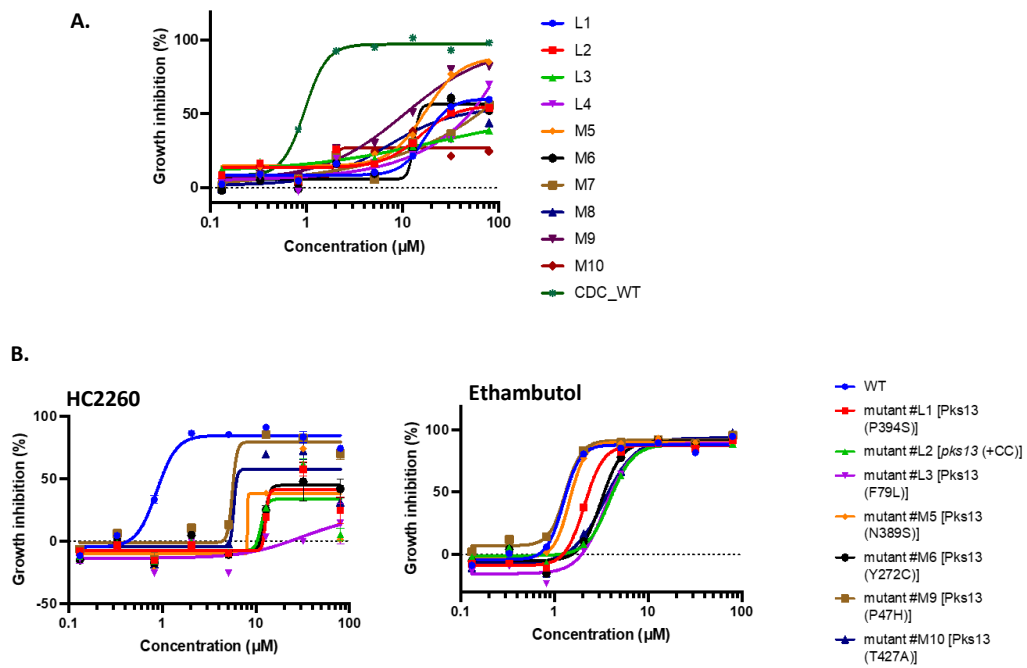
Figure A.4.5. Pks13 screening and cross-resistance studies. A. Confirmation of HC2259-resistant mutants. **B.** Cross-resistance screening of the mutants against HC2260 and ethambutol.
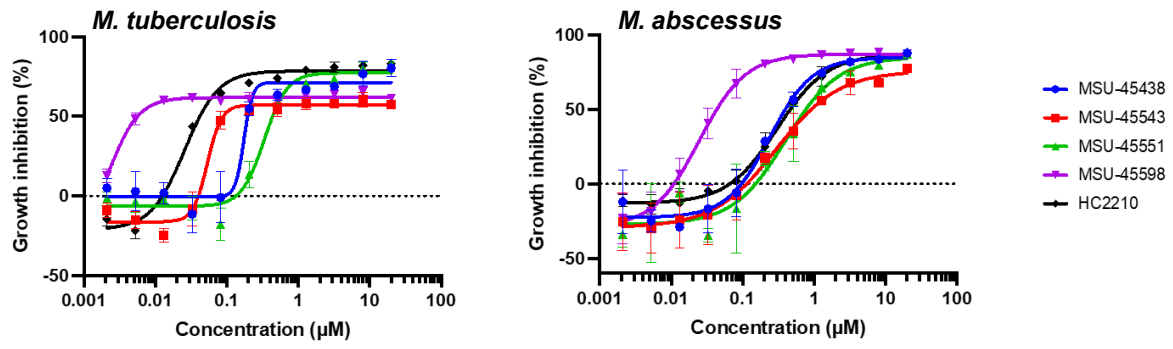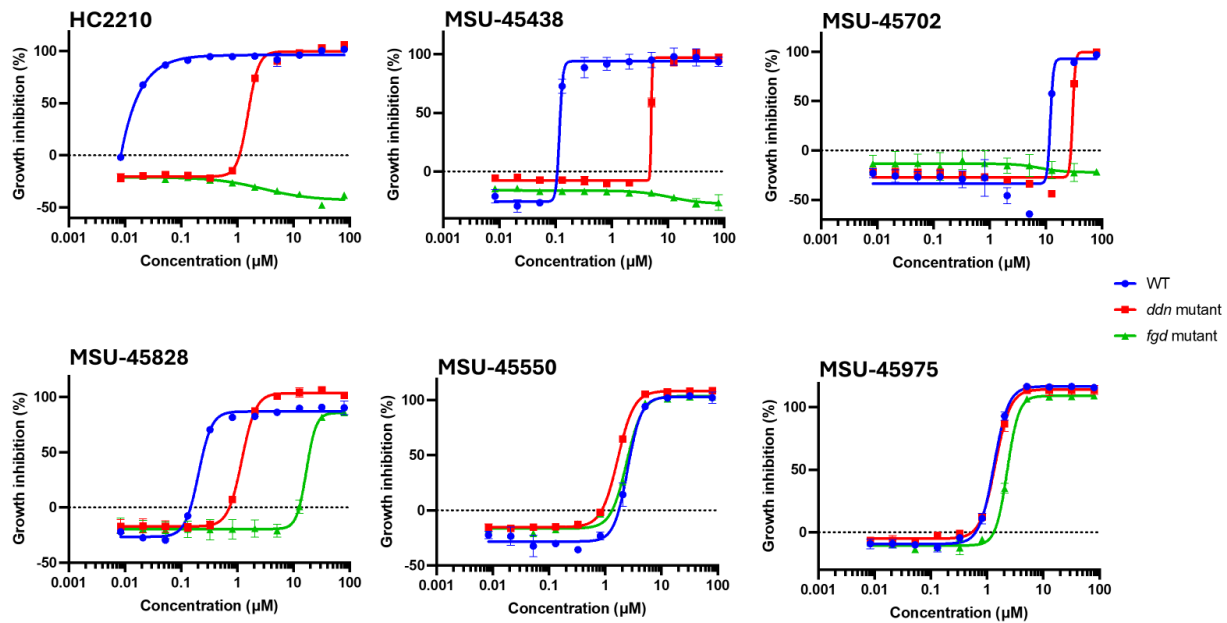
Figure A.5.1. Comparison of the activity of different HC2210 analogs against *M. tuberculosis* and *M. abscessus*.

Figure A.5.2. Cross-resistance screening of the some HC2210 analogs against *ddn* and *fgd* mutants.

Table A.1.1. Confirmation of commercially sourced compounds by mass spectrometry

Compound	Predicted mass (g/mol)	Observed mass (g/mol)*
HC2209	305.30	306.1249
HC2210**	332.31	333.1200
HC2211	287.31	288.1340
HC2217	406.40	407.1019
HC2226	265.22	266.0770
HC2233	386.40	387.1659
HC2234	400.40	401.1817
HC2238	333.27	334.0839
HC2239	361.31	362.0981
HC2250	289.24	290.0773

* ESI was run in the positive mode [M+H]+ resulting the observed masses having an additional H.
**HC2210 is composed of two distinct molecules – HC2210 (332.31g/mol) and oxalic acid (90.03g/mol). Oxalic acid cannot be detected using the ESI MS method employed.

Table A.2.1. Mutations in HC2210 resistant mutants from lower selection concentrations

Mutant strain	SNP location (nt)	Genes (s)	Protein	Nucleotide change	Amino acid substitution
m5	3,657,330	MAB_3607	CofD	GTC→CTC	V49L
m9	3,328,052	MAB_3289	CofC	+G	coding (587/615 nt)
m13	1,321,518	MAB_1319	CofGH	ACC→ATC	T578I
m16	1,322,252	MAB_1319	CofGH	CTC→TTC	L823F
m19	1,322,152	MAB_1319	CofGH	AAC→AAG	N789K
m48	3,327,979	MAB_3289	CofC	GCC→ACC	A172T
m53	1,322,403	MAB_1319	CofGH	(CAC)3→4	coding (2618/2646 nt)